

METABOLOMICS INVESTIGATIONS OF THE EFFECTS OF DRUGS ON MAMMALIAN CELLS

Surachai Ngamratanapaiboon

Thesis submitted to the University of Nottingham

for the degree of

Doctor of Philosophy

2nd December, 2016

DECLARATION

Except where acknowledged in the text, I declare that this dissertation is my own work and is based on research that was undertaken by me in the School of Pharmacy, University of Nottingham.

ABSTRACT

Cell-based metabolomics using LC-MS systemizes the study of the uniqueness of small-molecule metabolite (metabolomes) profiles in cellular processes. Cell-based metabolomics can potentially be used in many applications for the study of biological perturbation from stimulants in cellular pathways. The advantages of cell-based metabolomics include ease of control and interpretation when compared to the study of human subjects and animal models. Furthermore, this method can decrease some highly challenging problems that occur in genomics, transcriptomics and proteomics. Nowadays, cell culture in metabolomics studies has been used in many applications. These include cell culture and bioreactor optimisation, phenotype classification, stimulant testing effect, target and toxicity analysis, metabolic networks determination and modelling, and biomarker and drug target discovery.

In this study, the reverse phase-liquid chromatography-mass spectrometry and hydrophilic interaction chromatography-mass spectrometry for comprehensive metabolic profiling well suited to the untargeted analysis of non-polar and polar metabolites in mammalian cells were developed, optimized and validated. These methods can separate and detect most of hydrophobic and polar metabolites that are normally found in mammalian cell lines.

After that the LC-MS methods were applied to assess the effects of drugs with known and unknown cellular metabolic effects on three mammalian cell lines, namely HMVECs for antipsychotics experiment, MCF-7 cells for cordycepin experiment and MIN6 cells for fluoxetine experiment by using untargeted metabolic profiling.

The global effects of antipsychotics at high therapeutic dosage in HMVECs were investigated. The results support for the toxicity hypothesis with measurements that confirm previous findings and reveal the exact biological pathways of antipsychotic-altered BBB functions. It was found that antipsychotics may affect the bioenergetics pathway due to mitochondrial dysfunction resulted in ketoacidosis and inducing oxide stress by reactive oxygen species generation.

In the MCF- cell experiment, the results of the untargeted metabolite profiling demonstrated the clear anti-breast cancer effects of cordycepin and pentostatin. By investigating the metabolite profiles, clear synergistic effects of cordycepin and pentostatin combined in comparison to cordycepin activity alone in MCF-7 cells was observed. Furthermore, the pathway analysis indicated that anti-breast cancer activity was mainly responsible for alterations in purine and pyrimidine metabolism and bioenergetics. Additionally, cordycepin may be involved in the

inhibition of cell proliferation and differentiation, and the activation of cell apoptosis

The last experiment on MIN6 cells, the developed and optimized HILIC-MS approach in order to determine the biological pathways which are impaired by fluoxetine on glucose-stimulated insulin secretion on MIN6 cell lines was performed. It is found that fluoxetine may impair glycolysis, TCA and fatty acid metabolism on MIN6 cell lines. Moreover, it is also reveal that the alteration of biological pathways on MIN6 cells by known ETC inhibitors (rotenone (Complex I inhibitor, antimycin (Complex III inhibitor) and azide (a complex IV inhibitor). From comparison with these ETC inhibitors, it is found that fluoxetine may have the same effect pattern with azide.

ACKNOWLEDGEMENTS

First and foremost, all praise and thanks are due to my parents, the most gracious, and the Most Merciful for making me able to through this PhD journey and produce this dissertation.

I would like to extend my sincerest gratitude to my supervisor, Prof. Dr. David A. Barrett and Dr. Dong-Hyun Kim for their patience, encouragement, guidance and support throughout this work. The writing of this dissertation has been one of the most significant academic challenges I have ever had to face, without their support, patience and guidance, this study would not have been completed. It is to them that I owe my deepest gratitude.

I would also like to thank to the Royal Thai Government and Rajamangala University of Technlogy Krungthep for the fully funding throughout my postgraduate study. I wish to thank Dr. Catherine Ortori and Paul Cooling for all the technical help in the lab. I also thank to Dr. Ekramy Elmorsy and Dr. Paul A. Smith (Faculty of Medicine & Health Sciences, The University of Nottingham Medical School) for cell culture experiments on human microvascular endothelial cells from blood brain barrier and murine pancreatic beta cells. I would like to thank Mr. Lin Jia, Mrs. Wahyu Utami and Dr. Cornelia De Moor (School of Pharmacy, The University of

Nottingham) for cell culture experiments on human breast cancer cells.

I also to thank to all members of CAB groups who help me in my work. Your supports have taught me so much. I would like to thanks to Office of Educational Affairs, the Royal Thai Embassy, London, UK which gives me a support during the tough times.

CONTENTS

	Page
DECLARATION	i
ABSTRACT	ii
ACKNOWLEDGEMENTS	v
CONTENTS	vii
LIST OF FIGURES	xx
LIST OF TABLES	xxx
LIST OF ABBREVIATION	xxxii
CHAPTER I: INTRODUCTION	1
1.1 METABOLOMICS BACKGROUND	1
1.1.1 Types of metabolomics study	3
1.1.1.1 Metabolite target analysis	3
1.1.1.2 Metabolic profiling	3
1.1.1.3 Metabolic fingerprinting	4
1.1.2 Analytical technologies for metabolomics	4
1.1.2.1 Mass spectrometry	4
1.1.2.2 Orbitrap-Mass spectrometry	6
1.1.2.3 Liquid chromatography	8
A. Reversed phase-liquid chromatography	8

Page

B. Hydrophilic interaction chromatography 10

1.1.3 Metabolite Identification 11

1.1.4 Multivariate data analysis for metabolomics experiments 14

1.2 CELL-BASED METABOLOMICS 15

1.2.1 Overview 15

1.2.2 Definition of cell-based metabolomics 17

1.2.3 Advantages and disadvantages of cell-based metabolomics 18

1.3 BACKGROUND TO THE MAIN AREAS OF EXPERIMENTAL INVESTIGATION IN THE THESIS 19

1.3.1 Antipsychotics and the blood brain barrier 23

1.3.1.1 Typical antipsychotic (AP) drugs (First generation) 23

A. Chlorpromazine (CPZ) 24

B. Haloperidol (HAL) 26

1.3.1.2 Atypical antipsychotic medications 28

A. Clozapine (CLZ) 28

B. Risperidone (RIS) 29

1.3.1.3 Overdose problems of antipsychotics 31

Page

1.3.1.4 Blood brain barrier relevance 32

1.3.1.5 Antipsychotics and the blood brain barrier system 33

1.3.2 Breast cancer and cordycepin 35

1.3.2.1 Breast cancer cells 35

1.3.2.2 Problems with breast cancer treatments 36

1.3.2.3 Cordycepin 36

1.3.2.4 Role of pentostatin as a potentiator of cordycepin activity 39

1.3.2.5 Utility of cordycepin and pentostatin combinations in cell-based studies 40

1.3.3 Fluoxetine and pancreatic beta cells 41

1.3.3.1 Fluoxetine 41

1.3.3.2 Problems associated with fluoxetine 42

1.3.3.3 Pancreatic beta cells 43

1.3.3.4 Investigation of beta cell function using fluoxetine as a probe 43

1.4 AIMS OF THE THESIS 45

Page

CHAPTER II: MATERIALS AND METHODS 46

2.1 CHEMICALS 46

2.2 REVERSE PHASE LIQUID CHROMATOGRAPHY 54

2.3 HYDROPHILIC INTERACTION CHROMATOGRAPHY 54

2.4 MASS SPECTROMETRIC CONDITIONS 55

CHAPTER III: OPTIMISATION AND VALIDATION OF A LIQUID CHROMATOGRAPHY-MASS SPECTROMETRY METHOD 56

3.1 ABSTRACT 56

3.2 INTRODUCTION 58

3.3 OBJECTIVES 59

3.4 MATERIALS AND METHODS

3.4.1 Reverse phase liquid chromatography 60

3.4.1.1 Sample preparation for reverse Phase liquid chromatography 60

3.4.1.2 Mass spectrometric conditions for RP-LC method 61

3.4.2 Hydrophilic interaction chromatography 62

3.4.2.1 Sample preparation for hydrophilic interaction chromatography 63

Page

3.4.2.2 Mass spectrometric conditions 63

3.4.2.3 Chromatographic conditions 64

3.4.2.4 Method validation 64

3.5 RESULTS AND DISCUSSION 65

3.5.1 RP-LC method validation 65

3.5.2 Hydrophilic interaction chromatography 68

3.5.2.1 Mass spectrometric conditions 68

3.5.2.2 Chromatographic conditions 74

3.5.2.3 Method validation 85

CHAPTER IV: EFFECTS OF ANTIPSYCHOTIC DRUGS APPLIED TO HUMAN MICROVASCULAR ENDOTHELIAL CELLS ON THE INTRACELLULAR METABOLOME 90

4.1 ABSTRACT 90

4.2 INTRODUCTION 92

4.3 OBJECTIVES 95

4.4 MATERIALS AND METHODS 96

4.4.1 Chemicals and reagents 96

4.4.2 Study design 96

4.4.3 Human microvascular endothelia cells from blood brain barrier experiments 97

4.4.4 Metabolite extraction 98

4.4.5 LC-MS analysis 99

Page

4.4.6 Data analysis 102

4.5 RESULTS 104

4.5.1 Data Quality 104

4.5.2 Antipsychotic drug metabolism in HMVECs 109

4.5.3 Effects of antipsychotic drugs on lipid metabolites 115

4.5.4 Effects of antipsychotic drugs on polar metabolites in HMVECs 123

4.5.5 Biological significance of the metabolic effects of antipsychotics on HMVECs 127

4.6 DISCUSSION 129

4.6.1 Antipsychotics metabolites 129

4.6.2 Antipsychotic effects on HMVECs 131

4.7 CONCLUSION 137

CHAPTER V: LC-MS-BASED METABOLOMICS REVEALED SIGNIFICANT ALTERED INTRACELLULAR METABOLITES IN HUMAN BREAST CANCER (MCF-7) CELLS TREATED WITH CORDYCEPIN 138

5.1 ABSTRACT 138

5.2 INTRODUCTION 140

5.3 OBJECTIVES 143

5.4 MATERIALS AND METHODS 144

Page

5.4.1 Chemicals 144

5.4.2 Study design 144

5.4.2.1 The effect of pentostatin on the stability of cordycepin 144

5.4.2.2 The effect of cordycepin on metabolome changes 145

5.4.3 Pentostatin and cordycepin effects on MCF-7 cells 145

5.4.4 Metabolite extraction 145

5.4.5 Metabolomics analysis 146

5.4.6 Data processing and statistical analysis 147

5.5 RESULTS 149

5.5.1 Effects of pentostatin on cordycepin stability in MCF-7 cells 150

5.5.1.1 Multivariate statistical analysis of the metabolomics data 150

5.5.1.2 Feature selection: Potential key metabolites 157

5.5.2 Effects of cordycepin on MCF-7 cells 162

5.5.2.1 Metabolic profiles analysed by cell-based metabolomics using LC-MS approach 162

5.5.2.2 Cordycepin and its metabolites 163

Page

5.5.2.3 Metabolic identification of MCF-7 cells treated with cordycepin 166

5.5.3 Biological pathways analysis 170

5.6 DISCUSSION 173

5.6.1 Pentostatin effects on cordycepin stability in MCF-7 cells 173

5.6.2 Effects of combination of cordycepin And pentostatin on MCF-7 metabolite profile. 175

5.6.3 The effects of cordycepin on cellular metabolites of MCF-7 cells. 176

5.7 CONCLUSION 180

CHAPTER VI: CELL-BASED METABOLOMICS USING LC-MS TO STUDY THE METABOLIC EFFECTS OF FLUOXETINE ON GLUCOSE-TREATED MURINE PANCREATIC BETA (MIN6) CELLS 181

6.1 ABSTRACT 181

6.2 INTRODUCTION 183

6.3 OBJECTIVES 185

6.4 MATERIALS AND METHODS 186

6.4.1 Chemicals 186

6.4.2 Study design 186

6.4.3 Pancreatic beta cells 187

Page

6.4.4 MIN6 cell experiments 188

6.4.5 Metabolite extraction 188

6.4.6 Metabolomics analysis 188

6.4.7 HILIC-MS analysis 189

6.4.8 Data processing and statistical analysis 190

6.5 RESULTS 192

6.5.1 Data Quality 192

6.5.2 Metabolomic analysis of MIN6 cells 194

6.5.2.1 Metabolic signature of MIN6 cells exposure to glucose 194

6.5.2.2 Metabolic signature of glucose-treated MIN6 cells exposure to rotenone 200

6.5.2.3 Metabolic signature of glucose-treated MIN6 cells exposure to antimycin A 210

6.5.2.4 Metabolic signature of glucose-treated MIN6 cells exposure to azide 219

6.5.2.5 Metabolic signature of glucose-treated MIN6 cells exposure to fluoxetine 226

6.5.2.6 Overall effects 232

Page

6.5.3 Metabolic pathway analysis 234

6.6 DISCUSSION 237

6.6.1 Glucose effects 237

6.6.2 Fluoxetine effects on glucose-treated MIN6 cells 241

6.6.2.1 Lipids and lipid metabolism-related molecules 242

6.6.2.2 Bioenergetics 243

6.6.3 Comparison of the effects of fluoxetine and ETC inhibitors 244

6.6.3.1 Glycolysis 244

6.6.3.2 TCA cycle 245

6.7 CONCLUSION 248

CHAPTER VII: SUMMARY AND FUTURE DIRECTIONS 249

7.1 SUMMARY 249

7.1.1 Optimisation and validation of a liquid Chromatography-mass spectrometry Method 249

Page

7.1.2 Effects of antipsychotic drugs applied to human microvascular endothelial cells on the intracellular metabolome 253

7.1.3 LC-MS-based metabolomics revealed significant altered intracellular metabolites in human breast cancer (MCF-7) cells treated with cordycepin 256

7.1.4 Cell-based metabolomics using LC-MS to study the metabolic effects of fluoxetine on glucose-treated murine pancreatic beta (MIN6) cells 259

7.1.5 Overall summary 262

7.2 FUTURE WORK 268

7.2.1 Expanding metabolite identification 268

7.2.2 Expanding coverage of the metabolites 269

7.2.3 Improving metabolomics methods to obtain more quantitative data using multiple internal standards 270

PAGE

7.2.4 Integration of metabolomics data with metabolic pathway maps 271

7.2.5 Metabolomics for off-target effects of drugs in cells potential adverse effects in toxicology studies 272

APPENDIX 273

Supplementary Table 2.1 List of the first group of metabolite mixture. 273

Supplementary Table 2.2 List of the second group of metabolite mixture. 277

Supplementary Table 2.3 List of the third group of metabolite mixture. 278

Supplementary Table 3.1 Formula, monoisotopic molecular weight, type of adduct, detected mass, retention time and relative standard error of metabolites. 279

Supplementary Table 5.1 List of identified metabolites in MCF-7 cell extracts. 285

Supplementary Table 6.1 Details of detected ion (m/z) from cell extracts of untreated and glucose-treated MIN6 cells. 295

Page

Supplementary Table 6.2 Details of detected ion (m/z) from cell extracts of glucose- and glucose + DMSO-treated MIN6 cells. 300

Supplementary Table 6.3 Details of detected ion (m/z) from cell extracts of MIN6 cells treated with rotenone 301

Supplementary Table 6.4 Details of detected ion (m/z) from cell extracts of MIN6 cells treated with ethanol 307

Supplementary Table 6.5 Details of detected ion (m/z) from cell extracts of MIN6 cells treated with antimycin A 308

Supplementary Table 6.6 Details of detected ion (m/z) from cell extracts of MIN6 cells treated with azide 313

Supplementary Table 6.7 Details of detected ion (m/z) from cell extracts of MIN6 cells treated with fluoxetine 319

REFERENCES 323

LIST OF FIGURES

		Page
Figure 1.1	Overview of the interaction between different 'omics' sciences.	2
Figure 1.2	Overview of the Orbitap detector detailing the entrance of the ions into the detector, Orbitrap about the central electrode, and subsequent current-frequency detected by the systemetric exterior electrodes.	7
Figure 1.3	A schematic representing the mechanism in a RP separation.	9
Figure 1.4	A schematic representing the mechanism in a ZIC-HILIC separation.	11
Figure 1.5	Schematic of metabolite identification.	13
Figure 1.6	The general trend in the publication of cell-based metabolomics applications to study the effects and toxicology of drugs.	18

Page

Figure 1.7 Examples of cell culture applications in metabolomics studies. 21

Figure 1.8 Chemical structure of chlorpromazine. 24

Figure 1.9 Chemical structure of haloperidol. 26

Figure 1.10 Chemical structure of clozapine. 28

Figure 1.11 Chemical structure of risperidone. 30

Figure 1.12 Chemical structure of cordycepin. 37

Figure 1.13 Chemical structure of pentostatin. 40

Figure 1.14 Chemical structure of fluoxetine. 42

Figure 3.1 Chromatograms of the QC sample form lipid fraction. 66

Figure 3.2 Chromatograms of the QC sample form polar fraction. 67

Figure 3.3 Fingerprinting of three simultaneous standard polar metabolite mixtures in negative mode using HILIC-MS method. 69

		Page
Figure 3.4	Fingerprinting of three simultaneous standard polar metabolite mixtures in positive mode using HILIC-MS method.	70
Figure 3.5	Structures and mass spectra of the four analytes in ESI- and four analytes in ESI+.	73
Figure 3.6	Representative chromatograms of some compounds using HILIC-MS method.	77
Figure 3.7	Base peak chromatogram in ESI- mode of the three standard groups from HILIC-MS.	78
Figure 3.7	Base peak chromatogram in ESI+ mode of the three standard groups from HILIC-MS.	79
Figure 2.9	EICs of some standard organic acids studied by using HILIC-MS method.	82

Page

Figure 3.10 EICs of some standard L-amino acids studied by using HILIC-MS method. 83

Figure 3.11 EICs of some standard sugars by using HILIC-MS method. 84

Figure 4.1 Simple diagram of anatomical structure of the blood brain barrier. 93

Figure 4.2 Total ion chromatogram (TIC) of hydrophobic endogenous metabolites in ESI+ and ESI-. 106

Figure 4.3 Total ion chromatogram (TIC) of hydrophilic endogenous metabolites in ESI+ and ESI-. 107

Figure 4.4 PCA scores plots of lipid fraction (A) and polar fraction (B). 108

Figure 4.5 A schematic representation of the metabolism of chlorpromazine. 111

Figure 4.6 A schematic representation of the metabolism of haloperidol. 112

Page

Figure 4.7 A schematic representation of the metabolism of clozapine. 113

Figure 4.8 A schematic representation of the metabolism of risperidone. 114

Figure 4.9 OPLS-DA of untargeted metabolomics data from HMVECs treated with antipsychotics in the lipid fraction. 116

Figure 4.10 Level changes of the top ten significantly-changed metabolites from the lipid fraction. 121

Figure 4.11 OPLS-DA of untargeted metabolomics data from HMVECs treated with antipsychotics in the polar fraction. 124

Figure 4.12 Level changes of the top ten significantly-changed metabolites from the polar fraction 126

Page

Figure 4.13 Overall simple diagrams for biological pathways that are affected by high therapeutic dosage of antipsychotics. 128

Figure 5.1 Pie chart summarizing the distribution and information for MCF-7 cell metabolites. 150

Figure 5.2 PCA and OPLS-DA scores plots from MCF-7 cells exposed to DMSO), pentostatin, cordycepin and cordcepin + pentostatin combination. 152

Figure 5.3 PCA scores plot for among time treatments. 153

Figure 5.4 Cordycepin, cordycepin monophosphate and deoxyinosine levels in MCF-7 cells. 161

Figure 5.5 Scores plot of PCA and OPLS-DA of MS spectral data using all the detected ion features and samples. 164

Figure 5.6 Common pathway of cordycepin metabolism in mammalian cells. 165

		Page
Figure 5.7	The cordycepin metabolism and possible biological pathways that are affected by cordycepin in MCF-7 cells.	171
Figure 5.8	Level changes of some metabolites in MCF7 cells exposed to 50 μM cordycepin.	172
Figure 6.1	Scores plot of OPLS-DA of MS spectral data using all the detected ion features.	193
Figure 6.2	Scores plot from OPLS-DA analysis of control and glucose-treated MIN6.	196
Figure 6.3	Level changes of the top ten altered metabolites of 10 mM glucose treated MIN6 cells compared to untreated cells.	199
Figure 6.4	Scores plot from OPLS-DA analysis of basal, glucose and glucose+ DMSO treated MIN6 cells.	202
Figure 6.5	Scores plot from OPLS-DA analysis of basal, glucose + DMSO and glucose + DMSO + rotenone treated MIN6 cells.	203

		Page
Figure 6.6	Level changes of ten altered metabolites of 10 mM glucose treated MIN6 cells exposed to drugs compared to untreated cells.	209
Figure 6.7	Scores plot from OPLS-DA analysis of basal, glucose and glucose+ ethanol treated MIN6 cells.	212
Figure 6.8	Scores plot from OPLS-DA analysis of basal, glucose + ethanol and glucose + ethanol + antimycin A treated MIN6 cells.	213
Figure 6.9	Level changes of ten altered metabolites of 10 mM glucose-treated MIN6 cells exposed to 1 μM of antimycin A and ethanol compared to untreated cells.	218
Figure 6.10	Scores plot from OPLS-DA analysis of basal, glucose and glucose + azide treated MIN6 cells.	220

Page

Figure 6.11 Level changes of ten altered metabolites of 10 mM glucose treated MIN6 cells exposed with 6 mM of azide compared to untreated cells. 225

Figure 6.12 Scores plot from OPLS-DA analysis of basal, glucose and glucose + fluoxetine treated MIN6 cells. 227

Figure 6.13 Level changes of ten altered metabolites of 10 mM glucose treated MIN6 cells exposed to 30 μM of fluoxetine compared to untreated cells. 231

Figure 6.14 Fold changes of shared altered metabolites of 10 mM glucose treated MIN6 cells exposed to glucose, rotenone, antimycin A and fluoxetine. 233

Page

Figure 5.15 Model for the coupling of glucose metabolism to insulin secretion and the effects of fluoxetine, rotenone, antimycin A and azide in the MIN6 cell. 235

LIST OF TABLES

	Page
Table 2.1 Chemical lists were used in the study	47
Table 3.1 Details of MS parameters for RP-LC method	62
Table 3.2 Reproducibility expressed as percentage of relative standard deviation	86
Table 4.1 Details of LC conditions for lipidomic and metabolic profiling	100
Table 4.2 Details of MS parameters for lipidomic and metabolic profiling	101
Table 4.3 Metabolism of chlorpromazine, haloperidol, clozapine and risperidone	110
Table 4.4 Details of metabolites from the lipid fraction which changed significantly during treatment with chlorpromazine, clozapine, haloperidol and risperidone	117
Table 4.5 Details of metabolites from the polar fraction which changed significantly during treatment with chlorpromazine, clozapine, haloperidol and risperidone	125
Table 5.1 Summary of the parameters for assessing modeling quality	154

Page

Table 5.2 Metabolites identified in MCF-7 cells exposed to drugs at different time points 157

Table 5.3 The identified metabolites that were changed significantly during the treatment with cordycepin 168

Table 6.1 The details of metabolites from cell extracts of untreated MIN6 cells (Basal) and 10 mM glucose treated MIN6 cells 197

Table 6.2 The details of significantly altered metabolites of MIN6 cells exposed with rotenone (10 μM in final concentration 204

Table 6.3 The details of significantly altered metabolites of MIN6 cells exposed to antimycin A (1 μM in final concentration) 214

Table 6.4 The details of significantly altered metabolites of MIN6 cells exposed to azide (6 mM in final concentration) 221

Table 6.5 The details of significantly altered metabolites of MIN6 cells exposed to fluoxetine (30 μM in final concentration) 228

LIST OF ABBREVIATIONS

ADA	Adenosine deaminase
ADP	Adenosine diphosphate
AMP	Adenosine monophosphate
ATP	Adenosine triphosphate
AP	Antipsychotic
BBB	Blood brain barrier
CLZ	Clozapine
CE	Capillary electrophoresis
CNS	Central nervous system
CPZ	Chlorpromazine
Da	Dalton
dGMP	Deoxyguanosine monophosphate
LC	Liquid chromatography
EIC	Extracted ion chromatogram
ESI-	Negative electrospray ionisation mode
ESI+	Positive electrospray ionisation mode
ETC	Electron transport chain

FDA	Food and Drug Administration
GC	Gas chromatography
GDP	Guanosine diphosphate
GMP	Guanosine monophosphate
GTP	Guanosine triphosphate
HAL	Haloperidol
HCA	Hierarchical cluster analysis
HILIC	Hydrophilic interaction chromatography
HMVEC	Human microvascular endothelial cell
HRMS	High resolution mass spectrometry
Hz	Hertz
IDP	Inosine diphosphate
IMP	Inosine monophosphate
NMR	Nuclear magnetic resonance
M	Molar
mM	Millimolar
MS	Mass spectrometry
m/z	Mass per charge ratio
PAP	Polyadenylate polymerase pathway

PCA	Principal Component analysis
PCs	Principal Components
PLS-DA	Partial least square-discriminant analysis
PS	Phosphatidylserine
QC	Quality control
RIS	Risperidone
ROS	Reactive oxygen species
RP-LC	Reverse phase-liquid chromatography
RSD	Relative standard error
RT	Retention time
TCA	Tricarboxylic acid
ToF	Time-of-Flight
UDP	Uridine diphosphate
UMP	Uridine monophosphate
UTP	Uridine triphosphate
UHPLC	Ultra-high performance liquid chromatography
UV	Ultra violet
V	Voltage
v	Volume

ZIC	Zwitterionic
μM	Micromolar
n	number

CHAPTER I: INTRODUCTION

1.1 METABOLOMICS BACKGROUND

Metabolomics is a recent 'omics' science that evaluates downstream differences in biological endogenous metabolite levels resulting from therapeutic treatments or diseases (1–3). Metabolites are generally defined as a low molecular weight biomolecules which play an important, essential and diverse role in normal metabolic pathways. Metabolites consist of a very large variety of biochemical compounds when compared to the proteome and the transcriptome (4). Metabolomic studies are sometimes viewed as the important piece of the 'Rosetta Stone' needed for understand the puzzle of complex biological systems (5) as illustrated in Figure 1.1. This field of study could be viewed as the fusion methods among metabolite analysis, bioanalytical science and chemometrics (6).

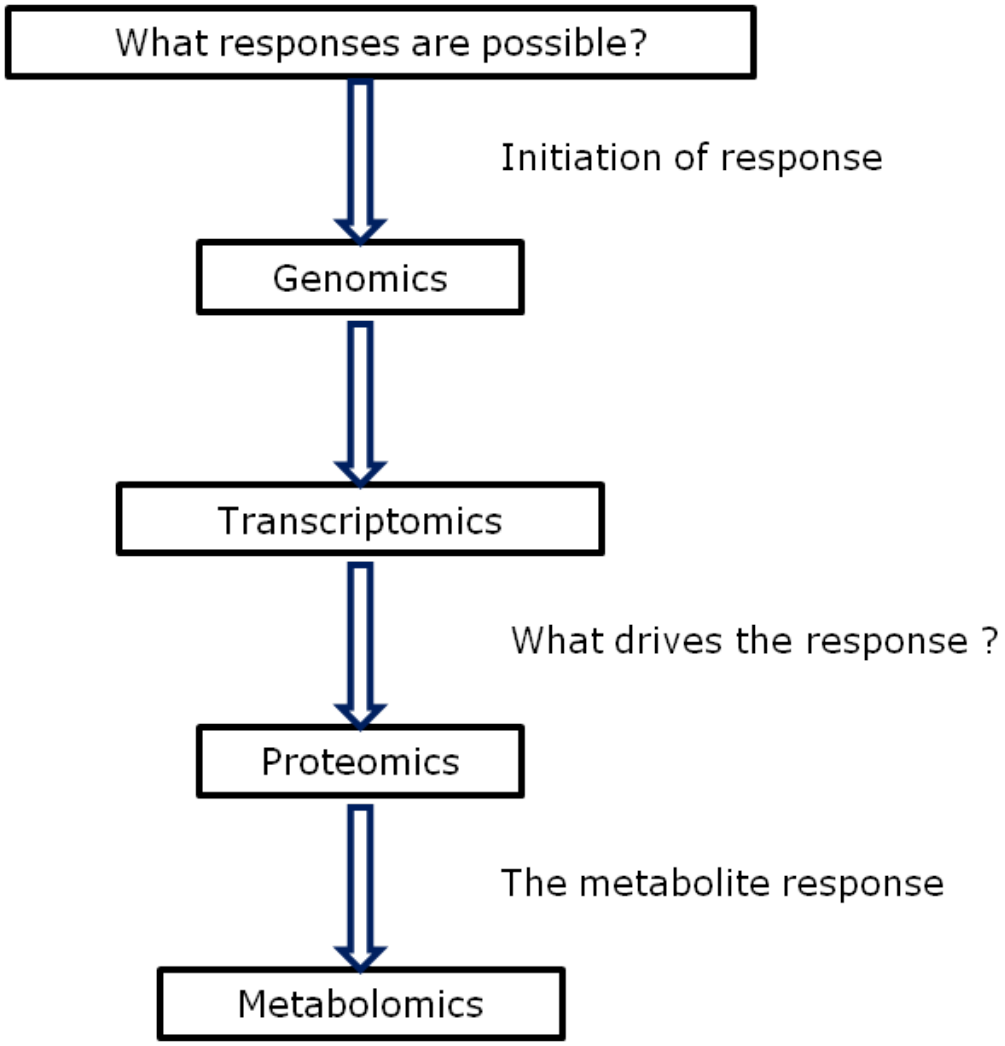


Figure 1.1 Overview of the interaction between different 'omics' sciences.

1.1.1 Types of metabolomics study

Metabolomics commonly consists of metabolite target analysis, metabolic profiling and metabolic fingerprinting (7).

1.1.1.1 Metabolite target analysis

Metabolite target analysis is a direct approach which focuses on quantitative study of one or a few biological metabolites that are related to a specific metabolic pathway (8,9). This approach requires extensive sample preparation and separation from untargeted metabolites. It is particularly useful when metabolites are present in very low concentrations. Often, chromatographic separation and sensitive MS detection are used to provide the requisite specificity and sensitivity (10).

1.1.1.2 Metabolic profiling

The concept of metabolic profiling allows the monitory of metabolites in a biochemical reaction of interested. Normally, metabolic profiling uses chromatographic separation before detection, with minimal metabolite isolation after sampling. This technique can provide an effective, investigative and quantitative approach for studying biological metabolism in cells, giving the best knowledge of changes to intracellular metabolite concentrations (9,11).

1.1.1.3 Metabolic fingerprinting

Metabolic fingerprinting is defined as a global, rapid, and high-throughput screening approach and is used for sample identification based on metabolite patterns of fingerprint which change to disease, drug, or environmental fluctuations (11–13). Generally, this approach is not used to quantify and identify metabolites. It is only used to discriminate between samples which originate from different biological status (14).

1.1.2 Analytical technologies for metabolomics

A comprehensive, non-biased, high-throughput method for a mixture of complex metabolites derived from a biological system is required in metabolomics (15). There are different kinds of analytical approaches that have been applied to metabolite study, such as nuclear magnetic resonance spectrometry (NMR) and mass spectrometry (MS), coupled with gas chromatography (GC), liquid chromatography (LC), or capillary electrophoresis (CE) (16–18).

1.1.2.1 Mass spectrometry (MS)

The advantages and disadvantages of both NMR and MS technologies have been delineated by Pan et al (19) and Dieterle et al (20). Briefly, NMR spectroscopy is a non-destructive and non-invasive method. Furthermore, it is claimed to be a highly discriminatory and fast approach. It can directly measure biological

samples without many extraction and separation processes. This technique provides complex analysis of a wide range of small hydrophobic and hydrophilic molecules in biological samples through analysis of various spectral window settings. However, the major disadvantage of a NMR approach is its relatively low sensitivity (19,20), which limits the amount of detailed metabolite information obtained from biological samples.

Providing higher sensitivity, MS technologies are constantly expanding in metabolomics studies, especially in targeted analysis, metabolic profiling and metabolic finger-printing. Nowadays, the rapid development of technologies in separation methods, ion sources and mass analysers has provided an ever increasing sensitivity, selectivity, specificity and speed of acquisition and detection (7,21,22). Electrospray ionisation, atmospheric pressure chemical ionisation, atmospheric pressure photoionisation and atmospheric pressure matrix-assisted laser desorption and ionisation has expanded the range of compounds detected. Furthermore, the number of detected compounds can be raised by changing the polarity of the ion source (23).

The type of data acquired with MS is dependent upon the MS technologies. (Triple-) Quadrupole MS frequently provides the best detection limits for targeted profiling. Time-of-flight (ToF) MS platform with orthogonal acceleration and reflection optics provides

higher scan speeds, spectral sensitivity and mass resolution. However, the main limitation of ToF technology has been its relatively narrow dynamic range which covers only one or two orders of magnitude (24) and the lack of high resolution, although these areas have been improved on in recent MS instruments (Orbitrap).

1.1.2.2 Orbitrap-Mass spectrometry (Orbitrap MS)

An Orbitrap MS platform is a relatively new mass analyser technology and has been successfully applied in quantification due to its accuracy, resolution and high dynamic range (25,26). The Orbitrap instrument was originally introduced by Kingdon in 1923 (27) and was modified by Knight in 1981 (28). However, the early Orbitrap was used as a mass detector in 2000 by Makarov (29). Later, the first commercial Orbitrap MS was introduced by Thermo Electron in 2005 (30). Figure 1.2 shows the schematic of Orbitrap mass spectrometer. An Orbitrap consists of a spindle shaped central electrode. This electrode is surrounded by two symmetrical electrodes (25). Ionised ions enter the Orbitrap off axis from the centre rod's equatorial position and are allowed to settle into ring-like orbitrap around the rod. The rings oscillate back and forth over the electrode as a frequency dependent upon the *m/z* of ionised ions. The change of current of the charged rings is recorded by the

split outer electrodes and converted into signal amplitude vs time (25,30).

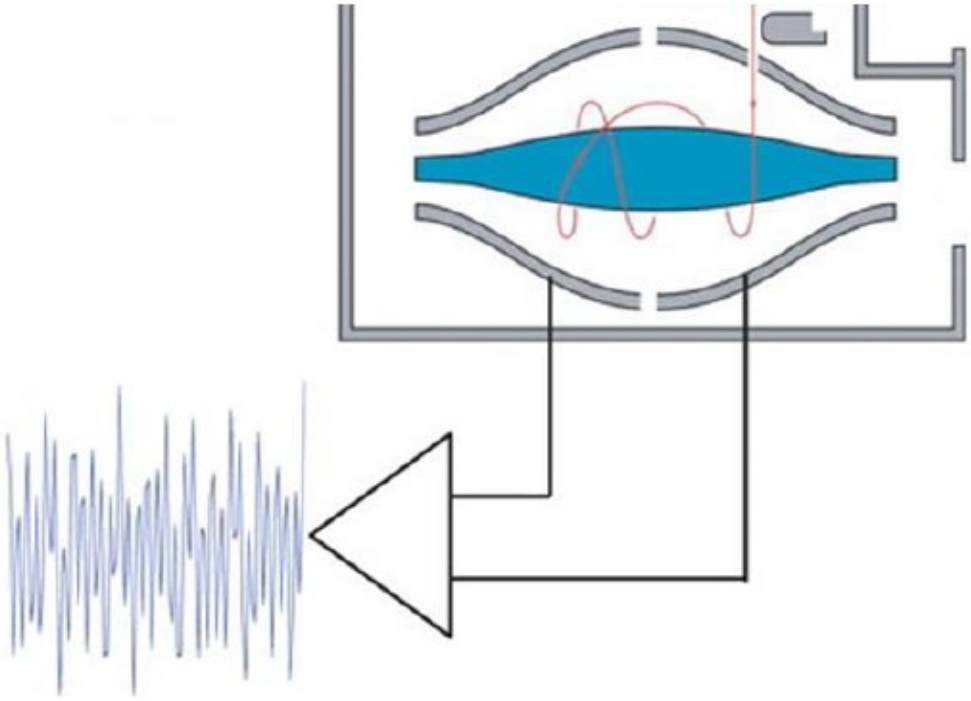


Figure 1.2 Overview of the Orbitap detector detailing the entrance of the ions into the detector, orbitrap about the central electrode, and subsequent current-frequency detected by the systemetric exterior electrodes (25).

1.1.2.3 Liquid chromatography (LC)

Separation is very important in metabolomics studies because it decreases sample complexity and provides further information about characteristics of metabolites that aid in their identification (31–33). Moreover, it allows the detection of low abundance metabolites whose ionisation could be suppressed by more high abundant metabolites (31). Improvements to LC equipment have led to the development of ultra-high performance liquid chromatography (UHPLC). Direct coupling of UHPLC to high resolution mass spectrometry (UHPLC-HRMS) represents the best technique of choice for metabolomics studies due to its capability to allow the detection of thousands of peaks (with unique mass and retention time) from samples (34–36). Normally, nonpolar and polar metabolites are separated and analysed in parallel due to the limitations of analytical column technologies.

A. Reversed phase-liquid chromatography (RP-LC)

In the past, metabolomics studies extensively used RP-LC, which give a good separation of semi- and non-polar metabolites, but which discriminates against polar metabolites since these are often not retained for analysis (37). RP-LC is popularly used because of its reproducible and predictable retention times, wide applicability to various classes of metabolites, and mobile phase compatibility for MS (37–39). Figure 1.3 illustrates a schematic representing the

mechanism in a RP separation However, RP-LC has the major disadvantage in the analysis of polar and/or ionic metabolites, which are typically poorly retained and eluted in the solvent front (38). Polar metabolites include amines, organic acids, amino acids, and others involved in biochemical pathways and influxes (33).This problem can be solved by the used of hydrophilic interaction chromatography.

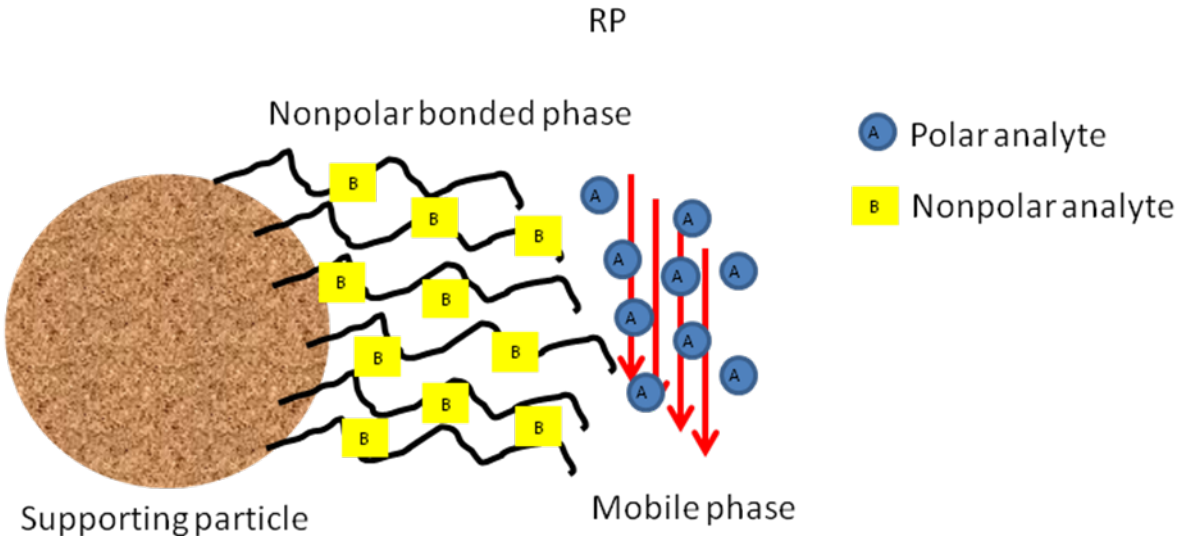


Figure 1.3 A schematic representing the mechanism in a RP separation (modified from (39)).

B. Hydrophilic interaction chromatography (HILIC)

While RP-LC is suitable for non-polar and lipid metabolites, HILIC is good for polar and hydrophilic metabolite analytes. Polar and hydrophilic metabolites with little or no retention on RP-LC could in general have a strong retention on HILIC. In practice, zwitterionic-HILIC (ZIC-HILIC) is popularly used in metabolomics studies. Figure 1.4 illustrates a schematic representing the mechanism in a ZIC-HILIC separation. It shows that the separation is based on a partitioning between the bulk eluent and a water-rich layer, internally not only dipole-dipole force, but also hydrogen bonds as well as ion exchange present (40).

The main advantage of HILIC lies in the application of retaining polar and hydrophilic compounds, particularly in the analysis of small polar and hydrophilic metabolites in metabolomics studies. Often metabolites and intermediate metabolites are hydrophilic, especially small organic acids (40,41). Several applications have been developed using HILIC, in particular for the analysis of polar and hydrophilic metabolites from biological samples (42–47). Tang et al has showed that HILIC coupled MS can enhance the comprehensiveness of polar and hydrophilic metabolite detection and add significant value for metabolomics studies (48). Wernisch et al has also presented a comparison of the chromatographic performance of RP-C18 and HILIC columns and showed that HILIC

was highly effective for the analysis of polar and hydrophilic metabolites (42). Recently, Gunda et al have applied HILIC-MS method for study cellular metabolites and suggested that superior peak shapes and efficiencies of cellular metabolites could be achieved by using HILIC (44).

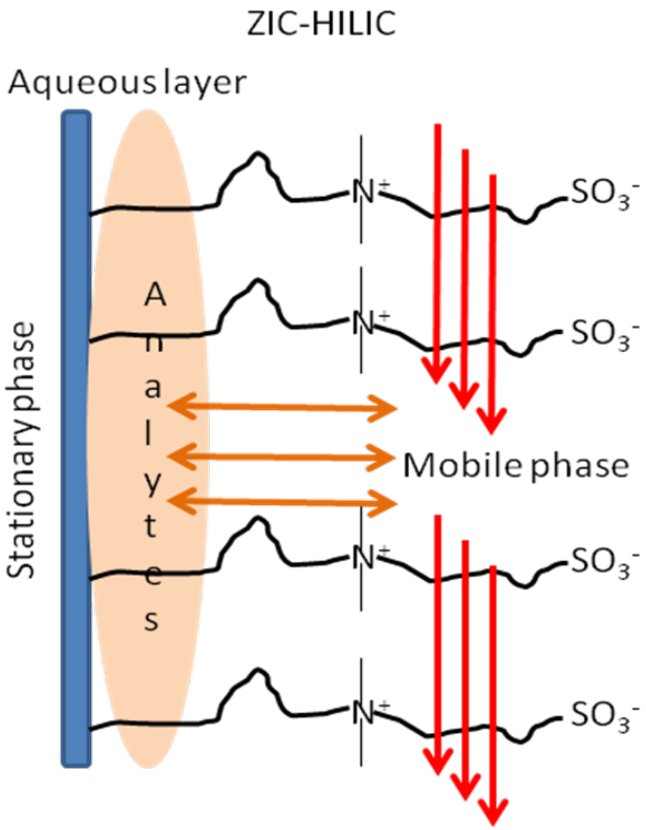


Figure 1.4 A schematic representing the mechanism in a ZIC-HILIC separation (modified from (40)).

1.1.3 Metabolite Identification

One of the important challenges in metabolomics analysis is to identify metabolites. Nowadays, metabolite identification in metabolomics analysis is primarily based on a *m/z* search followed by manual identification (49,50) as shown in Figure 1.5. First, the *m/z* value of the detected metabolite is matched against database(s). The metabolites have *m/z* values within specific tolerance criteria to the query *m/z* and are searched from the databases as accepted metabolites. Second, the MS/MS spectral (if they are available) and retention times of each authentic metabolite of the accepted compounds are compared.

However, putative metabolites from *m/z* verification are rarely unique because of the existence of isomers and the limited accuracy of MS approaches. In some cases, a *m/z* value can have be attributed many chemical identities by *m/z*, which makes the manual identification costly and laborious. Because of this limitation, this method is appropriate to only a limited number of biological metabolites. To enhance the efficiency of metabolite verification for a large number of biological metabolites, standard metabolites can be analysed. This decreases the amount of manual verification required.

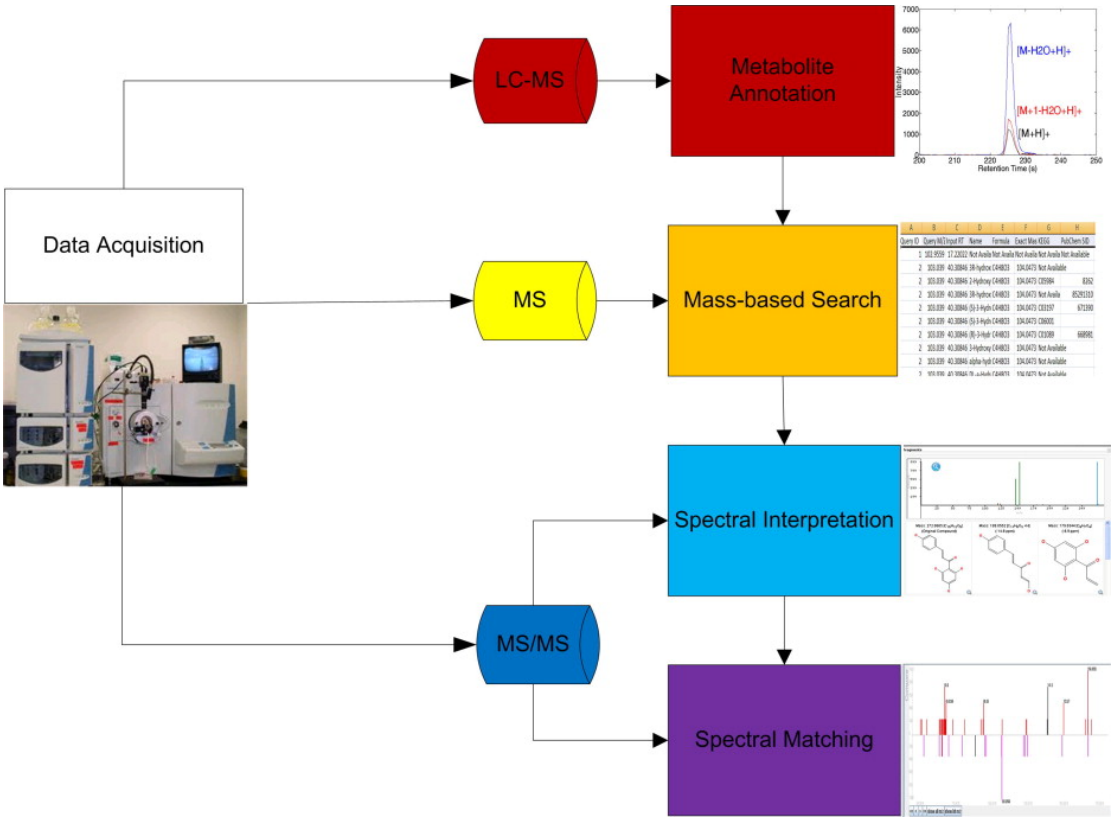


Figure 1.5 Schematic of metabolite identification.

1.1.4 Multivariate data analysis for metabolomics experiments

The complexity of dataset which is obtained from metabolite profiling by LC-MS is three-dimensionally related to the *m/z* ratio, mass ion intensity and retention time of the metabolites. In order to validate the metabolomics studies, it is necessary to optimise the quality of these complex datasets. Different data pre-treatment processes are applied to minimise unexpected analytical and biological variances. This includes the replacement of missing data by studying of particular metabolic levels across all replicates, or taking the mean of the nearest neighbour (51).

The intensity of detected metabolites can differ by several orders of magnitude between samples and metabolites, and may require data transformation to correct relative influences with new weighting. Modification includes log transformation, range transformation, (the minimum and maximum value for the variable set between 0 and 1), z-score-mean centring of the variable divided by its standard deviation, and mean centring. The multidimensional MS dataset is frequently applied by different supervised and unsupervised statistical calculation, such as a decision tree, partial least square-discriminant analysis (PLS-DA), hierarchical cluster analysis (HCA), and principal component analysis (PCA) (52–54).

PCA, an unsupervised, multivariate statistical analysis, is widely applied to minimise the dimensional data while retaining as much information as possible. PCA transforms the set of originally-correlated variables into a new set of few uncorrelated variables. This new set is called principal components (PCs). The greatest amount of variation and the greatest amount of remaining variation are shown in the first and second components, respectively (55,56).

1.2 CELL-BASED METABOLOMICS

1.2.1 Overview

In most recent metabolomic studies, body fluids were widely used in metabolomic studies concerning human biology and health, as these studies had a mainly holistic focus in terms of biological systems. The clinical application of metabolomic, involves the collection of large datasets requiring large numbers of clinical patients or volunteers. These datasets can decipher different endogenous and exogenous metabolites in humans and can lead to the discovery of novel biomarkers and new metabolites (42,49,55). These aspects are based on high anticipations in the development of new diagnostic technologies, risk factor evaluations of diseases and toxic assessment of many compounds (1,57,58). However, for a more holistic understanding of the function and properties of a cell, there is a requirement for appropriate information about specific cell types under a variety of conditions. This is vital for a holistic

understanding and can be accomplished by shifting the focus from the whole organism to cultured cells (59). In this way, cell experiments can complement the results of the whole system and provide insight into the cellular and sub-cellular mechanisms underlying disease and health. In addition, cell culture is highly compatible with metabolomic analysis, as it provides a controlled system for available, direct access and evaluation of tissues. Tissue culture is a valuable tool with which to study problems of clinical relevance, especially those related to disease, screening, and studies of mechanism of cell toxicity (60). The ready access to cells provides the possibility of a straightforward method with which to study cellular mechanisms. This in turn may lead to the discovery of new potential drug targets and, in the case of pathologically-derived tissue, an interesting application for the evaluation of therapeutic agents that could potentially treat the dysfunction.

1.2.2 Definition of cell-based metabolomics

Cell-based metabolomics using LC-MS systemises the study of the uniqueness of small-molecule metabolite (metabolomes) profiles in cellular processes. While transcriptomics and proteomics address the altered phenotype of a cell, metabolomics can provide rapid read out about the physiology and biochemistry of an altered cell (60). Cell-based metabolomics can potentially be used in many applications for the study of biological perturbation from stimulants in cellular pathways. In addition, it had been shown that toxic effects applied to mammalian cell cultures can occur at concentrations equivalent to the doses in which in vivo effects are studied (61). Figure 1.6 shows an increasing number of cell-based metabolomics applications.

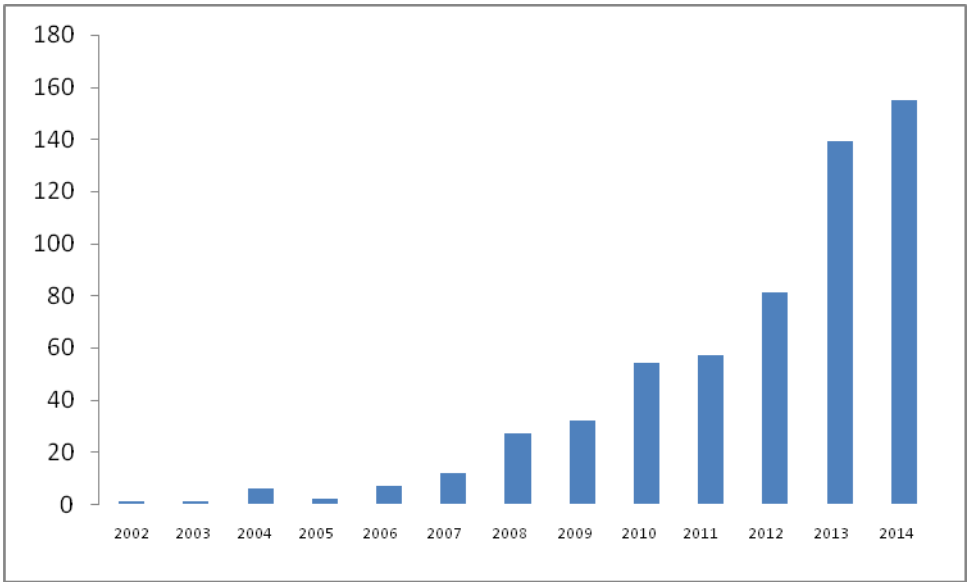


Figure 1.6 The general trend in the publication of cell-based metabolomics applications to study the effects and toxicology of drugs among 2002 to 2014 from the PubMed database, searching with the keywords "cells + metabolomics + drug effects".

1.2.3 Advantages and disadvantages of cell-based metabolomics

The advantages of cell-based metabolomics include ease of control and interpretation when compared to the study of human subjects and animal models. Furthermore, this method can decrease some highly challenging problems that occur in other metabolomics applications. For example, in metabolomics applications of human study, problems include individual variations across different subjects and different time points, difficulty in population control, and different confounding parameters (age, gender, health, etc) (61). Such problems do not arise in cell culture applications, where experimental and biological variation is kept under tight control and a smaller number of replicate experiments are needed to generate statistically valid results

In addition, cell culture study does not require ethics considerations in human studies and animal experiments, and using a specific type of cell can decrease variability and produce a more consistent background which becomes apparent in an experiment (60). Metabolites analysis in cell culture experiments can be directly correlated with other 'omics' sciences (preteomics, genomics, and transcriptomics) (61). Moreover, metabolomics data can be used for the investigation and identification of biochemical pathways, and can greatly help other cell culture analyses in the evaluation of different results. .

Although the cell-based metabolomics provides many benefits over other metabolomics applications, this approach has been impeded by several problems. Some of the main problems include the quenching processes, the variability of cell culture medium formulation and supplements, addition of chemical compounds or solvents during metabolite extraction procedures, time consuming metabolite extraction steps, and difficulties in obtaining sufficiently large numbers of cultured cells for analysis (60,61). In addition, some of the common problems, which are found in metabolomics studies, are also important in cell culture analysis. These include an inability to measure, quantify, and identify all metabolites and the problem with reproducibility and validity of data analysis. Many of these problems can be addressed by using appropriate study design and the application of appropriate analytical instruments and methodologies (44).

Nowadays, cell culture in metabolomics studies are used in many applications as shown in Figure 1.7. These include cell culture and bioreactor optimisation, phenotype classification, stimulant testing effect, target and toxicity analysis, metabolic networks determination and modelling, and biomarker and drug target discovery (34,44,47,57,58,60,61).

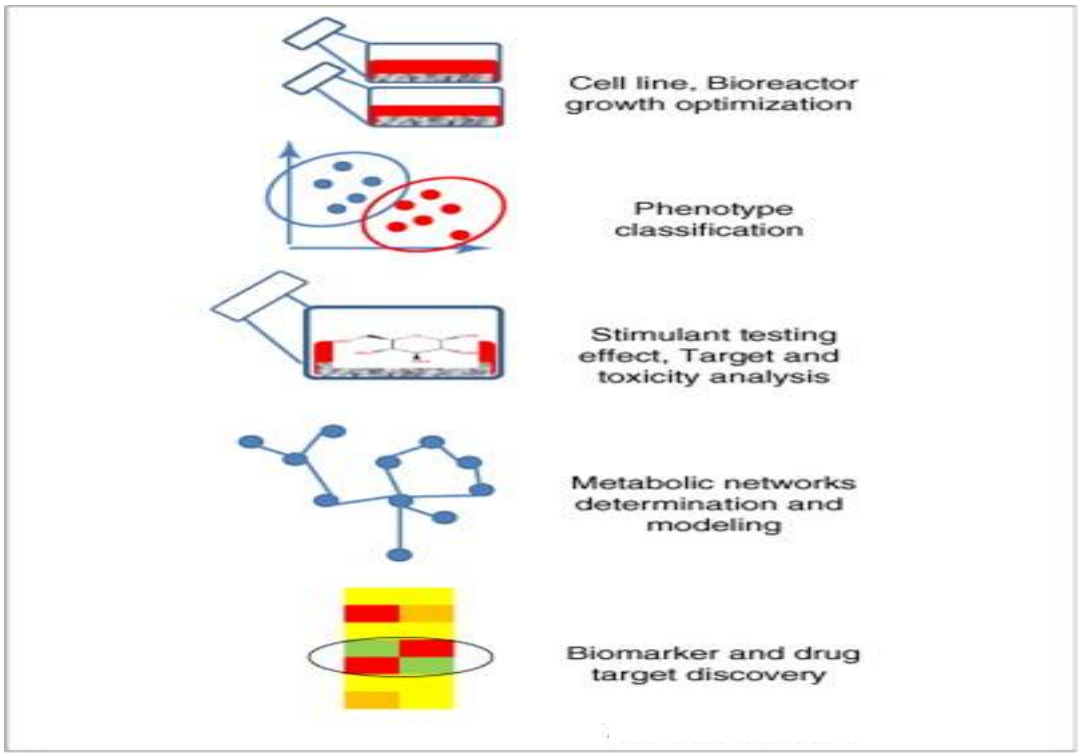


Figure 1.7 Examples of cell culture applications in metabolomics studies (41).

1.3 BACKGROUND TO THE MAIN AREAS OF EXPERIMENTAL INVESTIGATION IN THE THESIS

Both new drugs and old drugs can be approved by the Food and Drug Administration (FDA) if the chemicals can demonstrate therapeutic efficacy and an absence of serious adverse effects by a series of rigorous preclinical tests and clinical trials (62). Toxicology assessments are routinely used in preclinical animal studies to evaluate the harmful effects of a potential new drug candidate and its major drug metabolites (63,64). Despite the rigorous testing of new drug candidates in the screening and preclinical developmental phases, there are still some drugs that demonstrate toxic side effects in the clinical testing phase and/or post-market (62). The failure of a drug candidate as a result of safety concerns at the end stages of testing or its withdrawal from the market after approval, is a public safety concern and results in an enormous lost to the pharmaceutical company in terms of both time spent in development (65) (an average of 8-10 years from drug development to ultimate approval by US FDA (62)) and overall cost (the estimated cost of developing a new drug candidate being over 1 billion dollars in 2006 (66)). In response to this costly and timely attrition, many pharmaceutical companies have now increased their used of cell-based screening assays to identify potential hazards and take steps to design out or significantly reduce undesirable properties at an earlier stage, with the ultimate aim of enhancing

the probability of success in non-clinical and clinical drug development. There are many project that have successfully applied cell-based metabolomics for the study of pharmacoactivity and toxicity in many mammalian cell types (67,68),

1.3.1 Antipsychotics and the blood brain barrier

Psychotic disorders are severe mental illnesses that cause problems with thinking and perceptions. The main symptoms of people with psychoses are delusions (false beliefs) and hallucinations (false perceptions). One important aspect of psychotic disorders is schizophrenia; a debilitating problem of the central nervous system (CNS). The symptoms of individuals suffering from schizophrenia are hallucinations, delusions, conceptual disorganisation, social withdrawal and poor speech. Psychotic disorder treatments depend on the cause of the CNS disorder. One of the major treatments is to use drugs to control symptoms. Antipsychotic medications have been divided into two classes: typical (first generation) and atypical (second generation) (69–71).

1.3.1.1 Typical antipsychotic (AP) drugs (First generation)

The typical antipsychotics drugs have been used to treat psychotic disorders for more than six decades (72). Chlorpromazine (CPZ) and Haloperidol (HAL) are the standard antipsychotic agents in this class. CPZ and HAL are highly effective in treating schizophrenia,

but they cause severe extrapyramidal side effects including dystonia, parkinsonian-like syndrome, and tardive dyskinesia. These side effects interfere significantly with the social and occupational functioning of patients (69–71).

A. Chlorpromazine (CPZ)

CPZ is a typical potent antipsychotic drug which was first used clinically in 1951. This drug has been used to treat psychotic disorders and its pharmacology and side effects have been extensively reported (73). Chemically, CPZ belongs to the phenothiazine series of antipsychotic compounds. The structure is shown below:

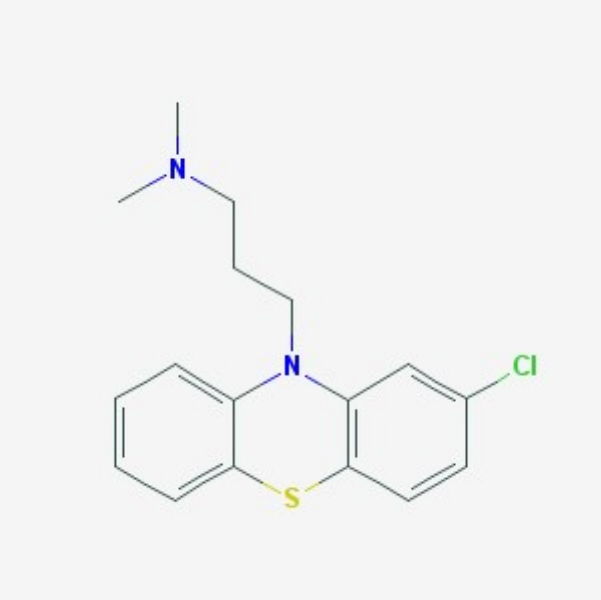


Figure 1.8 Chemical structure of chlorpromazine (3-(2-chlorophenothiazin-10-yl)-N,N-dimethylpropan-1-amine).

CPZ is a tertiary amine that tends to form an interface between water and lipid at a low concentration in the order of 10^{-2} M. It has been shown that CPZ tends to impair the permeability of cell membranes in a variety of mammalian cells, and it exerts this effect from minute to high concentration. In other words, this drug acts like a potent cell membrane permeability disruptor. CPZ is a dopamine antagonist and its major site of action is the dopamine D_2 receptors. The main metabolites of CPZ are CPZ N-oxide, CPZ sulfoxide and hydroxyl CPZ (73).

B. Haloperidol (HAL)

HAL is a typical potent antipsychotic drug which was first used clinically in 1960. This drug has been used to treat and manage the manifestations of acute and chronic psychotic disorders including schizophrenia, manic state, and drug-induced psychoses, such as steroid psychosis. Its pharmacology and side effects have been extensively reported (74,75). Chemically, HAL belongs to the butyrophenone series of antipsychotic compounds. The structure is shown below:

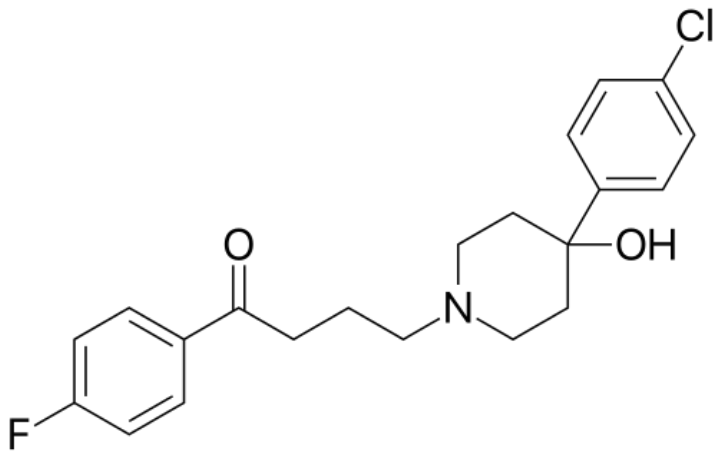


Figure 1.9 Chemical structure of haloperidol (4-[4-(4-chlorophenyl)-4-hydroxypiperidin-1-yl]-1-(4-fluorophenyl) butan-1-one)

HAL is a tertiary amine that tends to form an interface between water and lipid at very low levels in the order of 10^{-7} M. It has been shown that HAL tends to impair the permeability of cell membranes in a variety of mammalian cells, and that it exerts this effect from low to high concentration. That is, this drug acts like potent cell membrane permeability disruptor in the same way as CPZ. HAL is a dopamine antagonist and its major site of action is the dopamine D_2 receptors. The main metabolites of HAL are reduced haloperidol, hydroxyl HAL and 4-(4-chlorophenyl)-4-hydroxypiperidine (76).

1.3.1.2 Atypical antipsychotic medications

Because of CNS side effects caused by typical antipsychotics drugs, the so-called atypical AP drugs have been developed. They appear to have comparable clinical efficiency to the typical antipsychotics agents, but with minimal or no extrapyrimidal side effects. The first atypical AP medication that was used clinically to treat psychotic disorders was clozapine (CLZ). CLZ is used with caution and in restricted manner due to its severe side effect: potentially fatal agranulocytosis. The other drug is risperidone (RIS) which has been developed and used clinically without the risk agranulocytosis, but with potency equal to CLZ (77).

A. Clozapine (CLZ)

CLZ was first introduced in 1989 and has been used to treat schizophrenia. CLZ is a selective monoaminergic antagonist with high affinity for serotonin and histaminergic receptors. Unlike typical AP agents, it weakly blocks D_2 receptors (78). CLZ is a tricyclic dibenzodiazepine analog with the chemical name of 3-chloro-6-(4-methylpiperazin-1-yl)-5H-benzo[b] [1,4] benzodiazepine. Its structure is shown below.

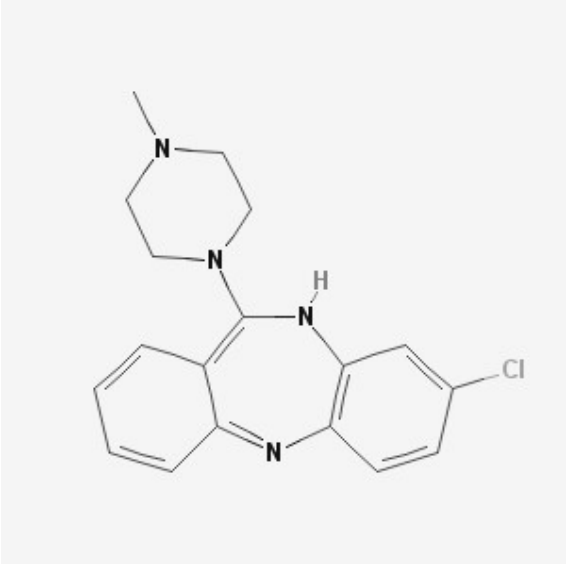


Figure 1.10 Chemical structure of clozapine (3-chloro-6-(4-methylpiperazin-1-yl)-5H-benzo[b][1,4]benzodiazepine)

CLZ is metabolised to N-oxide CLZ and N-desmethyl CLZ, which have less pharmacological activity than the parent drug (79).

B. Risperidone (RIS)

RIS was approved for clinical uses in 1989 and has been used to treat delusional psychosis (including schizophrenia), but it is also used to treat some forms of bipolar disorder and psychotic depression. RIS selectively antagonises serotonin effects and, to a lesser extent, competes with the D_2 receptor (80). RIS is a benzisoxazole derivative with the chemical name of 3-[2-[4-(6-fluoro-1,2-benzoxazol-3-yl)piperidin-1-yl]ethyl]-2-methyl-6,7,8,9-

tetrahydropyrido[1,2-a]pyrimidin-4-one. Its structure is given below.

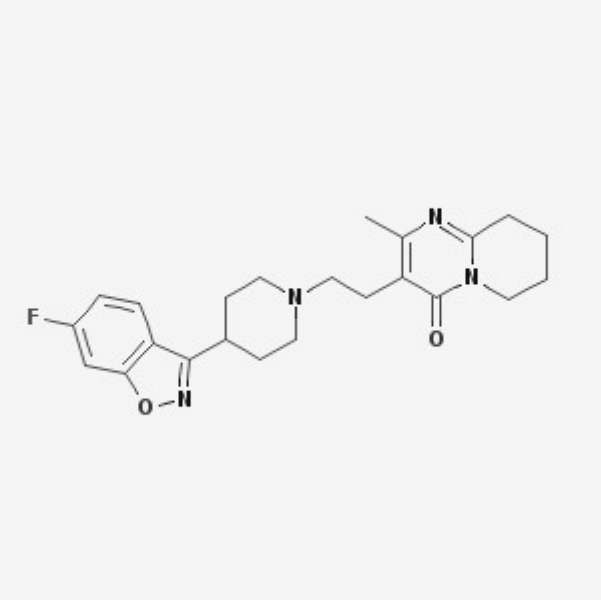


Figure 1.11 Chemical structure of risperidone (3-[2-[4-(6-fluoro-1,2-benzoxazol-3-yl)piperidin-1-yl]ethyl]-2-methyl-6,7,8,9-tetrahydropyrido[1,2-a]pyrimidin-4-one)

RIS is mainly metabolised by the liver and its main metabolic pathway is through hydroxylation of RIS to 9-hydroxyRIS. The 9-hydroxy-RIS metabolite has similar pharmacological activity to the parent drug (81).

1.3.1.3 Overdose problems of antipsychotics

One of the most two common problems of antipsychotics in clinical treatment is overdose. This problem is a common cause of out-of-hospital death and hospital admission due to poisoning in many countries (82,83). For examples, in the USA there were about 6.1 % of death due to AP overdose problems in 2010 (84) and 128 patients died from this problem in the UK in 2014 (85). One of the overdose side effects is extra pyramidal syndrome; this could result from a greater amount of APs passing to the CNS than would from a normal dose. This suggests that APs at overdose levels can affect the BBB functionalities and/or viabilities (86,87). The BBB is the primary interface of the brain, controlling the transport of neurotoxins, physiological metabolites, peripheral neurotransmitters, and xenobiotics into and out of the brain (88,89). Both typical and typical APs have been reported to impair BBB function and induce an apoptotic process in BBB cells (86,87).

1.3.1.4 Blood brain barrier relevance

The blood brain barrier (BBB) is a complex vascular structure that physically and physiologically separates the peripheral blood circulation from the central nervous system (CNS). The BBB acts very effectively to maintain brain homeostasis, regulate influx and efflux transport of nutrients, and protect the CNS from pathogen and toxins (88). The basic anatomy of the BBB consists of brain microvascular endothelial cells (HMVECs), pericytes, astrocyte foot processes and nerve endings. Although, these four structures contribute to the function of the microvasculatures of the brain, the permeability of the BBB is controlled only by the HMVECs. The other components do not contribute to any significant permeability-related exchange between blood and brain interstitial fluid. Once the HMVECs layer has been disrupted, the CNS will be directly exposed to the hazardous solutes, pathogens and toxins (89). Marchi et al. have shown that disruption of the BBB with mannitol increases the BBB permeability to intravascular substances resulting in epileptic seizures in rats (90). Furthermore, inflammation of the BBB caused by bacteria, viruses and other microorganisms breaks down the BBB and allows neurotoxins to enter the brain. This could lead to inflammation of the meninges (91). Moreover, BBB disruption plays a vital part in acute and chronic cerebral ischemia, brain trauma, multiple sclerosis, brain tumours, and brain infections (90). Recently, it has been reported that some antipsychotics such as

CPZ, HAL, RIS and CLZ can impair barrier functionality of the BBB and induce BBB cell apoptosis (86,87). At high dosage the APs break down and could induce cytotoxicity in HMVECs. These phenomena may also relate to antipsychotics-associated cerebral oedema.

1.3.1.5 Antipsychotics and the blood brain barrier system

The extent to which APs can affect the function of HMVECs, especially at high therapeutic dosage, is still not clearly understood. One hypothesis is that high doses of APs will increase the transport of APs into the CNS and cause side effects. Ben-Shachar et al. (92) and Pardridge et al. (93) suggested that APs, within the high therapeutic dosage range, induce gross permeability changes in the BBB allowing passage of $FeCl_3$, mannitol and inulin. These studies may indicate that APs at high dose can interfere with the barrier functionality and/or viability of the BBB. To date, the whole mechanism of how a high dosage of APs affects HMVEC function is not entirely clear; one important mechanism of APs could be the induction of phospholipidosis and cell apoptosis (86,87).

Phospholipidosis is characterised by intracellular accumulation of phospholipids that most likely result from impaired phospholipid metabolism of the lysosome. Lysosomes contain lysosomal phospholipase that play a critical role in the degradation of cellular

membranes (94). It has been reported that many amphiphilic drugs such as antidepressants, antibiotics and APs, can induce phospholipidosis in cells, organs and tissues (95–97). However, the relationship between APs and phospholipidosis in the BBB remains elusive.

Moreover, cell apoptosis results in the condensation of chromatin, and DNA fragmentation. Cell apoptosis is clearly marked by cell membrane disintegration in the early stages. The major component is phosphatidylserine (PS) translocated from the inner membrane to the outer membrane resulting in cell shrinking (98). AP drugs have been known to induce cell death in various mammalian cells. The cytotoxic effects of APs on BBB cells however are not yet clearly understood.

To understand how antipsychotics can affect the BBB, our study investigates the effect of four APs (CPZ, HAL, CLZ and RIS) at concentrations typical of high therapeutic dosage, on HMVECs from the BBB. For our investigation we decided to use cell-based metabolomics using a LC-MS approach to study the effects of antipsychotics.

1.3.2 Breast cancer and cordycepin

1.3.2.1 Breast cancer cells

Breast cancer develops in the cells of the breast and is hormone related. It is the most commonly diagnosed cancer and the second leading cause of cancer death in women worldwide. In 2015, there were approximately 231,840 new cases of breast cancer and 40,290 breast cancer deaths in the United States (99). The increase occurrence of this cancer could result from physical factors (such as UV radiation, pollution, and chemical exposure) and human behaviours (such as obesity, starvation, drinking and smoking) (100).

Nowadays, the advance of breast cancer treatments brings new hope and excitement to save patients' live. Instead of just one or two, various treatment approaches are now available for breast cancer. In addition, a choice of methods, based on individual factors such as age, condition of patient and stage of breast cancer, is possible (101). Breast cancer treatment can be divided into two options: local treatment and systemic treatment (102). Local treatment specifically targets the breast cancer tissue and has no effect on the rest of the body. Surgical removal and radiation therapy are commonly used in this type of treatment. Systemic therapy is the method that uses drugs, hormones, enzymes and antibodies to treat breast cancer.

1.3.2.2 Problems with breast cancer treatments

Nowadays, the available breast cancer treatments cause serious side effects and have limited effective options as mentioned above; thus, the discovery of novel, targeted and more effective therapy options is necessary. Natural products represent an abundance of source-derived remedies to discover novel pharmacologically active compounds for the treatment of breast cancer. One of important natural compound with potential anti-cancer effects is cordycepin, extracted from the insect fungus *Cordyceps spp.*

1.3.2.3 Cordycepin

Cordycepin or 3'-deoxyadenosine, is derivative of the nucleoside adenosine (shown in Figure 1.12). It was initially isolated from the *Cordyceps* species. The cordyceps species is a parasitic fungus and has been used as the active component of Chinese traditional medicine for many centuries. It is known to be, for the most past, very safe (103). Cordycepin has been proposed to have many biological activities: inhibition of cell proliferation, the induction of apoptosis, the inhibition of platelet aggregation, the inhibition of cell migration and invasiveness, inhibition of inflammation, and as an antifungal agent (104–111). Over the past decade, studies have focused on the effect of cordycepin on breast cancer cells with a view to its application in breast cancer treatment. Such studies have shown the efficacy of cordycepin in the inhibition of breast cancer cells (112). However, cordycepin is currently not medically used

because its pharmacology and toxicology are still not clearly understood.

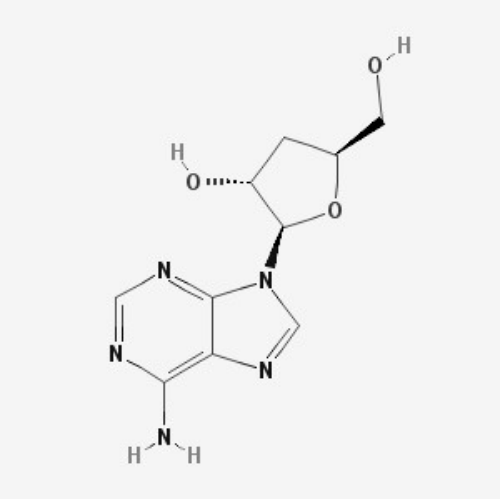


Figure 1.12 Chemical structure of cordycepin (3'-deoxyadenosine).

Cordycepin is known to interfere with a number of biochemical and molecular processes in many cancer cells. Recent research, however, has studied the possible anti-breast cancer ability of cordycepin. Investigations have been done with the breast cancer cell lines, MDA-MB-231, MDA-MB-453 and MCF-7 (104,112,113). Reports from these investigations have shown significant reductions in cancer cell proliferation.

Lu et al performed an in vitro study into the effect of cordycepin in breast cancer cell lines (MCF-7) and found that cordycepin suppresses MCF-7 proliferation (114). Thomadaki et al. investigated

the anti-cancer effect of cordycepin against MCF-7 cell lines, in which cordycepin showed cytotoxicity against MCF-7 cells. Thomadaki et al indicated that cordycepin affects the polyadenylate polymerase (PAP) pathway (115). Noh et al. also demonstrated that cordycepin inhibits MCF-7 cell growth by suppressing the MAPK/AP-1 pathway (116). Choi et al. reported that cordycepin induces apoptosis and autophagy in MDA-MB-231 and MCF-7 cell lines (104) and Lee et al. showed that cordycepin also causes DNA double strand breaks in MDA-MB-231, MDA-MB-453 and MCF-7 cells (113).

Although cordycepin has shown that it effectively kills MCF7 human breast cancer cell lines in vitro, the clinical application of cordycepin in breast cancer treatment still remains elusive. It is essential to gain an understanding of the exact biological effects of cordycepin. Moreover, one of the limitations of cordycepin as an anti-breast cancer drug is its stability.

Because cordycepin is an analogue of the nucleoside adenosine, it can be hydrolysed by adenosine deaminase (ADA). ADA is an enzyme that can be found in any mammalian cell and metabolised adenosine and its analogues yield inosine (117). Frederiksen et al. showed that the metabolite of cordycepin is 3’-deoxyinosine (118) and Cristalli et al. confirmed that cordycepin is metabolised by ADA to 3’-deoxyinosine (117). Once cordycepin has been metabolised by ADA, it has no anti-cancer activity. To extend the anti-cancer

activity of cordycepin, an ADA inhibitor is used. A variety of potential ADA inhibitors have been investigated to be used in synergy with cordycepin.

1.3.2.4 Role of pentostatin as a potentiator of cordycepin activity

Pentostatin, 2'-deoxycoformycin, is a purine nucleoside analogue (as shown in Figure 1.13) and a potent ADA inhibitor. It has been shown to possess activity in chronic lymphocytic leukaemia, prolymphocytic leukaemia, cutaneous T-cell lymphomas, adult T-cell lymphoma-leukemia, and low grade non-Hodgkin's lymphomas. The unique property pentostatin possesses is its significant ability to inhibit ADA; however, one problem with using pentostatin as an ADA inhibitor is that it can cause persistent immunosuppression. In addition, Rodman et al. found that pentostatin administered to dogs caused lymphopenia and thymus lymphoid depletion, thrombocytopenia, and a decrease in food consumption, but giving cordycepin alone did not cause these related toxicities. Moreover, severe gastrointestinal toxicity and bone marrow toxicity were detected in dogs given the combination of cordycepin and pentostatin (119). The efficacy of cordycepin in combination with pentostatin may still be limited in clinical applications; however, the administration of cordycepin and pentostatin could be effective in breast cancer treatment.

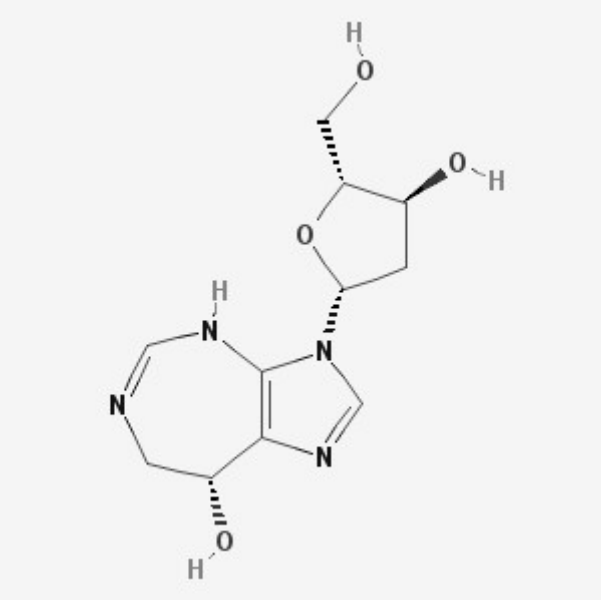


Figure 1.13 Chemical structure of pentostatin.

1.3.2.5 Utility of cordycepin and pentostatin combinations in cell-based studies

Although cordycepin has shown that it effectively kills MCF-7 human breast cancer cell lines and others in vitro by inducing cell death in association with the oestrogen receptor, inhibiting RNA synthesis and inducing DNA double strand breaks (104,113,116), there is still a lack of thorough insight into its anti-breast cancer effect from a

global perspective. Moreover, the efficacy of cordycepin in combination with pentostatin (ADA inhibitor) in breast cancer treatment has not been studied in terms of metabolome changes. This limitation inspired us to study how cordycepin and cordycepin in combination with pentostatin can affect metabolomes of MCF-7 cell lines by using a LC-MS cell-based metabolomics. The results could explain the biological effects of these drugs and may be used to predict the toxicology of cordycepin and pentostatin in breast cancer treatment.

1.3.3 Fluoxetine and pancreatic beta cells

1.3.3.1 Fluoxetine

Fluoxetine is a selective serotonin reuptake inhibitor antidepressant. It affects chemicals in the central nervous system by blocking only the serotonin transporter. Fluoxetine is used for the treatment of major depressive disorder, bulimia nervosa, obsessive-compulsive disorder, panic disorder, and premenstrual dysphoria (120).

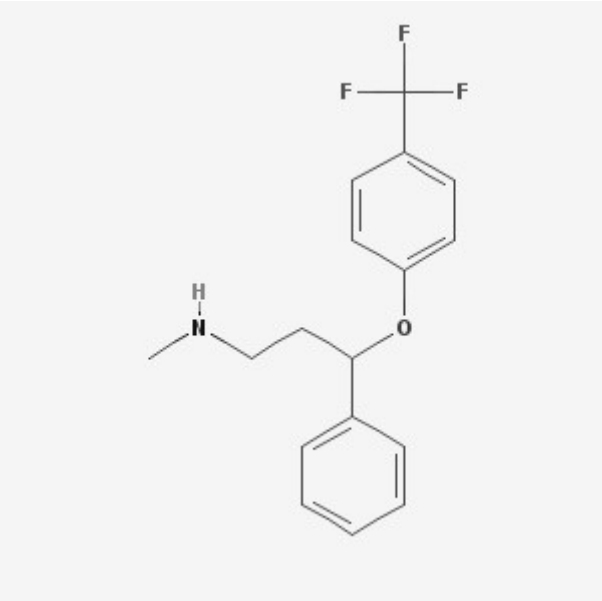


Figure 1.14 Chemical structure of fluoxetine.

1.3.3.2 Problems associated with fluoxetine

In the last decade, reports have indicated that the use of fluoxetine is associated with an increased risk of pancreatic beta cell dysfunction. This could result in weight gain and obesity, leading to an increased incidence of hypertension, dyslipidaemia, coronary artery disease, insulin resistance and overt diabetes (121–126). However, little is known about the effects of fluoxetine as an impairing agent of beta cell function. Impairment of beta cell function causes a pathological state in which it cannot maintain glucose homeostasis due to impaired insulin secretion and insulin resistance. Impaired beta cell function by fluoxetine may increase reactive oxygen species and oxidative damage. This may result in

decreased mitochondrial electron transport chain enzyme (ETC) activity (124). Therefore, in order to understand the effects of fluoxetine toxicity in beta cells, it is important to investigate the cellular responses associated with this drug.

1.3.3.3 Pancreatic beta cells

Beta cells are an important cell component in the pancreatic islets Langerhans of pancreatic islet. Its function is the secretion of insulin in response to elevated blood glucose through glucose stimulated insulin secretion. Insulin is a peptide hormone that sends signals to the liver, muscle and adipose tissue to absorb glucose from the blood and store it in the form of glycogen for later use. Dysfunction of beta cells results in a failure to adequately regulate insulin levels and consequently blood glucose, causing diabetes (127,128).

1.3.3.4 Investigation of beta cell function using fluoxetine as a probe

Fluoxetine has shown that it can impair beta cell function causing a pathological state in which its function cannot maintain glucose homeostasis due to impaired insulin secretion and insulin resistance. Impairment of beta cell function by fluoxetine may increase reactive oxygen species and oxidative damage. This may result in decreased mitochondrial electron transport chain enzyme (ETC) activity. Therefore, in order to understand the effects of

fluoxetine toxicity in beta cells, it is important to investigate the cellular responses associated with this drug.

These limitations inspired us to study how fluoxetine can affect metabolomes of MIN6 cell lines by using cell-based metabolomics using a LC-MS approach. The results obtained could explain the biological effects of these drugs and may be used to predict the toxicology of fluoxetine in clinical treatment.

1.4 AIMS OF THE THESIS

- To develop, optimise and validate a HILIC-MS approach for comprehensive metabolic profiling well suited to the untargeted analysis of polar metabolites in mammalian cells (Chapter III).
- To investigate the level and compositional changes in intracellular components of human microvascular endothelial cells from blood brain barrier upon exposure to a high concentration of four antipsychotics (chlopromazine, haloperidol, clozapine and risperidone) with cell-based metabolomics using HILIC MS (Chapter IV).
- To investigate the level and compositional changes in intracellular components of MCF-7 cells from upon treated with cordycepin with and without pentostatin with cell-based metabolomics using HILIC-MS (Chapter V).
- To investigate the level and compositional changes in intracellular components of murine pancreatic beta cells from upon treated with fluoxetine with cell-based metabolomics using HILIC-MS (Chapter VI).

CHAPTER II: MATERIALS AND METHODS

2.1 CHEMICALS

Chemicals used in the study can be summarised in Table 2.1. A stock solution of each authentic standard was prepared at 100 mM, 10 mM, 1 mM and 0.1 mM, separately in water or ethanol and stored at -80 ^{o}C. The standard mixtures were divided into 3 groups as summarised in Supplementary Tables 2.1 to 2.3. The final concentration of each standard metabolite was 100 μM. Working solutions containing analytes were prepared in acetonitrile by diluting 10 times to obtain a final concentration of 10 μM of each standard metabolite. The working solution was stored at -80 ^{o}C and brought up to room temperature before analysis.

Table 2.1 Chemical lists were used in the study.

Chemical	Grade	Supplier
(R)-2-Hydroxyglutarate	Analytical	Sigma-Aldrich (Poole, UK)
(R)-3-Hydroxybutanoate	Analytical	Sigma-Aldrich (Poole, UK)
(R)-Lactate	Analytical	Sigma-Aldrich (Poole, UK)
(S)-Malate	Analytical	Sigma-Aldrich (Poole, UK)
1,3-Diaminopropane	Analytical	Sigma-Aldrich (Poole, UK)
1-Aminocyclopropane-1-carboxylate	Analytical	Sigma-Aldrich (Poole, UK)
1-Aminopropan-2-ol	Analytical	Sigma-Aldrich (Poole, UK)
1-Butanol	Analytical	Sigma-Aldrich (Poole, UK)
1-Naphthylacetic acid	Analytical	Sigma-Aldrich (Poole, UK)
2,3-Bisphospho-D-glycerate	Analytical	Sigma-Aldrich (Poole, UK)
2-Aminobutan-4-olide	Analytical	Sigma-Aldrich (Poole, UK)
2-Deoxy-D-glucose	Analytical	Sigma-Aldrich (Poole, UK)
2-Hydroxyethyldisulfide	Analytical	Sigma-Aldrich (Poole, UK)
2-Methylcitrate	Analytical	Sigma-Aldrich (Poole, UK)
2-Oxobutanoate	Analytical	Sigma-Aldrich (Poole, UK)
2-Oxoglutarate	Analytical	Sigma-Aldrich (Poole, UK)
2-Phenylglycine	Analytical	Sigma-Aldrich (Poole, UK)
2-Phospho-D-glycerate	Analytical	Sigma-Aldrich (Poole, UK)
3-(4-Hydroxyphenyl)pyruvate	Analytical	Sigma-Aldrich (Poole, UK)
3-4-Dihydroxyphenylacetate	Analytical	Sigma-Aldrich (Poole, UK)
3'-5'-Cyclic AMP	Analytical	Sigma-Aldrich (Poole, UK)
3-Hydroxyphenylacetate	Analytical	Sigma-Aldrich (Poole, UK)
3-Phospho-D-glycerate	Analytical	Sigma-Aldrich (Poole, UK)
4-(beta-Acetylaminoethyl)imidazole	Analytical	Sigma-Aldrich (Poole, UK)
4-Aminobenzoate	Analytical	Sigma-Aldrich (Poole, UK)
4-Aminobutanoate	Analytical	Sigma-Aldrich (Poole, UK)
4-Coumarate	Analytical	Sigma-Aldrich (Poole, UK)
4-Trimethylammoniobutanoate	Analytical	Sigma-Aldrich (Poole, UK)
5-Aminolevulinate	Analytical	Sigma-Aldrich (Poole, UK)
5-Methoxytryptamine	Analytical	Sigma-Aldrich (Poole, UK)
5'-Methylthioadenosine	Analytical	Sigma-Aldrich (Poole, UK)
5-Oxoproline	Analytical	Sigma-Aldrich (Poole, UK)
6-Methylaminopurine	Analytical	Sigma-Aldrich (Poole, UK)
6-Phospho-D-gluconate	Analytical	Sigma-Aldrich (Poole, UK)
Acetoacetate	Analytical	Sigma-Aldrich (Poole, UK)
Acetonitrile	LC-MS	Acros Organics (Geel, Belgium)
Acetylcholine	Analytical	Sigma-Aldrich (Poole, UK)
Acetyl-CoA	Analytical	Sigma-Aldrich (Poole, UK)
Acetylcysteine	Analytical	Sigma-Aldrich (Poole, UK)
Adenine	Analytical	Sigma-Aldrich (Poole, UK)

Table 2.1 (Cont.) Chemical lists were used in the study.

Chemical	Grade	Supplier
Adenosine	Analytical	Sigma-Aldrich (Poole, UK)
Adenosine 2',5'-bisphosphate	Analytical	Sigma-Aldrich (Poole, UK)
ADP	Analytical	Sigma-Aldrich (Poole, UK)
Agmatine	Analytical	Sigma-Aldrich (Poole, UK)
Alanyl-Glycine	Analytical	Sigma-Aldrich (Poole, UK)
Allantoin	Analytical	Sigma-Aldrich (Poole, UK)
Ammonium carbonate	Analytical	Sigma-Aldrich (Poole, UK)
Ammonium acetate	LC-MS	Sigma-Aldrich (Poole, UK)
AMP	Analytical	Sigma-Aldrich (Poole, UK)
Antimycin A	Analytical	Sigma-Aldrich (Poole, UK)
Ascorbate	Analytical	Sigma-Aldrich (Poole, UK)
ATP	Analytical	Sigma-Aldrich (Poole, UK)
Benzoate	Analytical	Sigma-Aldrich (Poole, UK)
beta-Alanine	Analytical	Sigma-Aldrich (Poole, UK)
Betaine	Analytical	Sigma-Aldrich (Poole, UK)
Biopterin	Analytical	Sigma-Aldrich (Poole, UK)
Biotin	Analytical	Sigma-Aldrich (Poole, UK)
Bis-gamma-Glutamylcystine	Analytical	Sigma-Aldrich (Poole, UK)
Cholesterol	Analytical	Sigma-Aldrich (Poole, UK)
Choline	Analytical	Sigma-Aldrich (Poole, UK)
Choline phosphate	Analytical	Sigma-Aldrich (Poole, UK)
Chorpromazine	Analytical	Sigma-Aldrich (Poole, UK)
cis-Aconitate	Analytical	Sigma-Aldrich (Poole, UK)
Citrate	Analytical	Sigma-Aldrich (Poole, UK)
Clozapine	Analytical	Abcam (Cambridge, MA, USA)
CMP	Analytical	Sigma-Aldrich (Poole, UK)
CoA	Analytical	Sigma-Aldrich (Poole, UK)
Cordycepin	Analytical	Sigma-Aldrich (Poole, UK)
Creatinine	Analytical	Sigma-Aldrich (Poole, UK)
CTP	Analytical	Sigma-Aldrich (Poole, UK)
Cytidine	Analytical	Sigma-Aldrich (Poole, UK)
Cytosine	Analytical	Sigma-Aldrich (Poole, UK)
dAMP	Analytical	Sigma-Aldrich (Poole, UK)
D-Arabinose	Analytical	Sigma-Aldrich (Poole, UK)
dCMP	Analytical	Sigma-Aldrich (Poole, UK)
Deoxyadenosine	Analytical	Sigma-Aldrich (Poole, UK)
Deoxyribose	Analytical	Sigma-Aldrich (Poole, UK)
Deoxyuridine	Analytical	Sigma-Aldrich (Poole, UK)
D-Erythrose	Analytical	Sigma-Aldrich (Poole, UK)
D-Erythrose 4-phosphate	Analytical	Sigma-Aldrich (Poole, UK)

Table 2.1 (Cont.) Chemical lists were used in the study.

Chemical	Grade	Supplier
D-Fructose	Analytical	Sigma-Aldrich (Poole, UK)
D-Fructose 1,6-bisphosphate	Analytical	Sigma-Aldrich (Poole, UK)
D-Fructose 6-phosphate	Analytical	Sigma-Aldrich (Poole, UK)
D-Galactarate	Analytical	Sigma-Aldrich (Poole, UK)
D-Galacturonate	Analytical	Sigma-Aldrich (Poole, UK)
D-Gluconic acid	Analytical	Sigma-Aldrich (Poole, UK)
D-Glucono-1,4-lactone	Analytical	Sigma-Aldrich (Poole, UK)
D-Glucosamine	Analytical	Sigma-Aldrich (Poole, UK)
D-Glucosamine-6-phosphate	Analytical	Sigma-Aldrich (Poole, UK)
D-glucose	Analytical	Sigma-Aldrich (Poole, UK)
D-Glucose 6-phosphate	Analytical	Sigma-Aldrich (Poole, UK)
D-Glucuronolactone	Analytical	Sigma-Aldrich (Poole, UK)
dGMP	Analytical	Sigma-Aldrich (Poole, UK)
Dihydrolipoamide	Analytical	Sigma-Aldrich (Poole, UK)
dIMP	Analytical	Sigma-Aldrich (Poole, UK)
DL-Glyceraldehyde 3-phosphate	Analytical	Sigma-Aldrich (Poole, UK)
DMSO	HPLC	Acros Organics (Geel, Belgium)
Dopamine	Analytical	Sigma-Aldrich (Poole, UK)
D-Ribose	Analytical	Sigma-Aldrich (Poole, UK)
D-ribose 5-phosphate	Analytical	Sigma-Aldrich (Poole, UK)
D-Threose	Analytical	Sigma-Aldrich (Poole, UK)
dUMP	Analytical	Sigma-Aldrich (Poole, UK)
Eflornithine	Analytical	Sigma-Aldrich (Poole, UK)
Ethanol	LC-MS	Acros Organics (Geel, Belgium)
Ethanolamine phosphate	Analytical	Sigma-Aldrich (Poole, UK)
FAD	Analytical	Sigma-Aldrich (Poole, UK)
Fluoxetine	Analytical	Abcam (Cambridge, MA, USA)
FMN	Analytical	Sigma-Aldrich (Poole, UK)
Folate	Analytical	Sigma-Aldrich (Poole, UK)
Formic acid	LC-MS	Sigma-Aldrich (Poole, UK)
Fumarate	Analytical	Sigma-Aldrich (Poole, UK)
Gallate	Analytical	Sigma-Aldrich (Poole, UK)
gamma-L-Glutamyl-L-cysteine	Analytical	Sigma-Aldrich (Poole, UK)
GDP	Analytical	Sigma-Aldrich (Poole, UK)
Glutathione	Analytical	Sigma-Aldrich (Poole, UK)
Glutathione disulfide	Analytical	Sigma-Aldrich (Poole, UK)
Glyceraldehyde	Analytical	Sigma-Aldrich (Poole, UK)
Glycerol	Analytical	Sigma-Aldrich (Poole, UK)
Glycine	Analytical	Sigma-Aldrich (Poole, UK)

Table 2.1 (Cont.) Chemical lists were used in the study.

Chemical	Grade	Supplier
Glycolate	Analytical	Sigma-Aldrich (Poole, UK)
Glycylglycine	Analytical	Sigma-Aldrich (Poole, UK)
Glyoxylate	Analytical	Sigma-Aldrich (Poole, UK)
GMP	Analytical	Sigma-Aldrich (Poole, UK)
GTP	Analytical	Sigma-Aldrich (Poole, UK)
Guanine	Analytical	Sigma-Aldrich (Poole, UK)
Guanosine	Analytical	Sigma-Aldrich (Poole, UK)
Haloperidol	Analytical	Sigma-Aldrich (Poole, UK)
HEPES	Analytical	Sigma-Aldrich (Poole, UK)
Homocystine	Analytical	Sigma-Aldrich (Poole, UK)
Hypoxanthine	Analytical	Sigma-Aldrich (Poole, UK)
IDP	Analytical	Sigma-Aldrich (Poole, UK)
Imidazole	Analytical	Sigma-Aldrich (Poole, UK)
Imidazole-4-acetate	Analytical	Sigma-Aldrich (Poole, UK)
IMP	Analytical	Sigma-Aldrich (Poole, UK)
Inosine	Analytical	Sigma-Aldrich (Poole, UK)
Isonicotinic acid	Analytical	Sigma-Aldrich (Poole, UK)
Isopropanol	LC-MS	Acros Organics (Geel, Belgium)
Itaconate	Analytical	Sigma-Aldrich (Poole, UK)
L-2_3-Diaminopropanoate	Analytical	Sigma-Aldrich (Poole, UK)
L-2_4-Diaminobutanoate	Analytical	Sigma-Aldrich (Poole, UK)
L-2-Aminoadipate	Analytical	Sigma-Aldrich (Poole, UK)
L-Alanine	Analytical	Sigma-Aldrich (Poole, UK)
L-Arginine	Analytical	Sigma-Aldrich (Poole, UK)
L-Asparagine	Analytical	Sigma-Aldrich (Poole, UK)
L-Aspartate	Analytical	Sigma-Aldrich (Poole, UK)
L-Carnitine	Analytical	Sigma-Aldrich (Poole, UK)
L-Citrulline	Analytical	Sigma-Aldrich (Poole, UK)
L-Cystathionine	Analytical	Sigma-Aldrich (Poole, UK)
L-Cysteate	Analytical	Sigma-Aldrich (Poole, UK)
L-Cysteine	Analytical	Sigma-Aldrich (Poole, UK)
L-Cystine	Analytical	Sigma-Aldrich (Poole, UK)
L-Cystine	Analytical	Sigma-Aldrich (Poole, UK)
L-Dehydroascorbate	Analytical	Sigma-Aldrich (Poole, UK)
L-Glutamate	Analytical	Sigma-Aldrich (Poole, UK)
L-Glutamine	Analytical	Sigma-Aldrich (Poole, UK)
L-Gulono-1,4-lactone	Analytical	Sigma-Aldrich (Poole, UK)
L-Histidine	Analytical	Sigma-Aldrich (Poole, UK)
L-Homocysteine	Analytical	Sigma-Aldrich (Poole, UK)
L-Homoserine	Analytical	Sigma-Aldrich (Poole, UK)

Table 2.1 (Cont.) Chemical lists were used in the study.

Chemical	Grade	Supplier
Lipoamide	Analytical	Sigma-Aldrich (Poole, UK)
Lipoate	Analytical	Sigma-Aldrich (Poole, UK)
L-Isoleucine	Analytical	Sigma-Aldrich (Poole, UK)
L-Kynurenine	Analytical	Sigma-Aldrich (Poole, UK)
L-Leucine	Analytical	Sigma-Aldrich (Poole, UK)
L-Lysine	Analytical	Sigma-Aldrich (Poole, UK)
L-Methionine	Analytical	Sigma-Aldrich (Poole, UK)
L-Noradrenaline	Analytical	Sigma-Aldrich (Poole, UK)
L-Ornithine	Analytical	Sigma-Aldrich (Poole, UK)
L-Phenylalanine	Analytical	Sigma-Aldrich (Poole, UK)
L-Proline	Analytical	Sigma-Aldrich (Poole, UK)
L-Rhamnose	Analytical	Sigma-Aldrich (Poole, UK)
L-Serine	Analytical	Sigma-Aldrich (Poole, UK)
L-Threonine	Analytical	Sigma-Aldrich (Poole, UK)
L-Tryptophan	Analytical	Sigma-Aldrich (Poole, UK)
L-Tyrosine	Analytical	Sigma-Aldrich (Poole, UK)
L-Valine	Analytical	Sigma-Aldrich (Poole, UK)
Maleic acid	Analytical	Sigma-Aldrich (Poole, UK)
Malonate	Analytical	Sigma-Aldrich (Poole, UK)
Maltose	Analytical	Sigma-Aldrich (Poole, UK)
Melatonin	Analytical	Sigma-Aldrich (Poole, UK)
Menadione	Analytical	Sigma-Aldrich (Poole, UK)
Mercaptoethanol	Analytical	Sigma-Aldrich (Poole, UK)
Mesaconate	Analytical	Sigma-Aldrich (Poole, UK)
meso-2,6-Diaminoheptanedioate	Analytical	Sigma-Aldrich (Poole, UK)
Methanol	LC-MS	Acros Organics (Geel, Belgium)
Methylcysteine	Analytical	Sigma-Aldrich (Poole, UK)
Methylglyoxal	Analytical	Sigma-Aldrich (Poole, UK)
Methylguanidine	Analytical	Sigma-Aldrich (Poole, UK)
Methylmalonate	Analytical	Sigma-Aldrich (Poole, UK)
MOPS	Analytical	Sigma-Aldrich (Poole, UK)
N(pi)-Methyl-L-histidine	Analytical	Sigma-Aldrich (Poole, UK)
N2-Acetyl-L-lysine	Analytical	Sigma-Aldrich (Poole, UK)
N-Acetyl-D-glucosamine	Analytical	Sigma-Aldrich (Poole, UK)
N-Acetylglutamine	Analytical	Sigma-Aldrich (Poole, UK)
N-acetyl-L-glutamate	Analytical	Sigma-Aldrich (Poole, UK)
N-Acetylneuraminate	Analytical	Sigma-Aldrich (Poole, UK)
N-Acetylornithine	Analytical	Sigma-Aldrich (Poole, UK)
NAD+	Analytical	Sigma-Aldrich (Poole, UK)
NADH	Analytical	Sigma-Aldrich (Poole, UK)

Table 2.1 (Cont.) Chemical lists were used in the study.

Chemical	Grade	Supplier
NADP+	Analytical	Sigma-Aldrich (Poole, UK)
NADPH	Analytical	Sigma-Aldrich (Poole, UK)
Nicotinamide	Analytical	Sigma-Aldrich (Poole, UK)
Nicotinate	Analytical	Sigma-Aldrich (Poole, UK)
O-Acetylcarnitine	Analytical	Sigma-Aldrich (Poole, UK)
O-Acetyl-L-serine	Analytical	Sigma-Aldrich (Poole, UK)
Orotate	Analytical	Sigma-Aldrich (Poole, UK)
Orotidine	Analytical	Sigma-Aldrich (Poole, UK)
Orthophosphate	Analytical	Sigma-Aldrich (Poole, UK)
Oxalate	Analytical	Sigma-Aldrich (Poole, UK)
Oxaloacetate	Analytical	Sigma-Aldrich (Poole, UK)
Pantothenate	Analytical	Sigma-Aldrich (Poole, UK)
Pentostatin	Analytical	Tocris Bioscience (Bristol, UK)
Phenol	Analytical	Sigma-Aldrich (Poole, UK)
Phenolsulfonphthalein	Analytical	Sigma-Aldrich (Poole, UK)
Phenylacetylglycine	Analytical	Sigma-Aldrich (Poole, UK)
Phenylhydrazine	Analytical	Sigma-Aldrich (Poole, UK)
Phenylpyruvate	Analytical	Sigma-Aldrich (Poole, UK)
Phosphoenolpyruvate	Analytical	Sigma-Aldrich (Poole, UK)
Phthalate	Analytical	Sigma-Aldrich (Poole, UK)
Picolinic acid	Analytical	Sigma-Aldrich (Poole, UK)
Putrescine	Analytical	Sigma-Aldrich (Poole, UK)
pyrazinoate	Analytical	Sigma-Aldrich (Poole, UK)
Pyridoxal	Analytical	Sigma-Aldrich (Poole, UK)
Pyridoxal phosphate	Analytical	Sigma-Aldrich (Poole, UK)
Pyridoxine	Analytical	Sigma-Aldrich (Poole, UK)
Pyrophosphate	Analytical	Sigma-Aldrich (Poole, UK)
Pyruvate	Analytical	Sigma-Aldrich (Poole, UK)
Riboflavin	Analytical	Sigma-Aldrich (Poole, UK)
Risperidone	Analytical	Sigma-Aldrich (Poole, UK)
Rotenone	Analytical	Sigma-Aldrich (Poole, UK)
S-Adenosyl-L-homocysteine	Analytical	Sigma-Aldrich (Poole, UK)
S-Adenosyl-L-methionine	Analytical	Sigma-Aldrich (Poole, UK)
Selenomethionine	Analytical	Sigma-Aldrich (Poole, UK)
Serotonin	Analytical	Sigma-Aldrich (Poole, UK)
S-Glutathionyl-L-cysteine	Analytical	Sigma-Aldrich (Poole, UK)
sn-glycero-3-Phosphocholine	Analytical	Sigma-Aldrich (Poole, UK)
sn-Glycerol 3-phosphate	Analytical	Sigma-Aldrich (Poole, UK)
Sodium azide	Analytical	Sigma-Aldrich (Poole, UK)
Spermidine	Analytical	Sigma-Aldrich (Poole, UK)
Spermine	Analytical	Sigma-Aldrich (Poole, UK)

Table 2.1 (Cont.) Chemical lists were used in the study.

Chemical	Grade	Supplier
Succinate	Analytical	Sigma-Aldrich (Poole, UK)
Succinate semialdehyde	Analytical	Sigma-Aldrich (Poole, UK)
Sucrose	Analytical	Sigma-Aldrich (Poole, UK)
Taurine	Analytical	Sigma-Aldrich (Poole, UK)
Taurocholate	Analytical	Sigma-Aldrich (Poole, UK)
Thiamine	Analytical	Sigma-Aldrich (Poole, UK)
Thiamin diphosphate	Analytical	Sigma-Aldrich (Poole, UK)
Thiopurine S-methylether	Analytical	Sigma-Aldrich (Poole, UK)
Thymidine	Analytical	Sigma-Aldrich (Poole, UK)
Thymine	Analytical	Sigma-Aldrich (Poole, UK)
trans-4-Hydroxy-L-proline	Analytical	Sigma-Aldrich (Poole, UK)
Trypanothione	Analytical	Sigma-Aldrich (Poole, UK)
Trypanothione disulfide	Analytical	Sigma-Aldrich (Poole, UK)
UDP-glucose	Analytical	Sigma-Aldrich (Poole, UK)
UMP	Analytical	Sigma-Aldrich (Poole, UK)
Uracil	Analytical	Sigma-Aldrich (Poole, UK)
Uridine	Analytical	Sigma-Aldrich (Poole, UK)
Xanthine	Analytical	Sigma-Aldrich (Poole, UK)

2.2 REVERSE PHASE LIQUID CHROMATOGRAPHY (RP-LC)

Lipidomic chromatographic separations were performed on an Agilent SB C8 column (1.8 µm particle size, 2.1 x 100 mm, Crawford Scientific Ltd., Lancashire, UK) and metabolic chromatographic separations were performed on a C18 (2) column (2.5 µm particle size, 3 x 100 mm, Phenomenex Ltd, Cheshire, UK). The mobile phases were 0.1% w/v ammonium acetate in water and 0.1% ammonium acetate in mixture of acetonitrile and isopropanol (60:40 v/v) for lipidomics, and 0.1% v/v formic acid in water and 0.1% v/v formic acid in acetonitrile for polar compounds.

2.3 HYDROPHILIC INTERACTION CHROMATOGRAPHY (HILIC)

A ZIC-HILIC (betaine-sulfonate bonded phase) columns with a 5 µm particle size; 150 mm x 2.1 mm internal diameter (Millipore (U.K.) Limited, Hertfordshire, U.K.) at a column temperature of 30°C, using a mobile phase of 0.1% v/v formic acid in water and 0.08% v/v formic acid in acetonitrile at a flow rate of 0.200 mL/min. Sample injection volume was 10 µL. The total time for the analytical run was 20.00 minutes.

2.4 MASS SPECTROMETRIC CONDITIONS

Quadrupole time of flight (QToF) mass spectrometry (Waters, UK) performed in ESI negative and positive mode using an electrospray ionisation (ESI) source. Sodium formate solution was used as a calibrant in both negative and positive modes for the QToF calibration. Tuning parameters were optimised by infusing a standard solution containing 10 μM of standard compound mix and pumped at a flow rate of 10 μl/minute (using an injection syringe pump). The mass spectrometer was run with a scan time of 0.5 second, inter-scan time of 0.01 second, and resolution at 10,000. The mass range was 50 to 1,000 Da.

CHAPTER III: OPTIMISATION AND VALIDATION OF A LIQUID CHROMATOGRAPHY-MASS SPECTROMETRY METHOD

3.1 ABSTRACT

The objective of this part of my work described in this chapter was to optimise and validate the LC-MS method, for hydrophobic metabolites using reverse phase (RP), and small polar metabolites using hydrophilic interaction chromatography (HILIC) coupled with LC-MS. RP-LC-MS and HILIC-MS methods were optimised for analysing the standard mixtures, ranging from lipid compounds, the central carbon pathway, phosphate compounds, sugars and others. These compounds are all common in human cells. The RP-LC-MS and HILIC-MS method were tested for its sensitivity and effectiveness, and optimised and validated for its reliability and reproducibility. The RP-MS method was able to apply for hydrophobic metabolites. The HILIC-MS method was able to detect the most polar metabolites used in negative and positive electrospray ionisation modes (ESI- and ESI+) with mass spectrometers. Both RP-LC-MS and HILIC-MS methods showed good reliability and reproducibility, with the relative standard deviation of retention time and peak areas less than 2% and 20%

respectively, and can be applied to study the effects of pharmaceutical compounds (or others) in cell based-metabolomics.

Keywords: cell based metabolmics, liquid chromatography-mass spectrometry, reverse phase chromatography, hydrophilic interaction chromatography

3.2 INTRODUCTION

Liquid chromatography-mass spectrometry (LC-MS) is commonly used in metabolomics analysis, details of which may be found in references (129–131). Currently, analytical technologies, especially LC-MS, are making great progress in optimising and validating their methods for metabolomics analysis (132,133). However, there has been less attention given to the investigation of small polar molecules. Such molecules are limited by conventional reverse phase chromatography (RP-LC) because these metabolites are poorly retained and usually eluted in the void volume (48,131). On the other hand, it has been shown that the hydrophilic interaction chromatography (HILIC-MS) method easily resolves small polar metabolites for better identification and qualification (48,134). Thus, a comprehensive coverage of the study of small polar metabolites in mammalian cells has been developed, optimised and validated for the RP-LC and HILIC-MS analytical methods in metabolomics based mammalian cell culture study (134–138). However, effectiveness, reliability and reproducibility are all crucial for this type of study, since the efficiency of acquired data that is used in metabolomics analysis relies on this step. As metabolomics analysis is initiated with sample separation via liquid chromatography and detected with mass spectrometry, this chapter was designed firstly to optimise and validate the RP-LC-MS and

HILIC-MS method for facilitating comprehensive hydrophobic metabolites and small polar metabolite identification.

3.3 OBJECTIVES

This part of the works has two main objectives:

- to optimise the RP-LC-MS and HILIC-MS method for facilitating comprehensive hydrophobic metabolites and small polar metabolite identification
- to validate the RP-LC-MS and HILIC-MS method for facilitating comprehensive hydrophobic metabolites and small polar metabolite identification

3.4 MATERIALS AND METHODS

3.4.1 Reverse phase liquid chromatography (RP-LC)

Numerous RP-LC methods have been reported for the qualitative and quantitative analysis of lipids and hydrophobic compounds in mammalian cell lines (139–141). In this study, the RP-LC methods were based on the previous report (142). Lipidomic chromatographic separations were performed on an Agilent SB C8 column (1.8 µm particle size, 2.1 x 100 mm, Crawford Scientific Ltd., Lancashire, UK) and metabolic chromatographic separations were performed on a C18 (2) column (2.5 µm particle size, 3 x 100 mm, Phenomenex Ltd, Cheshire, UK). The mobile phases were 0.1% w/v ammonium acetate in water and 0.1% ammonium acetate in mixture of acetonitrile and isopropanol (60:40 v/v) for lipidomics, and 0.1% v/v formic acid in water and 0.1% v/v formic acid in acetonitrile for polar compounds.

3.4.1.1 Sample preparation for reverse phase liquid chromatography

To facilitate the extraction of cellular metabolites, the 0.50 ml of suspension of cell debris was vigorously vortexed for 5 minutes. The cell extraction was based on the method described by Bligh and Dyer (143). Briefly, 0.50 ml chloroform and 0.50 ml of water were added to the suspension and then vortexed vigorously for 10 minutes at 4°C. Then, the suspension was centrifuged at 15,000 g

for 10 minutes at 4°C. The polar (water soluble) fraction and non-polar (lipid) fraction were collected separately and transferred into fresh eppendorf tubes and evaporated to dryness at room temperature. The dried non-polar layer was reconstituted in 50.00 µl of chloroform and methanol (1:2 v/v), and the dried aqueous layer was reconstituted in 50.00 µl of water. The reconstituted samples were centrifuged at 15,000 g for 10 minutes at 4°C to remove any cell debris. Finally, the supernatant was transferred into an HPLC vial and stored at -80°C for further analysis.

3.4.1.2 Mass spectrometric conditions for RP-LC method

High resolution mass spectrometry (Exactive, Waters, UK) performed in ESI negative and positive mode using an electrospray ionisation (ESI) source. Calmix solution was used as a calibrant in both negative and positive modes for the MS calibration. For MS parameters are summarised in Table 3.1.

Table 3.1 Details of MS parameters for RP-LC method.

Parameters	Lipid profiling	Polar Metabolite profiling
Probe	A heated electrospray ionisation	A heated electrospray ionisation
Heat temperature (°C)	150	400
Capillary temperature (°C)	275	250
Flow rate of sheath gas (ml/min)	40	40
Flow rate of auxiliary gas (ml/min)	5	20
Flow rate of sweep gas (ml/min)	1	0
Spray voltage in positive mode (kV)	4.5	4.0

3.4.2 Hydrophilic interaction chromatography (HILIC)

Small and polar molecules are limited by RP-LC because these metabolites are poorly retained and usually eluted in the void volume (48). On the other hand, it has been shown that the hydrophilic interaction chromatography (HILIC-MS) method easily resolves small polar metabolites for better identification and qualification (144–146). Thus, a comprehensive coverage of the study of small polar metabolites in mammalian cells presents a major challenge in the optimisation and validation of the HILIC-MS analytical method in metabolomics based mammalian cell culture study. The reason this drawback is such a big challenge is because effectiveness, reliability and reproducibility are all crucial for this

type of study, since the efficiency of acquired data that is used in metabolomics analysis relies on this step. The HILIC-MS method of the study was modified from the previous study (135).

3.4.2.1 Sample preparation for hydrophilic interaction chromatography

The cell culture was removed and washed with 1 ml of PBS and then MCF-7 cell pellets were extracted with 0.5 ml cold methanol (-20°C) and cell suspensions were vortexed for 2 hr in cold room (4°C). The suspensions were centrifuged for 10 min at 15,000 rpm and temperature at 4°C. The supernatants were transfer to new eppendorf tubes and kept at -80°C for further analysis.

3.4.2.2 Mass spectrometric conditions

Quadrupole time of flight (QToF) mass spectrometry (Waters, UK) performed in ESI negative and positive mode using an electrospray ionisation (ESI) source. Sodium formate solution was used as a calibrant in both negative and positive modes for the QToF calibration. Tuning parameters were optimised by infusing a standard solution containing 10 µM of standard compound mix and pumped at a flow rate of 10 µl/min (using an injection syringe pump). The mass spectrometer was run with a scan time of 0.5 second, inter-scan time of 0.01 second, and resolution at 10,000. The mass range was 50 to 1,000 Da.

3.4.2.3 Chromatographic conditions

Chromatographic separation was achieved on a ZIC-HILIC column with a 5 µm particle size; 150 mm x 2.1 mm internal diameter (Millipore (U.K.) Limited, Hertfordshire, U.K.) at a column temperature of 30°C, using a mobile phase of 0.1% v/v formic acid in water and 0.08% v/v formic acid in acetonitrile at a flow rate of 0.200 mL/min. Sample injection volume was 10 µL. The total time for the analytical run was 20.00 minutes.

3.4.2.4 Method validation

The HILIC-MS method was validated by three consecutive analytical studies on three separate days. Each study contained the three standard mixtures and a single QC sample. Each of the samples was repeated six times, and these samples were studied in random order. Before an analysis, the column was conditioned by five injections of the QC sample. During the analysis, the QC sample was injected after every six samples. A solvent blank of 50% v/v of acetonitrile in water was also run after twelve samples.

3.5 RESULTS AND DISCUSSION

3.5.1 RP-LC method validation

For checking the instrument performance in the RP-LC methods, QC samples were analysed throughout the whole analysis procedure for both lipid and polar fractions. Figure 3.1 and 3.2 shows chromatogram of QC samples.

The data from the QC samples of both lipid fraction and polar fraction were then analysed to determine the number of ions present in the samples, their intensity and their % RSD values. The average RSDs of peak abundance for the QC samples was 17.9% with a standard deviation of 7.84% for the lipid fraction, and 22.86% with a standard deviation of 10.17% for the polar fraction. Since the recommendations of the FDA are that biochemical analysis ions should show % RSDs less than 30, these were used in the subsequent analysis of the test and control sample data. Our values showing average %RSD demonstrated that the system had excellent stability during the analysis procedure for RP-LC method.

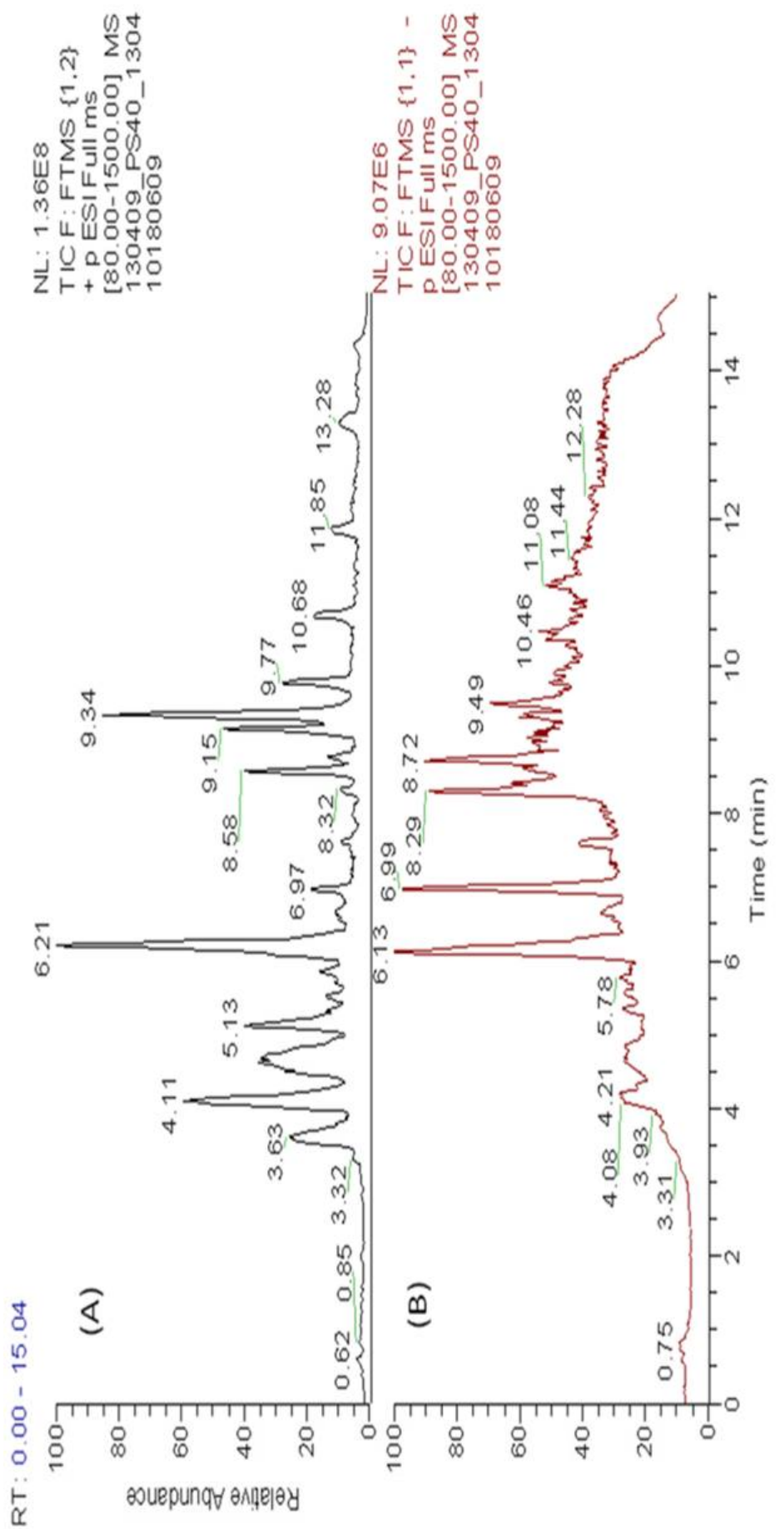


Figure 3.1 Chromatograms of the QC sample form lipid fraction in (A) positive and (B) negative mode using RP-LC-MS method.

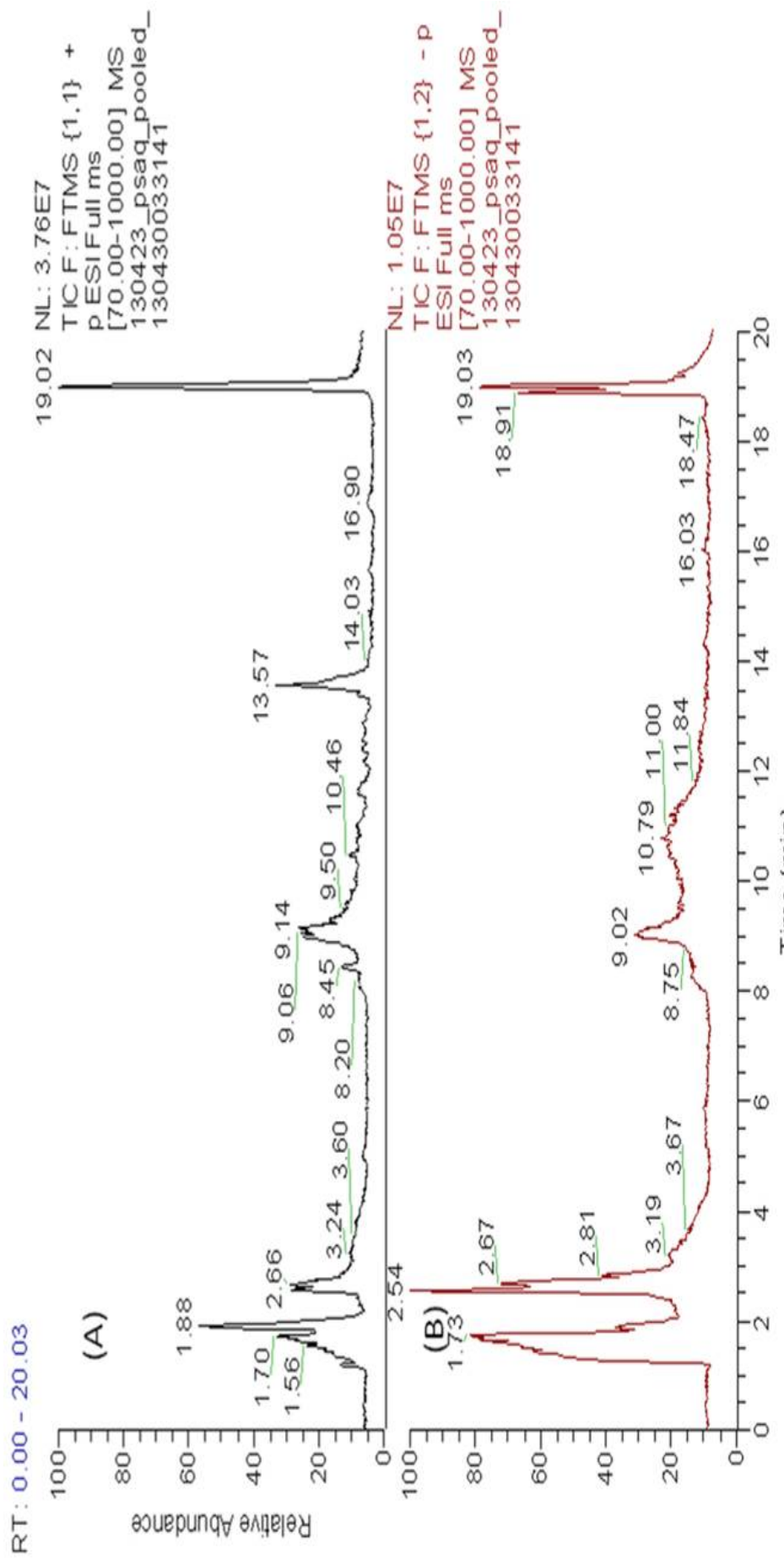


Figure 3.2 Chromatograms of the QC sample form polar fraction in (A) positive and (B) negative mode using RP-LC-MS method.

3.5.2 Hydrophilic interaction chromatography (HILIC)

3.5.2.1 Mass spectrometric conditions

It is important to optimise MS conditions because doing so will provide a good selectivity and sensitivity (147). In this study, the conditions QToF/MS were optimised by introducing standard mixtures directly into the MS detector. Both ESI- and ESI+ ionization and parameters such as capillary, sampling and extraction cone, source and desolvation temperature, cone and desolvation gas, and ion guide were determined to increase the sensitivity of the compounds. The optimal parameters for both ESI- and ESI+ condition were 3000 V for capillary cone, 34 V for sampling cone, 5 V for extraction cone, 2 V for ion guide, 100°C of source temperature, 250°C for desolvation temperature, 70 L/hour for cone gas and 600 L/hour for desolvation gas. The data were acquired in centroid mode from *m/z* 50 to 1,000 at a scan rate of 1.0 Hz and an interscan rate of 0.5 Hz. The mass accuracy was adjusted by external calibration using sodium formate clusters in both ESI+ and ESI- before starting an analysis. Figures 3.3 and 3.4 present the optimised MS/QToF method capability on the detection of different polar metabolites found in three simultaneous standard mixtures, typical mass spectra in ESI- and ESI+ modes, respectively. .

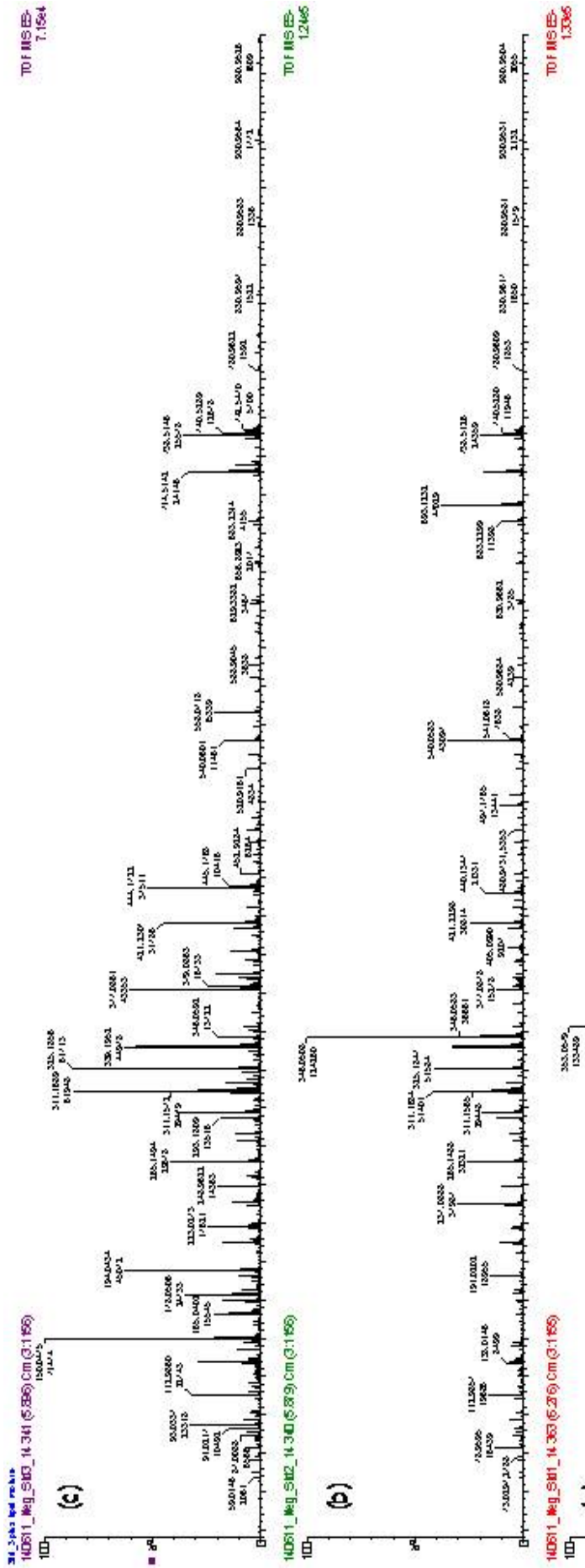


Figure 3.3 Fingerprinting of three simultaneous standard polar metabolite mixtures in negative mode using HILIC-MS. Typical optimised MS spectra of the (A) first, (B) second and (C) third standard mixtures.

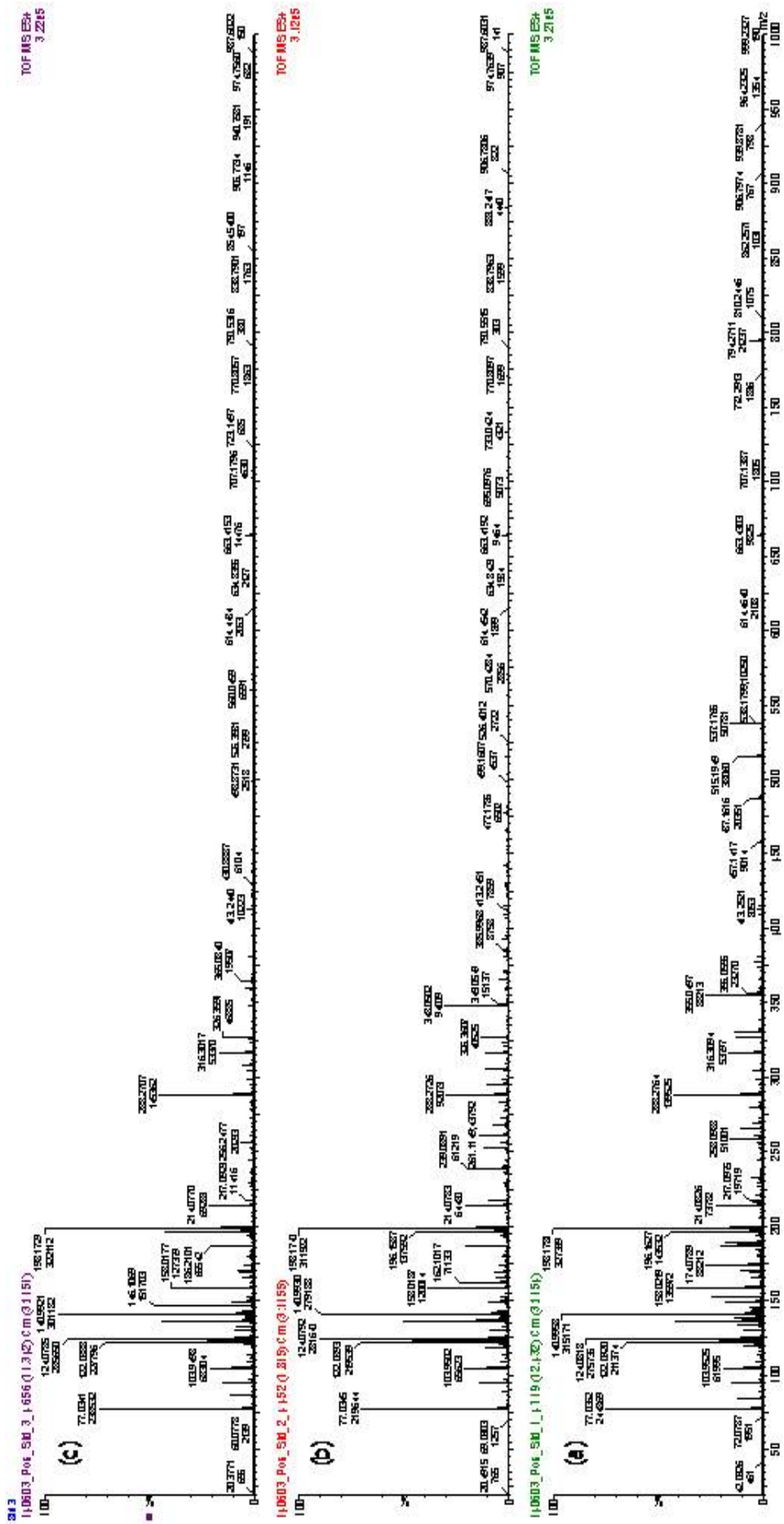


Figure 3.4 Fingerprinting of three simultaneous standard polar metabolite mixtures in positive mode using HILIC-MS method. Typical optimised MS spectra of the (A) first, (B) second and (C) third standard mixtures.

The standard mixtures contained a variety of different metabolites which are dominantly deprotonated and protonated molecules ($[M-H]^-$ and $[M+H]^+$). Figure 3.5 illustrated the structures and the mass spectrum of $[M-H]^-$ and $[M+H]^+$ ions from some compounds in the standard mixtures. For example, in ESI -, (R)-lactate, 2-oxoglutarate, D-gluconic acid and folate showed an intense ion at *m/z* 89.0244, 101.0244, 195.0510 and 440.1324, respectively, corresponding to the loss of a proton $[M-H]^-$. In ESI+, L-proline, deoxyadenosine, glutathione and riboflavin showed an intense ion at *m/z* 116.0706, 252.1091, 308.0911 and 377.1456, respectively, corresponding to the acceptance of proton $[M+H]^+$.

Moreover, a good signal was achieved using an ESI negative ion mode (ESI-) for most polar metabolites and ESI positive ion mode (ESI+) for some metabolites, such as nicotinamide, 2-phenyl glycine, methylguanidine, cytosine and some L-forms of amino acid. For example, the ion spectrum production for lactic acid, 1-naphthylacetic acid and deoxyuridine yielded a high abundance of ions of *m/z* 89.0244, 185.0608 and 227.0673 in ESI-, respectively. For ESI+, the ion spectrum production for methylguanidine, nicotinamide and deoxyadenosine yielded a high abundance of ions of *m/z* 74.0713, 123.0553 and 252.1091, respectively.

As described above, these mass spectra were consistent with the in the published literatures (144,148), as these protonated or

deprotonated metabolites were injected into the MS spectrometer. These polar metabolites produce the best signal quality in their respective negative or positive ionisation modes. Therefore, the MS full scan modes with negative and positive ionisation modes were preferable for simultaneous polar metabolites.

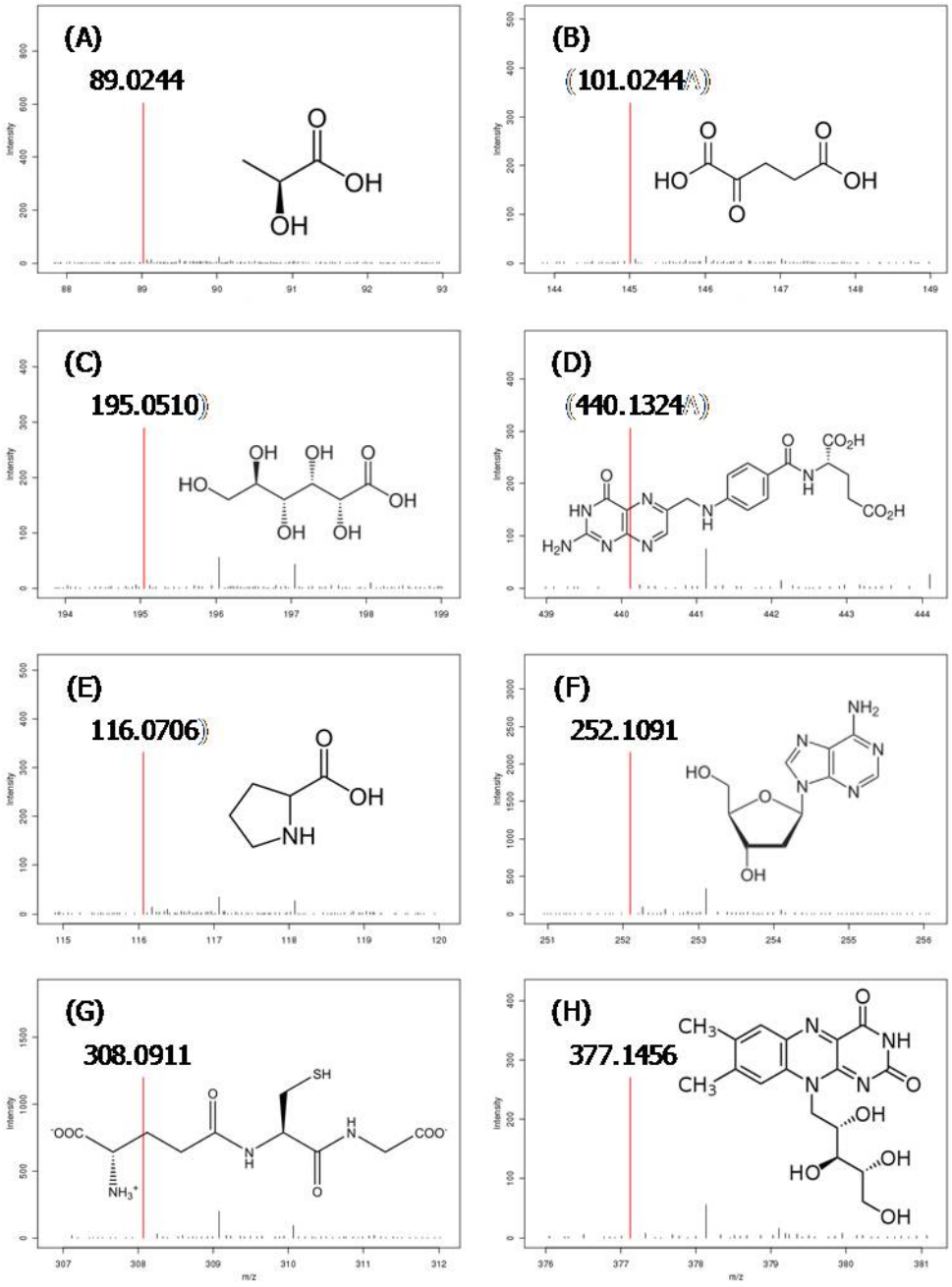


Figure 3.5 Structures and mass spectra of the four analytes in ESI- ((R)-lactate: *m/z* 89.0244 (A), 2-oxoglutarate(B): *m/z* 101.0244, D-gluconic acid (C): *m/z* 195.0510 and folate: *m/z* 440.1324) (D) and four analytes in ESI+ (L-proline: *m/z* 116.0706 (E), deoxyadenosine *m/z*: 252.1091 (F), glutathione: *m/z* 308.0911 (G) and riboflavin: *m/z* 377.1456 (H)). .

3.5.2.2 Chromatographic conditions

It is important to optimise LC conditions because the optimised condition can provide good selectivity and sensitivity, fast speed, and symmetrical peak shape. Most studies have developed the LC-MS method for investigating the intracellular metabolic profile of mammalian cells, using reverse phase (RP) with or without a pairing reagent to identify polar metabolites (149). However, this work has failed to detect many key polar metabolites that are known to be present in mammalian cells, due to the fact that they are poorly retained and usually eluted in the void volume (139). Moreover, a pairing reagent which was used suppressed the detected ions (130). Currently, the HILIC-MS method has demonstrated that it can resolve polar metabolites for better identification and quantification (134). Nowadays, it is more widely used to study the polar metabolites in microorganisms (138,150,151), plant cells (152–154), sera and plasma (18,136), and drugs (137,155,156). In this study, the HILIC conditions were optimised in an attempt to achieve reliable analysis of cell-based samples.

One hundred and fifty-eight metabolites, commonly found intracellularly in mammalian cells, were used for HILIC- MS/QToF method optimisation. The parameters chosen for MS conditions were used, as described in section 2.4. The simultaneous polar metabolite mix (n = 6 for each mix) were used to check the

performance of the optimised HILIC- MS/QToF. Both negative and positive ionisation modes (ESI- and ESI+) were used in separate runs.

The aqueous solvent choice in HILIC-MS is very important for metabolic separation because it has a great effect on retention time, peak shapes, sensitivity and efficiency. In this work, water (mobile phase A) and acetonitrile (mobile phase B) were chosen as the main components of the mobile phase because they are common and frequently used. Acetonitrile provides a better retention of analytes than methanol, because it is an aprotic solvent, which means it is less likely to create hydrogen bonds with the functional group of the stationary phase or with the polar metabolites (156). The suitable pH range for the HILIC column has been reported to be 3-8 (144). Commonly, the polar metabolites are strongly affected by the pH of the mobile phase (144). In order to establish an HILIC separation, various concentrations of formic acid were investigated by adjusting the percentage of this acid. It was found that under a gradient elution mode with 0.10% formic acid in water (pH = 3.0) and 0.08% formic acid in acetonitrile, most peaks of compounds are quite symmetrical, with good separation, as shown in Figure 3.6. However, this condition resulted in poor chromatographic peak shapes of the phosphorylated metabolites, such as GDP, AMP and ADP, resulted in poor chromatographic peak shapes. In particular, these three metabolites have shown that they

could be well separated using basic conditions (149). Nevertheless, the developed HILIC-MS could separate these metabolites as shown in Supplementary Table 3.1.

The gradient rate has a major impact on the polar metabolite separation in ESI-MS analysis. Various gradient and flow rates were then studied to determine the optimal condition that provides high resolution separations [data not shown]. In this work, a water/acetonitrile mobile phase containing 0.1% and 0.08% v/v formic acid, respectively, was used. Initially, linear gradients from 95%-5%B at 8, 10, 13 and 15 min were used. In this study, the 13 min gradient time, from 95% of mobile phase B to 5% of mobile phase B, was selected because a good baseline separation and quick speed were achieved. The total analysis time was 20 minutes per injection. Figure 3.7 and 3.8 show the base peak chromatograms (BPIs) in ESI- and ESI+ modes of three standard mixtures.

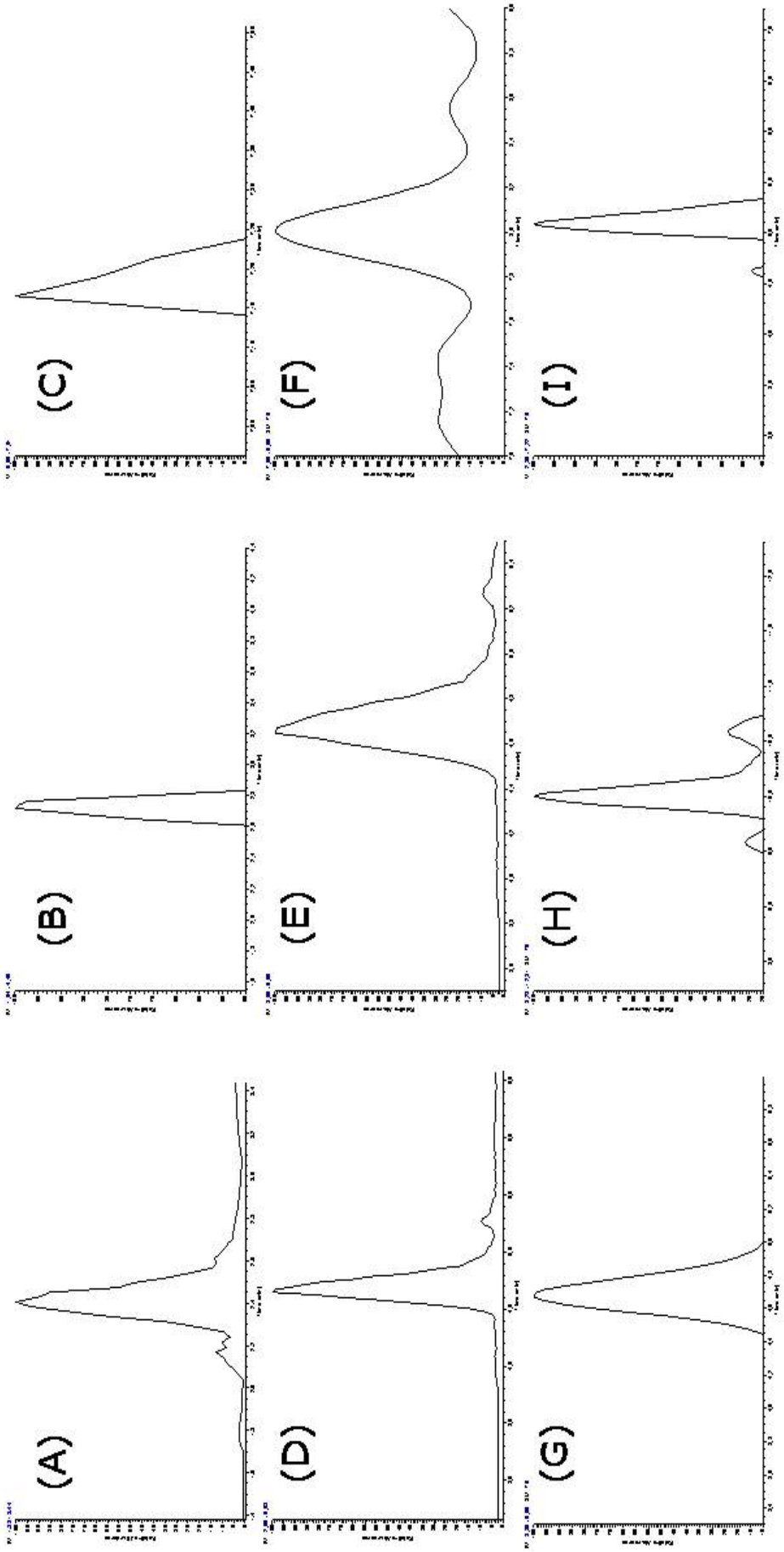


Figure 3.6 Representative chromatograms of some compounds using HILIC-MS method, corresponding to the deprotonated ion $[M-H]^-$: (A) urea (*m/z* 59.0251), (B) lactate (*m/z* 89.0244), (C) taurine (*m/z* 124.0074), (D)L-Lysine (*m/z* 145.0983), (E) uric acid (*m/z* 167.0211), (F) myoinositol (*m/z* 179.0561), (G) N2-acetyl-L-lysine (*m/z* 187.1088), (H) L-Tryptophan (*m/z* 203.0826), (I) sucrose (*m/z* 341.1089).

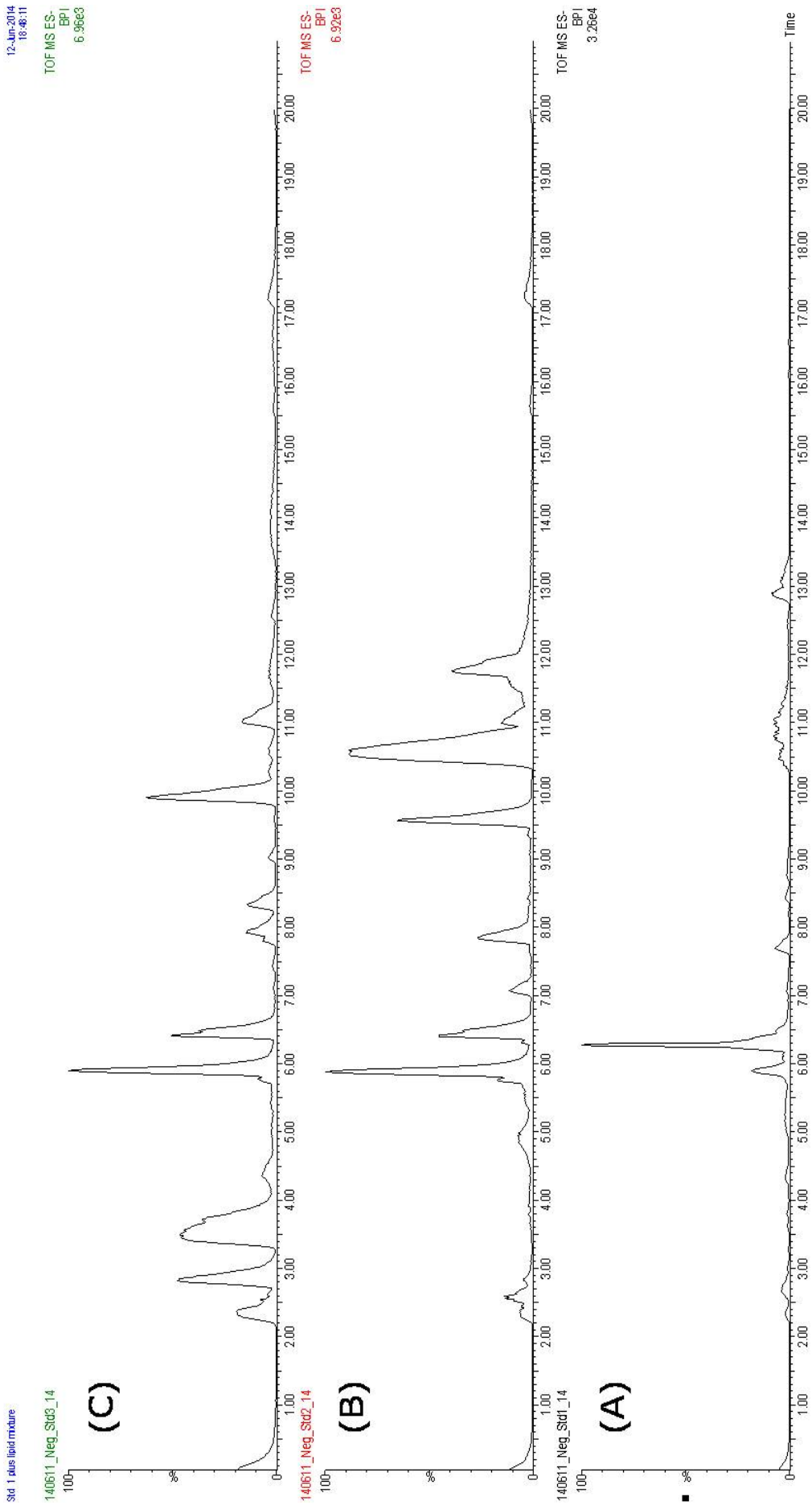


Figure 3.7 Base peak chromatogram in ESI- mode of the three standard groups from HILIC-MS method: (A) first, (B) second, and (C) third mixtures.

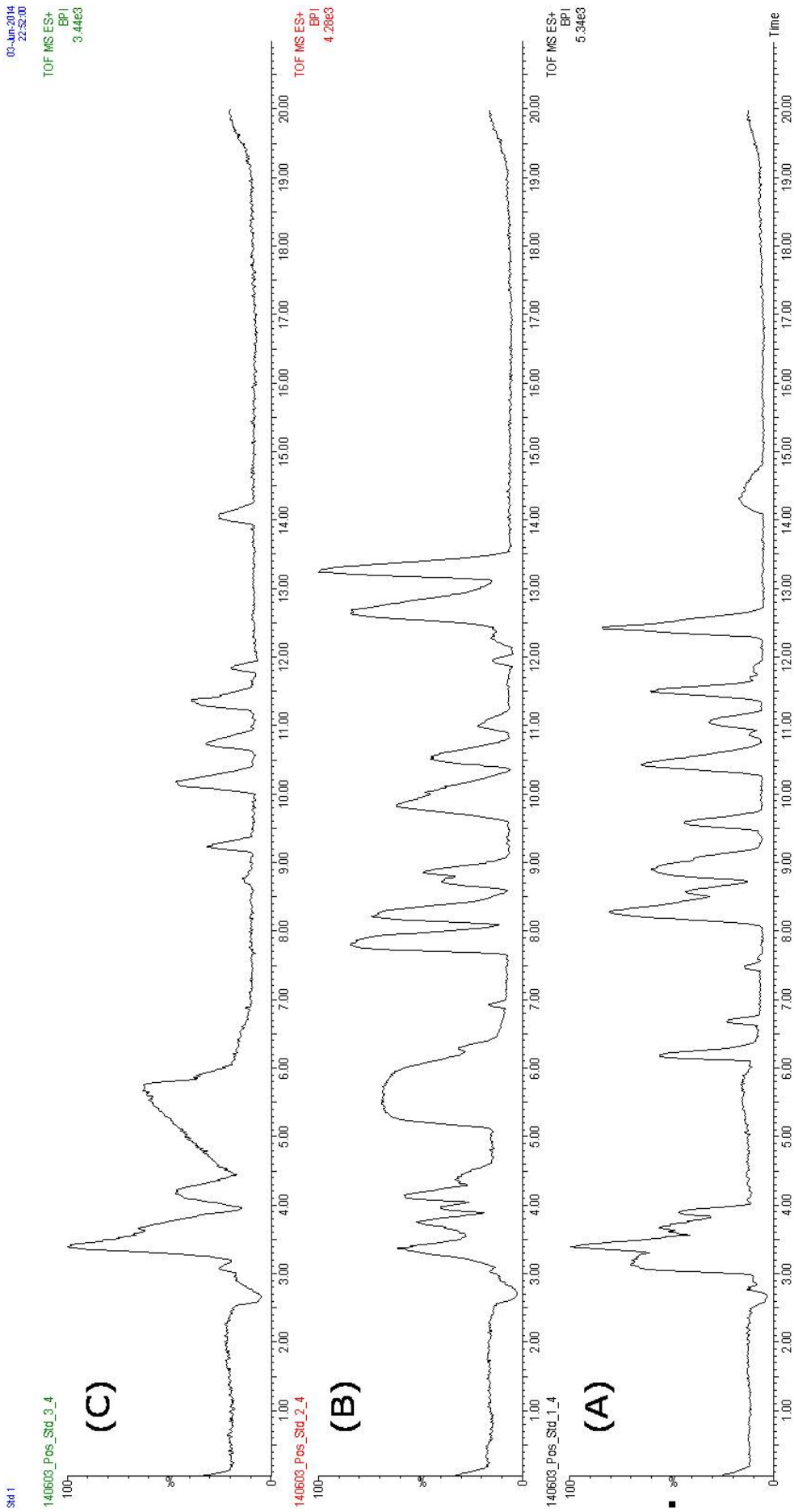


Figure 3.8 Base peak chromatograms in ESI+ mode of the three standard groups from HILIC-MS method: (A) first, (B) second, and (C) third mixtures

The extracted ion chromatograms (EICs), after injection of some standard polar metabolites, are shown in Figures 3.9 to 3.11. All of the small organic acids were detected in the ESI- mode, due to their carboxylic acid groups carrying a negative charge responsible for the ESI signal. The EICs of some standard organic acids (1-naphtylacetic acid, gallic acid, 3-hydroxyphenylacetic acid, (R)-3-hydroxybutanoic acid, 3,4-dihydroxyphenyl acetic acid, 2-oxobutanoic acid, fumaric acid, glycolic acid and pyruvic acid) are illustrated in Figure 3.9. Retention times of these organic acids were achieved as follows: (1-naphtylacetic acid = 2.52 min, gallic acid = 2.62 min, 3-hydroxyphenylacetic acid = 2.98 min, (R)-3-hydroxybutanoic acid = 3.12 min, 3,4-dihydroxyphenyl acetic acid = 3.25 min, 2-oxobutanoic acid = 3.68 min, fumaric acid = 3.89 min, glycolic acid = 4.34 min and pyruvic acid = 4.56). It was found that amino acids can be detected in both ESI- and ESI+. However, most of these metabolites registered larger dynamic responses in ESI+. Higher signal intensity was detected for protonated adduct ions, as compared to deprotonated adduct ions, due to amino acid functionality carrying the positive charge responsibility. For example, EICs of 9 standard L-amino acids (phenylalanine, leucine, tryptophan, methionine, valine, proline, glutamate, serine and asparagine) are shown in Figure 3.10. These examples are chromatographically resolved by the optimised method.

Figure 3.11 shows the EICs of some standard sugar compounds in the mixture (DL-rhamnose, DL-ribose, D-erythrose, D-fructose, D-mannitol, sucrose, DL-maltose, trehalose and deoxyribose. The mixture contains two forms of rhamnose, ribose and maltose (D- and L-forms), hence giving two peaks with identical mass. Moreover, the developed method is able to resolve the nucleosides, phosphate compounds and others chromatographically or by mass difference, as shown in Supplementary Table 3.1.

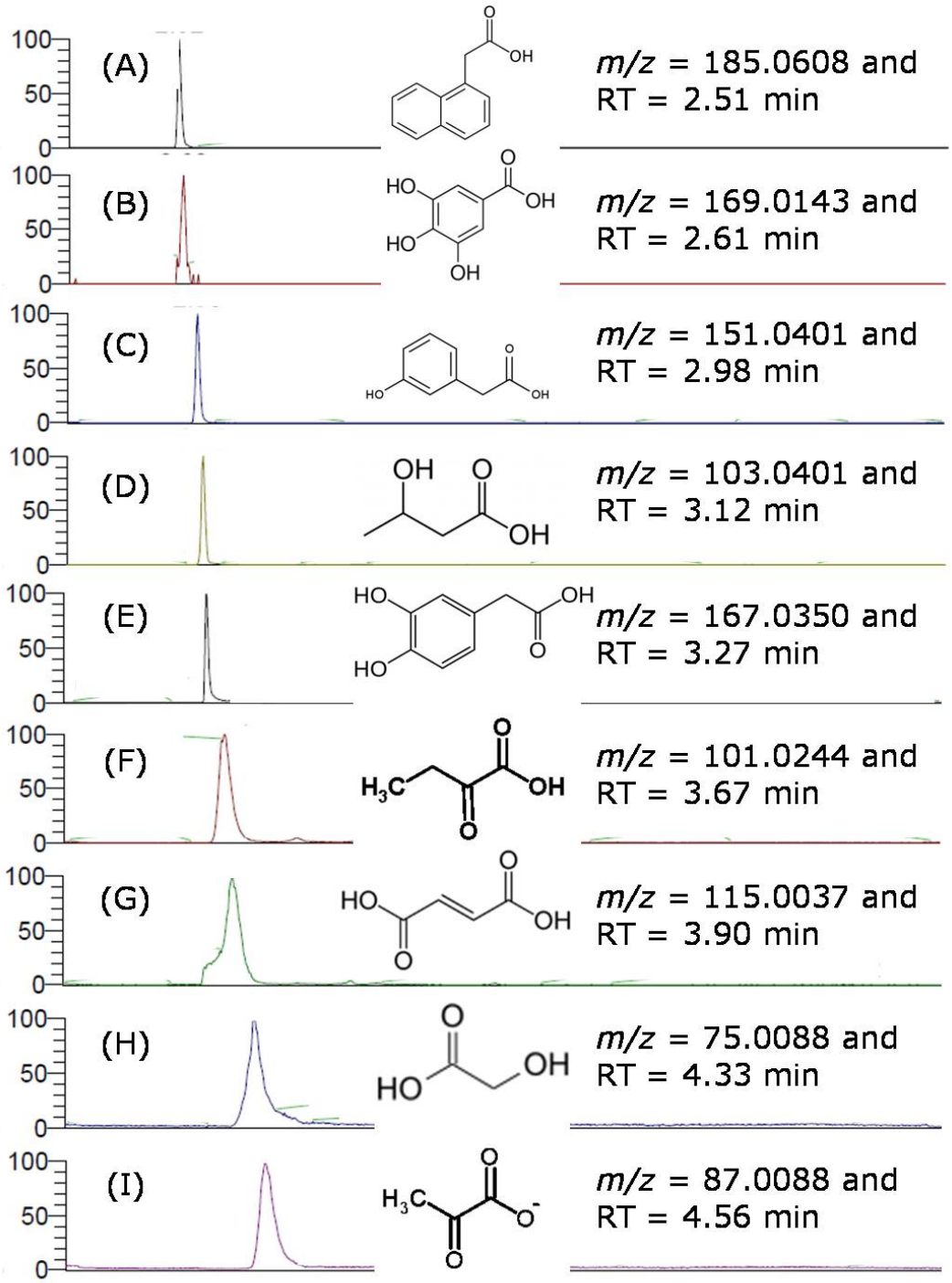


Figure 3.9 EICs of some standard organic acids studied by using HILIC-MS method: (A) 1-naphtylacetic acid, (B) gallic acid, (C) 3-hydroxyphenylacetic acid, (D) (R)-3-hydroxybutanoic acid, (E) 3,4-dihydroxyphenyl acetic acid, (F) 2-oxobutanoic acid, (G) fumaric acid, (H) glycolic acid and (I) pyruvic acid. (RT = Retention time)

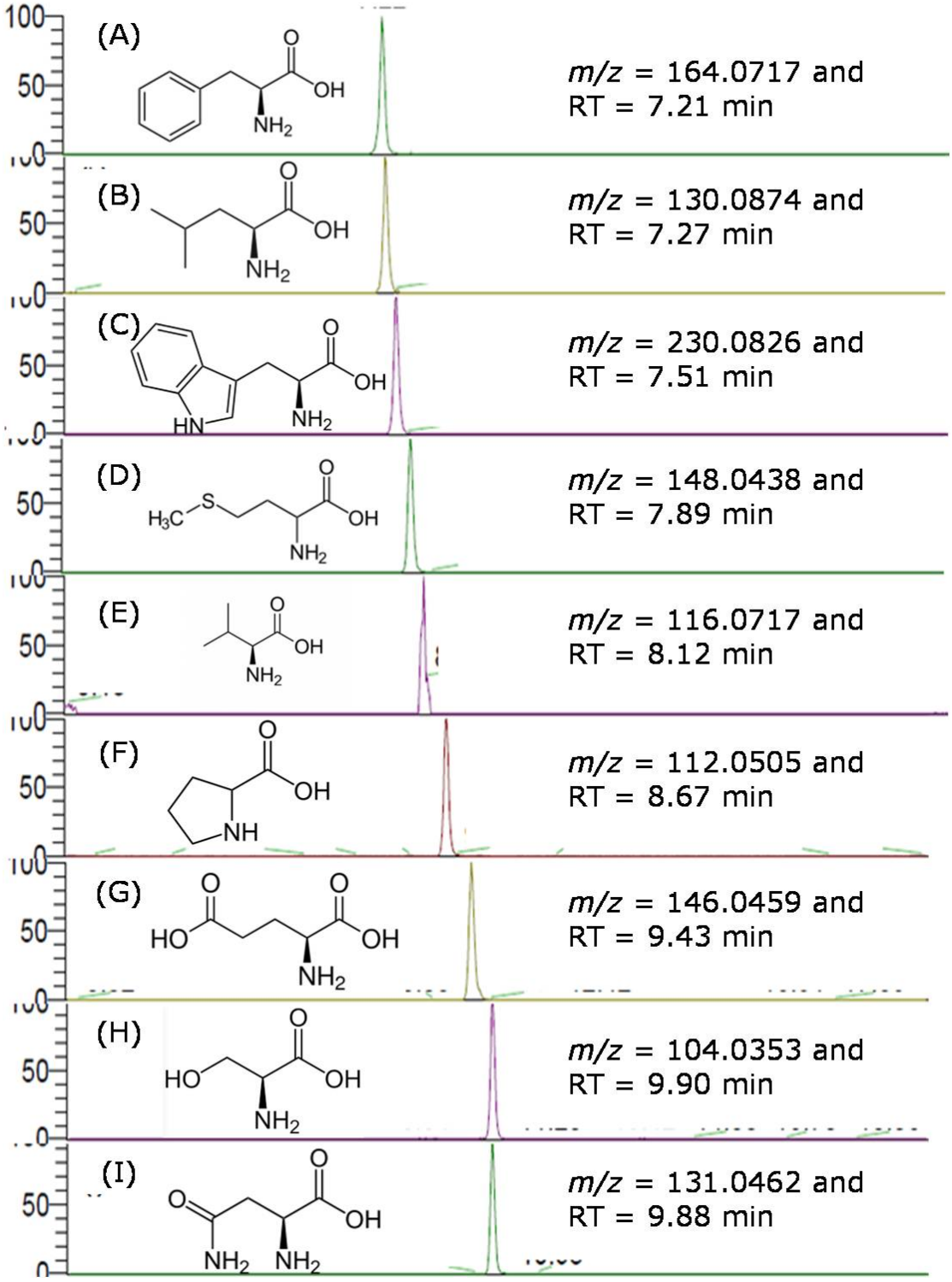


Figure 3.10 EICs of some standard L-amino acids studied by using HILIC-MS method: (A) phenylalanine, (B) leucine, (C) tryptophan, (D) methionine, (E) valine, (F) proline, (G) glutamic acid, (H) serine and (I) asparagine. (RT = Retention time) .

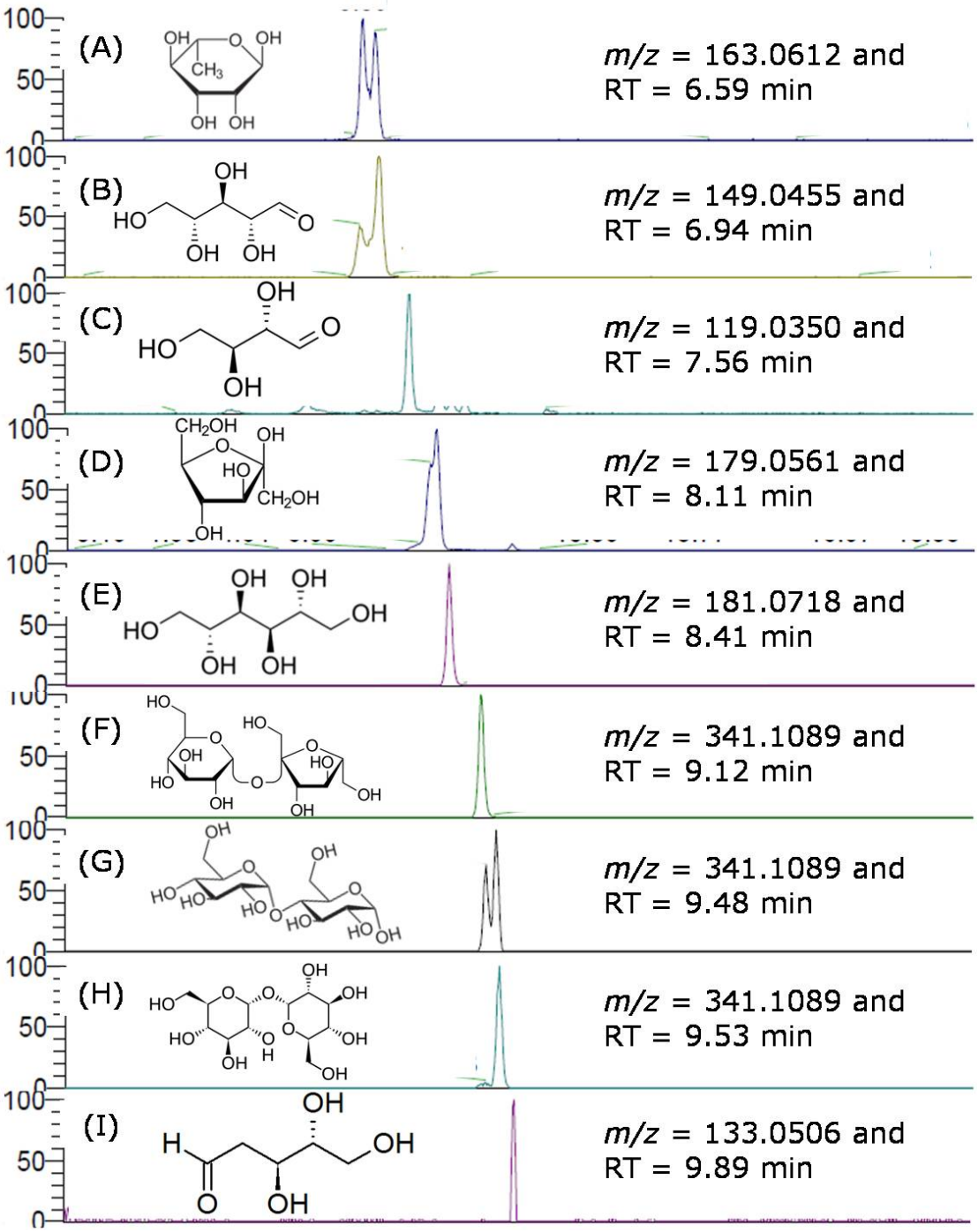


Figure 3.11 EICs of some standard sugars by using HILIC-MS method: (A) DL-rhamnose, (B) DL-ribose, (C) D-erythrose, (D) DL-fructose, (E) D-manitol, (F) sucrose, (G) DL-maltose, (H) trehalose and (I) deoxyribose.

3.5.2.3 Method validation

Raw data obtained from HILIC-MS/QToF were processed with MarkerLynx. Across the replicate (n =6), the percentage of relative standard deviations (%RSD) of the retention times and peak areas were used to investigate intra-day variation for all detected metabolites, as listed in Tables 3.2. Inter-day variation for detected metabolites was determined in replicate (n = 6) over three different days. In practice, the percentage of relative standard deviation should be within 15% and should not deviate by more than 20%. For intra-day and inter-day reproducibility, most of the detected metabolites were less than 15%.

Table 3.2 Reproducibility expressed as percentage of relative standard deviation

Compound Name	Peak area (n =6)	
	%RSD Intra-day	%RSD Inter-day
(R)-2-Hydroxyglutarate	4.88	16.45
(R)-3-Hydroxybutanoate	2.28	12.46
(R)-Lactate	2.53	11.31
(S)-Malate	5.96	22.31
1-Naphthylacetic acid	2.69	12.92
2-Hydroxy isobutyric acid	11.11	26.16
2-Hydroxyhippuric acid	10.77	19.48
2-Methylcitrate	10.62	14.95
2-oxobutanoate	0.93	11.68
2-Oxoglutarate	10.86	15.67
2-Phenylglycine	14.09	15.67
3_4-Dihydroxyphenylacetate	5.82	12.06
3'_5'-Cyclic AMP	4.92	11.01
3-Hydroxyphenylacetate	3.44	13.97
3-Methylhistidine	7.67	13.19
4-Aminobutanoate	9.41	10.44
4-Hydroxyphenyacetate	18.75	22.67
6-Phospho-D-gluconate	12.37	24.68
Adenine	2.51	14.67
AMP	2.49	15.78
ascorbate	18.88	24.82
Benzoate	18.64	19.91
Betaine	14.75	14.70
CDP	17.74	23.08
cis-Aconitate	1.06	12.62
CMP	13.32	13.52
Creatine	15.69	17.20
Creatinine	15.02	17.62
Cytidine	8.53	12.99
cytosine	9.52	13.15
D-Arabinose	8.47	14.33
Deoxyadenosine	19.80	20.22
Deoxyribose	9.03	13.26
Deoxyuridine	3.12	13.71
D-Erythrose	5.09	9.71
D-Fructose	17.59	24.79

Table 3.2 (Cont.) Reproducibility expressed as percentage of relative standard deviation

Compound Name	Peak area (n =6)	
	%RSD Intra-day	%RSD Inter-day
D-Fructose 6-phosphate	18.25	20.77
D-Galactarate	9.67	11.20
D-Galacturonate	6.39	8.71
D-Gluconic acid	7.44	12.06
D-Glucosamine	12.15	20.80
D-glucose 6-phosphate	16.40	22.63
dGMP	16.43	24.79
DL-Glyceraldehyde 3-phosphate	18.49	22.09
D-Mannitol	16.79	25.65
D-Ribose	10.30	11.30
D-ribose 5-phosphate	11.13	17.71
Ethanolamine phosphate	9.79	12.45
Folate	4.37	11.96
Fumarate	4.69	15.65
Gallate	15.57	18.22
GDP	17.17	23.18
Glutathione	12.86	15.23
Glyceraldehyde	5.24	12.09
Glycine	10.68	11.27
Glycolate	3.18	8.02
Glycylglycine	13.63	14.34
Glyoxylate	5.68	11.93
GMP	17.65	24.27
Guanine	8.59	11.27
Hippuric acid	4.62	13.14
Homocystine	12.21	12.89
Hypoxanthine	12.02	17.69
Imidazole-4-acetate	3.31	8.75
IMP	11.29	15.16
Inosine	2.72	6.87
Isocitric acid	9.77	13.21
L-2,4-Diaminobutanoate	19.59	21.72
L-Alanine	7.78	11.96
L-Arginine	10.38	14.57
L-Asparagine	6.03	10.87
L-Aspartate	3.60	11.97
L-Carnitine	18.12	19.71
L-Citrulline	10.79	11.30

Table 3.2 (Cont.) Reproducibility expressed as percentage of relative standard deviation

Compound Name	Peak area (n = 6)	
	%RSD Intra-day	%RSD Inter-day
L-Cysteate	7.01	11.27
L-Cysteine	18.84	22.48
L-Cystine	8.37	19.06
L-Glutamate	7.32	11.53
L-Histidine	7.22	14.21
L-Homocysteine	5.91	11.24
L-isoleucine	2.07	13.64
L-Leucine	5.47	10.12
L-Lysine	3.52	17.91
L-Methionine	3.70	14.23
L-Ornithine	7.24	12.35
L-Phenylalanine	4.62	14.92
L-Rhamnose	5.77	12.59
L-Serine	5.83	10.68
L-Threonine	4.74	13.73
L-Tryptophan	5.68	14.36
L-Tyrosine	0.54	7.05
L-Valine	1.88	8.51
Malonate	3.21	10.30
Maltose	8.22	14.16
Melatonin	7.92	10.38
meso-2_6-Diaminoheptanedioate	8.66	11.88
Methylguanidine	11.61	12.48
Methylmalonate	2.27	7.49
Myoinositol	7.96	17.79
N2-Acetyl-L-lysine	2.55	11.11
N-Acetyl-D-glucosamine	5.92	13.24
Nicotinamide	6.29	13.78
Orotate	8.31	13.60
Phenolsulfonphthalein	3.98	4.05
Phosphoenolpyruvate	9.50	10.56
Phthalate	7.00	13.54
Pyridoxine	2.21	12.56
Pyruvate	7.71	10.53
S-Adenosyl-L-homocysteine	6.40	12.14
Selenomethionine	3.76	8.76
Serotonin	6.23	14.46

Table 3.2 (Cont.) Reproducibility expressed as percentage of relative standard deviation

Compound Name	Peak area (n =6)	
	%RSD Intra-day	%RSD Inter-day
sn-Glycero-3-Phosphocholine	3.46	13.42
Succinate	7.05	12.25
Sucrose	4.72	11.30
Taurine	5.94	6.86
trans-4-Hydroxy-L-proline	4.76	9.03
Trehalose	5.22	14.82
Trehalose	5.22	14.82
UDP	15.11	18.22
UMP	21.39	27.85
Uric acid	9.68	13.89
Uridine	4.40	12.18
Xanthine	5.84	11.40

CHAPTER IV: EFFECTS OF ANTIPSYCHOTIC DRUGS APPLIED TO HUMAN MICROVASCULAR ENDOTHELIAL CELLS ON THE INTRACELLULAR METABOLOME

4.1 ABSTRACT

The effects of antipsychotics at high therapeutic dosage on blood brain barrier (BBB) dysfunction and breakdown remain unknown. Cell-based metabolomics using a liquid chromatography-mass spectrometry (LC-MS) approach was employed on human microvascular endothelial cells (HMVECs) from BBB treated with chlorpromazine, clozapine, haloperidol and risperidone to explore changes in the intracellular metabolome change. The significantly altered lipids and metabolites were associated with mitochondrial function and oxidative stress responses. It is proposed that chlorpromazine, clozapine, haloperidol and risperidone at high therapeutic dosage could affect the bioenergetics pathway due to mitochondrial dysfunction resulting in ketoacidosis and oxide stress by reactive oxygen species generation in HMVECs. This might address why antipsychotics could induce dysfunction and breakdown of the BBB.

Keywords: antipsychotics, blood brain barrier, cell-based metabolomics, liquid chromatography-mass spectrometry, mitochondria, oxidative stress

4.2 INTRODUCTION

Antipsychotics have been widely used and play a role in treating mental health illnesses such as schizophrenia and bipolar disorder (157–159). Antipsychotics are normally classified as typical (first generation) or atypical (second generation) (160–162). The two classes block off central dopaminergic and serotonergic pathways (86); however, atypical antipsychotics provide important modulation of serotonergic neurotransmission (70). While such antipsychotics have proven effective in schizophrenia and bipolar disorder treatment, the pattern of antipsychotic neurotoxicity and other central nervous system (CNS) side effects when taken in high therapeutic doses is not clearly understood. A possible major concern and contributor to the neurotoxicity of high dosage therapeutic antipsychotics could be due to antipsychotics affecting the transport properties of the blood brain barrier (BBB) causing BBB dysfunction and/or breakdown (86,92).

The BBB is a complex vascular structure that physically and physiologically separates the peripheral blood circulation from the central nervous system (CNS). It acts very effectively in maintaining brain homeostasis, regulating influx and efflux transport of nutrients, and protecting the CNS from pathogens and toxins (89,163,164). The basic anatomy of the BBB consists of brain microvascular endothelial cells (HMVECs), pericytes, astrocyte foot

processes and nerve endings as shown in Figure 4.1. Although, these four structures contribute to the function of the microvasculatures in the brain, the permeability of the BBB is controlled only by the HMVECs (89).

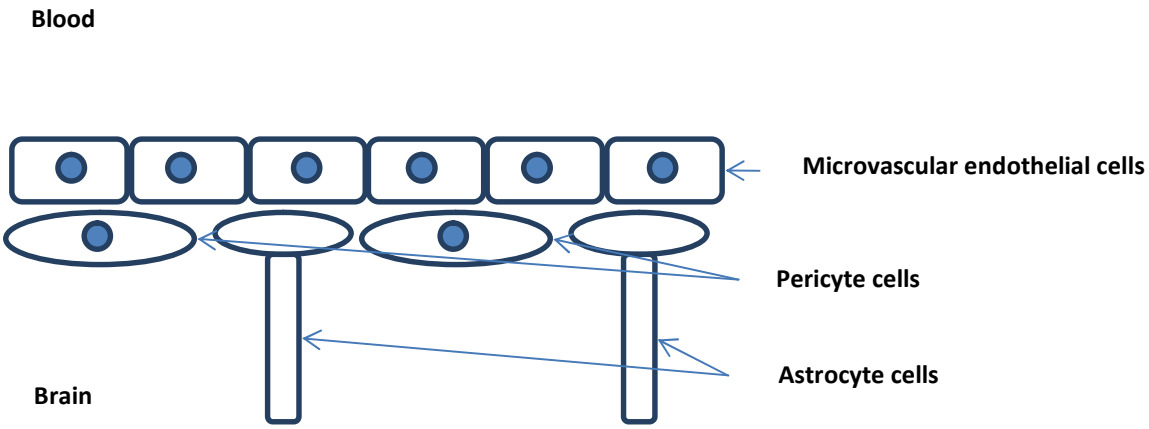


Figure 4.1 Simple diagram of anatomical structure of the blood brain barrier (adapted from reference (165)).

HMVECs are endowed with a requisite network of specific transport systems to shuttle essential nutrients and metabolites across the BBB including tight junctions, expression of nutrient transporters, and polarised efflux transporter activity (166). The tight junctions and nutrient transporters limit the passive diffusion of nutrients, drugs, and other molecules from the bloodstream into the brain. In contrast, the efflux transporters diffuse small lipophilic and toxic molecules form the brain back to the bloodstream (167). Therefore, breakdown and dysfunction of the BBB are associated with HMVEC

functions. Factors that can cause the breakdown and dysfunction of the BBB are varied, ranging from immune cells, pathogens, chemicals and drugs (168). Use of antipsychotics at high therapeutic dosage and other drugs have been associated with adverse effects leading to the breakdown and dysfunction of HMVECs of the BBB (86,169–171). Pardrige et al. (93) suggested that antipsychotics might be responsible for the disruptive effects of HMVECs of the BBB. Ben-Shachar et al. (92) showed that typical and atypical antipsychotics induced gross permeability changes in iron transportation within HMVECs of the BBB. Moreover, Zetterberg et al. (172) reported that antipsychotics impaired HMVECs function of the BBB in patients with bipolar disorder. Currently, Elmorsy et al. (86) have shown that at high therapeutic concentration of antipsychotics, the ability of HMVECs associated with oxidative stress, cellular ultrastructure and morphology, and viability is impaired. These events could damage the barrier functionality of the BBB. Although there is evidence to show antipsychotics at high therapeutic dosage can impair the functionality of HMVECs of the BBB, it is still not a clearly understood mechanism. Furthermore, the metabolic effects of antipsychotics at high therapeutic dosage and their metabolites have not been revealed, although this is clearly very meaningful for exploring antipsychotic mechanisms of causing the breakdown and dysfunction of the BBB. These considerations

prompted us to study the metabolic alterations induced by antipsychotics treatment at high therapeutic dosage in HMVECs.

The aim of the current study was to examine the effect of four antipsychotics (chlorpromazine, clozapine, haloperidol and risperidone) at high therapeutic dosage on HMVEC intracellular metabolome using a LC-MS metabolomics-analysis. Multiple metabolites that could facilitate our understanding of the in vitro actions and incorporation of antipsychotics were identified. This in turn could aid understanding of the breakdown and dysfunction of the BBB caused by high dose antipsychotics.

4.3 OBJECTIVES

This part of the works has three main objectives:

- to apply cell-based metabolomics using LC-MS to reveal the effects of four antipsychotics (chlorpromazine, clozapine, haloperidol and risperidone) on human microvascular endothelial cells (HMVECs) from the blood brain barrier
- to Identify the significant cellular metabolites of HMVECs that are affected by chlorpromazine, clozapine, haloperidol and risperidone
- to identify the possible pathways that are disturbed by chlorpromazine, clozapine, haloperidol and risperidone

4.4 MATERIALS AND METHODS

4.4.1 Chemicals and reagents

Mass spectrometer grade acetonitrile, chloroform, isopropanol, and methanol were purchased from VWR International Co Ltd (Leicestershire, UK), formic acid from Fisher Scientific Co Ltd (Leicestershire, UK), and ammonium acetate from Sigma-Aldrich Co Ltd (Ayrshire, UK). HPLC grade water was obtained from an ELGA system with 18.2 ՝Ω (ELGA LabWater Co Ltd, High Wycombe, UK). Chlorpromazine,haloperidol and risperidone were purchased from Sigma-Aldrich Co Ltd (Ayrshire, UK) and clozapine was obtained from Abcam Co Ltd (Cambridge, USA).

4.4.2 Study design

Cell lines were treated with

- DMSO as a control,
- 3 μM of chlorpromazine,
- 5 μM of clozapine,
- 0.7 μM of haloperidol and
- 0.8 μM of risperidone.

For 24 hours. These concentrations used in this study are near to the top of therapeutic serum levels and are similar to those measured as an overdosed in patients (86,87). Additionally, these concentrations with IC50 were used to accelerate and evoke

detectable effects of the APs within the time frame of cell division as not to be confounded by affects on cell proliferation (86). Each of the above groups has six biological replicates.

4.4.3 Human microvascular endothelia cells from blood brain barrier experiments

HMVECs were cultured by Ekramy Elmorsy (Faculty of Medicine & Health Sciences, University of Nottingham Medical School, Queen's Medical Centre, Nottingham UK). HMVECs were used in passages 21-23 at a density of 1 x 10^8 cell/ml and were cultured and maintained as described in the previous protocol (86). When 80% confluence had been achieved, unattached HMVECs and cell culture media were discarded and attached HMVECs were washed with 5 ml of PBS. Then, 10 ml of fresh cell culture media was added, followed by antipsychotics. This was then incubated for 48 hours. The cell culture media was then removed and attached HMVECs were washed with 5.00 ml of PBS followed by 0.50 ml of cold methanol (4^oC). Then a cell scraper was used to detached cells from a flask and the cell suspension was transferred to an Eppendorf tube and kept at -80^oC for further processes.

4.4.4 Metabolite extraction

To facilitate the extraction of cellular metabolites, the 0.50 ml of suspension of cell debris in each dish was transferred to an Eppendorf tube and vigorously vortexed for 5 minutes. The cell extraction was based on the method described by Bligh and Dyer (143). Briefly, 0.50 ml of 4°C chloroform and 0.50 ml of 4°C water were added to the suspension and then vortexed vigorously for 10 minutes at 4°C. Then, the suspension was centrifuged at 15,000 g for 10 minutes at 4°C. The polar (water soluble) fraction and non-polar (lipid) fraction were collected separately and transferred into fresh Eppendorf tubes and evaporated to dryness at room temperature. The dried non-polar layer was reconstituted in 50.00 µl of chloroform and methanol (1:2 v/v), and the dried aqueous layer was reconstituted in 50.00 µl of water. The reconstituted samples were centrifuged at 15,000 g for 10 minutes at 4°C to remove any cell debris. Finally, the supernatant was transferred into an HPLC vial and stored at -80°C for further analysis.

4.4.5 LC-MS analysis

As described in Chapter III, lipidomic and metabolic profiling was performed on an LC Accela^{TM} system (Thermo Scientific Ltd, Loughborough, UK) coupled with high resolution mass spectrometry (Exactive, Thermo Scientific Ltd, Loughborough, UK). Lipidomic chromatographic separations were performed on an Agilent SB C8 column (1.8 µm particle size, 2.1 x 100 mm, Crawford Scientific Ltd., Lanarkshire, UK) and metabolic chromatographic separations were performed on a C18 (2) column (2.5 µm particle size, 3 x 100 mm, Phenomenex Ltd, Cheshire, UK). The details of LC and MS conditions are summarised in Tables 4.1 and 4.2. In both lipid and polar metabolic profiling, samples were performed in six replicates, to account for any biological variability. The retention time consistency and mass accuracy were confirmed though the pooled QC samples.

Table 4.1 Details of LC conditions for lipidomic and metabolic profiling.

Systems and parameters	**Lipid profiling**			**Polar Metabolite profiling**		
LC system	Accela™ system			Accela™ system		
MS system	Exactive(R)			Exactive(R)		
Column type	Agilent SB C8 column (1.8 µm, 2.1 x 100 mm)			C18(2) column (2.5 µm, 3 x 100 mm)		
Column Temperature (°C)	40			40		
Mobile phase A	0.1% w/v Ammonium acetate in water			0.1 % v/v formic acid in water		
Mobile phase B	0.1% Ammonium acetate in mixture of acetonitrile/isopropanol (60:40 v/v)			0.1 % v/v formic acid in acetonitrile		
Gradient step	**Time (min)**	**%A**	**%B**	**Time (min)**	**%A**	**%B**
	0	75	25	0	80	20
	5	10	90	5	40	60
	10	0	100	10	20	80
	12	0	100	12	20	80
	15	75	25	15	80	20
Flow rate (µl/min)	500			500		
Sample injection volume (µl)	10			10		

Table 4.2 Details of MS parameters for lipidomic and metabolic profiling.

Parameters	**Lipid profiling**	**Polar Metabolite profiling**
Probe	A heated electrospray ionisation	A heated electrospray ionisation
Heat temperature (°C)	150	400
Capillary temperature (°C)	275	250
Flow rate of sheath gas (ml/min)	40	40
Flow rate of auxiliary gas (ml/min)	5	20
Flow rate of sweep gas (ml/min)	1	0
Spray voltage in positive mode (kV)	4.5	4.0
Spray voltage in negative mode (kV)	3.5	4.0
Scan range (*m/z*)	100-1,500	70-1,000
Resolution (Hz)	2-50,000	2-50,000
Maximum injection time (ms)	100	100

4.4.6 Data analysis

The feasibility of the method was first performed by using an Orbitrap mass spectrometer. Six replicates of each drug-treated sample were analysed by LC-MS. Typical LC-MS total ion chromatogram (TIC) of hydrophobic and hydrophic endogenous metabolite extracts analysed by LC-MS in both positive and negative ion mode (ESI +ve and –ve) are illustrated in Figure 4.2 to 4.3. Principal component analysis (PCA) and orthogonal partial least squares discriminant analysis (OPLS-DA) were employed to process the acquired LC-MS data. Samples were grouped together for OPLS-DA modelling. The PCA and OPLS-DA results were displayed as scores plots to visualise sample clustering and to indicate sample similarity. Discriminatory metabolites between the treated and the control for each antipsychotic drug were first screened with the variable importance in the projection (VIP) ranks $\geq$ 1.00 and then validated using ANOVA statistical analysis of false discovery rate (FDR) with a significant level of 0.05 for antipsychotic treatments. According to the identity check based on raw data and the features of peaks, the target masses of candidate metabolites identified in the profiling process were searched over a narrow ± 5 ppm mass window in the HMDB, METLIN and LIPIDMAP databases. The possible pathway analysis combines results from the publications to help our studies identify the most relevant pathways involved in the conditions under study. A results report was then presented

graphically as well as in a detailed table. Potential antipsychotic effects were recognised based on the identified metabolic pathways and statistics.

4.5 RESULTS

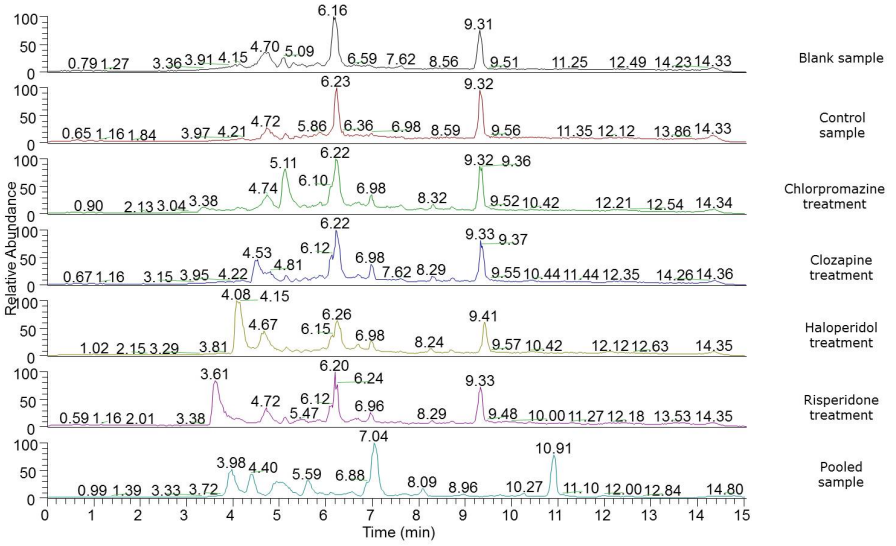
4.5.1 Data Quality

Figure 4.2 shows examples of LC-MS chromatograms of positive and negative for lipid fraction and Figure 4.3 for polar fraction. For checking the instrument performance in this study, 10 µL of cellular extraction from each HMVECs treated drug, control, and system blank were pooled to get a QC sample in both lipid and polar fractions. A number of consecutive injections of the pooled QC sample were made to obtain a stable LC-MS system (173–175). Pooled QC samples were analysed every five samples throughout the whole analysis procedure for both lipid and polar fractions.

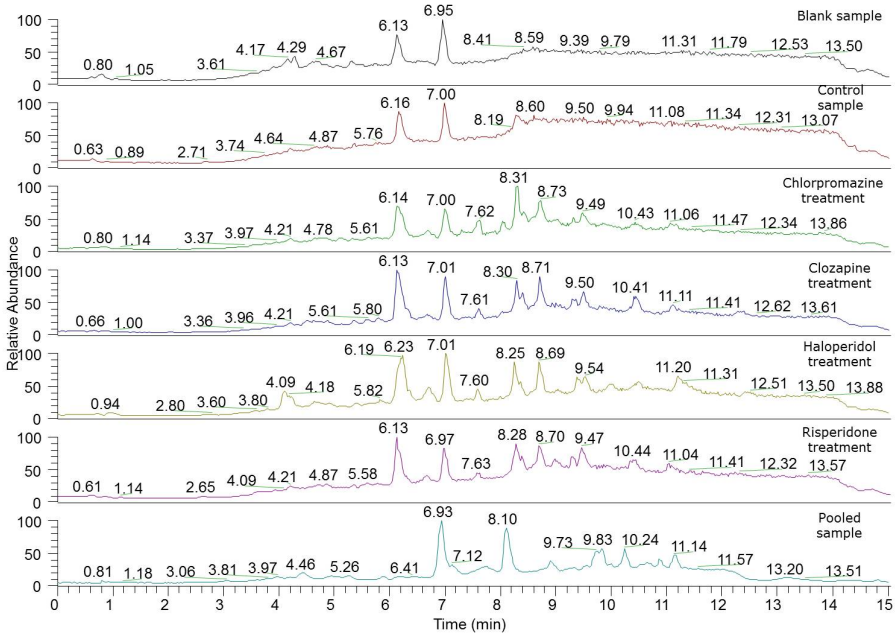
According to the optimised conditions of both lipid and polar fraction analysis, principal component analysis of pooled QC samples from HMVECs is shown in Figure 4.4 (A) for lipid fraction and Figure 4.4 (B) for polar fraction. Pooled QC samples were gathered together for analysis during the data collection. The data from the pooled QC samples of both lipid fraction and polar fraction were then analysed to determine the number of ions present in the samples, their intensity and their % RSD values. The average RSDs of peak abundance for the pooled QC samples was 17.9% with a standard deviation of 7.84% for the lipid fraction, and 22.86% with a standard deviation of 10.17% for the polar fraction. Since the recommendations of the FDA is that biochemical analysis ions

should show % RSDs less than 30, these were used in the subsequent analysis of the test and control sample data (176). Our values showing average %RSD demonstrated that the system had excellent stability during the analysis procedure for both lipid and polar fractions.

For data analysis, the aligned data array for both lipid fraction and polar fraction ion MS data were filtered using the pooled lipid and pooled polar QC samples. In line with the recommendations of the FDA for biomarker analysis ions (176), those showing %RSD less than 30 were used in the subsequent analysis of the HMVECs treated with four antipsychotics at high therapeutic dosage and control cell sample data. Thus, the pooled QC filters were prepared so that ions were present in the pooled QC samples and had a variability of lower than 30% RSD (abundance intensity). Profiling solution software produced a data array of 961 ions for lipid fraction and 860 mass ions for the polar fraction. This met the above criteria for each fraction.

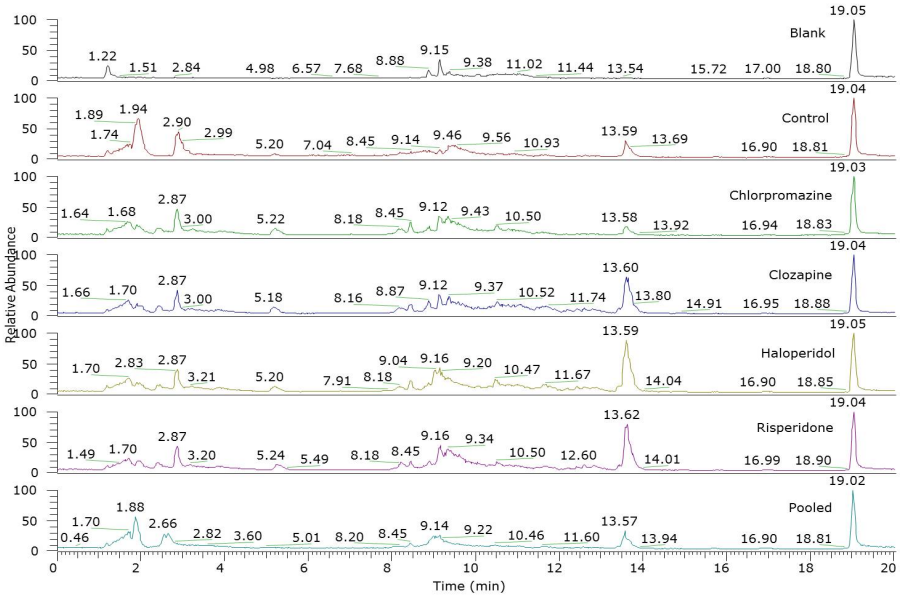


(A)

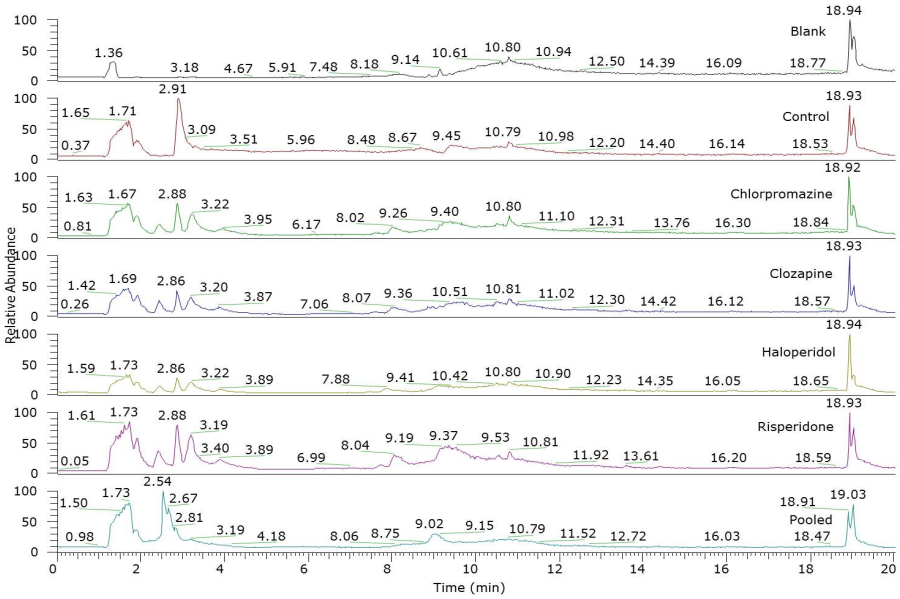


(B)

Figure 4.2 Total ion chromatogram (TIC) of hydrophobic endogenous metabolites in ESI+ve (A) and ESI-ve (B) of blank, control, chlorpromazine, clozapine, haloperidol and risperidone-treated HMVECs, and pooled samples.



(A)



(B)

Figure 4.3 Total ion chromatogram (TIC) of hydrophilic endogenous metabolites in ESI+ve (a) and ESI-ve (b) of blank, control, chlorpromazine, clozapine, haloperidol and risperidone-treated HMVECs, and pooled samples.

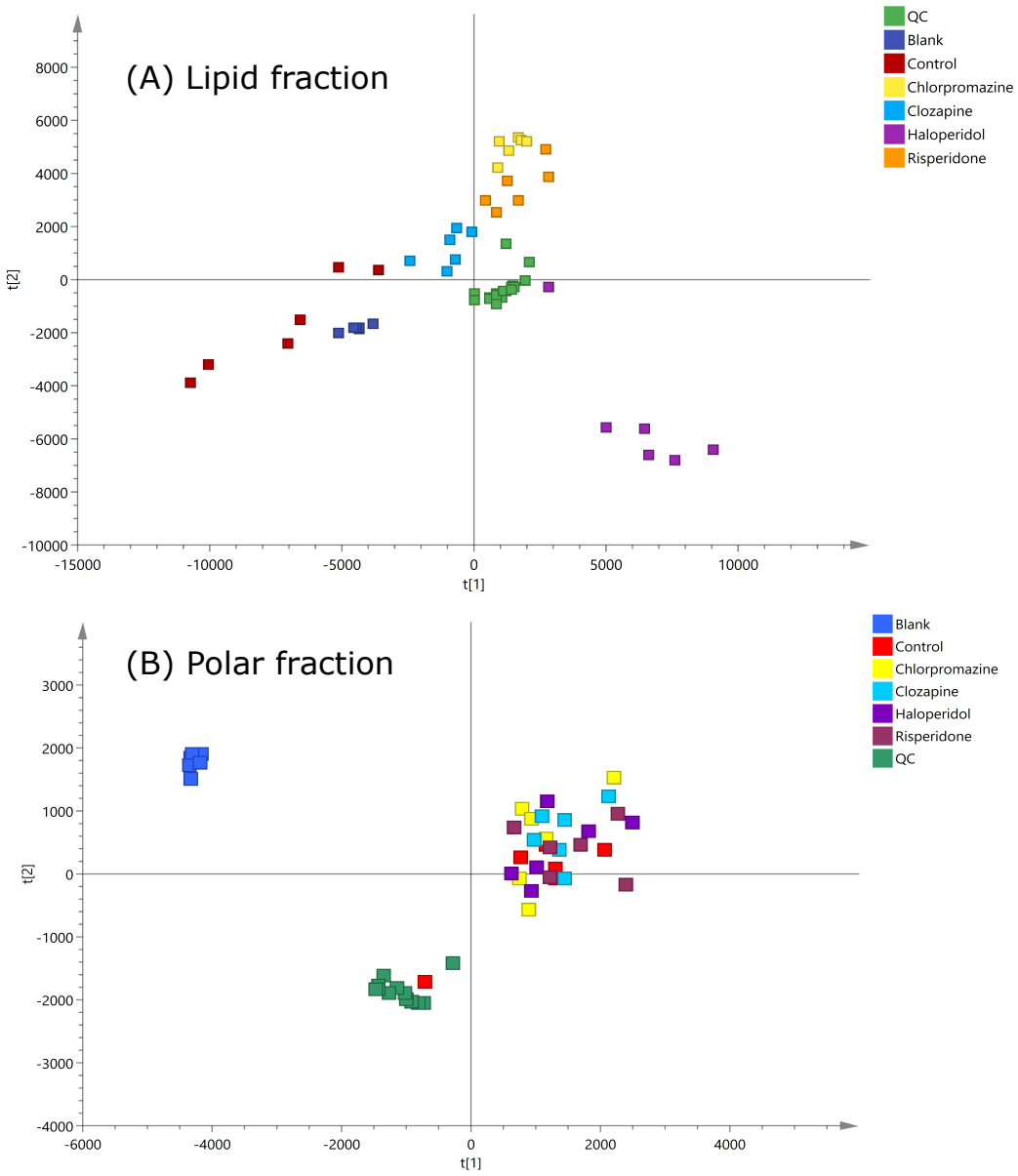


Figure 4.4 PCA scores plots of lipid fraction (A) and polar fraction (B) of human microvascular endothelia cells treated with chlorpromazine (yellow boxes), clozapine (blue boxes), haloperidol (violet boxes), and risperidone (brown boxes). Control samples, pooled samples (QC) and system blank samples are shown in red boxes, green boxes and dark blue boxes, respectively.

4.5.2 Antipsychotic drug metabolism in HMVECs

For the LC-Orbitrap/MS analysis of the four antipsychotic drugs, samples generated from incubation with human microvascular endothelial cells with high dosage of each drug were extracted by liquid extraction and concentrated by speed vacuum. The MS spectrum of the chlorpromazine $[M+H]^+$, haloperidol $[M+H]^+$, clozapine $[M+H]^+$, and risperidone $[M+H]^+$ revealed ions at *m/z* = 319.1028, 376.1473, 327.1327, and 411.2190, respectively. Of interest from the current perspective was the detection of each drug metabolism as shown in Table 4.3 with *m/z* $[M+H]^+$ at 335.0978, 305.0872, and 285.1419 in chlorpromazine-treated samples, at 392.1421 and 342.1863 in haloperidol-treated samples, at 343.1319, 313.1213, and 307.1553 in clozapine-treated samples, and at 427.2139 in risperidone-treated samples. Table 4.3 summarises possible drug metabolites of each antipsychotic and Figures 4.5 to 4.8 shows possible chemical structures.

Table 4.3 Metabolism of chlorpromazine, haloperidol, clozapine, and risperidone

Name	m/z	Adduct	RT (min.)	M.W.	Formula
Chlorpromazine	319.1028	[M+H]+	5.08	318.0957	$C_{17}H_{19}ClN_2S$
7-Hydroxy-chlorpromazine	355.0978	[M+H]+	6.72	334.8636	$C_{17}H_{19}ClN_2OS$
3-Hydroxy-chlorpromazine	355.0978	[M+H]+	6.72	334.8636	$C_{17}H_{19}ClN_2OS$
Norchlorpromazine	305.0872	[M+H]+	4.69	304.8376	$C_{16}H_{17}ClN_2S$
Chlorpromazine-N-oxide	335.0978	[M+H]+	3.37	334.0907	$C_{17}H_{19}ClN_2OS$
Promazine	285.1419	[M+H]+	4.53	284.4191	$C_{17}H_{20}N_2S$
Haloperidol	376.1473	[M+H]+	4.06	375.8642	$C_{21}H_{23}CLFNO_2$
Haloperidol-N-oxide	392.1421	[M+H]+	3.27	391.8636	$C_{21}H_{23}CLFNO_3$
Hydroxy-haloperidol	392.1434	[M+H]+	4.34	377.8801	$C_{21}H_{25}CLFNO_2$
Dechlorinated-haloperidol	342.1863	[M+H]+	3.61	341.1492	$C_{21}H_{24}FNO_2$
Clozapine	327.1327	[M+H]+	4.46	326.8233	$C_{18}H_{19}ClN_4$
Hydroxy-clozapine	343.1319	[M+H]+	3.40	342.8227	$C_{18}H_{19}ClN_4O$
Clozapine-N-oxide	343.1318	[M+H]+	6.41	342.8227	$C_{18}H_{19}ClN_4O$
Norclozapine	313.1213	[M+H]+	3.78	312.7967	$C_{17}H_{17}ClN_4$
Hydroxyl-desmethyl-clozapine	307.1553	[M+H]+	3.32	294.3510	$C_{17}H_{18}N_4O$
Risperidone	411.2190	[M+H]+	3.61	410.4845	$C_{23}H_{27}FN_4O_2$
Hydroxy-risperidone	427.2139	[M+H]+	3.67	426.4839	$C_{23}H_{27}FN_4O_3$

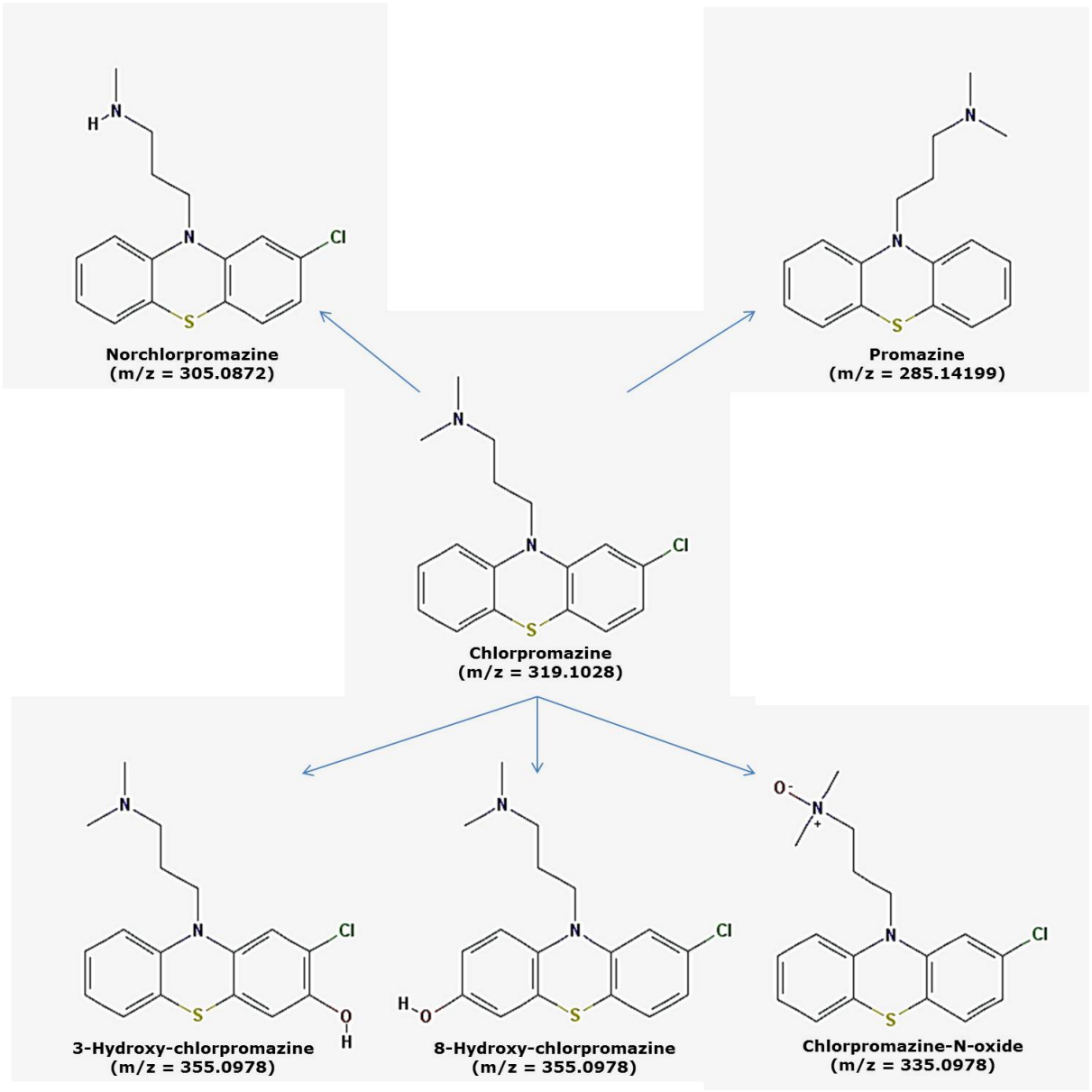


Figure 4.5 A schematic representation of the metabolism of chlorpromazine.

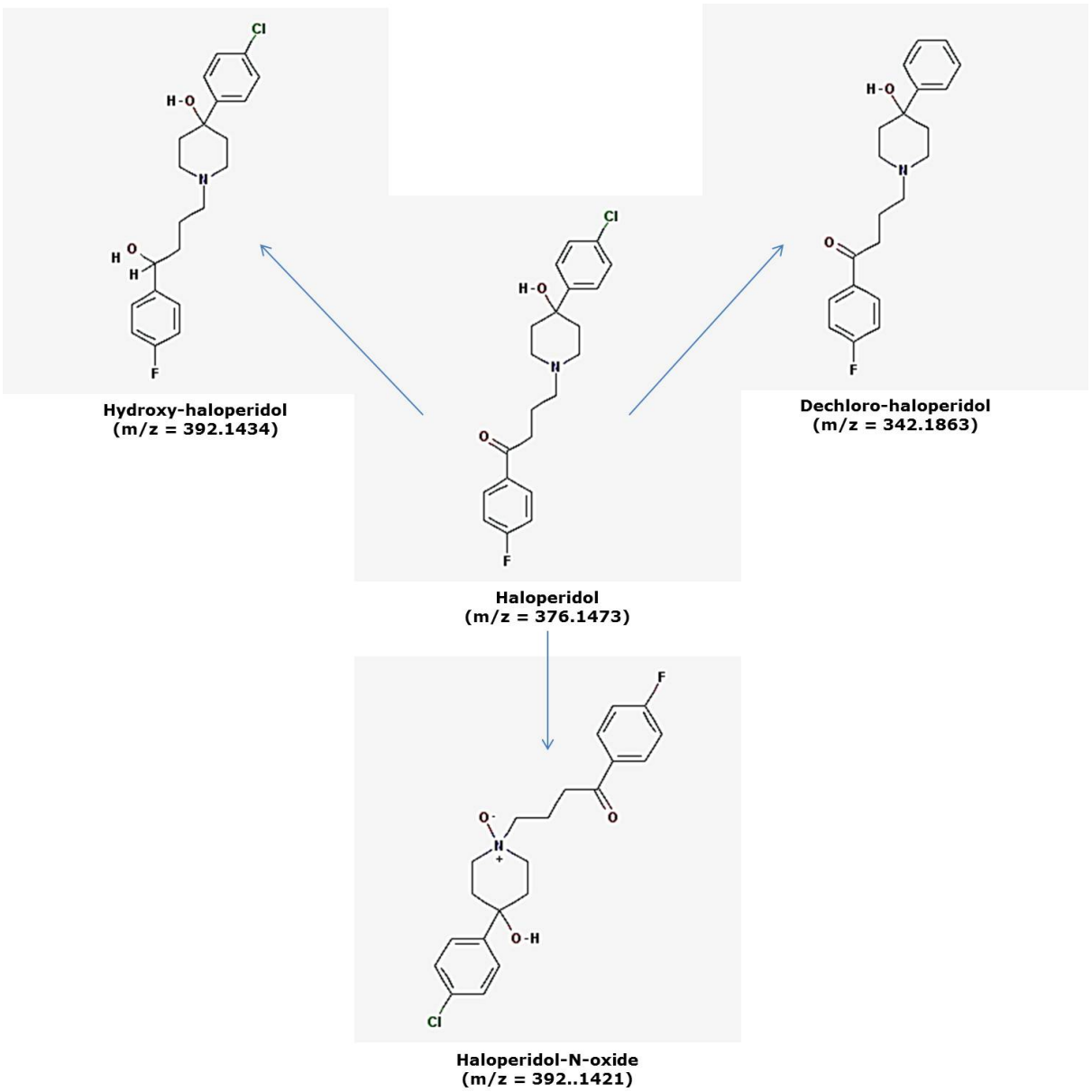


Figure 4.6 A schematic representation of the metabolism of haloperidol.

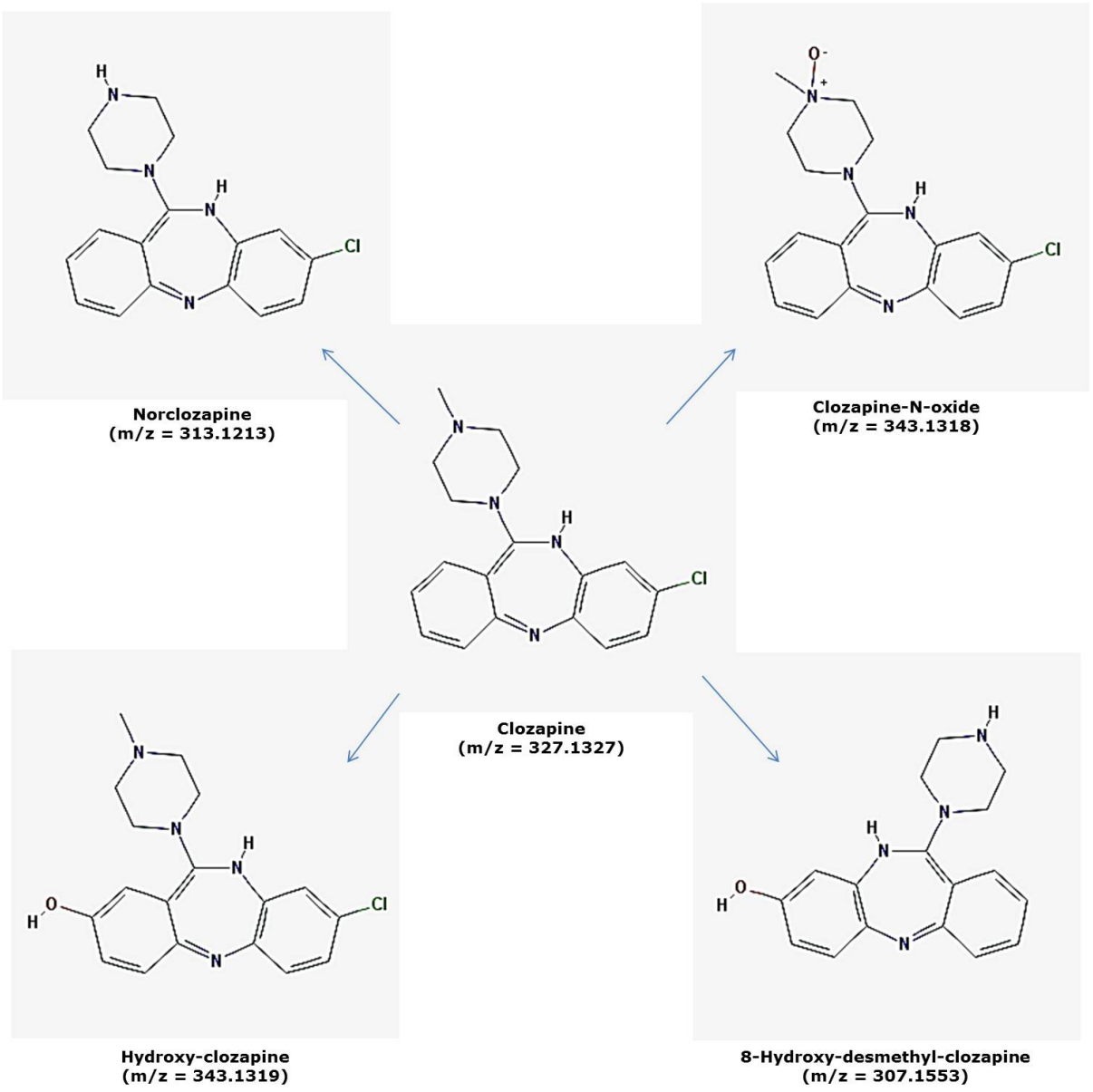


Figure 4.7 A schematic representation of the metabolism of clozapine.

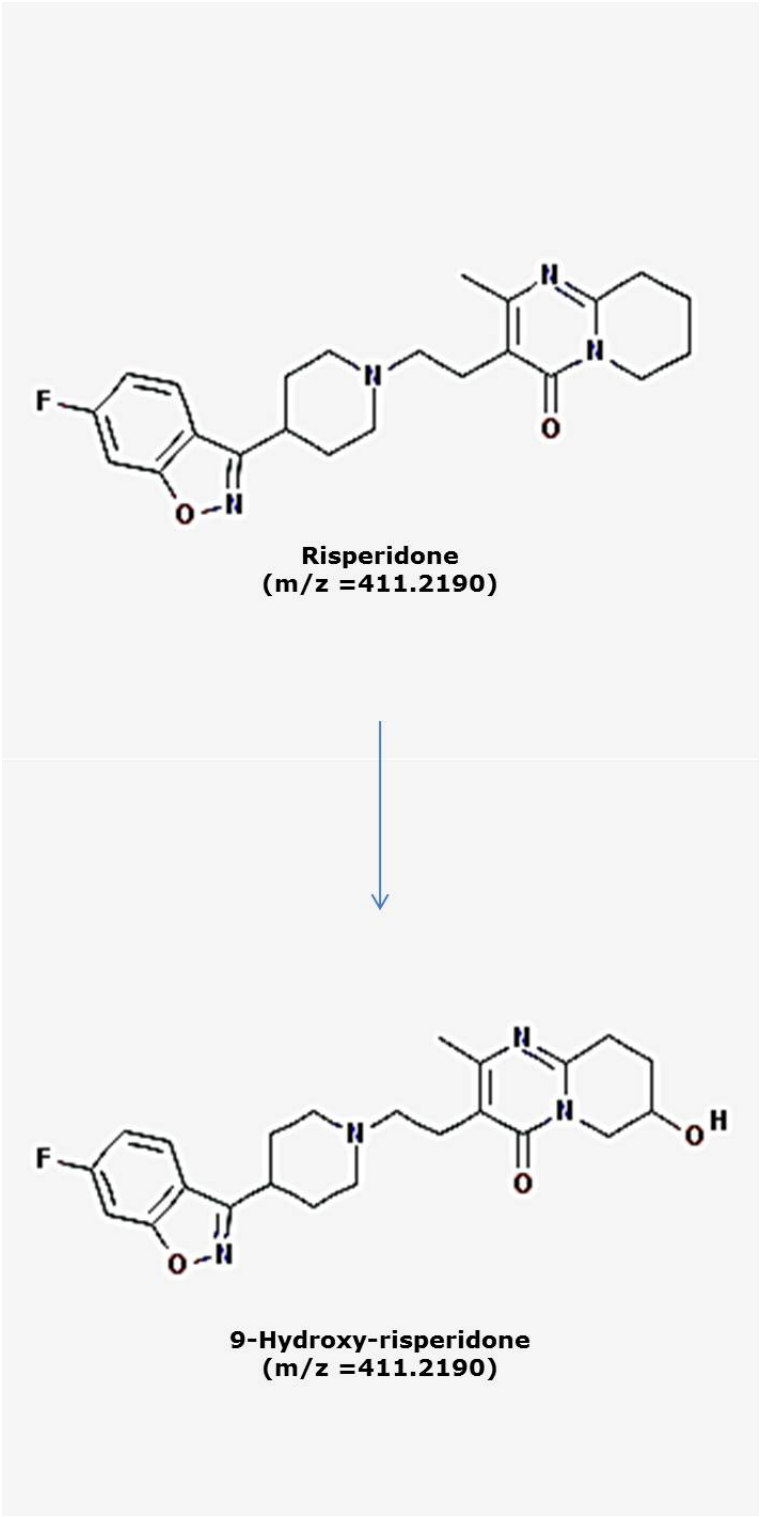


Figure 4.8 A schematic representation of the metabolism of risperidone.

4.5.3 Effects of antipsychotic drugs on lipid metabolites in HMVECs

From our data, PCA scores plots showed clear separation between control and antipsychotic treatment of HMVECs in the lipid fraction (Figure 4.3 (A)). Figure 4.9 shows that separate clusters from each model are revealed, which indicates metabolic differences in terms of level and compositional changes of cellular lipid metabolites among control, chlorpromazine treatment, clozapine treatment, haloperidol treatment and risperidone treatment. Then, OPLS-DA was applied to visualise samples in an attempt to distinguish between control and each antipsychotic treatment, which revealed a very clear separation in the lipid fraction. In order to identify which detected ions account for such a significant separation in the case of OPLS-DA modelling, VIP statistics (VIP $\geq$ 1.0) were initially used to pre-select detected mass ions. Then, from those detected mass ions with FDR (ANOVA) $\leq$ 0.05 selection was made of those which were most correlated with the OPLS-DA discriminant scores in order to decrease the risk of false positives in the selection of significantly altered mass ions. According to these criteria, the 57 identified metabolites by exact mass from antipsychotics treatment on HMVECs were obtained as being significantly different from the control. These metabolites contributed most towards discriminating the metabolic profiles between control and antipsychotic treatments

summarised in Table 4.4 and Figure 4.10 which show the top ten significant changes in levels of identified metabolites.

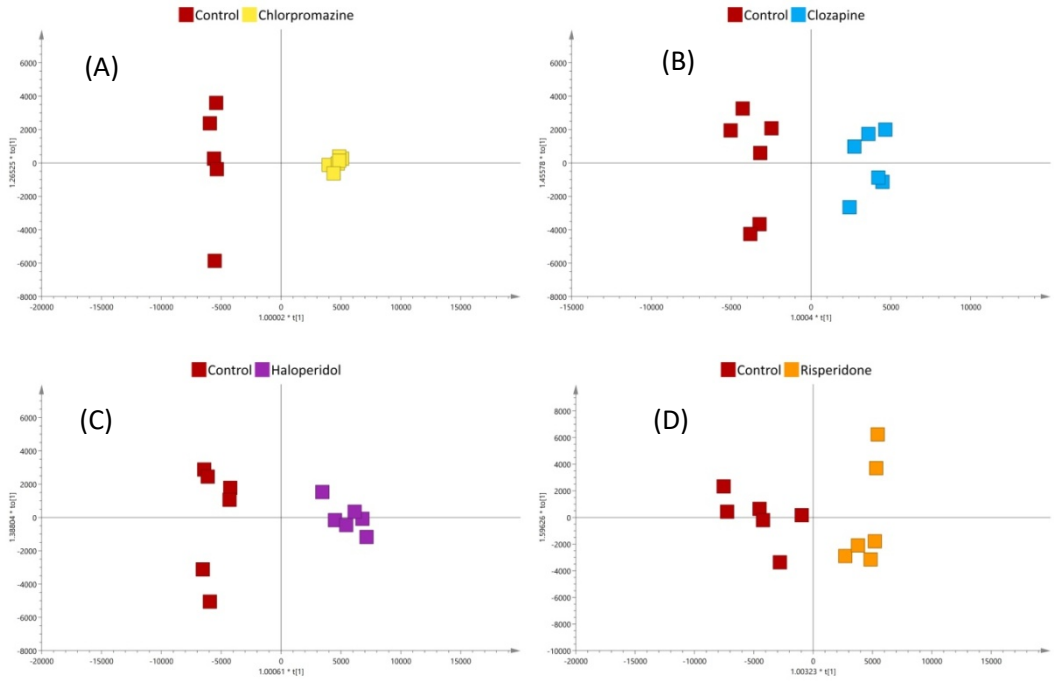


Figure 4.9 OPLS-DA of untargeted metabolomics data from HMVECs treated with antipsychotics at high therapeutic dosage in the lipid fraction. Two-dimensional OPLS-DA scores plots reveal separation between untreated cells and chlorpromazine-treated cells (A), untreated cells and clozapine-treated cells (B), untreated cells and haloperidol-treated cells (C), and untreated cells and risperidone-treated cells (D). Untreated (red boxes), chlorpromazine (yellow boxes), clozapine (blue boxes), haloperidol (violet boxes) and risperidone (brown boxes).

Table 4.4 Details of metabolites from the lipid fraction which changed significantly during treatment with chlorpromazine, clozapine, haloperidol and risperidone in HMVECs.

m/z	Annotation	Formula	Mass error (ppm)	RT (min)	Control		Chlorpromazine		Clozapine		Haloperidol		Risperidone		VIP	FDR
					Abundance	SD	Abundance	SD	Abundance	SD	Abundance	SD	Abundance	SD		
337.0945	Unidentified			3.36	2954	2535	436892	38737	77	56	152	83	356	42	1.88	0.00E+00
191.1178	N-Methylserotonin	C11H14N2O	1	3.61	2429	1232	3609	279	7538	7915	4108	532	176606	11709	1.18	2.55E-15
350.2301	Hexadecanedioic acid	C16H30O4	0	3.92	142549	67476	194912	45010	197166	37163	343190	59321	204562	69567	1.06	1.34E-06
336.2509	Palmitoylglycine	C18H35NO3	0	4.08	84439	40458	117774	20824	116844	21707	261959	48119	121426	35329	1.02	3.92E-11
165.0710	Unidentified			4.10	115	76	649	513	398	184	216748	75496	617	657	1.20	0.00E+00
270.0793	Unidentified			4.47	392	294	660	118	160721	24095	380	102	859	239	1.40	0.00E+00
329.1338	Unidentified			4.50	4359	2825	7348	1023	1303623	185970	40628	16488	9259	2462	3.98	0.00E+00
434.1528	Dimethyluric acid	C7H8N4O3	1	4.61	253	439	0	0	47	54	5957732	2443885	3176	4265	6.33	8.69E-12
354.1054	Unidentified			4.61	0	0	58	91	0	0	232063	103669	23	37	1.26	3.99E-12
840.5684	Phosphoserine	C44H84NO10P	4	4.68	38789	16662	69418	13300	5621	6083	76056	17842	157868	108032	1.07	5.29E-08
757.4727	Phosphoserine	C39H66NO10P	4	4.68	44144	31127	82960	12381	7108	8426	150440	34084	163085	90556	1.15	9.93E-10
796.5426	Phosphoserine	C42H80NO9P	4	4.68	78641	28553	128951	18454	13417	9299	142114	31911	286481	202376	1.43	4.26E-09
752.5166	Cardiolipin	C85H148O17P2	0	4.68	125668	45788	187521	30688	19053	12251	214617	46301	417885	297066	1.71	3.51E-10
713.4449	Galbeta1-4(NeuAcalpha2-3)Galbeta1-4Glcbeta-Cer(d18:1/24:1(15Z))/ GalNAcbeta1-4(KDNalpha2-3)Galbeta1-4Glcbeta-Cer(d18:1/24:1(15Z))	C71H128N2O26	0	4.70	70178	47964	127220	16992	12391	14360	228028	51097	228937	128480	1.36	6.86E-09
669.4194	Phosphatidylethanolamine	C31H60NO8P	3	4.70	94811	63917	161191	21262	24271	19195	280125	62626	278489	151291	1.48	1.76E-09
708.4908	Butyl 4'-O-butanoyl-6-O-hexadecanoyl-neohesperidoside	C36H66O12	2	4.70	204714	68840	292289	40074	36939	21555	343689	79727	643756	466748	2.12	5.36E-10
664.4627	N-(hexadecanoyl)-sphinganine-1-phosphate	C34H70NO6P	3	4.70	237819	87117	328679	50210	27359	25051	389058	97474	723292	526844	2.27	1.10E-09
537.3403	Cardiolipin	C94H146O17P2	3	4.73	74260	45080	111106	13515	24764	19492	186957	46282	177904	84053	1.15	3.29E-08
625.3922	Neurosporaxanthin β-D-glucopyranoside	C41H56O7	3	4.73	110205	73613	178809	20468	25865	24778	313967	70547	309168	166096	1.56	2.16E-08

VIP is a variable importance in the projection that shows the importance of a variable. FDR is a false discovery rate.

Table 4.4 (Cont.) Details of metabolites from the lipid fraction which changed significantly during treatment with chlorpromazine, clozapine, haloperidol and risperidone in HMVECs.

m/z	Annotation	Formula	Mass error (ppm)	RT (min)	Control		Chlorpromazine		Clozapine		Haloperidol		Risperidone		VIP	FDR
					Abundance	SD	Abundance	SD	Abundance	SD	Abundance	SD	Abundance	SD		
532.3842	26,27-diethyl-1α,25-dihydroxy-22-thiavitamin D3 / 26,27-diethyl-1α,25-dihydroxy-22-thiacholecalciferol	C30H50O3S	4	4.73	154806	55784	191848	25292	38362	23203	233906	73379	391369	257889	1.62	9.63E-09
576.4106	Trihexosylceramide (d18:1/24:1(15Z))	C60H111NO18	0	4.73	206305	72449	268793	39422	31615	27221	320322	97418	567407	397226	2.00	4.52E-09
620.4369	Lysophosphoethanolamine	C27H56NO7P	5	4.73	248294	89363	329760	47560	30457	28543	392198	105124	714601	515033	2.25	3.70E-09
581.3661	Unidentified			4.73	94159	62847	149428	18156	24158	23696	261928	62302	249381	126365	1.39	6.69E-08
488.3580	Thyroxine glucuronide	C21H19I4NO10	0	4.75	102381	38703	132758	14306	40464	17220	165822	46419	246661	146138	1.25	2.53E-08
569.2147	8Z,11Z,14Z-eicosatrienoyl-CoA	C44H72N7O17P3S	3	4.96	0	0	34	82	0	0	205485	90202	13	21	1.18	1.69E-13
567.2176	7-Methylinosine	C11H15N4O5	3	4.96	0	0	44	85	0	0	274250	119380	64	102	1.37	1.25E-11
452.1786	Unidentified			5.05	0	0	0	0	0	0	179413	79202	10	15	1.11	0.00E+00
280.2635	Linoleamide	C18H33NO	0	5.14	215317	129030	206596	51090	328347	77117	446364	102814	360439	146812	1.32	6.86E-05
298.2739	Palmitoleoyl Ethanolamide	C18H35NO2	0	5.14	229372	136097	216600	55680	350344	80123	477430	107306	383848	155374	1.37	3.59E-05
321.0997	Unidentified			5.14	15127	16075	2730780	210552	729	174	938	358	2604	508	4.73	0.00E+00
681.3497	Unidentified			5.23	42	32	81	50	103	54	316466	151407	846	235	1.46	0.00E+00
430.1943	Normetanephrine/Epinephrine	C9H13NO3	1	5.28	0	0	0	0	1	1	218082	93994	275	125	1.22	0.00E+00
695.3104	N2-Succinyl-L-ornithine	C9H16N2O5	0	6.09	144615	111219	433367	89864	406583	135064	336365	35478	446877	159787	1.74	1.86E-04
892.5616	Phosphatidylethanolamine	C47H72NO8P	2	6.12	73036	61258	242936	48933	210764	70229	200175	41270	216803	98959	1.26	6.52E-04
695.3584	25-O-(2''-beta-D-glucopyranosyl-beta-D-glucopyranosyl)-25-hydroxy-11E-eicosenoic acid/3-O-(alpha-L-rhamnopyranosyl-(1-2)-alpha-L-rhamnopyranosyl)-3-hydroxydecanoyl-3-hydroxydecanoic acid	C32H58O13	0	6.12	722884	403885	1661030	293589	1610924	424216	1201025	219261	1727060	400459	3.11	1.10E-02
637.3055	D-Pantethine	C22H42N4O8S2	1	6.12	909435	720509	2873438	645097	2713069	955412	2077931	303355	3064660	1173915	4.57	4.28E-04
659.2872	Unidentified			6.14	101067	73015	221520	38318	222949	60585	184136	18964	256889	67408	1.19	1.56E-03
918.5774	Phosphatidylethanolamine	C49H74NO8P	2	6.16	90793	89864	287386	51028	259902	104885	222132	21804	309457	129868	1.41	1.25E-03

VIP is a variable importance in the projection that shows the importance of a variable. FDR is a false discovery rate.

Table 4.4 (Cont.) Details of metabolites from the lipid fraction which changed significantly during treatment with chlorpromazine, clozapine, haloperidol and risperidone in HMVECs.

m/z	Annotation	Formula	Mass error (ppm)	RT (min)	Control		Chlorpromazine		Clozapine		Haloperidol		Risperidone		VIP	FDR
					Abundance	SD	Abundance	SD	Abundance	SD	Abundance	SD	Abundance	SD		
575.5033	Diacylglycerols	C37H68O5	1	6.16	72734	49494	586484	78548	369102	96840	543159	198198	154325	54501	2.12	2.18E-10
601.5188	Diacylglycerols	C39H70O5	1	6.27	116313	79281	668440	132463	492515	143591	829349	300307	285682	106693	2.34	1.21E-07
627.5349	1-(9Z,12Z,15Z-octadecatrienoyl)-2-(11Z-eicosenoyl)-sn-glycerol	C41H72O5	0	6.68	296878	227745	947254	203221	829398	229276	1107197	295982	619451	274282	2.51	5.10E-04
391.2841	12-Ketodeoxycholic acid/7-Hydroxy-3-oxocholanoic acid/Nutriacholic acid	C24H38O4	0	7.00	112107	70274	309363	43871	303795	88320	249009	32553	295398	78310	1.44	6.86E-05
149.0233	Unidentified			7.00	72241	45460	201857	31022	202854	64516	166432	23509	197778	52238	1.19	5.17E-05
906.5489	Phosphoserine	C49H82NO12P	1	7.28	965	551	215835	76166	59625	13997	5126	1917	2116	575	1.27	0.00E+00
966.6177	Phosphatidylethanolamine	C52H92NO10P	1	7.30	51	91	171175	77117	46633	11554	1301	940	111	126	1.12	3.62E-10
605.5501	Diacylglycerols	C39H74O5	1	7.37	78625	44497	295142	87221	220538	58979	280380	72631	122511	53772	1.36	5.38E-05
577.5185	Diacylglycerols	C37H70O5	1	7.44	2376	1853	135971	44152	51540	11538	8743	2169	4586	1487	1.01	1.11E-16
653.5718	1,2-didodecanoyl-3-tridecanoyl-sn-glycerol	C40H76O6	0	7.54	26357	13445	173044	41292	87270	19328	60768	18741	44750	12569	1.04	2.29E-11
858.5468	Phosphatidylcholine	C52H80NO8P	3	7.58	3890	430	321912	114925	79931	18168	9825	2908	4520	1074	1.54	0.00E+00
918.6176	1-(11Z-docosenoyl)-2-(4Z,7Z,10Z,13Z,16Z,19Z-docosahexaenoyl)-glycero-3-phospho-(1'-sn-glycerol)/1-(4Z,7Z,10Z,13Z,16Z,19Z-docosahexaenoyl)-2-(11Z-docosenoyl)-glycero-3-phospho-(1'-sn-glycerol)	C50H85O10P	4	7.58	168	236	188177	85338	44421	10205	1579	840	140	171	1.17	9.63E-07
860.5706	Ceramide 1-phosphate	C46H90NO6P	1	7.61	6340	6731	139879	44915	35146	8866	6702	3797	2349	1738	1.00	1.15E-09
682.5608	N-(hexadecanoyl)-1-beta-glucosyl-sphing-4-enine	C40H77NO8	1	7.61	174114	112197	445423	31619	358938	89332	294848	42307	302495	78415	1.48	1.75E-03
603.5340	TG(12:0/12:0/12:0)	C39H74O6	2	7.61	10176	5567	355682	108425	120908	30654	20500	7656	13567	3599	1.62	8.09E-12
862.5882	Phosphoserine	C45H88NO9P	3	8.03	12562	5734	150232	49274	67417	12967	13015	3961	10681	7321	1.03	1.54E-12
920.6319	Phosphoserine	C48H94NO10P	0	8.05	423	405	424629	206493	104969	26656	6394	3576	467	291	1.75	1.67E-08
824.5408	Phosphoserine	C45H80NO10P	4	8.28	17273	10533	269429	101962	74283	30524	53296	17031	30445	6198	1.30	1.16E-11

VIP is a variable importance in the projection that shows the importance of a variable. FDR is a false discovery rate.

Table 4.4 (Cont.) Details of metabolites from the lipid fraction which changed significantly during treatment with chlorpromazine, clozapine, haloperidol and risperidone in HMVECs.

m/z	Annotation	Formula	Mass error (ppm)	RT (min)	Control		Chlorpromazine		Clozapine		Haloperidol		Risperidone		VIP	FDR
					Abundance	SD	Abundance	SD	Abundance	SD	Abundance	SD	Abundance	SD		
577.5195	Diacylglycerols	C37H70O5	1	8.30	52688	34833	266378	60515	148745	36269	167193	30601	114633	30039	1.22	2.57E-07
651.5778	Unidentified			8.40	124817	66284	266097	47008	225901	46333	255403	45432	201155	58510	1.07	3.37E-04
603.5349	1,2-Dioleoyl-sn-glycerol	C39H72O5	0	8.54	125642	52336	731431	156063	392260	79035	334822	114351	190700	39899	2.07	4.53E-08
800.5418	Phosphoserine	C43H80NO10P	3	8.70	46378	20721	576428	230362	182182	52906	141847	55512	76759	15698	1.83	1.51E-08
536.5039	N-Palmitoylsphingosine	C34H67NO3	1	8.71	121227	97150	433533	117004	408113	140791	458071	107568	347948	107213	1.77	5.27E-05
520.5091	Linolenyl palmitate	C34H62O2	0	8.72	204958	148226	670015	150229	650160	204911	700654	155568	567790	168898	2.22	5.27E-05
596.5721	Unidentified			8.72	90885	65862	279610	56552	292559	88981	308896	75394	268801	66222	1.50	3.80E-05
970.7168	N-(docosanoyl)-1-β-lactosyl-sphinganine	C52H101NO13	0	9.04	73969	60518	177847	41171	167812	57567	135994	20323	198182	85231	1.04	1.03E-02
972.7345	Galabiosylceramide/Lactosylceramide	C54H101NO13	0	9.06	97066	83951	236138	59102	214737	68740	173102	28256	245743	111903	1.17	1.74E-02
808.6656	Galactosylceramide/Glucosylceramide	C48H91NO8	2	9.49	171901	142013	445123	89313	386872	133301	328603	79201	464124	201245	1.61	4.94E-03
832.6603	Phosphocholine	C50H94NO8P	1	9.50	204450	129997	466403	63409	419480	134858	347082	63746	470101	166105	1.59	1.40E-02
810.6775	1-(2E,6E-phytadienyl)-2-(2E,6E-phytadienyl)-sn-glycero-3-phosphocholine	C48H92NO6P	4	9.50	277932	206537	688196	133605	592504	184393	514349	107960	679798	273592	1.95	8.78E-03
701.5113	Phosphatidic acid	C39H75O8P	1	11.02	52773	35630	193857	33293	88716	16853	153701	88321	79965	18643	1.04	1.45E-02
727.5271	Phosphatidic acid	C41H77O8P	1	11.44	50077	29283	225943	43335	101905	25927	160046	84709	86224	19188	1.15	1.69E-03

VIP is a variable importance in the projection that shows the importance of a variable. FDR is a false discovery rate.

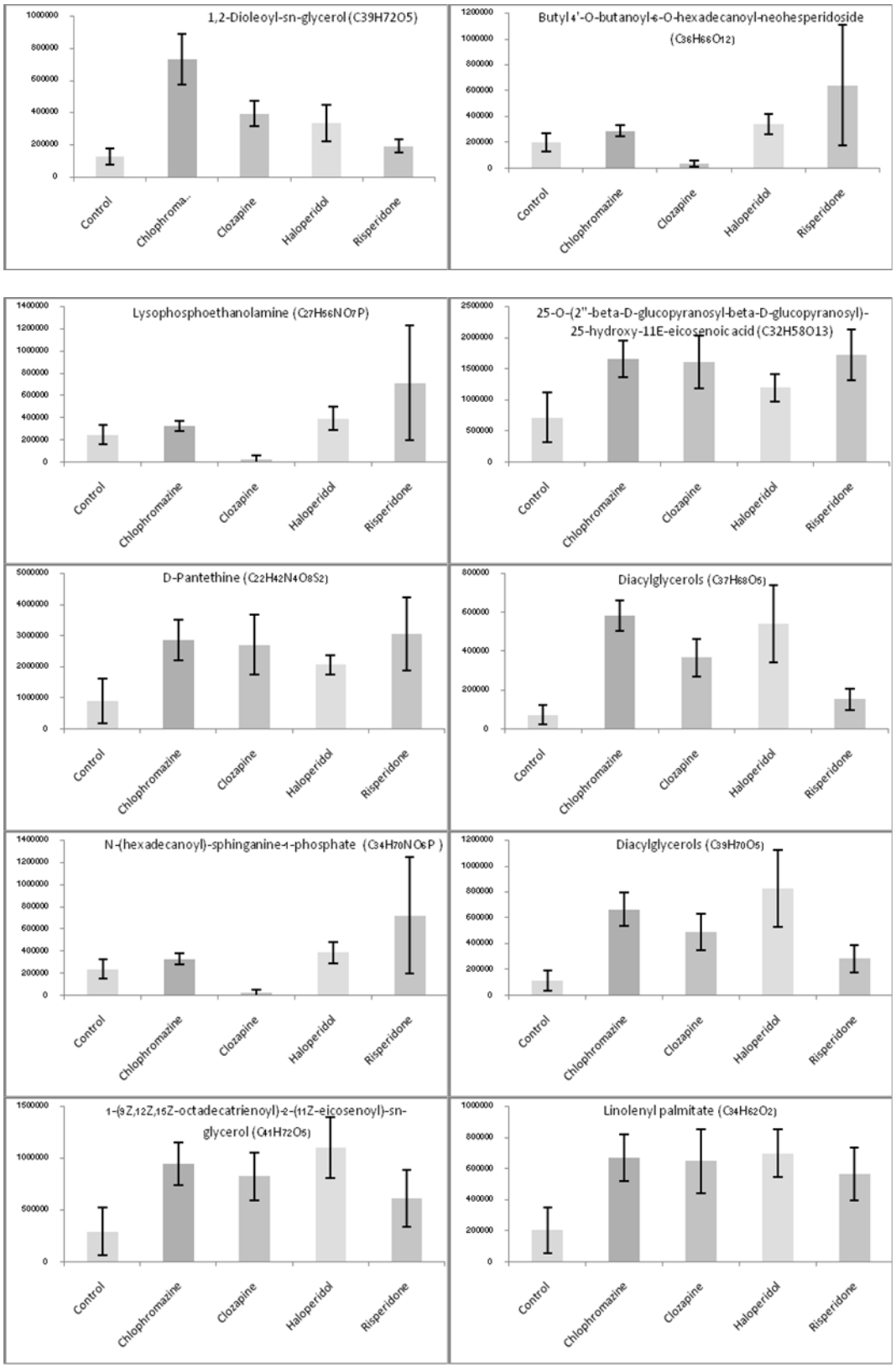


Figure 4.10 Level changes of the top ten significantly-changed metabolites from the lipid fraction in HMVECs treated with chlorpromazine, clozapine, haloperidol and risperidone and untreated HMVECs.

Interestingly, all of the top significant metabolites detected were found to be hydrophobic compounds. There were five lipid compounds (25-O-(2''-beta-D-glucopyranosyl-beta-D-glucopyranosyl)-25-hydroxy-11E-eicosenoic acid or 3-O-(alpha-L-rhamnopyranosyl-(1-2)-alpha-L-rhamnopyranosyl)-3-hydroxydecanoyl-3-hydroxydecanoic acid, 2 diacylglycerols, 1-(9Z,12Z,15Z-octadecatrienoyl)-2-(11Z-eicosenoyl)-sn-glycerol, and linolenyl palmitate that were significantly and similarly changed by all antipsychotics treated HMVECs. Butyl 4'-O-butanoyl-6-O-hexadecanoyl-neohesperidoside, N-(hexadecanoyl)-sphinganine-1-phosphate and lysophosphoethanolamine were found to be significantly increased in chlorpromazine-, haloperidol- and risperidone-treated cells while these lipids were significantly decreased in the clozapine treatment group. In addition, D-pantethine was significantly changed in all of the antipsychotic treatments.

4.5.4 Effects of antipsychotic drugs on polar metabolites in HMVECs

For global metabolic profiling, unsupervised PCA was performed to separate the groups. From our data, PCA score plots did not show clear separation between control and antipsychotic treatment of HMVECs in the polar fraction (Figure 4.3 (B)). Then OPLS-DA was applied to visualise samples in an attempt to distinguish between control and each antipsychotic treatment, which revealed a very clear separation in the polar fraction (Figure 4.11). According to the criteria as previously mentioned in section 4.5.3, the nineteen identified metabolites from antipsychotics treatment on HMVECs were obtained as summarised in Table 4.5. These metabolites contributed most toward discriminating between the metabolic profiles of control and antipsychotic treatments. Figure 4.12 provides the top ten significant level changes of the identified metabolites.

Intriguingly, four of the top significant metabolites detected (1,2-dihexanoyl-sn-glycero-3-phosphate, 3-hydroxymelatonin, acetoacetic acid and (iso)butyrylcarnitine) were found to be significantly increased in four antipsychotics-treated HMVECs and 2 (3-hydroxyoctanoyl carnitine and heptanoylcholine) were increased in clozapine-, haloperidol- and risperidone-treated cells. Moreover, octenedioic acid was found to be increased only in risperidone-

treated cells. L-Carnitine and succinic acid semialdehyde were decreased. In addition, D-arabitol was decreased only in haloperidol-treated cells.

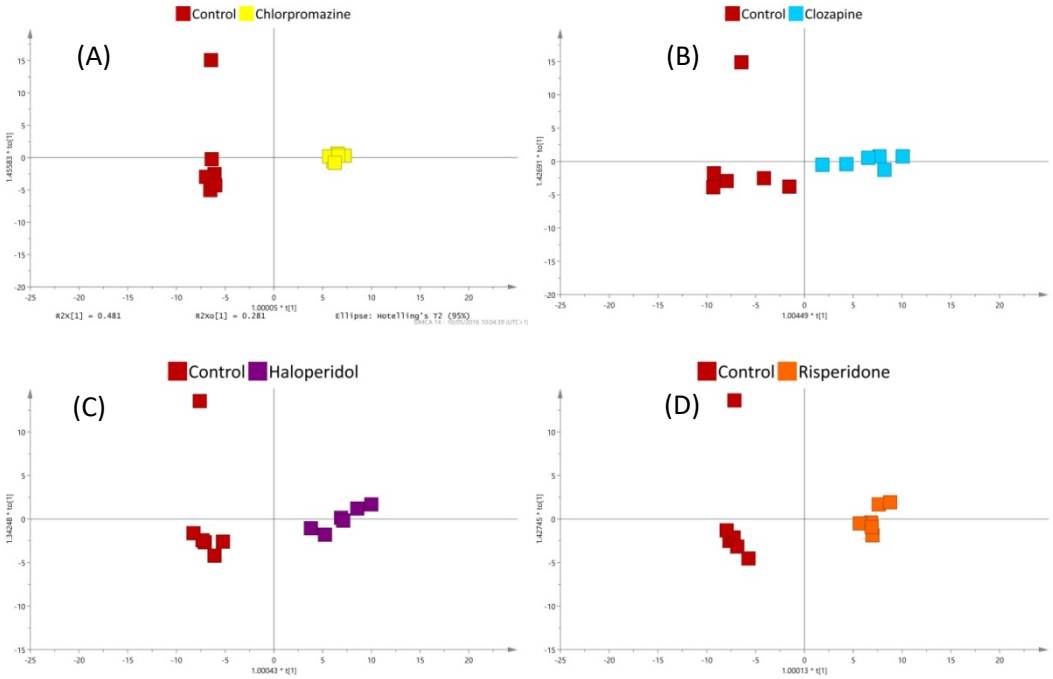


Figure 4.11 OPLS-DA of untargeted metabolomics data from HMVECs treated with antipsychotics at high therapeutic dosage in the polar fraction. Two-dimensional OPLS-DA scores plots reveal separation between untreated cells and chlorpromazine-treated cells (A), untreated cells and clozapine-treated cells (B), untreated cells and haloperidol-treated cells (C), and untreated cells and risperidone-treated cells (D). Untreated (red boxes), chlorpromazine (yellow boxes), clozapine (blue boxes), haloperidol (violet boxes) and risperidone (brown boxes).

Table 4.5 Details of metabolites from the polar fraction which changed significantly during the treatment with chlorpromazine, clozapine, haloperidol and risperidone in HMVECs.

m/z	Annotation	Formula	Mass error (ppm)	RT (min)	Control		Chlorpromazine		Clozapine		Haloperidol		Risperidone		VIP	FDR
					Abundance	SD	Abundance	SD	Abundance	SD	Abundance	SD	Abundance	SD		
327.0511	3-Hydroxymelatonin	C13H18N2O3	1	1.70	589	108	1087	48	751	265	1074	196	950	74	1.626	1.11E-05
348.0793	Unidentified			1.80	1219	395	667	175	600	104	1139	351	653	187	1.946	1.09E-04
280.0918	Glycerophosphocholine	C8H20NO6P	0	1.82	16308	10159	5642	1483	5313	944	9182	3103	5497	1457	1.06	2.26E-05
152.0317	Pyroglutamic acid	C5H7NO3	0	1.84	1629	496	1066	113	1142	103	796	169	994	179	1.00	7.51E-06
162.1124	L-Carnitine	C7H15NO3	0	1.92	1808	255	1868	77	1767	92	1512	340	666	48	1.631	9.56E-13
175.0576	D-Arabitol	C5H12O5	0	1.94	7689	1024	9225	2390	7802	1453	3560	927	7307	769	2.64	4.79E-08
168.0271	L-Glutamate	C5H9NO4	4	1.97	4461	948	3390	367	3492	217	2677	402	3150	417	1.14	8.37E-06
133.0133	Unidentified			2.29	544	220	876	135	912	69	1105	64	1480	118	1.139	1.27E-06
213.1232	L-prolyl-L-proline	C10H16N2O3	0	2.34	812	318	2223	1771	1290	271	2024	267	1359	285	1.16	8.82E-04
85.0292	Succinic acid semialdehyde	C4H6O3	2	2.74	1383	328	1666	58	1526	60	1133	299	721	89	1.71	7.19E-09
129.0188	Oxoglutaric acid	C5H6O5	0	2.97	26426	7260	26270	3000	22598	3139	21387	4004	15580	1954	1.11	1.37E-04
85.0291	Acetoacetic acid	C4H6O3	2	3.89	371	80	578	47	605	17	560	62	1122	106	1.703	1.11E-11
232.1542	Butyrylcarnitine/Isobutyryl-L-carnitine	C11H21NO4	0	3.89	2408	923	6245	483	6594	375	5259	818	15882	1869	1.807	1.84E-10
173.0809	Octenedioic acid	C8H12O4	0	3.92	618	48	641	91	625	64	712	85	1024	129	1.642	3.66E-05
577.8956	Unidentified			4.09	1886	612	718	243	896	383	1074	376	1069	246	1.004	1.41E-03
190.9926	Oxoglutaric acid	C5H6O5	0	5.57	787	386	1349	192	1480	199	1996	241	2793	303	1.24	3.53E-06
276.0755	Unidentified			8.15	1563	315	1770	136	2320	272	1422	191	2743	204	2.364	3.40E-09
384.1149	Succinyladenosine	C14H17N5O8	0	8.62	767	268	1359	164	1168	159	1567	339	1316	183	1.20	5.98E-04
410.1920	1,2-dihexanoyl-sn-glycero-3-phosphate	C15H29O8P	4	8.64	921	347	2546	1386	1345	399	2039	360	1607	334	1.48	5.00E-04
558.2769	Unidentified			8.64	1986	728	5434	3278	2822	859	4225	701	3200	876	1.432	1.23E-03
304.2116	3-hydroxyoctanoyl carnitine	C15H29NO5	1	8.76	292	123	294	39	432	46	1470	465	3041	369	1.687	4.20E-13
363.1611	Unidentified			8.93	2127	837	2617	795	2255	794	4631	1395	3955	812	1.832	3.38E-04
128.0713	Isobutyrylglycine/ N-Butyrylglycine	C6H11NO3	0	9.02	569	437	219	82	1449	709	1673	726	2151	1386	1.46	1.54E-06
196.0580	N-Acetyl-L-glutamate 5-semialdehyde	C7H11NO4	0	9.04	393	190	294	116	956	500	965	430	1349	899	1.25	3.15E-04
255.1588	Heptanoylcholine	C12H26NO2	2	10.63	954	611	590	253	1799	804	1618	370	1794	616	1.826	7.07E-05

VIP is a variable importance in the projection that shows the importance of a variable. FDR is a false discovery rate.

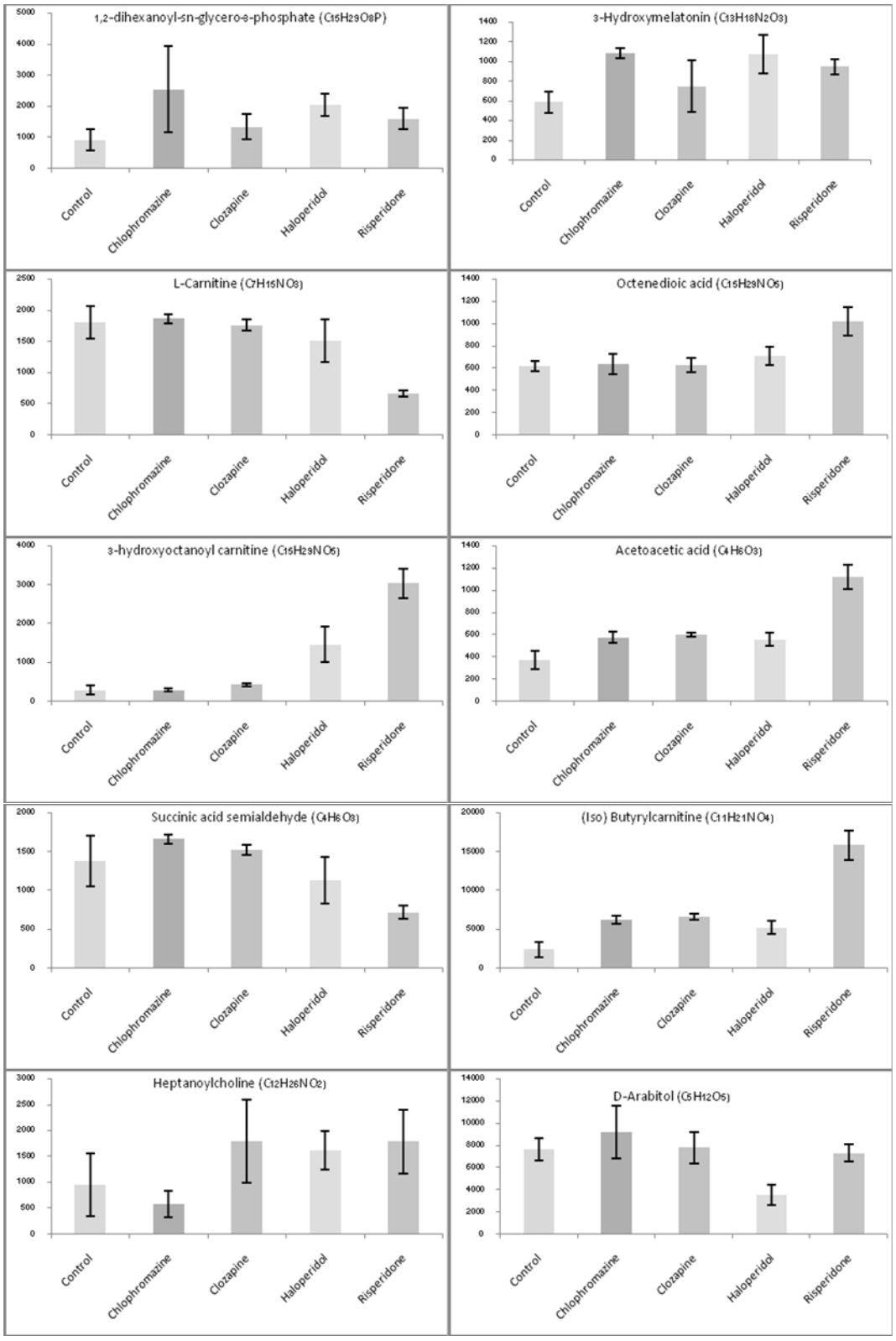


Figure 4.12 Level changes of the top ten significantly-changed metabolites from the polar fraction in HMVECs treated with chlorpromazine, clozapine, haloperidol and risperidone and untreated HMVECs.

4.5.5 Biological significance of the metabolic effects of antipsychotics on HMVECs

To characterise biological pathways that may be affected by chlorpromazine, clozapine, haloperidol and risperidone at high therapeutic dosage in HMVECs, and distinguish them from the control cells, various changes in levels of lipid compounds and polar metabolites were determined. These are summarised in Tables 4.4 and 4.5. Treatment with the four antipsychotic medications caused, changes in the levels of lipid compounds and polar metabolites. In brief, the significantly altered lipid compounds and polar metabolites were associated with bioenergetics and lipid metabolism as illustrated in Figure 4.13.

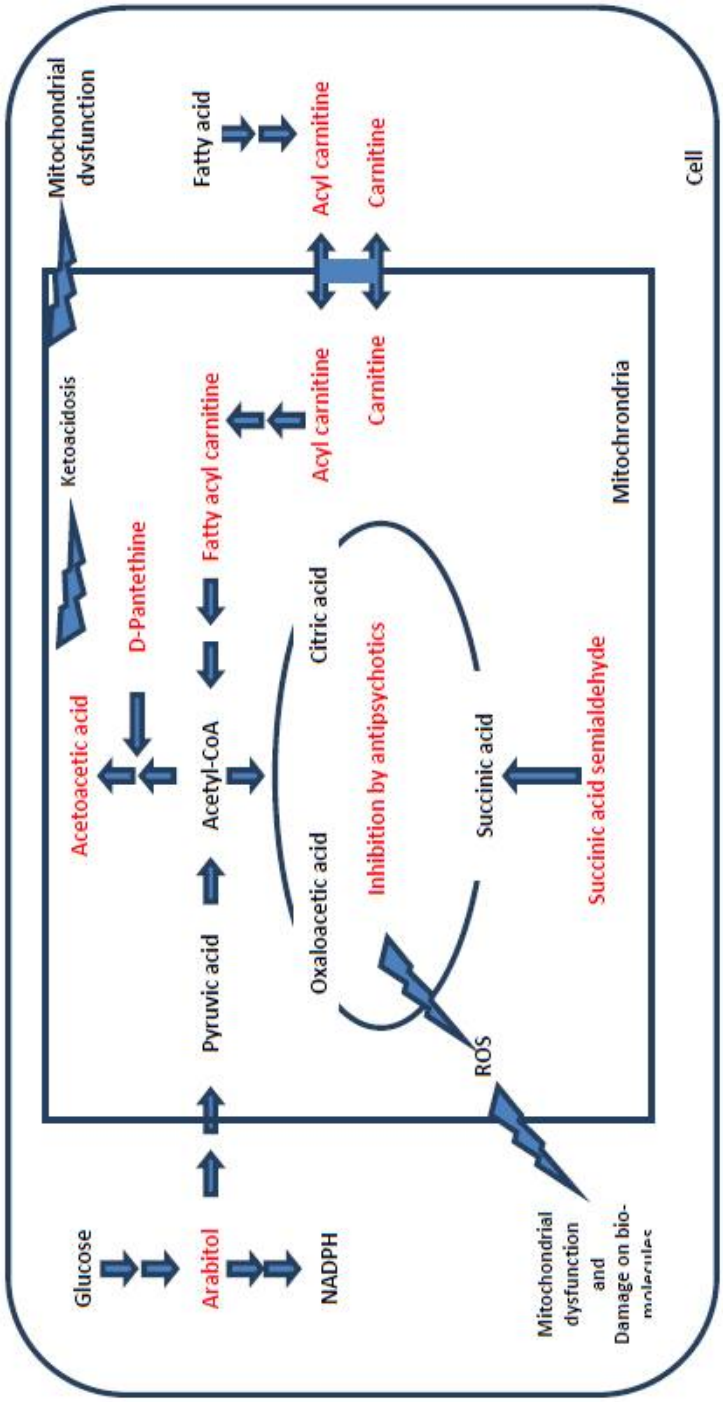


Figure 4.13 Overall simple diagrams for biological pathways that are affected by high therapeutic dosage of antipsychotics in HMVECs. Mitochondrial functions altered during the treated with antipsychotic drugs. Significantly changed metabolites are marked Red.

4.6 DISCUSSION

The purpose of this work was to describe the outcomes of an untargeted lipidomic and metabolomic analysis of the effects of chlorpromazine, clozapine, haloperidol and risperidone at high therapeutic dosage in human microvascular endothelial cells (HMVECs) from the blood brain barrier (BBB) using cell-based LC-MS metabolomics analysis. This approach has been widely used and expanded greatly in recent years (59,60). The analyses presented in this chapter address BBB dysfunction and breakdown caused by high therapeutic dosage of antipsychotics.

4.6.1 Antipsychotics metabolites

Although only four chlorpromazine metabolites were identified in this study, these metabolites were identified in the urine of psychiatric patients (177) and in vitro study (178). Previous studies have suggested that chlorpromazine can be transformed into other metabolites through hydroxylation, N-oxidation, demethylation, and dechlorination. To achieve chlorpromazine metabolites, LC-MS analysis was applied to screen for these compounds. The ions were identified as the putative chlorpromazine metabolites based on the exact *m/z* as shown in Table 4.3. This in vitro study detected the two hydroxylation chlorpromazine metabolites (8-hydroxychlorpromazine and 3-hydroxychlorpromazine), one demethylation chlorpromazine metabolite (N-

desmethylchlorpromazine), one N-oxidation chlorpromazine metabolite (chlorpromazine-N-oxide), and one chlorination chlorpromazine metabolite (promazine).

Using LC-MS/ToF, Tolonen and Rousu et al. (179) reported 14 haloperidol metabolites formed from an in vitro study of human liver microsomal incubation. In this study they found only 3 drug metabolites in HBMVECs as shown in Table 4.3 and Figure 4.4. This illustrates the possible chemical structures of the detected metabolites: N-oxidation, hydroxylation, and dechlorination forms. These drug metabolites were similarly found in the previous study.

There were 12 clozapine metabolite forms of clozapine which were reported in previous studies (180,181). In our study, there were 4 clozapine metabolites forms detected in HMVECs treatment group: one oxidation, one hydroxylation, one dechlorination, and one oxidative dechlorination (as shown in Table 4.3 and Figure 4.5). 9-Hydroxy risperidone was detected for risperidone as shown in Table 4.3 and Figure 4.6, according to the previous experiment [66].

Interestingly, in all treatments, the identified antipsychotic metabolites appeared to be derived from cytochrome P450-mediated oxidative metabolism. Pereira and Berbkop-Schnurch et al showed that BBB could have drug-inactivating enzymes as presentas found in the intestine and liver (182). Dauchy et al found

CYPs in microvessels of BBB (183) and Shawahna found Phase I and Phase II metabolizing enzymes in human brain microvessels (184).

Drug-inactivating enzymes metabolise drug and modify its response, liming the risk of developing adverse drug reactions with antipsychotics affecting the CNS. Moreover, these CYP enzymes in the BBB may constitute an additional protecting mechanism against antipsychotics, which may act regardless of their lipophilicity.

However, the drug metabolite identifications were based on the accurate and exact mass measurement (*m/z*) and calculated using Mathwork® software. Thus, the results in this report suggest the possible drug metabolite, only. To confirm these metabolites, the MS/MS patterns and available standard will be employed to confirm the future works.

4.6.2 Antipsychotic effects on HMVECs

Our data shows that significantly altered levels of lipids and polar metabolites (as shown in Figure 4.8 and 4.10) are found in HMVECs treated with antipsychotics at high therapeutic dosage when compared with untreated cells. These findings are consistent with, and substantially add to, previous reports of alteration in lipid metabolism and cellular metabolism in the BBB (91,185–187). Taken together, the data indicate that high therapeutic dosage of antipsychotics might potentially be involved in HMVECs dysfunction.

Interestingly, studying the results from the changes of lipid and polar metabolites shows that antipsychotics at high therapeutic dosage affect lipid profiles and intracellular metabolic profiles of HMVECs. In cellular processes, lipid metabolism is mainly involved in mitochondrial functions (188). Thus, the alteration of lipid profiles and metabolic profiles could result in the impairment of mitochondrial function. Antipsychotics have been reported to impair mitochondrial function (189–191), and cellular and mitochondrial membrane structure (94,192,193) resulting in cell apoptosis.

Mitochondria are complex organelles found in every human cell. They are responsible for the vast majority of cellular energy production in the form of adenosine triphosphate (ATP). ATP is the energy currency for almost all cellular processes (194). Impaired function of mitochondria leads to impaired bioenergetics which in turn causes a lack of cellular energy (195). Recently, studies by Elmorsy et al. have demonstrated bioenergetic impairment in HMVECs treated with four antipsychotics (chlorpromazine, clozapine, haloperidol and risperidone) and subsequent mitochondrial dysfunction (86,87). The results indicated changes in level of acetoacetic acid, D-pantethine, (iso)butyrylcarnitine, 3-hydroxyactanoyl carnitine, L-carnitine, succinic acid semialdehyde and D-arabitol in HMVECs treated with antipsychotics. Alterations of these metabolites could be involved in mitochondrial dysfunction as shown in Figure 4.11. .

Mitochondrial dysfunction leads to impaired bioenergetics in HMVECs treated with antipsychotics. As a result of energy deficiency, fatty acids are used for energy production as a compensatory mechanism. The metabolism of fatty acids generates several acid substances including acyl carnitine compounds and related compounds, and acetoacetic acid. In our results the levels of acyl carnitine compounds ((iso)butyrylcarnitine and 3-hydroxyactanoyl carnitine) were significantly increased, while the level of carnitine (an amino acid which play an important role in fatty acid transportation into mitochondria (196)) was significantly decreased. These changes could confirm that there is a high rate of fatty acid metabolism in HMVECs treated with high dosage antipsychotics. Moreover, it was found that the level of acetoacetic acid and D-pantethine were significantly raised in all HMVECs treated with high dosage antipsychotics (Figure 4.8 and 4.10). Acetoacetic acid and D-pantethine are not normally found at a high level in HMVECs and other cells. These metabolites increase when cells have no oxaloacetic acid available for the conversion of acetyl-CoA to citric acid, or have excessive fatty acid metabolism. According to the results, the level of fatty acids and related compounds were significantly changed. These alterations could suggest that the increase of acetoacetic acid and D-pantethine levels may result from mitochondrial dysfunction and an excess of

fatty acid metabolism resulting in an excess of acetyl-CoA. The excess acetyl-CoA is then metabolised to acetoacetic acid.

When even larger amounts of acetoacetic acid accumulate such that the cell's pH is lowered to dangerously acidic levels, a state of ketoacidosis is reached. Ketoacidosis is a metabolic state disorder associated with high concentrations of ketone bodies (aceto acetic acids) and results in HMVECs dysfunction and apoptosis (197,198).

In addition, mitochondrial dysfunction and increased fatty acid metabolism can generate reactive oxygen species (ROS) resulting in oxidative stress in cells (199). This stress can cause severe damage to all components of the cell, including DNA, protein, and lipids. Elmorsy et al. demonstrated that the cellular structure and morphology of HMVECs was disrupted by chlorpromazine, clozapine, haloperidol and risperidone treatment. This disruption by the antipsychotics was associated with oxidative stress (86,87). The results revealed pronounced changes in 10 lipid compounds (see Figures 4.8 and 4.10) in HMVECs treated with chlorpromazine, clozapine, haloperidol and risperidone. These lipids are constituents of the cellular membrane and are involved in cell proliferation, differentiation, apoptosis and oxidative stress (200).

In addition, there are a number of antioxidant defences to detoxify fluctuations in ROS and its reactive intermediates in cells, but ROS generation often exceeds the antioxidant capacity of cells (188).

The result indicates that the levels of 3-hydroxymelatonin and D-arabitol were significantly increased and decreased respectively in HMVECs treated with antipsychotics. 3-Hydroxymelatonin is an intermediate product of melatonin's interaction with ROS in cells. It has been reported that melatonin may act as a direct scavenger of ROS (thus, not only playing a role in sleep and circadian rhythm regulation) and yields 3-hydroxymelatonin in human cells. The level of 3-hydroxymelatonin is proportional to the level of oxidative stress by ROS in cells (201). In addition, D-arabitol is a substance in the pentose phosphate pathway of glucose metabolism that is used in the biosynthetic reaction of NADPH. NADPH protects against oxidative stress directly by neutralizing ROS and the level of D-arabitol is decreased when cells have high oxidative stress by ROS (202). The Antipsychotics have been reported to induce production of ROS in cells. Chlorpromazine and clozapine have demonstrated that they can induce ROS generation in HepaRG and SKNSH respectively and also in other cells (185,203). It has also been reported that haloperidol and risperidone can generate ROS in astroglia cells (204). The data which are consistent with, and substantially add to, the previous reports of oxidative stress by ROS in BBB cells (86,87), could indicate that antipsychotics are involved in ROS generation resulting in oxidative stress in HMVECs treated with antipsychotics. In conclusion, chlorpromazine, clozapine,

.

haloperidol and risperidone at high therapeutic dosage could affect the bioenergetics pathway due to mitochondrial dysfunction resulting in keto-acidosis and inducing oxide stress by reactive oxygen species generation in HMVECs.

In this study, the global effects of antipsychotics at high therapeutic dosage in HMVECs and the important of finding the metabolic pathways which have been altered were explored. Future studies should be designed to target lipidomic and metabolic profiling on mitochondrial function and fatty acid metabolism in order to determine lipids and metabolites which correlate with metabolome change for each antipsychotic drug. This could address why antipsychotics induce dysfunction and breakdown of the BBB, causing the aetiology of neuroleptic associated cerebral oedema and neuroleptic malignant syndrome.

While observation of HMVECs by using cell-based LC-MS metabolomics may not be fully applicable to the whole BBB system, our study affords several advantages over in vivo study and more precise measurement due to ease of manipulation and procurement.

4.7 CONCLUSION

Data generated using cell-based metabolomics in the study of HMVECs exposed to antipsychotics has provided a novel way to test and extend several hypotheses when studying effects of drugs and other compounds on biochemical mechanisms of the BBB. The simultaneous measurement of lipid and polar metabolites shows a novel interaction of metabolites that are vital in both the triggering and amplifying pathways of the BBB thus helping to refine the global view. The results are found support for the toxicity hypothesis with measurements that confirm previous findings and reveal the exact biological pathways of antipsychotic-altered BBB functions. Finally, we find that antipsychotics may affect the bioenergetics pathway due to mitochondrial dysfunction resulted in ketoacidosis and inducing oxide stress by reactive oxygen species generation.

CHAPTER V: LC-MS-BASED METABOLOMICS REVEALED SIGNIFICANT ALTERED INTRACELLULAR METABOLITES IN HUMAN BREAST CANCER (MCF-7) CELLS TREATED WITH CORDYCEPIN

5.1 ABSTRACT

Cordycepin, 3 deoxyadenosine, has the potential to become an anti-breast cancer drug with promising prospects. LC-MS-based metabolomics has been a powerful method to study metabolic profiles in cell line after drug treatment, which can be used for investigating of cordycepin effects in a cell culture model. The effectiveness of cordycepin is limited by its rapid deamination to an inactive metabolite by adenosine deaminase (ADA). Co-administration of a potent inhibitor of ADA, pentostatin, can be used to increase a half-life of cordycepin. In the present work, cell-based metabolomics using LC-MS was applied to analyze the metabolic changes induced by cordycepin treatment in MCF-7 cells. A cell-based metabolomics using LC-MS coupled pathway analysis was successfully applied to explore the metabolome changes induced by cordycepin with or without pentostatin on MCF-7 cells. It is revealed that pentostatin can inhibit cordycepin degradation by ADA leading to the enhancement of cordycepin effectiveness. Furthermore, the

pathway analysis indicated that anti-breast cancer was mainly responsible for alterations in purine and pyrimidine metabolism and bioenergetics. In addition, it was found that topaquinone, which involves in degradation of DNA, dramatically and significantly increased in MCF-7 cells exposed to cordycepin. This may indicate that cordycepin may be involved in the inhibition of cell proliferation and differentiation, and the activation of cell apoptosis.

Keywords: LC-MS, cell-based metabolomics, MCF-7 cells, cordycepin, pentostatin, breast cancer

5.2 INTRODUCTION

Although there are many advances in screening, surveillance and interventions, breast cancer is still the most common cancer problem among women globally (205–207). It is reported that there are 232,670 of new cases and 40,430 of deaths from breast cancer in US in 2014 (208), and 464,000 of new cases and 131,000 of deaths from this cancer in UK in 2012 (209). In addition, in Europe 458,337 and 131,259 of incidence and mortality numbers were reported in 2012 (210). Breast cancer is curable in the early stages (211–213); however, currently available breast cancer treatments cause serious side effects (214–216) and have limited effective therapy options is necessary (217–219). For example, the most common side effects of chemotherapeutic drugs using in breast cancer treatment are hair loss, low blood counts (causing an increased risk infection), feeling and being sick, loss of appetite and mouse ulcers (220–222); thus, the discovery of novel, targeted and more effective therapeutic options are necessary.

Natural products represent an abundance of source-derived remedies to discovery novel pharmacological active compounds for the development of anti-breast cancer drugs (223–225). Cordycepin, also known as 3'-deoxyadenosine, is originally found in the insect fungus *Cordyceps* spp., and its structure is similar to adenosine but it lacks of 3' hydroxyl group (226). Cordycepin have

been reported that it has various biological activities such as anti-fungal (103), immunomodulatory (107), anti-inflammatory (105,106,227), and anti-cancer effects (110,111,228). In addition, cordycepin is reported to be inhibitor of purine biosynthesis, DNA/RNA synthesis and mammalian target of rapamycin (mTOR) (113,229–231) and therefore exhibited a great potential for cancer prevention and treatment (110,111,113,228,230,231). As a result of its potential, investigation on therapeutic efficacy of cordycepin against various cancer cells has become a promising approach for the discovery of new anti-cancer drug. Recently, cordycepin has been shown that it is a clinically useful in treatment human breast cancer (104,108,113,116). Cordycepin has also shown that it effectively kills MCF-7 human breast cancer cell line in vitro study by inducing cell death association with estrogen receptor (104), inhibiting RNA synthesis and inducing DNA double strand breaks (113); however, there is still lack of thorough insight into the mechanism of anti-breast cancer effect.

Cell based-metabolomics is an approach that is used to characterize the metabolomic profile of cells (232). Since the profile of metabolites with relatively low molecular weight (commonly less than 1.5 KDa) are downstream products of biological processes, their identity and concentration in biological system can provide biochemical signatures for globally monitoring the physiological effects, and exploring the effects of drug (233).

Particularly, because cellular metabolism of cancer cells is different from that of normal cells, such as high energy metabolism, high enzyme activities and high phosphate compound metabolites levels, cell based-metabolomics has been a powerful approach employed for further investigation of biomarkers for cancer diagnosis and drug treatment (232,233).

Compared to nuclear magnetic resonance (NMR) spectroscopy and gas chromatography-mass spectrometry (GC-MS), liquid chromatography-mass spectrometry (LC-MS) has proven to be an effective combination for metabolites identification and quantifications in human biological samples because of its excellent resolution and sensitivity (234). Cell-based metabolic profiling using LC-MS has been used widely for metabolomic studies in vivo and in vitro models due to its high throughput, soft ionisation and good coverage of metabolites (234). The success of cell-based metabolomics using LC-MS combined with uni- and multivariate statistical tools has been proven as a powerful technique in rapidly identifying drug metabolites and providing useful metabolic information about the mechanisms of drug in human (232–234).

The aim of this present study was to apply cell-based metabolomics using LC-MS to investigate changes in intracellular metabolome caused by the cellular responses to cordycepin with or without in MCF7 cell lines.

The identification of multiple metabolites could facilitate the understanding of the in vitro actions of cordycepin and aid in understanding the biological mechanisms of this drug resulting in future applications for breast cancer treatment. Untargeted LC-MS-based metabolite profiling was employed to functionally assign cordycepin induced changes in the cellular metabolism of MCF-7 cells. Furthermore, this study investigated and identified the differential effects of this drug on intracellular metabolites including those involved in the metabolic pathway responsible for killing MCF-7 cells.

5.3 OBJECTIVES

This part of project has three main objectives:

- to apply the LC-MS-based metabolomics to investigate the metabolic changes of MCF-7 cells exposed to pentostatin, cordycepin and cordycepin + pentostatin.
- to study the effect of pentostatin on cordycepin stability on MCF-7 cells that are affected by cordycepin at different time points (15, 30, 60 and 120 min).
- to identify which metabolic pathway within MCF-7 cells are affected by cordycepin.

5.4 MATERIALS AND METHODS

5.4.1 Chemicals

LC-MS-grade acetonitrile and methanol were purchased from Fisher Scientific (Leicestershire, UK). HPLC-grade water obtained from Elga Purelab Genetic (Buckinghamshire, UK). Formic acid (LC-MS grade) was purchased from Acros Organics (Leicestershire, UK), and all standard chemical compounds were purchased from Sigma-Aldrich (Dorset, UK). These standards are HPLC or LC-MS grade.

5.4.2 Study design

5.4.2.1 The effect of pentostatin on the stability of cordycepin

Cell lines were treated with either:

- 1 μM of pentostatin,
- 50 μM of cordycepin,
- 50 μM of cordycepin + 1 μM of pentostatin

for two, eight and 24 hours. Each of the above groups was set up in triplicate. The concentration and the time treatment do not affect on MCF-7 cell viability with previous report (235).

5.4.2.2 The effect of cordycepin on metabolome changes

Cell lines were treated with 50 μM of cordycepin for 15, 30, 60 and 120 minutes. There were six biological replicates of each group.

5.4.3 Pentostatin and cordycepin effects on MCF-7 cells

MCF-7 cell lines were cultured in Dulbecco's modified Eagle medium (DMEM) high glucose (4.5 g/L), supplemented with 10% foetal bovine serum (FBS) and 2mM L-glutamine at 37 ^{o}C and 5% CO_2 as described previously in (236). MCF-7 cells were seeded in a 6 well plate at a density of 10^8 cells/ml and grow up to 80% confluence. MCF-7 cells were treated with DMSO (control), pentostatin, cordycepin and cordycepin + pentostatin for 2, 8 and 24 hr for the investigation of pentostatin effects. The cells were also exposed to DMSO (control) and cordycepin for 15, 30, 60 and 120 min for the cordycepin study. These were performed by a PhD student, Mrs. Utami Wahyu and Mr. Lin Jia from the Division of Molecular and Cellular Science, School of Pharmacy, University of Nottingham, UK for pentostatin and cordycepin studies, respectively.

5.4.4 Metabolite extraction

The cell culture was removed and washed with 1 ml of PBS and then MCF-7 cell pellets were extracted with 0.5 ml cold methanol (-20°C) and cell suspensions were vortexed for 2 hr in cold room (4°C). The suspensions were centrifuged for 10 min at 15,000 rpm

at 4°C. The supernatants were transferred to new eppendorf tubes and kept at -80°C for further analysis.

5.4.5 Metabolomics analysis

Analyses were performed using non-targeted protocols using Exactive Orbitap MS with HILIC-MS instrumentation previously reported in Chapter II. The initial method development was carried out on the Water Q-ToF Premier instrument and these methods were then transferred to the Thermo Exactive LC-MS system. A mixture of authentic standard compounds was injected before sample analysis for metabolite identification. The pooled QC sample was obtained by taking a 10 µl aliquot of all samples from the study. The pooled QC sample was injected every 6 sample injections and was used to assess instrument performance.

Liquid chromatography was performed using the Thermo Scientific Accela LC system coupled with the Exactive Orbitrap MS as previous described (135). Briefly, HILIC separations were achieved using a ZIC-pHILIC column with a 150 x 2.1 mm, 3.5 µm particle size, equipped with a ZIC-pHILIC PEEK guard column with a 20 x 2.1 mm, 5 µM particle size. The mobile phases were acetonitrile (A) and 20 mM ammonium carbonate (pH 9.2) (B) at the flow rate of 0.20 ml/minute at 40°C. At t=0 minutes run, at 5% B, a gradient to 95% B was concluded at 13 minutes and a gradient to 5%B was completed at 15 minutes.

Following column wash and equilibration, the run was concluded with 5% B at 20 minutes. Data acquisition of ion detection was performed between 70 to 1,400 m/z in positive and negative modes.

5.4.6 Data processing and statistical analysis

LC-MS data was pre-processed (filtering and alignment) and extracted by using Progenesis QI software. The extracted m/z data was exported to text file data for further analysis. Manual inspection and duplicates removal was performed to form a final data by using Xcalibur software version 2.0. Statistical analyses were performed using univariate (Student's T-Test) and multivariate (OPLS-DA) approaches. Simca P version 14.0 was used for statistical analyses. Detected ions were pre-selected as candidates when their VIP values were $\geq$ 1.00. The VIP value indicates the importance of each metabolite for group separation. Then, among these detected ions with ANOVA (FDR < 0.05) was then selected as significantly changed ions that were most correlated with the OPLS-DA discriminant scores in order to assess levels of significant difference for each ion between control and cordycepin treated samples. In addition, features that were detected in every chromatogram and had < 30% CV with each group were included in the analysis.

The identification of significantly altered ions was performed by matching accurate masses and retention times of authentic standards using standard peak assignment but when standards

were not available, metabolites were tentatively identified through accurate mass search of the Human Metabolome database and the METLIN data base with a mass error less than 5 ppm (237).

5.5 RESULTS

5.5.1 Effects of pentostatin on cordycepin stability in MCF-7 cells

In order to study the effects of pentostatin on cordycepin stability, the MCF7 cells were treated with 50 μM cordycepin and 1 μM pentostatin for 2, 8 and 24 hr and analysed by LC-MS.

After the preprocessing steps by the Progenesis-QI software, the number of detected features in MCF-7 cell extracts from the intervention study was 3,470 in total (ESI+ and ESI-). Of these, 291 features were identified putatively. These identified metabolites include cordycepin and its metabolism compounds, amino acids, fatty acids, lipids, sugars and organic acids (see Figure 5.1 and Supplementary Table 5.1).

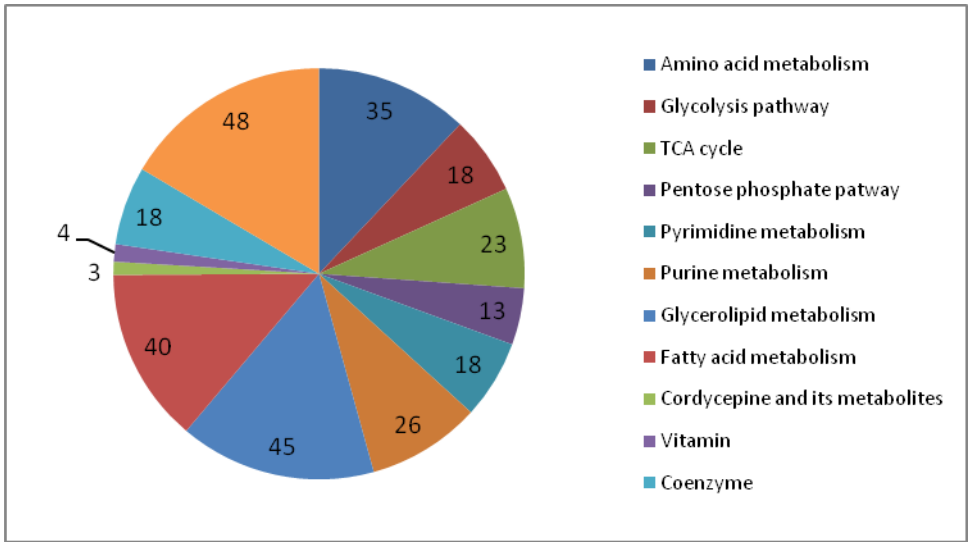


Figure 5.1 Pie chart summarising the distribution and information for MCF-7 cell metabolites, detected by untargeted metabolic profiling.

5.5.1.1 Multivariate statistical analysis of the metabolomics data

Using principal component analysis (PCA) to visualize general clustering, trend, or outlines among the observation, the set of spectral data from MCF-7 cell samples was analyzed as shown in Figure 5.2. In the PCA scores plot, each time treatment condition was separated. For each PCA scores plot of time treatment conditions as shown in Figure 5.3, control (DMSO), cordycepin, pentostatin and cordycepin + pentostatin were clearly separated from each sample. As can be seen in Figure 5.2 and 5.3, trends among control, pentostatin, cordycepin and cordycepin +

pentostatin combination groups were observed indicating feasibility to investigated relationships between time series and drug treatment conditions. As the time points increases, the clusters spread from the middle left (2 hr) to the middle right (8 hr) and to the middle top (24 hr) of the PCA scores plot (Figure 5.2(A). The clusters spread from the middle right (2 hr) to the middle left (8 hr) and to the middle top (24 hr) of the OPLS-DA scores plot (Figure 5.2(B)).

Next, separate PCAs of time treatment series of DMSO, pentostatin, cordycepin and cordycepin + pentostatin combination were performed to investigate how pentostatin can increase an activity of cordycepin (Figure 5.3). As can be seen in Figure 5.3(A) to (C), clear separation among DMSO, pentostatin, cordycepin and cordycepin + pentostatin at different time points were observed, except cordycepin and cordycepin + pentostatin was not clear separation. However, the clusters spread from the top right to bottom right and to middle left. The percentages of each PC were summarised in Table 5.1.

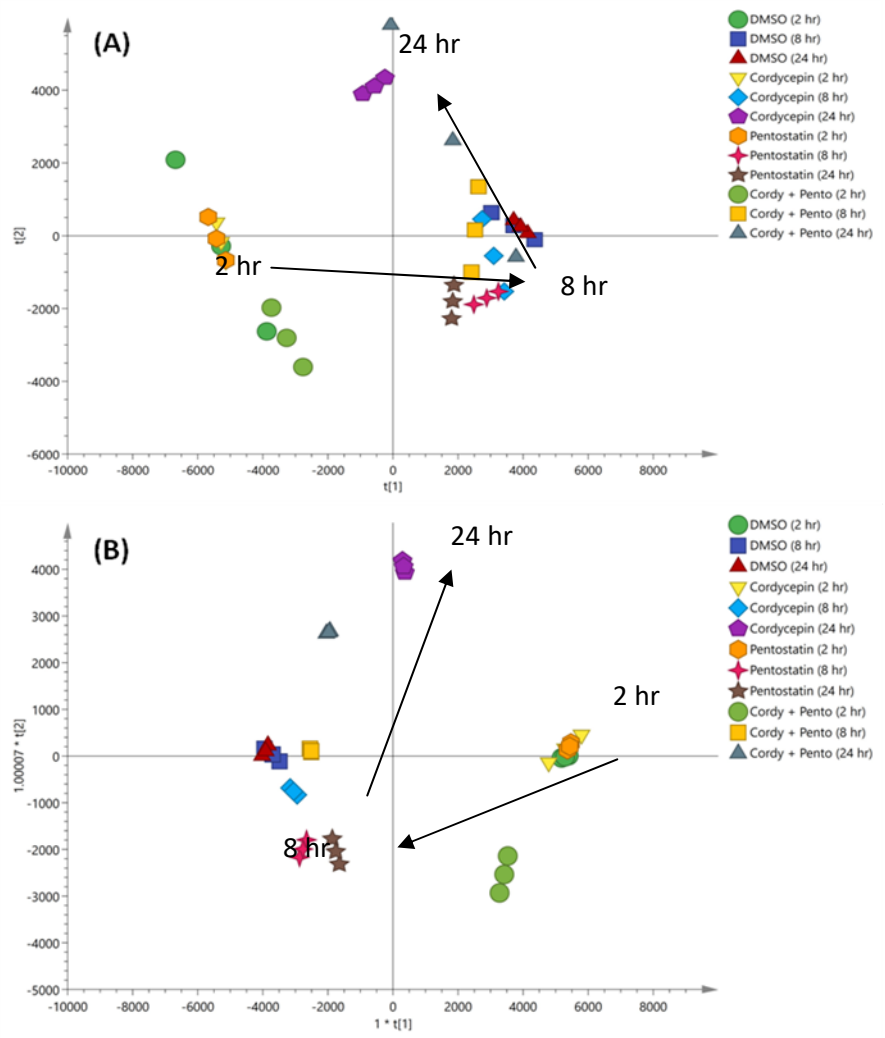


Figure 5.2 (A) PCA scores plot from MCF-7 cells exposed to DMSO (as a control), pentostatin, cordycepin and cordycepin + pentostatin combination at 2, 8 and 24 hr with PC1 (54.41%) versus PC2 (19.23%). (B) OPLS-DA scores plot with R^2X = 0.999, R^2Y = 0.97 and Q^2 = 0.84. Metabolic profiling was carried out on MCF-7 cell extracts upon exposure to vehicle and drugs; 2 hr DMSO treatment (green circulars), 8 hr DMSO treatment (blue squares), 24 hr DMSO treatment (red triangles), 2 hr cordycepin treatment (yellow inversed triangles), 8 hr cordycepin treatment (blue diamonds), 24 hr cordycepin treatment (violet pentagons), 2 hr pentostatin treatment (orange hexagons), 8 hr pentostatin treatment (pink four point-stars), 24 hr pentostatin treatment (brown five point-stars), 2 hr cordycepin + pentostatin treatment (pale green circular), 8 hr cordycepin + pentostatin (orange squares), and 24 hr cordycepin + pentostatin (gray triangles). Arrows are draw as a visual guide indicating the relationship between time point and mass spectra.

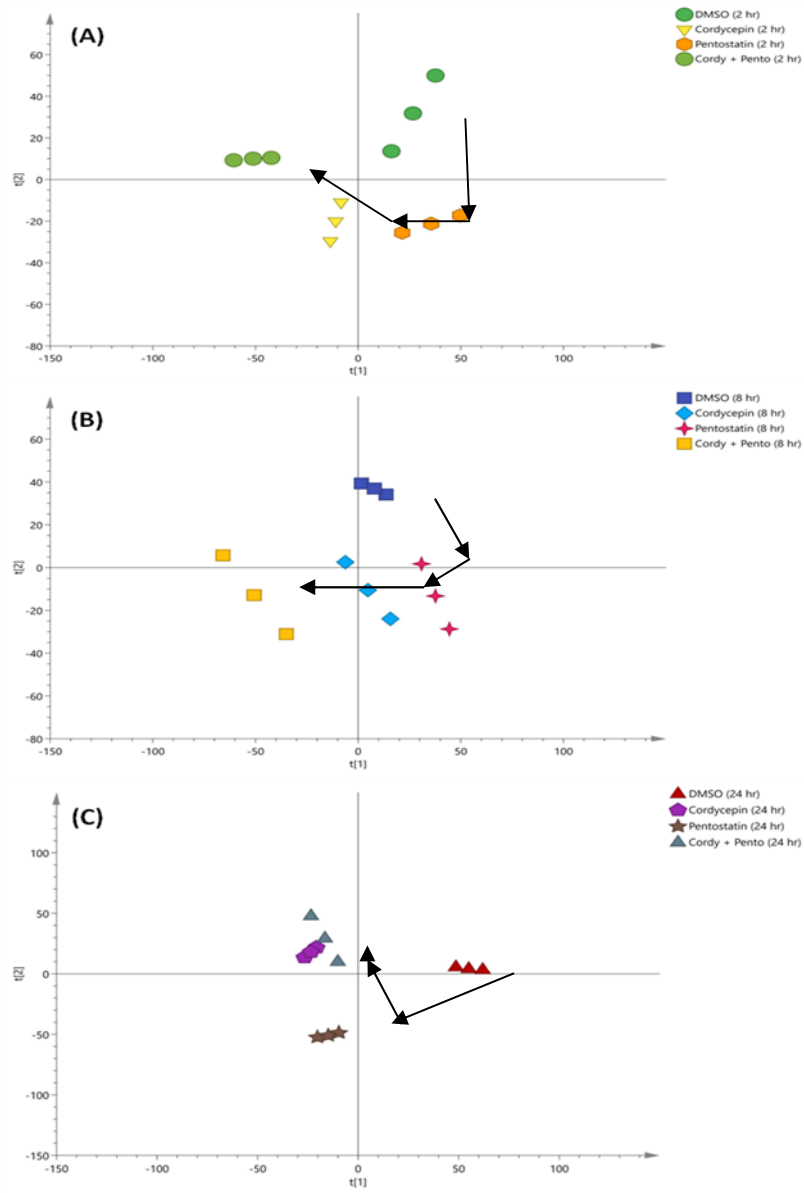


Figure 5.3 PCA scores plot for among time treatments (A) 2 hr with PC1 (96.07%) versus PC2 (0.98%), (B) 8 hr with PC1(87.30%) versus PC2 (11.69%) and (C) 24 hr with PC1(60.98%) versus PC2 (20.89%);2 hr DMSO treatment (green circulars), 8 hr DMSO treatment (blue squares), 24 hr DMSO treatment (red triangles), 2 hr cordycepin treatment (yellow inversed triangles), 8 hr cordycepin treatment (blue diamonds), 24 hr cordycepin treatment (violet pentagons), 2 hr pentostatin treatment (orange hexagons), 8 hr pentostatin treatment (pink four point-stars), 24 hr pentostatin treatment (brown five point-stars), 2 hr cordycepin + pentostatin treatment (pale green circular), 8 hr cordycepin + pentostatin (orange squares), and 24 hr cordycepin + pentostatin (gray triangles). Arrows are draw as a visual guide indicating the relationship between drugs and mass spectra.

Table 5.1 Summary of the parameters for assessing modelling quality

Groups	No.[a]	PC1 (%)	PC2 (%)
2 hr	2	86.07	13.98
8 hr	2	87.30	11.69
24 hr	2	60.98	20.89

[a] Number of component.

An OPLS-DA was applied in order to better understand and the different metabolic patterns and to detect potential metabolites showing prominent level changes in our models. Quality of the resulting discriminant models are $R^2X = 0.999$, $R^2Y = 0.97$ and $Q^2 = 0.84$. These parameters larger than 0.50 suggest that all model were robust and had good fitness and prediction (238). OPLS-DA scores plot (Figure 5.2(B)) showed that the combination of cordycepin and pentostatin for each time point had distinctive metabolic profiles and clear separaion from vehicles, cordycepin and pentostatin.

5.5.1.2 Feature selection: Potential key metabolites

In order to identify which metabolites contributed to the group separations, the variable importance for projection (VIP) based on OPLS-DA models was used and ANOVA was also performed. Only metabolites with VIP values $\geq$ 1.00 were selected as candidates. Then, among these, variables with FDR < 0.05 in ANOVA analysis were selected as metabolites that were most correlated with the OPLS-DA discriminant scores in order to decrease the risk of false positives in the selection of potential metabolites. Applying such an approach, significant metabolites related to the effects of pentostatin on cordycepin activity in MCF-7 cell lines were identified.

After two hours of treatment with drugs, the levels of 35 metabolites were significantly changed (Supplementary Table 5.2) and for the eight and 24 hour time points, 38 and 42 metabolites, respectively, were significantly altered (Supplementary Table 5.3 and 5.4). To identify most significant metabolites, a fold change cut-off value was set at 1.50, which narrowed the search to only include features that were increased and decreased at least 1.50 times after the drug treatment compared to the controls. The number of remaining features was reduced to 24, 29 and 37 in 2, 8 and 24 hour drug treatments, respectively. The remaining features were summarised in Table 5.2. However, it was found that cordycepin and cordycepin monophosphate were dramatically increased as

shown in Figure 5.4 (A) and (B), but deoxyinosine was significantly decreased (Figure 5.4 (C)).

Table 5.2 Metabolites identified in MCF-7 cells exposed to drugs at different time points (2, 8 and 24 h) with VIP value ≥ 1.00 and FDR < 0.05.

m/z	RT (min)	Metabolites	2 hr (Fold change)			8 hr (Fold change)			24 hr (Fold change)		
			Pentostatin	Cordycepin	Cordycepin + Pentostatin	Pentostatin	Cordycepin	Cordycepin + Pentostatin	Pentostatin	Cordycepin	Cordycepin + Pentostatin
369.3518	2.40	3-Deoxyvitamin D3	x	x	-1.68	x	x	x	x	2.58	0.00
338.3422	2.43	Eicosanoyl-EA	2.11	1.83	-1.51	x	x	x	x	2.61	0.00
538.5204	2.43	N-Palmitoylsphingosine	x	x	-3.77	x	x	x	x	4.67	0.00
330.2644	2.65	Undecanoylcarnitine/4,8 Dimethylnonanoyl carnitine	x	x	x	x	x	x	1.02	-1.02	-1.07
201.1599	2.72	Spermine dialdehyde	x	x	x	3.16	3.91	x	x	x	x
220.1181	2.90	Pantothenic acid	x	x	x	x	x	-1.79	x	x	-1.83
748.5309	2.90	CL	x	x	-1.74	x	x	x	x	2.34	0.00
429.2426	2.90	Glycyl-Lysine/Lysyl-Glycine	x	x	3.05	x	x	x	x	x	x
117.0192	2.91	Succinic acid	x	x	x	3.34	2.58	x	4.60	2.02	x
89.0243	2.91	Lactic acid	x	x	x	x	x	x	-1.88	x	x
129.0556	2.96	4-Acetylbutyrate/2-Methyl-3-ketovaleric acid	x	x	x	x	x	x	-2.44	-1.52	x
298.0975	3.07	5'-Methylthioadenosine	x	x	x	x	-2.94	-15.43	x	x	x
246.1704	3.44	2-Methylbutyroylcarnitine/Pivaloylcarnitine/Isovalerylcarnitine/Valerylcarnitine	x	x	x	x	x	-2.15	x	x	-6.37
232.1546	3.58	Butyrylcarnitine/Isobutyryl-L-carnitine	x	x	-1.70	x	x	-1.83	x	-1.78	-6.08
218.1389	4.89	Propionylcarnitine	x	x	x	x	x	-3.26	x	x	-20.32
176.0554	5.27	N-Formyl-L-glutamic acid	x	x	x	x	x	x	x	-2.18	-1.98
204.1231	5.61	L-Acetylcarnitine	x	x	1.52	x	x	x	x	-2.16	-4.19
252.1091	5.63	Cordycepin	x	x	x	> 1000.00	> 1000.00	>1000.00	> 1000.00	>1000.00	> 1000.00
133.0141	5.72	Malic acid	x	x	x	-2.91	x	x	-3.97	-2.03	x

Metaboloites in red were identified by using commercially available standards and the others were identified by comparison with the MS library.

Table 5.2 (Cont.) Metabolites identified in MCF-7 cells exposed to drugs at different time points (2, 8 and 24 h) with VIP value ≥ 1.00 and FDR < 0.05.

m/z	RT (min)	Metabolites	2 hr (Fold change)			8 hr (Fold change)			24 hr (fold change)		
			Pentostatin	Cordycepin	Cordycepin + Pentostatin	Pentostatin	Cordycepin	Cordycepin + Pentostatin	Pentostatin	Cordycepin	Cordycepin + Pentostatin
253.0934	5.79	Deoxyinosine	-1.76	712.04	x	x	93.62	33.09	x	x	x
137.0458	5.81	Hypoxanthine	-2.74	5.63	-1.67	-4.27	6.16	x	2.27	8.62	0.00
788.5456	6.10	PS	x	x	x	-3.10	-2.01	x	x	x	x
268.1046	6.28	Adenosine	x	x	x	x	-3.29	-13.70	x	x	x
229.1549	6.33	Pro (iso)Leu/(iso)Leu Pro	x	x	x	x	x	-3.84	x	-3.71	-8.28
261.1272	6.46	Pantetheine	x	x	x	x	x	1.89	x	x	x
170.0811	6.55	Pyridoxine	x	x	x	x	x	x	x	-1.89	-1.91
294.2434	6.58	4,8 dimethylnonanoyl carnitine	x	x	-1.53	x	x	x	x	x	x
269.0885	6.63	Inosine	x	x	x	-4.45	x	0.00	x	x	x
731.6077	6.63	SM	x	x	-3.04	x	x	x	x	4.88	0.00
148.0427	6.65	Thiomorpholine 3-carboxylate	1.98	4.33	2.56	x	x	x	1.51	-1.72	-1.74
136.0617	6.67	Adenine	1.61	3.87	2.64	x	x	x	x	x	x
191.0195	6.88	D-Glucaro-1,4-lactone	x	x	x	-2.58	-4.32	-1.71	x	x	x
205.0972	6.92	L-Tryptophan	x	x	x	x	x	x	x	-1.54	x
213.1234	6.99	L-prolyl-L-proline	x	x	x	x	x	-1.97	x	-3.59	-4.51
182.0813	7.68	L-Tyrosine	x	x	x	x	x	x	x	-1.56	x
225.0613	7.94	Glucoheptonic acid	x	x	x	x	x	x	1.86	1.52	x
130.0620	7.96	Creatine	x	x	x	x	x	x	-2.12	-2.85	x
166.0177	8.20	Homocysteinesulfinic acid	x	x	x	x	x	x	-5.48	-2.03	-1.62
156.0421	8.48	N-Methylethanolaminium phosphate	x	x	x	x	x	1.78	x	x	x

Metaboloites in red were identified by using commercially available standards and the others were identified by comparison with the MS library.

Table 5.2 (Cont.) Metabolites identified in MCF-7 cells exposed to drugs at different time points (2, 8 and 24 h) with VIP value ≥ 1.00 and FDR < 0.05.

m/z	RT (min)	Metabolites	2 hr (Fold change)			8 hr (Fold change)			24 hr (Fold Change)		
			Pentostatin	Cordycepin	Cordycepin + Pentostatin	Pentostatin	Cordycepin	Cordycepin + Pentostatin	Pentostatin	Cordycepin	Cordycepin + Pentostatin
213.0491	8.74	Serinyl-Serine	-3.15	-2.33	x	x	-1.57	x	x	x	x
147.0764	8.75	Ureidoisobutyric acid	x	-1.95	-2.93	x	x	x	x	x	0.00
488.6558	8.92	(2E)-Tetradecenoyl-CoA	x	2.17	2.90	x	x	1.55	x	x	x
210.0283	9.39	Phosphocreatine	x	-2.11	x	x	x	x	x	x	x
332.0760	9.43	Cordycepin monophosphate	x	>1000.00	>1000.00	x	>1000.00	>1000.00	x	>1000.00	>1000.00
258.1107	9.62	Glycerophosphocholine	x	-1.64	-2.24	x	x	x	x	x	x
348.0711	9.72	Adenosine monophosphate	x	x	x	-2.56	-5.56	-11.68	-1.88	-6.34	-1.88
307.0838	9.72	Oxidized glutathione	x	-1.58	-1.94	x	x	x	x	x	x
928.2119	9.73	Nonanoyl-CoA	-5.28	-2.46	x	x	x	x	x	x	x
161.1285	9.74	Isoputreanine/N(6)-Methyllysine	x	x	x	x	-1.66	-2.40	x	x	x
223.0748	10.01	L-Cystathionine	x	x	x	x	x	x	x	-2.57	-6.63
175.1190	10.15	L-Arginine	x	x	x	x	x	1.89	x	x	x
664.1168	10.22	NAD	x	x	-1.91	x	x	-2.73	x	x	-2.08
184.0734	10.24	Phosphocholine	x	x	-1.55	x	x	x	x	x	x
323.0283	10.64	Uridine monophosphate	x	x	x	-6.07	-4.35	-1.60	-3.99	-7.12	-1.63
168.9905	10.96	Glyceraldehyde-3-phosphate	x	x	x	x	x	x	-1.68	-3.75	x
364.0659	11.17	Guanosine monophosphate	x	x	x	x	x	x	-1.82	-8.73	-2.16
184.0014	11.25	Phosphoserine	-2.26	x	x	x	x	x	x	x	x
472.0981	11.72	CMP-2-aminoethylphosphonate	x	x	x	x	x	x	-1.67	-1.59	-1.51
428.0375	14.92	Adenosine diphosphate	x	x	x	-1.66	-2.03	-3.19	-1.83	-2.57	-1.53

Metaboloites in red were identified by using commercially available standards and the others were identified by comparison with the MS library.

Table 5.2 (Cont.) Metabolites identified in MCF-7 cells exposed to drugs at different time points (2, 8 and 24 h) with VIP value ≥ 1.00 and FDR < 0.05.

m/z	RT (min)	Metabolites	2 hr			8 hr			24 hr		
			Pentostatin	Cordycepin	Cordycepin + Pentostatin	Pentostatin	Cordycepin	Cordycepin + Pentostatin	Pentostatin	Cordycepin	Cordycepin + Pentostatin
412.0424	14.92	dADP	x	x	x	3.78	x	48.45	-6.06	-23.01	0.00
341.0041	16.33	Fructose-1,6-bisphosphate	x	x	x	x	x	x	2.16	1.88	-1.86

Metaboloites in red were identified by using commercially available standards and the others were identified by comparison with the MS library.

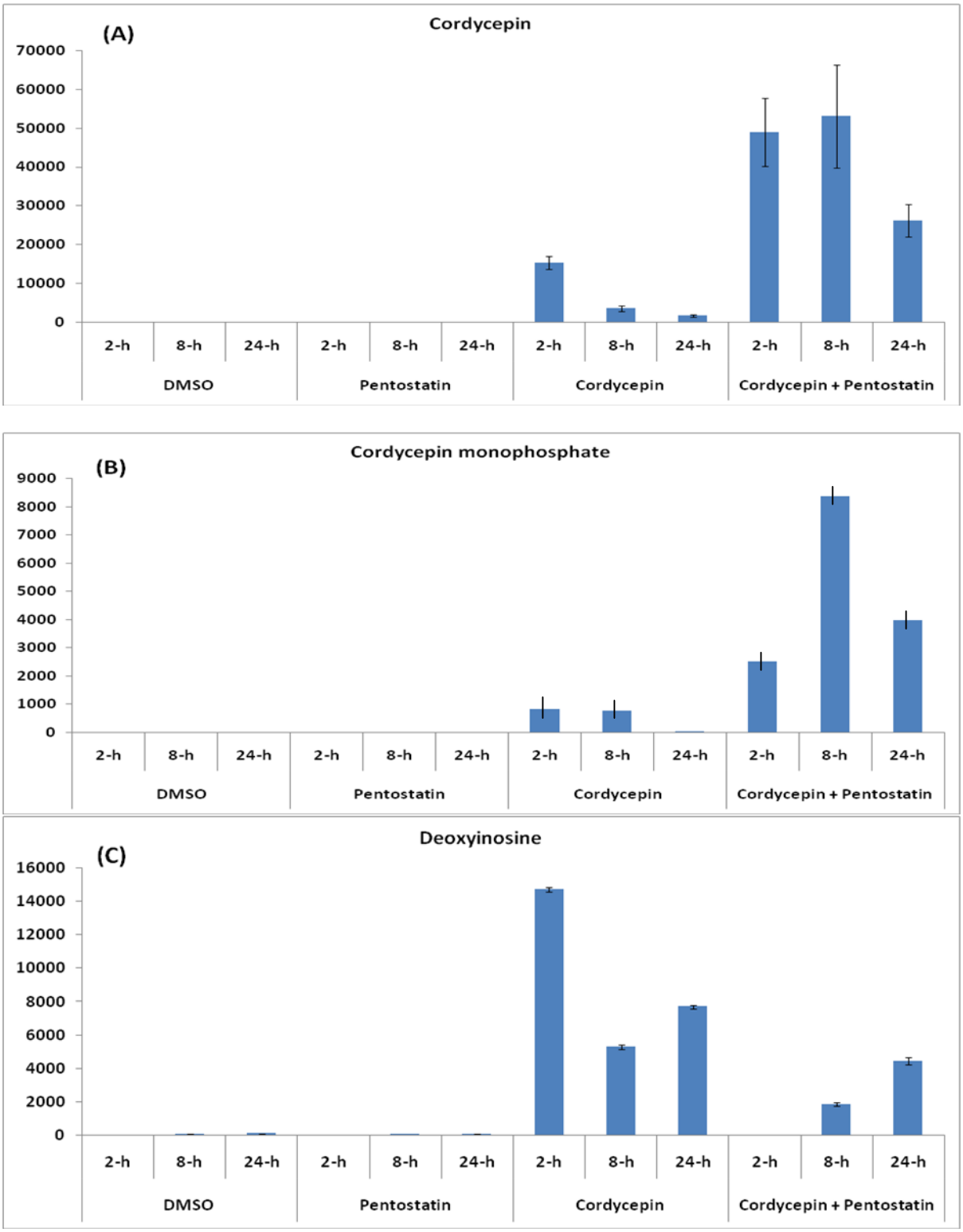


Figure 5.4 Cordycepin (A), cordycepin monophosphate (B) and deoxyinosine (C) levels in MCF-7 cells exposed with pentostatin, cordycepin and cordycepin + pentostatin at different time points (2-, 8- and 24- h).

5.5.2 Effects of cordycepin on MCF-7 cells

To understand the metabolomic signature of cordycepin on MCF-7 cells, a cell-based metabolomics analysis using LC-MS was performed. The MS spectral data of the control, vehicle and different time points of cordycepin treatment (15, 30, 60 and 120 min) were used and the metabolomic profile of overall group and each pair group (control vs vehicle, control vs cordycepin (15 min), control vs cordycepin (30 min), control vs cordycepin (60 min), and control vs cordycepin (120 min)) were subjected to multivariate statistical analysis.

5.5.2.1 Metabolic profiles analysed by cell-based metabolomics using LC-MS approach

MS spectral data was aligned by using a pooled QC sample. Importantly, the alignment process did not affect the clustering of the samples. An un-supervised multivariate statistical method, principal component analysis (PCA), was applied. Close clustering of pooled QC samples in the PCA using all these features indicates minimal sample processing and instrument-related variation (see Figure 5.5(A)). The PCA showed that the six experimental conditions are clearly distinguishable and suggests that cordycepin caused an unambiguous change in the MCF-7 cell metabolome underlining the sensitivity of this analysis to differentiate among metabolic states of MCF-7 cells. Due to possible fluctuation of

metabolic status of the MCF-7 cells, an OPLS-DA was applied to better understand the different metabolic pattern and to detect significant ions showing prominent level changes in the models. Any difference between the classes, the untreated, vehicle, and cordycepin with different time points were also clearly separated in the OPLS-DA scores plot as shown in Figure 5.5(B).

5.5.2.2 Cordycepin and its metabolites

Among these metabolic features, cordycepin and cordycepin metabolites (cordycepin monophosphate and cordycepin diphosphate) were detected successfully in the samples (Figure 5.6). Figure 5.6(A) illustrates the cordycepin metabolism in mammalian cells. The identities of these drugs and known metabolites of cordycepin and its metabolites were confirmed by running commercial standards. Whereas cordycepin showed a decrease in level over the time point, the cordycepin metabolites increased over the time points (Figure 5.6 (B)).

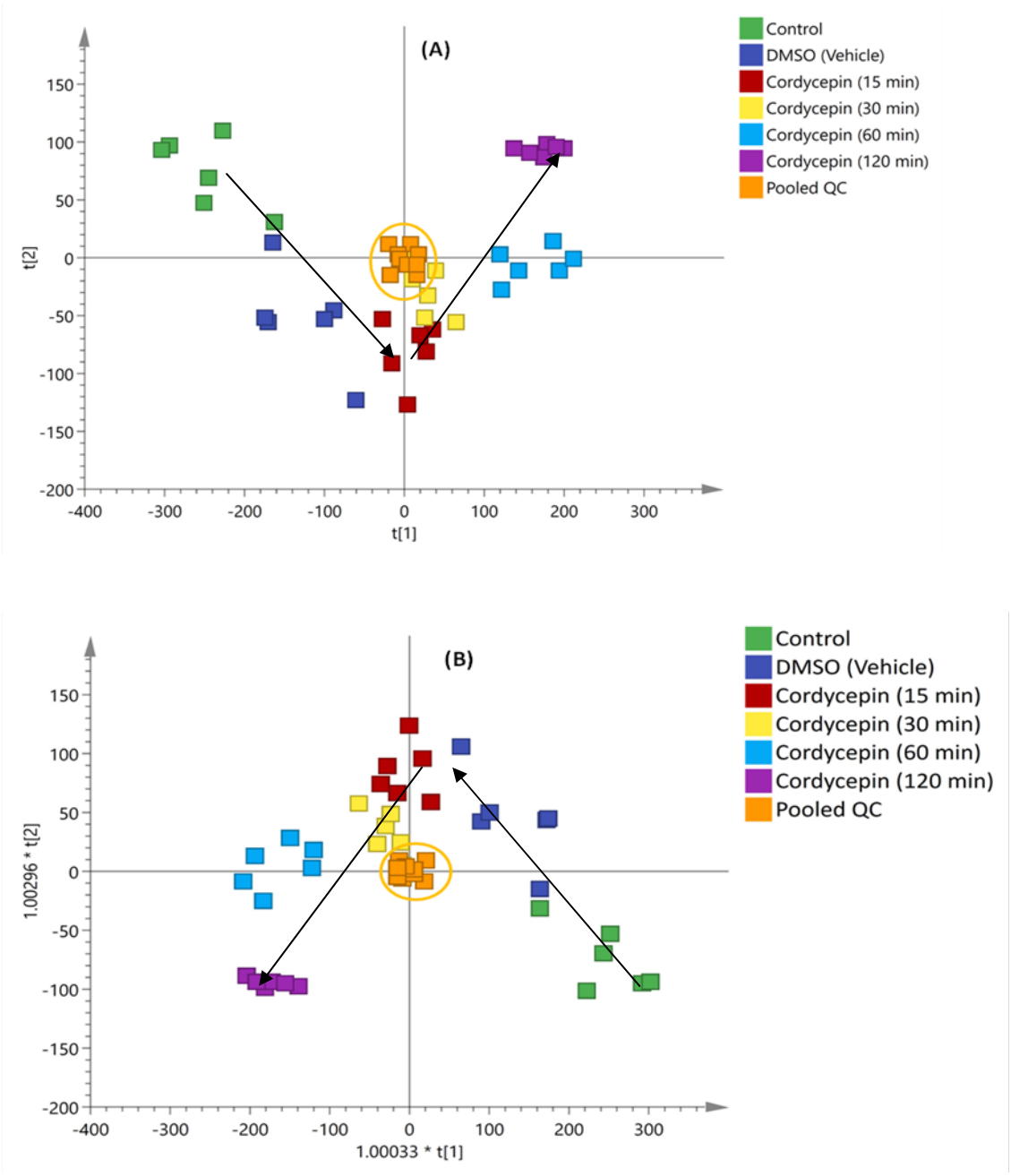


Figure 5.5 Scores plot of principal component analysis (PCA) (A) and OPLS-DA (B) of MS spectral data using all the detected ion features and samples (n = 50 including 8 quality controls: Pooled QC and 6 systems blank). Close clustering of pooled QC samples indicates limited method associated variation. 15 (red boxes), 30 (yellow boxes), 60 (blue boxes) and 120 (violet boxes) min cordycepin treated MCF-7 cells, DMSO treated MCF-7 cells (dark blue boxes) and control (green boxes). Arrows are drawn as a visual guide indicating the relationship between the time points and the mass spectra. .

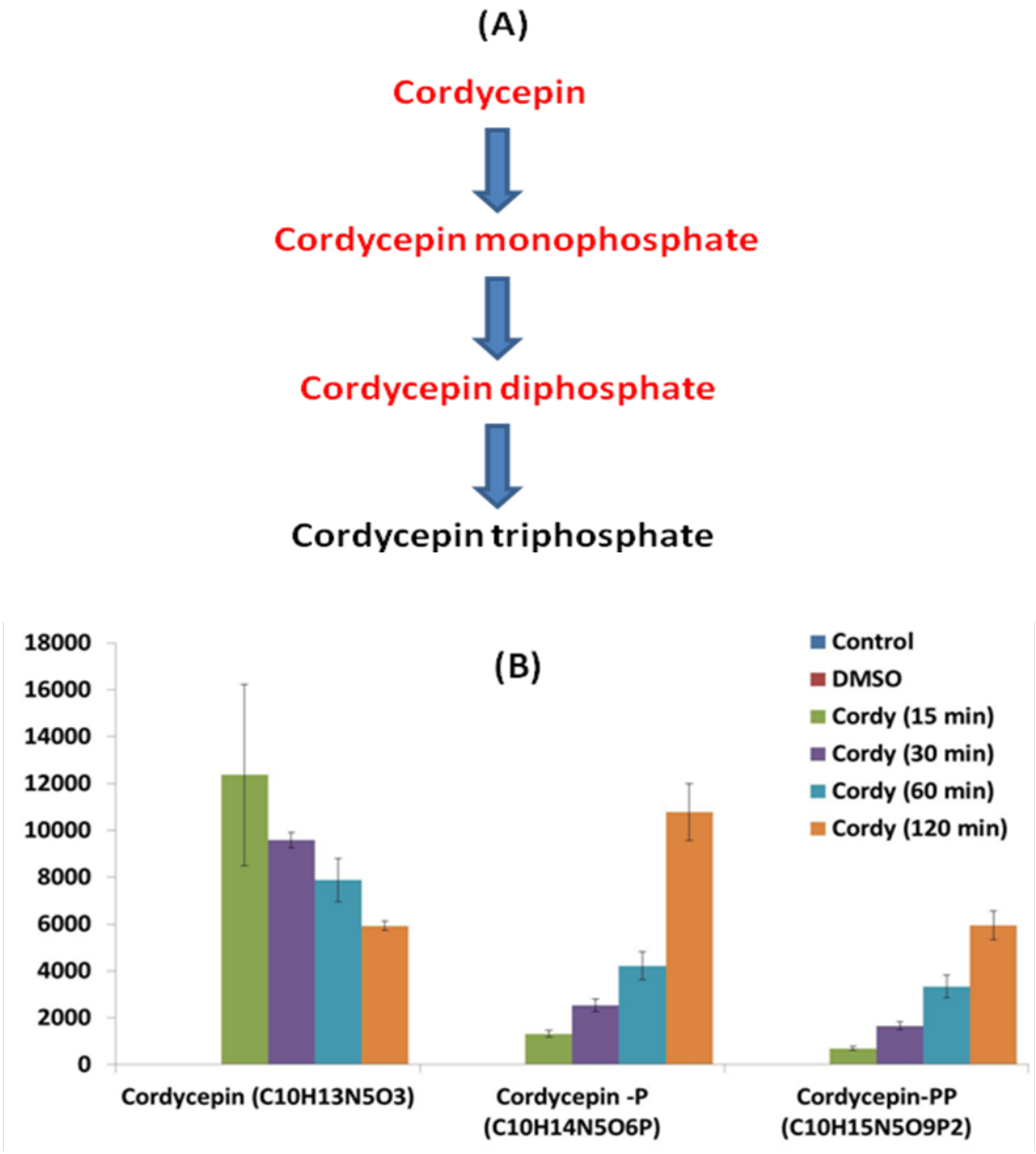


Figure 5.6 (A) Common pathway of cordycepin metabolism in mammalian cells. Metabolites highlighted in red are identified in MCF-7 cells. (B) The abundance of cordycepin and its metabolites varies in MCF-7 cell treated with cordycepin at different time points (15 (green), 30 (violet), 60 (blue) and 120 (orange)). The mean abundance of each analyte is represented by a horizontal bar.

5.5.2.3 Metabolic identification of MCF-7 cells treated with cordycepin

A PCA and OPLS-DA based on cellular metabolites demonstrated that the control and vehicle (DMSO treatment) clustered closely within each group and separately from each other, indicating different metabolic patterns among the time points (Figure 5.5). Exposure to cordycepin caused significant changes in the MCF-7 metabolic pattern which indicated a distinct modulation of the MCF-7 cell metabolism. For the investigation of metabolome change in MCF-7 cells treated with cordycepin at the different time points (15, 30, 60 and 120 min), detected ions were pre-selected as candidates when their VIP values were $\geq$ 1.00. Detected ions with FDR $\leq$ 0.05 (ANOVA) were then selected as those which showed greatest correlation with the OPLS-DA discriminant scores, in order to decrease the risk of false positive in the selection of potentially significant ions. Applying such an approach, mass ions for discriminating metabolome changes and chemical compound types were identified. Differences between sample classes are summarised in the accompanying tables (Supplementary Table 5.1), with tentative identities. 1,670 ions were initially detected and 78 ions were found to be significantly altered. Based on exact mass (with mass error $\leq$ 5 ppm) and compared to authentic standards (if they are available) and data from literatures, 42 of the significantly detected ions were identified as shown in Table 5.3. The list was

refined to present only identified metabolites showing significant differences among control, vehicle (DMSO) and cordycepin treatment samples (FDR < 0.05). 15 and 30 min after a treatment with cordyceycepin 22 metabolite levels were significantly altered, with 9 metabolites reduced and 13 metabolites increased in cordycepin-treated MCF-7 cells and untreated MCF-7 cells. For the 60-minute time point, 26 metabolites were detected with 9 metabolites decreased and 17 metabolites increased. In the 120-minute treatment, 28 metabolites were changed with 7 metabolites reduced and 21 metabolites increased. In addition, in the DMSO treated samples were no significantly changed metabolites in MCF-7 cells. This indicated that the DMSO used as vehicle did not significantly affect the metabolome of MCF-7 cells in this study.

Table 5.3 The identified metabolites that were changed significantly during the treatment with cordycepin

Metabolites	m/z	RT (Min)	mass error (ppm)	FDR	Fold change (X/Control)				
					DMSO	Cordycepin (15 min)	Cordycepin (30 min)	Cordycepin (60 min)	Cordycepin (120 min)
Homogentisic acid	85.0282	8.20	0	1.42E-09	1.01	1.31	1.28	1.46	1.74
Sarcosine	88.0403	8.15	2	4.54E-03	1.03	1.85	2.04	2.06	1.90
(S)-2-Acetolactate	113.0243	8.18	1	1.00E-03	0.85	1.05	1.00	1.19	1.40
Creatinine	114.0660	7.81	1	2.12E-10	1.00	0.64	0.53	0.58	0.70
Creatine	132.0765	8.17	1	2.33E-05	1.00	1.74	1.91	2.03	2.08
L-Homocysteic acid	138.0491	6.16	1	1.24E-03	0.89	2.21	2.45	2.51	3.79
Phenylpyruvic acid	165.0543	8.01	1	0.00E+00	1.07	1.18	1.20	1.25	1.52
Pyridoxine	170.0808	7.03	2	3.06E-05	0.96	1.16	1.30	1.33	1.55
Citrulline	176.1029	8.69	1	1.49E-03	0.88	1.23	1.35	1.69	2.80
Phosphohydroxypyruvic acid	184.9852	17.37	1	3.94E-04	1.26	1.52	1.07	0.75	0.75
Phosphocreatine	210.0284	8.37	0	2.28E-04	1.04	0.49	0.47	0.50	0.69
L-Valine	90.0548	17.08	3	2.35E-04	1.18	1.52	0.88	0.77	0.79
L-Arginine	99.0551	0.66	1	1.30E-03	0.98	0.85	0.70	0.92	0.67
Tyrosine	182.0808	8.01	1	3.34E-08	1.06	1.16	1.17	1.24	1.49
Octenedioic acid	171.0660	2.84	1	1.73E-03	0.92	1.08	1.19	4.15	5.12
Suberic acid	173.0816	2.74	1	1.81E-05	0.92	0.87	1.20	3.57	2.94
Hydroxyadipic acid	180.0866	7.64	1	2.13E-05	0.78	0.97	0.93	1.03	1.22
Glyceraldehyde	71.0135	8.22	1	6.86E-04	0.84	1.06	0.99	1.17	1.40
D-Glyceraldehyde phosphate	168.9907	8.34	1	3.79E-06	0.99	0.36	0.34	0.28	0.30
Myoinositol	198.0971	8.05	1	1.65E-05	0.75	1.17	1.10	1.26	1.55
Adenine	136.0617	7.47	3	1.17E-04	1.13	6.77	13.10	18.44	41.26
Hypoxanthine	137.0457	6.16	2	1.99E-04	0.85	13.10	15.18	16.37	27.10
Phosphoenolpyruvic acid	166.9751	9.22	0	2.55E-03	1.18	0.23	0.19	0.33	0.38
5'Deoxyadenosine	252.1092	3.25	1	2.23E-04	0.90	>1000.00	>1000.00	>1000.00	>1000.00
Uracil	79.0023	2.80	2	2.70E-07	-	>1000.00	>1000.00	>1000.00	>1000.00
4,5-Dihydroorotic acid	80.0243	3.31	1	5.50E-03	-	>1000.00	>1000.00	>1000.00	>1000.00

Metaboloites in red were identified by using commercially available standards and the others were identified by comparison with the MS library.

Table 5.3 (Cont.) The identified metabolites that were changed significantly during the treatment with cordycepin

Metabolites	m/z	RT (Min)	mass error (ppm)	p-value	Fold change (Drug/Control)				
					DMSO	Cordycepin (15 min)	Cordycepin (30 min)	Cordycepin (60 min)	Cordycepin (120 min)
Dihydrothymine	129.0656	17.20	1	3.69E-03	1.08	1.26	0.87	0.70	0.75
Ureidosuccinic acid	175.0358	7.01	1	3.56E-03	0.93	0.11	0.03	0.01	0.00
Deoxyribose 1-phosphate	195.0064	7.43	0	8.03E-04	0.00	87.41	179.53	289.76	718.65
Acetic acid	59.0134	8.18	1	1.27E-05	0.82	0.98	1.00	1.07	1.27
Dihydroxyacetone	71.0135	8.22	3	6.86E-04	0.84	1.06	0.99	1.17	1.40
Topaquinone	128.5134	3.21	1	2.82E-03	-	>1000.00	>1000.00	>1000.00	>1000.00
cis-Aconitic acid	173.0091	9.57	1	9.60E-06	0.99	1.54	1.42	1.53	1.51
Citric acid	191.0198	9.51	1	1.01E-05	1.18	1.58	1.76	1.64	1.76
Phenylalanylphenylalanine	127.0389	2.06	1	1.70E-07	0.98	0.90	0.96	0.65	0.38
Trimethylamine N-oxide	76.0755	17.17	1	4.70E-03	1.00	1.19	0.76	0.61	0.69
3-keto-2-Methylbutyrate	79.0400	2.80	1	3.24E-05	4.72	4.88	4.62	5.01	5.26
PC/PE	742.5389	5.69	1	1.10E-03	0.90	0.65	0.53	0.67	0.70
Niacinamide	123.0550	17.20	0	1.51E-03	0.90	1.02	0.78	0.60	0.66

Metaboloites in red were identified by using commercially available standards and the others were identified by comparison with the MS library.

5.5.3 Biological pathways analysis

To characterise biological pathways that may be affected by 50 μM of cordycepin in MCF-7 cells compared with control cells, various changes in levels of intermediate compounds in amino acid metabolism, TCA intermediate compounds and intermediate compounds in purine and pyrimidne metabolism were determined and are summarised in Table 5.3. In brief, the significantly altered these intermediate compounds were associated with bioenergetics as illustrated in Figure 5.7 and Figure 5.8 shows some other changes in metabolite levels.

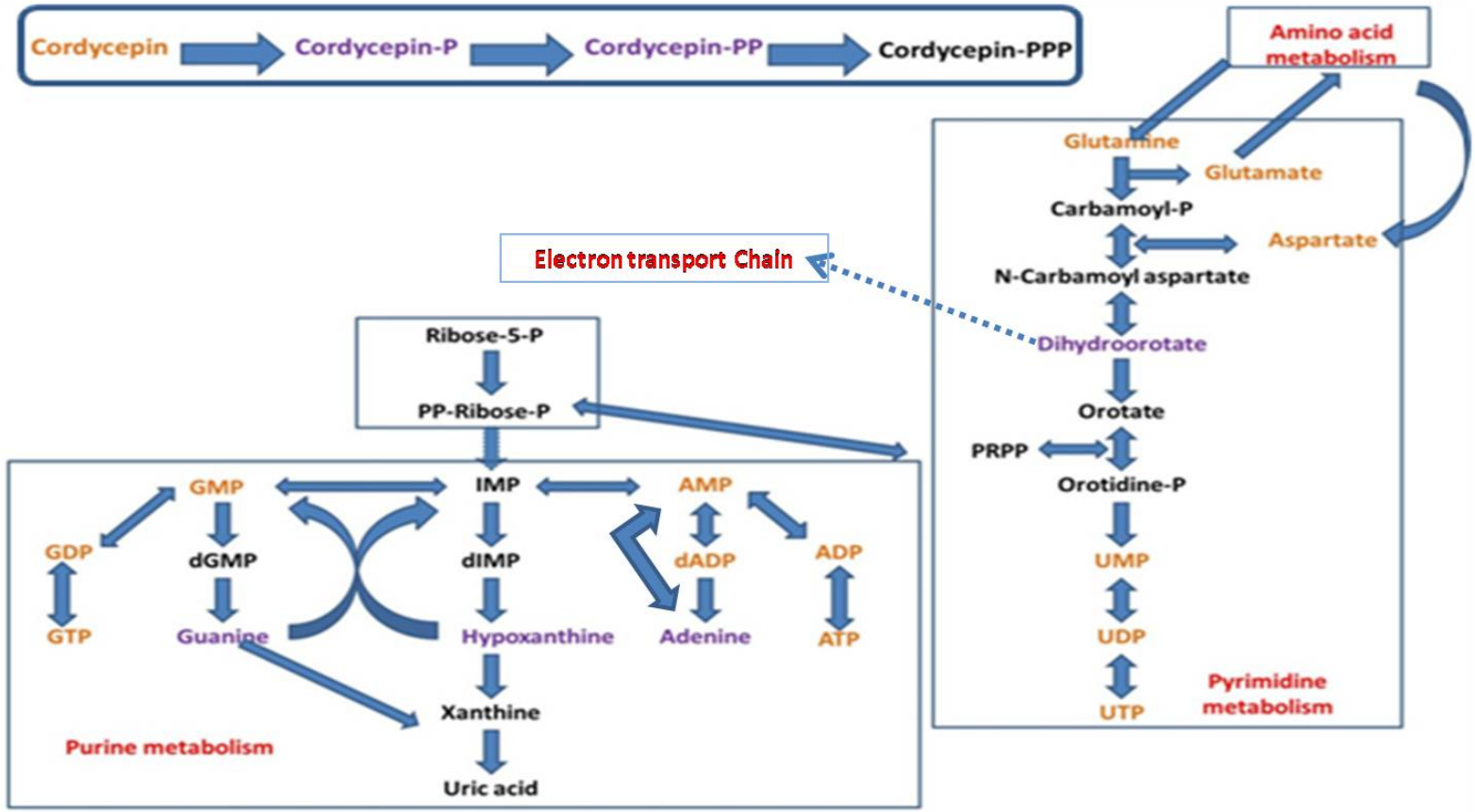
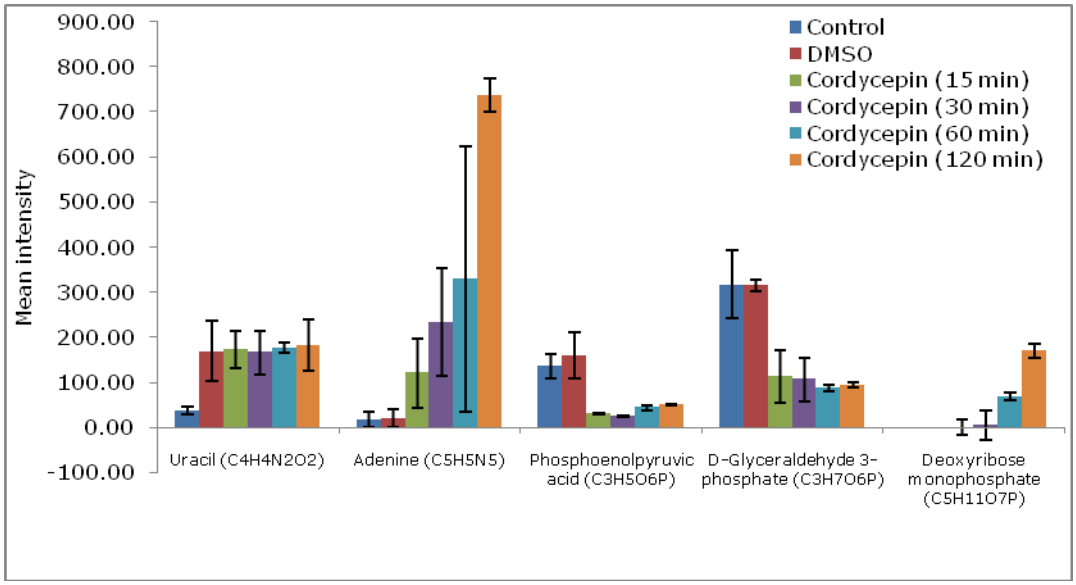


Figure 5.7 The cordycepin metabolism and possible biological pathways that are affected by cordycepin in MCF-7 cells. Metabolites in brown indicate the decrease in their levels and in violet indicate the increase in their levels.



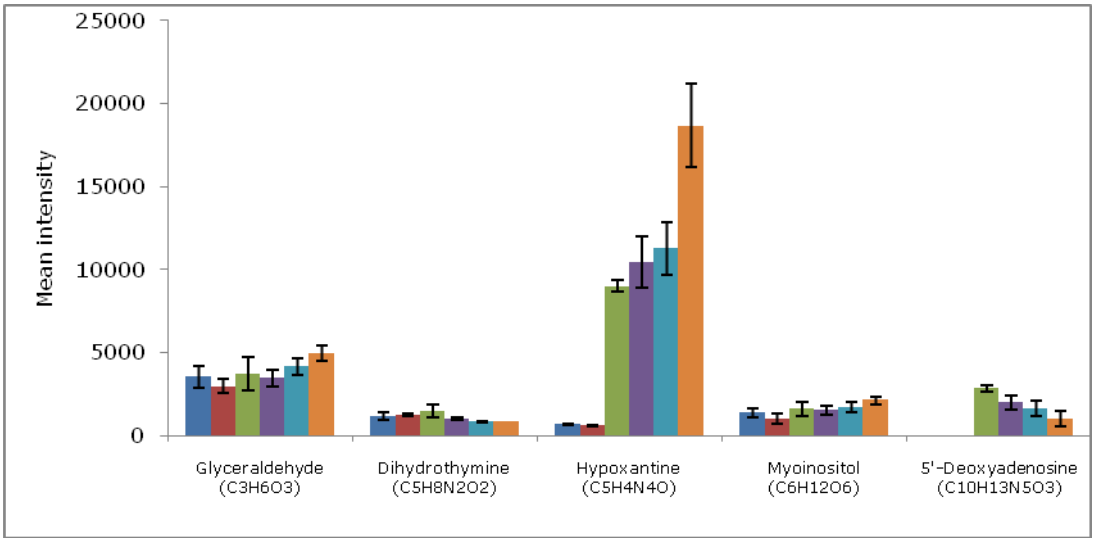


Figure 5.8 Level changes of some metabolitesin MCF7 cells exposed to 50 μM cordycepin at 15, 30, 60 and 120 min.

5.6 DISCUSSION

Cell based metabolomics using LC-MS approach provides a powerful analytical tool for the identification of cellular pathway alterations and possible mechanism of drugs. This is the first study that identifies metabolite alterations, affected pathways and key metabolites for the cordycepin with or without pentostatin response in MCF-7 cells.

5.6.1 Pentostatin effects on cordycepin stability in MCF-7 cells

The significantly increased levels of cordycepin and cordycepin monophosphate and the significantly decreased levels of deoxyinosin in MCF-7 over the time point as summarised in Table 4.2 and shown in Figure 4.4 indicated pentostatin can inhibit adenosine deaminase. Several previous analyses by others have also shown the inhibitory effect of pentostatin on adenosine deaminase (239–241). Cordycepine is an analogue of the nucleoside adenosine that is converted into mono, di and tri-phosphates. These phosphate forms have been shown to be active forms of cordycepin (226). In the results, it is found that only cordycepin monophosphate was significantly enriched; these may form the degradation of cordycepin di- and tri-phosphates in during an extraction process or storage time. This is not surprise because nucleoside phosphates compounds have been reported that they

can be easily hydrolysed (240). Moreover cordycepin and its phosphate compounds have a very short half-life (240,242,243).

Tsai et al. has found that cordycepin is eliminated in 1.6 min in rats (243). Adenosine deaminase is an enzyme that is commonly found in most of mammalian cells. The adenosine deaminase catalyzes the hydrolysis of deoxyadenosine to yield deoxyinosine (239). It has been reported that adenosine deaminase inhibitors such as pentostatin can inhibit the activity of adenosine deaminase and thus increase the half-life of cordycepin in vitro and in vivo studies (239–241). These studies and the data in this study are confirmed that pentostatin can increase the activity of cordycepin by an inhibition of adenosine deaminase in MCF-7 cells.

However, pentostatin itself can affect on cellular metabolites of MCF-7 cells as summarised in Table 4.2. Pentostatin has been reported that it has a cytotoxic effect on cancer cells (244–247). Soares et al. have shown that pentostatin can decrease inosine levels in cancer cells resulted to decrease proliferation (247). This work and the data may indicate that pentostatin can effect inosine metabolism.

5.6.2 Effects of combination of cordycepin and pentostatin on MCF-7 metabolite profile.

In previous study by Wahyu, she characterised the anti-breast cancer activity of the combination of cordycepin and pentostatin in the same drug concentrations as the results in this study and showed the effects of the drug combination by the intracellular reduction of nucleoside phosphate compounds as a consequence of treatment (235). In the results, it is found that the levels of adenine and adenosine in MCF-7 cells treated with 50 μM of cordycepin alone and 50 μM cordycepin + pentostain 1 μM combined were significantly increased and decreased, respectively (Table 4.2). Adenine and adenosine are used in AMP, ADP and ATP biosynthesis (248). It is found that the level of AMP and ADP were significantly reduce after treatment with drugs, however, the highest changes in the levels of AMP, ADP and GMP were found with cordycepin and pentostatin combined (Table 4.2). Furthermore, it is also observed that the levels of GMP and ureidoisobutyric acid involved in GMP biosynthesis (249) were also significantly decreased in MCF-7 cells exposed to cordycepin and pentostatin combined. From the Wahyu's work (235) and the results obtained in this study it is confirmed that pentostain can increase effects of cordycepin on MCF-7 cells through the nucleoside phosphate synthesis.

Interestingly, it is found that the level of NAD^+ was significantly decreased in MCF-7 cells treated with cordycepin + pentostatin combined (see Table 4.1). NAD^+ is a coenzyme found in all mammalian cells. NAD^+ is the crucial intermediate metabolites in electron transport chain (ETC) generating ATP (250). This finding may suggest that cordycepin + pentostatin combined may interfere with ETC in MCF-7 cell. Moreover, it is found that level of pantothenate was significantly decreased and the level of pantetheine was significantly increased. Both pantothenate and pantetheine are intermediates in CoA biosynthesis; pantetheine is a substrate needed to form pantothenate. CoA is a coenzyme in the synthesis and oxidation of fatty acid in all mammalian cells (251). This finding may indicate that cordycepin + pentostatin combined may also inhibit CoA biosynthesis.

5.6.3 The effects of cordycepin on cellular metabolites of MCF-7 cells.

In previous section, the effects of cordycepin with or without pentostatin were investigated and it is found that the metabolome of MCF-7 cells was changed after two hour treatment. In order to understand how cordycepin can affect metabolic profiles of MCF-7 cells, the effects of cordycepin at different time points (15, 30, 60 and 120 min) were studied. The results indicate significant metabolite levels and metabolites ratio changes that are part of

several pathways including amino acid metabolism, purine and pyrimidine metabolism, and TCA cycle. This is summarised in Table 5.3.

Alterations in purine and pyrimidine metabolism including ATP, CTP, GTP, and UTP have been previous implicated in the MCF-7 cells exposed to cordycepin (235). Several metabolite level and metabolite ratio changes in adenine, hypoxanthine and deoxyribose phosphate at 30 min and in myoinositol at 120 min post-cordycepin treatment (see Table 4.2) were observed. Alterations of these metabolite ratios can reflect change in purine and pyrimidine metabolsim. Cordycepin phosphate compounds have been reported to inhibit purine and pyrimidine metabolsim in many cells (109,241,252,253). This inhibition causes the reduction of nucleoside phosphate levels. Results from previous studies have associated the cordycepin treatment response with reduced levels and ratios of nucleoside triphosphate compounds (ATP, CTP, GTP and UTP) (235,252). The results in this study, it is observed that most levels and ratios of intermediate compounds of purine and pyrimidine metabolism were altered at 30 min post-cordycepin treatment, and increased or decreased according to the specific time points. This suggests that cordycepin may interfere with the purine and pyrimidine metabolism at 30 min in MCF-7 cells.

The inhibition of purine and pyrimidine metabolism could ultimately be the cause for an activations of bioenergetics which has previously been implicated in ATP synthesis in many anticancer drugs (254,255). It is observed that several metabolite level changes of the bioenergetics intermediate compounds at 30 minutes post-cordycepin treatment (D-glyceraldehyde phosphate, phosphoenolpyruvic acid, cis-aconitic acid and citric acid) as summarised in Table 5.2. Alteration of these metabolites can reflect changes in bioenergetics of MCF-7 cells.

Moreover, it is found that the levels of creatinine and phosphocreatine were significantly decreased and creatine significantly increased at 15 minutes post-cordycepin treatment (Table 5.2). These metabolites are intermediate compounds in cell's energy shuttle (256,257) as following:

Creatine + ATP <----------> Phosphocreatine + ADP

Phosphocretaine ---------> Creatinine + PO_4^{2-}

This finding may suggest that cordycepin may affect cell's energy shuttle only 15 minutes after treatment.

Surprisingly, in these studies topaquinone and its level was dramatically and significantly increased in MCF-7 cells exposed to cordycepin (Table 5.3). Topaquinone, the cofactor in most human copper-containing amine oxidase, has been reported to oxidise

DNA-bound polyamines leading to degradation of DNA, and is involved in cell proliferation, differentiation and apoptosis (258,259). This finding suggests that one possible mechanism of cordycepin in MCF-7 cells might be the induction of human copper-containing amine oxidase activity, causing the inhibition of cell proliferation and differentiation and/or the activation of apoptosis.

5.7 CONCLUSION

The results of the untargeted metabolite profiling demonstrated clear anti-breast cancer effects of cordycepin and pentostatin. By investigating the metabolite profiles, clear synergistic effect of cordycepin and pentostatin combined in comparison to cordycepin activity alone in MCF-7 cells was observed.

Untargeted cell-based metabolomics using LC-MS coupled pathway analysis was successfully applied to explore the metabolome changes induced by cordycepin with or without pentostatin on MCF-7 cells. Based on the data extracted through the statistical multivariate analysis, differences in the metabolic alterations were detected. Significantly altered metabolites, including amino acids, fatty acids, lipids, organic acids and phosphate compounds, were identified as potential key metabolites in cordycepin-treated MCF-7 cells. Moreover, it is found that pentostatin can inhibit cordycepin degradation by ADA, resulting in an increase in the effects of cordycepin.

Furthermore, the pathway analysis indicated that anti-breast cancer activity was mainly responsible for alterations in purine and pyrimidine metabolism and bioenergetics. Additionally, cordycepin may be involved in the inhibition of cell proliferation and differentiation, and the activation of cell apoptosis.

CHAPTER VI: CELL-BASED METABOLOMICS USING LC-MS TO STUDY THE METABOLIC EFFECTS OF FLUOXETINE ON GLUCOSE-TREATED MURINE PANCREATIC BETA (MIN6) CELLS

6.1 ABSTRACT

Fluoxetine is used as an effective antidepressant. However, patients using fluoxetine have a risk of pancreatic beta cell malfunction resulting in diabetes. Previous studies have revealed that fluoxetine could decrease mitochondrial electron transport chain enzyme activity in beta cells. However, the exact mechanism underlying its mode of action in beta cells remains largely unclear. In this study, murine pancreatic beta (MIN6) cells were exposed to 30 μM fluoxetine; 7 minutes post-treatment, cell-based metabolomics using LC-MS coupled with uni- and multivariate statistical analysis was used to characterise the metabolic variations of intracellular metabolites. Moreover, the effects of 10 μM rotenone, 1 μM antimycin A and 6 mM azide on MIN6 cells was investigated to compare with fluoxetine treatment. The orthogonal partial least-squares discriminant analysis (OPLS-DA) scores plots of the MS spectra demonstrated that the fluoxetine-treated MIN6 cells were clearly distinguished from the glucose treatment. In total, 66

differential metabolites were identified to discriminate the two groups. These key metabolites were mainly involved in bioenergetics. This study indicates that fluoxetine may exert beta cell dysfunction by affecting ETC complex IV. These findings should aid in the understanding of the biological mechanisms underlying fluoxetine induced diabetes.

Keywords: fluoxetine, MIN6 cells, beta cell dysfunction, cell-based metabolomics using LC-MS

6.2 INTRODUCTION

Fluoxetine is a selective serotonin reuptake inhibitor (SSRI) antidepressant drug. It affects neurotransmitters in the central nervous system by blocking only the serotonin transporter. Fluoxetine is used for the treatment of major depressive disorder, bulimia nervosa obsessive-compulsive disorder, panic disorder, and premenstrual dysphoric disorder (260–263). Use of fluoxetine is associated with an increased risk of pancreatic beta cell dysfunction. This could lead to diabetes resulting to weight gain and obesity which turn leads to an increased incidence of hypertension, dyslipidaemia, coronary artery disease, insulin resistance and overt diabetes (121–126,260,264). SSRI drugs have been currently reported that they can directly impact pancreatic beta cell function (122). De long et al. demonstrated that fluoxetine decrease beta cell function and led to an increased production of reactive oxygen species and oxidative damage. This may contribute to decrease mitochondrial electron transport chain enzyme activity (124). Since fluoxetine targets mitochrondrial function and as the latter is an important component of the glucose stimulated-insulin secretion pathway, the glycaemic affects of fluoxetine may result from a direction on beta-cell function (126).

Despite this evidence, little is known about the metabolic effects of fluoxetine as an agent of impaired beta cell function. Impairment of beta cell function causes a pathological state in which its function cannot maintain glucose homeostasis due to impaired insulin secretion and insulin resistance. Impairment beta cell function by fluoxetine may increase reactive oxygen species and oxidative damage. This may result in decreased mitochondrial electron transport chain enzyme (ETC) activity (126). Therefore, in order to understand the effects of fluoxetine toxicity in beta cells, it is important to investigate the cellular responses associated with this drug.

Only a few experiments investigating the cellular responses to fluoxetine have been reported (122,124,125). De Long et al have found that fluoxetine increases a production of reactive oxygen species and oxidative damage in rat beta cells. This may contributes to decreased mitochondrial electron transport chain enzyme activity (124). Paul has suggested that fluoxetine inhibits mitochondrial respiration in murine beta cells (126). Moreover, Isaac et have shown that fluoxetins inhibit insulin secretion and induce apoptosis of pancreatic murine beta cells (122). Since the mechanism of these compounds on cell function is clearly understood, this comparison study provides insight into how fluoxetine disturbs cellular function on pancreatic beta cells.

Herein, the HILIC-MS method was applied to investigate the cellular response of MIN6 cells to fluoxetine. Short-time reaction response was observed to assess the effect of this drug. In addition, antimycin A-, azide- and rotenone-treated-MIN6 cells were investigated to compare with the fluoxetine-treated MIN6 cell result. The biological pathways that are involved in fluoxetine, antimycin A, azide and rotenone function were also investigated.

6.3 OBJECTIVES

This part of the project has three main objectives:

- to apply cell-based metabolomics using pHILIC-MS to investigate the metabolic profile of MIN6 cells exposed to fluoxetine, antimycin A, sodium azide and rotenone.
- to identify the significant cellular metabolites of MIN6 cells that are affected by fluoxetine, antimycin A, sodium azide and rotenone.
- to identify the possible biological pathways that are affected by fluoxetine, antimycin A, sodium azide and rotenone in MIN6 cells.

6.4 MATERIALS AND METHODS

6.4.1 Chemicals

LC-MS-grade acetonitrile and methanol were purchased from Fisher Chemicals (Laoughborough, UK). HPLC-grade water was obtained from Elga Purelab Genetic (, Buckingham, UK). Formic acid (LC-MS grade) was purchased from Acros Organics (Geel, Belgium), and all standard chemical compounds were purchased from Sigma-Aldrich (Poole, UK). These standard chemical compounds are all HPLC or LC-MS grade.

6.4.2 Study design

Cell lines were treated with 20 µl of 1M glucose for 7 minutes to give a 10 mM final concentration. The concentration and time treatment give a maximal insulin secretion with previous reports of glucose-stimulated insulin secretion in islets and INS-1 832/13 cells (126). The glucose-treated cells were then exposed to:

- 2 µl of 10mM dimethyl sulfoxide (DMSO) as a vehicle control,
- 2 µl of 10mM rotenone (in DMSO) to give a final concentration of 10 µM,
- 2 µl of ethanol as a vehicle control,
- 2 µl of 1mM antimycin A (in ethanol) to give a final concentration of 1 µM,

- 4 µl of 3 M Na_3N (in H_20) to give a final concentration of 6 mM and
- 6 µl of 10 mM fluoxetine (in H_20) to a give final concentration of 30 µM.

Each group had 6 biological replicates.

6.4.3 Pancreatic beta cells

MIN6 cells, a murine pancreatic beta cell line, were cultured by Paul A. Smith (Faculty of Medicine & Health Sciences, University of Nottingham Medical School, Queen's Medical Centre, Nottingham, NG7 2UH, UK) as previously described (126). Briefly, MIN6 cells were cultured in DMEM containing 25 mM glucose supplement with 15% fetal calf serum, 100 u/ml penicillin, 100 µg/ml streptomycin and 5 µl/l β-mercaptoethanol. MIN 6 cell were seeded 5 days before the experiment in 25 ml polystyrene non-pyrogenic culture flasks at a density of 1.4 x 10^8 cells/ml, in a humidified atmosphere to about 80% confluence. For the studies MIN6 cells were used between passages 10 and 30. MIN6 cells were discarded and washed with 5 ml of PBS. Next, 3 ml of trypsin/EDTA was added and put in a 32°C water bath for 3 minutes. To stop the reaction in culture flasks, 17 ml of HANKs BSA (0.1% wt/vol bovine serum albumin) was added to give a final total volume of 20 ml. MIN6 cells were precipitated by centrifugation for 2 min at 1,000 rpm. The supernatant was discarded and the MIN6 cells resuspended in 6 ml of HANKs BSA.

6.4.4 MIN6 cell experiments

1 ml of cell suspension ($1x10^{14}$cells/ml) and 1 ml of HANKs BSA were added to 8 chambers of Rank Brothers dual digital model 20 oxygen measurement controllers at 32°C with magnetic spinner at low speed for 10 min to equilibrate the system. 20 µl of 1 mM glucose was added to each of 7 chambers and leaving one chamber as a basal control. After a further 10 minutes, additions to 6 chambers with various conditions were made. This left one chamber as a glucose control. After 8 minutes, MIN6 cells were transferred to fresh Eppendorff tubes and centrifuged for 2 minutes at 1,000 rpm to stop the reaction. The supernatants were poured off and cell pellets kept at -80°C for further processes.

6.4.5 Metabolite extraction

MIN6 cell pellets were extracted with cold methanol (-20°C) and the cell suspensions vortexed for 2 hours in a cold-room (4°C). The suspensions were centrifuged for 10 minutes at 15,000 rpm at 4°C. The supernatants were transferred to new eppendorf tubes and kept at -80°C for further analysis.

6.4.6 Metabolomics analysis

Analyses were performed using non-targeted protocols using Exactive Orbitap MS with pHILIC-MS instrumentation previously reported in Chapter II. A mixture of authentic standard compounds

was injected before sample analysis for metabolite identification. The pooled QC sample was obtained by taking a 10 µl aliquot of all samples from the study. The pooled QC sample was injected every 6 sample injections and was used to assess instrument performance.

6.4.7 HILIC-MS analysis

Liquid chromatography was performed using the Thermo Scientific Accela LC systems coupled with the Exactive Orbitrap MS as previously described (13). HILIC separations were achieved using a ZIC-pHILIC column with a 150 x 2.1 mm, 3.5 µm particle size, equipped with a ZIC-pHILIC PEEK guard column with a 20 x 2.1 mm, 5 µM particle size. The mobile phases were acetonitrile (A) and 20 mM ammonium carbonate (pH 9.2) (B) at the flow rate of 0.20 ml/minute at 40°C. At t=0 minutes run, at 5% B, a gradient to 95% B was concluded at 13 minutes and a gradient to 5%B was completed at 15 minutes. Following column wash and equilibration, the run was concluded with 5% B at 20 minutes. Data acquisition of ion detection was performed between 70 to 1,400 *m/z* in positive and negative modes.

6.4.8 Data processing and statistical analysis

LC-MS data were pre-processed (filtering and alignment) and extracted using Progenesis QI software. The extracted *m/z* data was exported to text file data for further analysis. Manual inspection and duplicate removal was performed to form final data by using Xcalibur software version 2.0. Statistical analyses were performed using univariate (Student's T-Test) and multivariate (OPLS-DA) approaches. Simca P version 14.0 was also used for statistical analyses. Detected ions were pre-selected as candidates when their VIP values were $\geq$ 1.00. The VIP value indicates the importance of each metabolite for group separation. Then, these detected ions with a p-Value $\leq$ 0.05 (T-test) were selected as significantly changed ions that were most correlated with the OPLS-DA discriminant scores in order to decrease the risk of false positive in the selection of significantly potentially detected ions. P-value describes a measure of the likelihood that the association between a set of metabolites in the dataset, and a related function, is random. In general, a p-value < 0.05 indicates a statistically significant, non-random association. In addition, features that were detected in every chromatogram and had < 30% of covariant with each group were included in the analysis.

The identification of significantly altered ions in our work was confirmed with authentic standards that are available in our

laboratory using standard peak assignment. Some metabolites were tentatively identified through an accurate mass search of the Human Metabolome database and the METLIN data base with an error rate of less than 5 ppm.

6.5 RESULTS

The metabolomes of murine pancreatic beta cells (MIN6) were investigated by untargeted cell based metabolomics using LC-MS to evaluate which metabolites are affected by fluoxetine. Moreover, rotenone, antimycin A, and azide were also investigated in order to compare their effects with those of fluoxetin: rotenone is a complex I inhibitor of the ETC system, antimycin A is a complex III inhibitor of the ETC system and azide is a complex IV inhibitor of the ETC system. The observed altered metabolites are shown in the next section.

6.5.1 Data Quality

For checking the instrument performance in this study, 5 µL of each sample was pooled to generate a quality control (QC) sample. MS spectral data was aligned using the QC samples. Importantly, the alignment process was applied to the aligned data to identify significant clusters in an unsupervised manner and did not affect the clustering of the samples. An OPLS-DA was applied to better understand the different metabolic patterns and to detect significant ions showing prominent level changes in the models. Any difference between the classes, untreated (basal), vehicles (DMSO and ethanol), rotenone, antimycin A, azide and fluoxetine were also clearly separated in the OPLS-DA scores plot as shown in Figure 6.1.

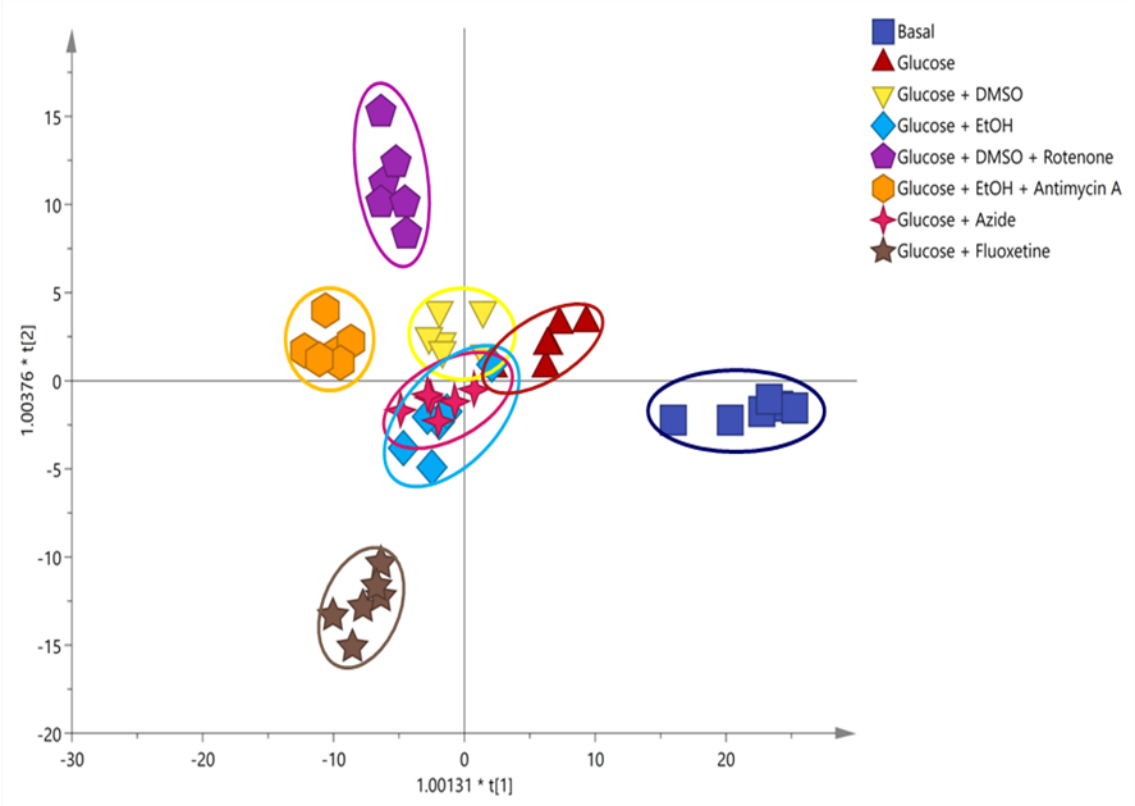


Figure 6.1 Scores plot of OPLS-DA of MS spectral data using all the detected ion features and samples (with R^2X =0.78, R^2Y = 0.973 and Q^2 = 0.868) : basal or untreated (dark blue squares), glucose treatment (red triangles), glucose + dimethyl sulfoxide (DMSO) treatment (yellow inverted triangles), glucose + ethanol (EtOH) treatment (blue diamonds), glucose + DMSO + rotenone treatment (violet pentagons), glucose + EtOH + antimycin A treatment (orange hexagons), glucose + azide treatment (pink four peak stars) and glucose + fluoxetine treatment (brown five peak stars).

6.5.2 Metabolomic analysis of MIN6 cells

An OPLS-DA based on cellular metabolites demonstrated that the basal (untreated), glucose, DMSO (as a vehicle in rotenone samples), ethanol (as a vehicle in antimycin A treatment), rotenone, antimycin A, azide and fluoxetine clustered closely within each group and separately from each other, indicating different metabolic patterns among each sample type. For the investigation of metabolome change in MIN6 cells treated with four compounds, detected ions were pre-selected as candidates with the criteria aforementioned in the experimental section.

6.5.2.1 Metabolic signature of MIN6 cells exposure to glucose

First, the effects of glucose on MIN6 cells were examined. The final concentration of glucose in the cell culture media used in this experiment was determined according to previous publications (265,266). Lorenz et al have shown that the 50 percentage of effective concentration value for insulin secretion from beta cells in response to glucose was 10 mM glucose (265). In addition, Eiazzouny et al have shown that 10 mM glucose did not affect on beta cell survival (266). To investigate the metabolome changes of MIN6 cells which are caused by 10 mM glucose, cell-based metabolomics using LC-MS was performed on the cellular extract. Representative OPLS-DA scores plot of MS spectra obtained from

the basal samples and samples treated with glucose are illustrated in Figure 6.3. The differentiation model featured better predictability with $R^2X = 0.93$, $R^2Y = 0.99$, $Q^2 = 0.9$, and the scores plot showed that there are clear differences between the basal samples and samples treated with glucose. VIP values were used to identify ions responsible for class separation based on multivariate analysis of treated versus control (untreated) groups. In VIP analysis, a VIP value is greater than 1.0 are considered important (267). Statistical analyses for the comparison between treated versus control groups were conducted using ANOVA and FDR values were used to determine statistical differences in ion intensity between treated and control groups (268). In this exploratory analysis, FDR values < 0.05 were considered to be statistically significant. Results are presented as significantly changed if the signal intensity $\geq$ 1.50 fold. The criteria (VIP $\geq$ 1.00, FDR $\leq$ 0.05 and fold change $\geq$ 1.50) was applied to choose the ions that were altered in the glucose treatment in MIN6 cells. Significant results are based on the average of six biological replicates per treatment condition for each compound. At least 44 ions were identified as summarised in Table 6.1. Figure 6.3 shows the level changes of the top ten significantly altered metabolites.

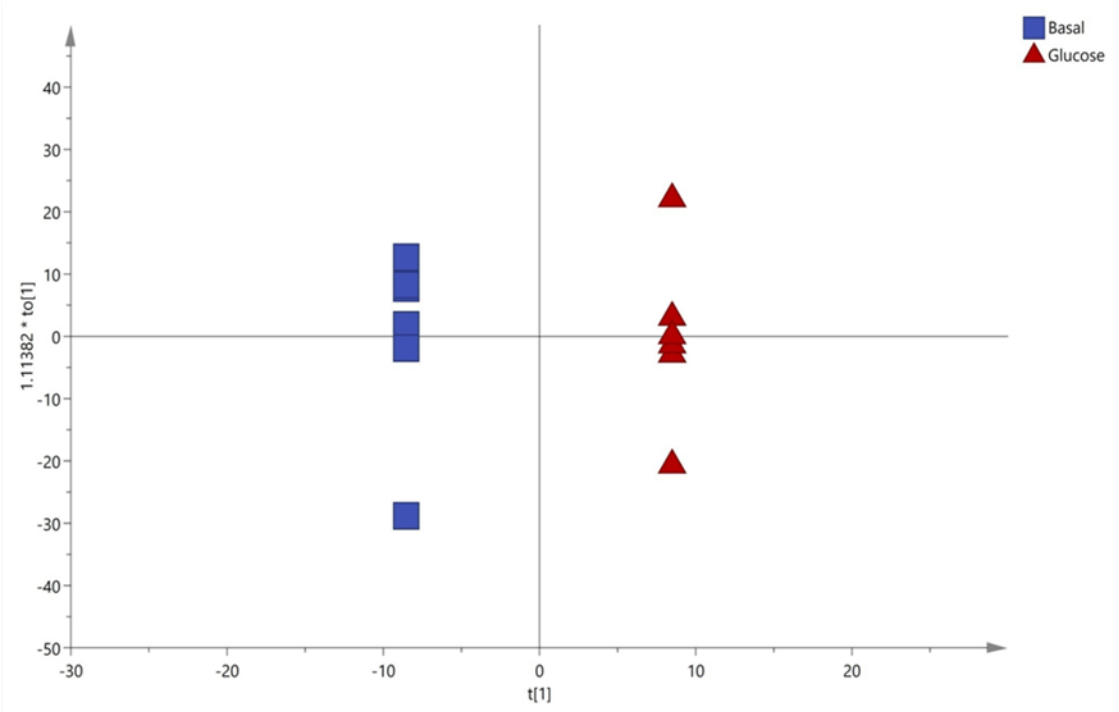


Figure 6.2 Scores plot from OPLS-DA analysis of control and glucose-treated MIN6 cells (with R^2X = 0.94, R^2Y = 1.00 and Q^2 = 0.96). Each point represents cell extracts from one sample of MIN6 cells under control or glucose treatment. Extracts from the same condition are grouped and enclosed with ellipses: basal (blue squares) and glucose (red triangles). .

Table 6.1 The details of metabolites from cell extracts of untreated MIN6 cells (Basal) and 10 mM glucose treated MIN6 cells.

m/z	Polarity	RT (min)	Metabolites	Formula	M.W.	Adduct	Error (ppm)	VIP	FDR	Fold
87.0089	-	3.36	Malonic semialdehyde	C3H4O3	88.0160	M-H	1	1.14	1.55E-02	10.03
87.0089	-	8.62	Pyruvate	C3H4O3	88.0160	M-H	1	1.11	2.27E-04	2.55
89.0246	-	2.63	Dihydroxyacetone	C3H6O3	90.0317	M-H	2	3.26	1.09E-02	9.90
89.0246	-	5.48	Lactic acid	C3H6O3	90.0317	M-H	2	7.12	1.83E-03	14.00
89.0246	-	3.67	Glyceraldehyde	C3H6O3	90.0317	M-H	2	3.89	1.08E-05	14.14
90.0551	+	8.87	β-Alanine	C3H7NO2	89.0477	M+H	1	1.89	3.79E-05	2.53
96.9699	-	7.55	Phosphoric acid	H3O4P	97.9769	M-H	3	7.08	2.17E-03	1.71
101.0245	-	8.60	Succinic acid semialdehyde	C4H6O3	102.0317	M-H	1	3.31	3.00E-06	31.41
102.0551	+	8.47	Acetic acid	C2H4O2	60.0211	M+ACN+H	2	1.28	5.26E-03	2.06
110.9854	-	8.11	Methylphosphate	CH5O4P	110.9853	M-H	1	1.12	6.51E-03	7.45
113.0246	-	8.65	2-Hydroxy-2,4-pentadienoate	C5H6O3	114.0317	M-H	1	2.21	1.88E-06	63.73
115.0038	-	8.87	Fumaric acid	C4H4O4	116.0110	M-H	1	1.35	1.23E-04	8.86
116.0707	+	8.12	L-Proline	C5H9NO2	115.0633	M+H	1	4.85	7.08E-04	1.69
120.0657	+	8.72	L-Threonine	C4H9NO3	119.0582	M+H	1	1.05	3.40E-03	2.45
131.0351	-	8.62	2-Acetolactic acid/3-hydroxy-3-methyl-2-oxo-Butyric acid	C5H8O4	132.0423	M-H	1	1.33	2.60E-05	5.68
132.0769	+	8.87	Creatine	C4H9N3O2	131.0695	M+H	1	1.50	1.42E-03	1.75
133.0144	-	8.82	Malic acid	C4H6O5	134.0215	M-H	1	6.64	7.82E-05	22.10
143.0351	-	8.65	Methylitaconate/2-Methyleneglutarate	C6H8O4	144.0423	M-H	1	2.45	4.40E-06	79.23
145.0144	-	8.55	Oxoglutaric acid	C5H6O5	146.0215	M-H	1	1.91	1.23E-04	16.66
146.0460	-	8.40	L-Glutamate	C5H9NO4	147.0532	M-H	1	4.45	2.64E-03	1.95
162.1126	+	8.52	L-Carnitine	C7H15NO3	161.1052	M+H	1	2.35	7.38E-04	2.65
179.0564	-	8.62	Myoinsoitol	C6H12O6	180.0634	M-H	1	8.07	8.70E-06	51.42
180.0868	+	8.20	Glucosamine	C6H13NO5	179.0794	M+H	1	1.91	8.23E-03	172.13
191.0200	-	9.84	Citric acid/Isocitric acid	C6H8O7	192.0270	M-H	1	4.92	2.37E-03	3.75
232.1546	+	6.65	O-Butyryl-L-carnitine/Isobutyryl carnitine	C11H21NO4	231.1471	M+H	1	1.51	2.92E-04	5.01
246.2428	+	2.60	Myristic acid/Isomyristic acid	C14H28O2	228.2089	M+NH4	0	1.20	2.11E-03	2.14
258.1103	+	8.92	Glycerophosphocholine	C8H20NO6P	257.1028	M+H	1	13.86	4.72E-02	2.06
260.1859	+	6.16	L-Hexanoylcarnitine	C13H25NO4	259.1784	M+H	1	2.50	9.60E-05	7.61
288.2171	+	2.60	L-Octanoylcarnitine	C15H29NO4	287.2097	M+H	1	2.19	4.83E-03	7.85

Metaboloites in red were identified by using commercially available standards and the others were identified by comparison with the MS library.

Table 6.1 (Cont.) The details of metabolites from cell extracts of untreated MIN6 cells (Basal) and 10 mM glucose treated MIN6 cells.

m/z	Polarity	RT (min)	Metabolites	Formula	M.W.	Adduct	Error (ppm)	VIP	FDR	Fold
290.2691	+	2.55	3-hydroxyhexadecanoic acid/2-Hydroxyhexadecanoic acid	C16H32O3	272.2351	M+NH4	1	1.56	6.32E-04	1.92
294.9039	-	14.70	PE	C51H102NO8P	887.7343	M-3H	1	4.26	1.15E-03	1.73
308.0992	-	7.84	N-Acetylneuraminic Acid	C11H19NO9	309.1060	M-H	2	1.20	3.85E-02	3.09
336.0534	+	7.37	5'-Methylthioadenosine	C11H15N5O3S	297.0896	M+K	2	1.07	7.39E-03	1.63
338.0504	+	7.37	8-Hydroxyguanosine	C10H13N5O6	299.0866	M+K	2	1.53	6.82E-03	1.63
349.1178	+	7.83	Glutathione	C10H17N3O6S	307.0838	M+ACN+H	0	2.12	1.73E-02	3.11
359.1202	-	8.62	Glucose	C6H12O6	180.0634	2M-H	2	6.60	9.29E-06	100.40
565.0488	-	9.19	UDP-glucose	C15H24N2O17P2	566.0550	M-H	2	1.79	1.92E-03	2.90
592.8298	+	14.73	Dynorphin A 9-17	C53H85N17O14	1183.6462	M+2H	1	1.16	1.18E-03	2.06
613.1412	-	8.77	CMP-N-acetylneuraminic acid	C20H31N4O16P	614.1473	M-H	2	1.40	1.12E-02	1.99
664.1176	+	8.50	Nicotinamide adenine dinucleotide (NAD)	C21H27N7O14P2	664.1169	M	1	1.72	3.32E-03	1.52
703.5758	+	2.57	Palmitoyl sphingomyelin/SM(d18:0/16:1(9Z))	C39H79N2O6P	702.5676	M+H	1	1.74	3.14E-02	2.22
707.0767	+	7.37	Nicotinamide ribotide	C11H15N2O8P	334.0566	2M+K	1	1.03	2.36E-03	2.00
715.0650	+	7.37	Imidazoleacetic acid ribotide	C10H15N2O9P	338.0515	2M+K	2	3.55	2.80E-03	1.73
760.5858	+	2.35	PE or PC	C42H82NO8P	759.5778	M+H	1	2.64	4.06E-02	1.68
1189.4883	-	6.99	Taurocholic acid 3-sulfate	C26H45NO10S2	595.2485	2M-H	1	1.44	3.89E-03	3.08

Metaboloites in red were identified by using commercially available standards and the others were identified by comparison with the MS library.

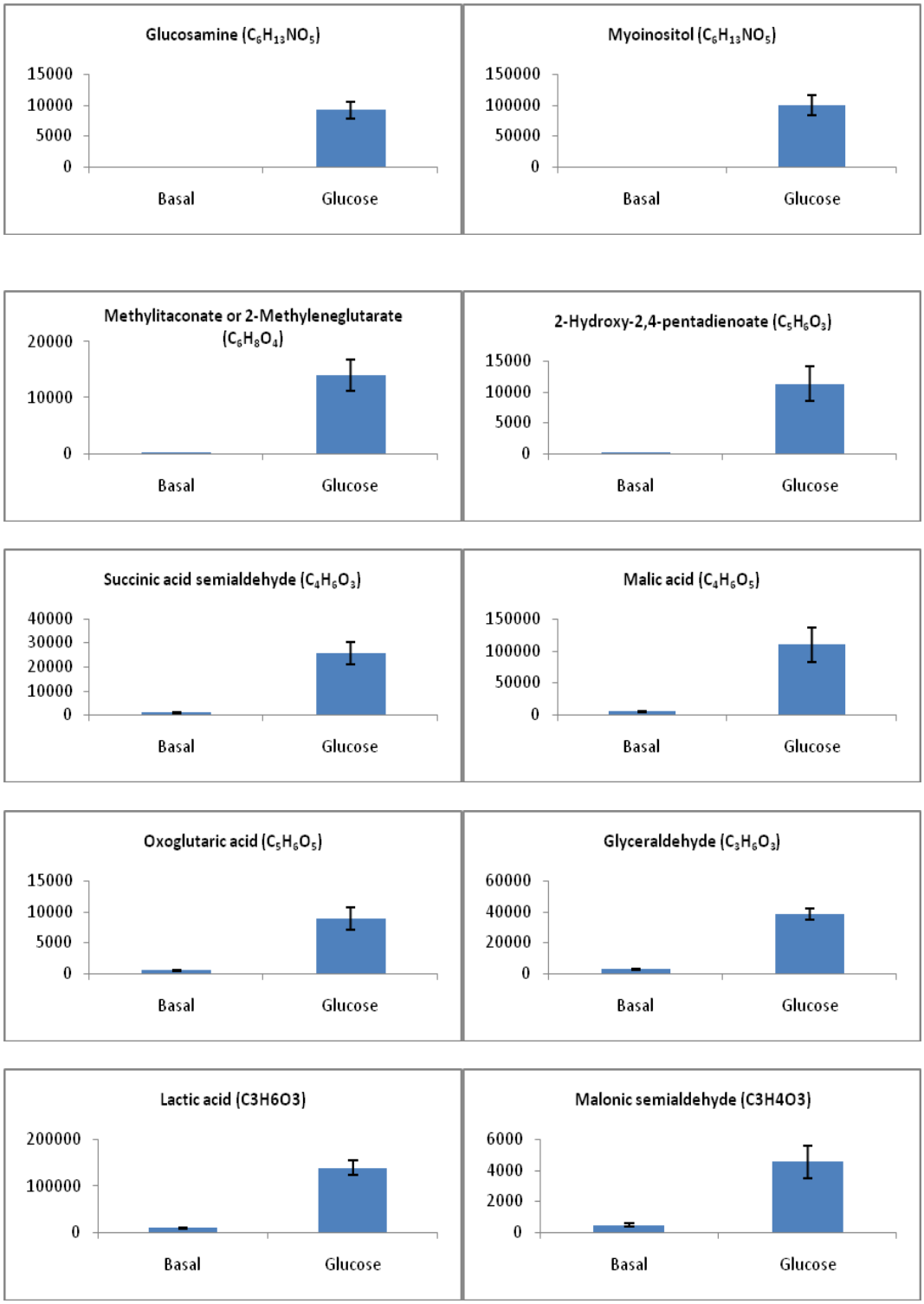


Figure 6.3 Level changes of the top ten altered metabolites of 10 mM glucose treated MIN6 cells (Glucose) compared to untreated cells (Basal).

6.5.2.2 Metabolic signature of glucose-treated MIN6 cells exposure to rotenone

DMSO was used as a vehicle investigating how it compared with the glucose treated samples. The OPLS-DA scores plot shown in Figure 6.4 did not indicate a clear separation in the metabolite profiles between the samples treated with DMSO and those treated with glucose. It is found that 19 ions were significantly altered (VIP $\geq$1.00 and FDR < 0.05) as summarised in Supplementary Table 6.2. Based on exact mass (with mass error $\leq$ 5 ppm) and comparison to authentic standard, none of them were identified. This could indicate that the amount of DMSO used as a vehicle did not affect the main metabolic profile of glucose-treated MIN6 cells.

The effects of rotenone on glucose-treated MIN6 cells were investigated. The OPLS-DA scores plot shown in the Figure 6.5 indicates that the metabolite profile of the rotenone cells were distinct from DMSO treated and glucose treated. This explains the significant separation of metabolite profiles among the treatments and indicates that metabolite profiles of glucose-treated MIN6 cells were altered by rotenone. Then, applying the criteria for identifying the significant ions (VIP $\geq$ 1.00, FDR < 0.05) in order to study the effects of rotenone on the metabolite profile of glucose-treated MIN6 cells, 179 significant ions were detected (see Supplementary Table 6.3). Based on exact mass (with mass error $\leq$ 5 ppm) and

compared to authentic standards, and data from free databases (HMDB and MetLin) and literature, 96 of the significant ions were identified in the samples as summarised in Table 6.2. Figure 6.6 shows the level changes of the ten significantly altered metabolites (involved in bioenergetics) in MIN6 cells exposed to rotenone, compared with controls.

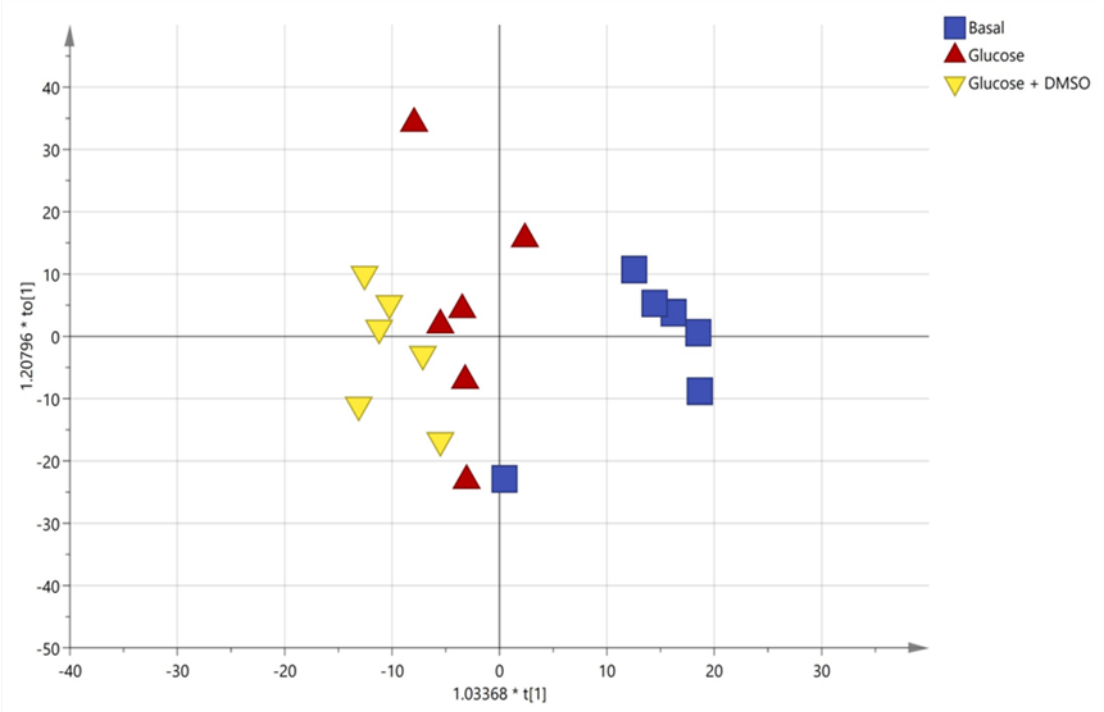


Figure 6.4 Scores plot from OPLS-DA analysis of basal, glucose and glucose+ DMSO treated MIN6 cells. Each point represents cell extracts from one sample of MIN6 cells under control or compound treatments. Extracts from the same condition are grouped: basal (blue squares), glucose (red triangles) and glucose + DMSO combined (yellow inverted triangles).

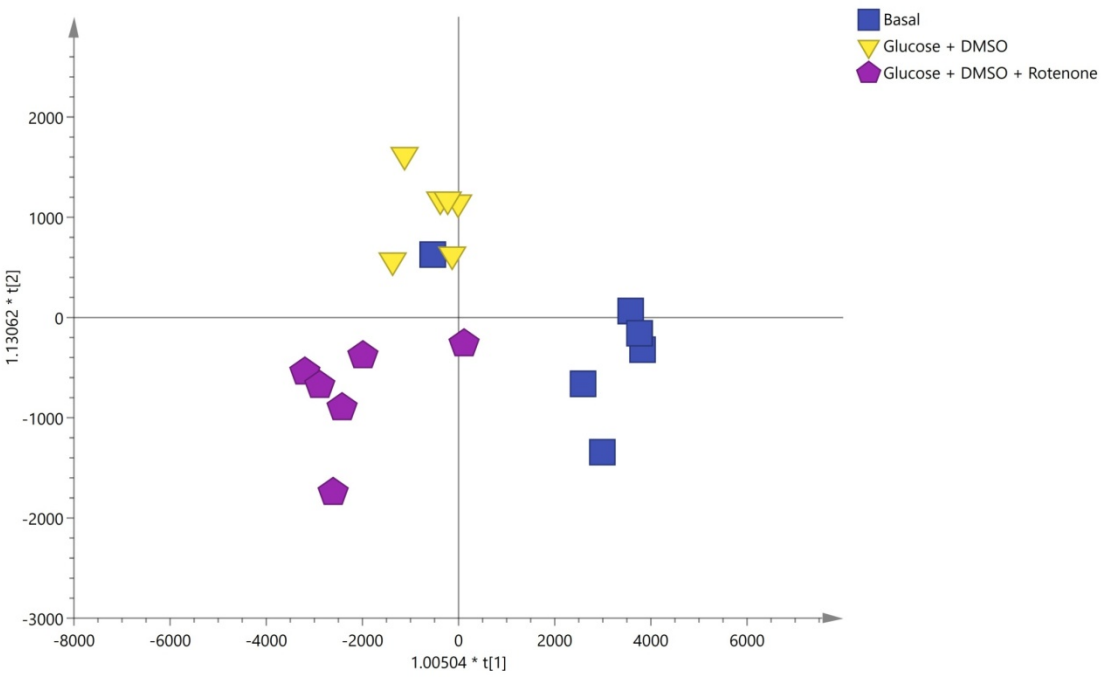


Figure 6.5 Scores plot from OPLS-DA analysis of basal, glucose + DMSO and glucose+ DMSO + rotenone treated MIN6 cells (with R^2X = 0.95, R^2Y = 0.97 and Q^2 =0.96). Each point represents cell extracts from one sample of MIN6 cells under control or compound treatments. Extracts from the same condition are grouped: basal (blue squares), glucose + DMSO combined (yellow reverted triangles) and glucose + DMSO + rotenone combined (violet octagons).

Table 6.2 The details of significantly altered metabolites of MIN6 cells exposed with rotenone (10 μM in final concentration).

m/z	Polarity	RT (min)	Metabolites	Formula	M.W.	Adduct	Error (ppm)	VIP	FDR	Fold
87.0089	-	2.54	Pyruvic acid	C3H4O3	88.0160	M-H	1	1.11	2.32E-05	1.13
89.0246	-	2.63	L-Lactic acid	C3H6O3	90.0317	M-H	2	2.19	6.07E-04	1.66
90.0551	+	8.87	L-Alanine	C3H7NO2	89.0477	M+H	1	1.49	3.12E-08	1.23
101.0245	-	8.60	Succinic acid semialdehyde	C4H6O3	102.0317	M-H	1	1.71	4.12E-14	1.31
110.9854	-	8.11	Hydroxyacetone	C3H6O2	74.0368	M+K-2H	0	1.50	1.68E-07	3.76
112.0507	+	7.61	Cytosine	C4H5N3O	111.0433	M+H	1	1.29	2.68E-05	2.04
114.0664	+	6.26	Creatinine	C4H7N3O	113.0589	M+H	2	1.41	8.48E-04	1.39
115.0038	-	8.87	Fumaric acid	C4H4O4	116.0110	M-H	1	1.62	4.33E-15	1.85
116.0707	+	8.12	L-Proline	C5H9NO2	115.0633	M+H	1	2.59	4.44E-07	1.11
117.0195	-	8.24	Succinic acid	C4H6O4	118.0266	M-H	1	1.40	1.06E-04	1.94
131.0715	-	2.31	Leucinic acid	C6H12O3	132.0786	M-H	1	1.17	1.12E-08	4.14
132.0304	-	8.75	L-Aspartic acid	C4H7NO4	133.0375	M-H	1	1.56	1.64E-04	1.12
133.0144	-	8.82	Malic acid	C4H6O5	134.0215	M-H	1	4.34	5.58E-11	2.14
133.0610	+	9.10	L-Asparagine	C4H8N2O3	132.0535	M+H	2	1.16	2.34E-06	2.43
133.0762	+	2.64	2-Keto-3-deoxy-D-gluconic acid	C6H10O6	178.0477	M+2Na+H	3	1.21	4.03E-08	2.58
137.0459	+	7.29	Hypoxanthine	C5H4N4O	136.0385	M+H	1	1.36	1.76E-06	2.03
143.0351	-	8.65	3-Methylglutaconic acid	C6H8O4	144.0423	M-H	1	1.58	2.83E-08	1.36
147.0765	+	9.05	L-Glutamine	C5H10N2O3	146.0691	M+H	1	1.09	2.09E-06	1.65
152.0566	+	7.75	Guanine	C5H5N5O	151.0494	M+H	0	1.31	2.58E-07	2.18
159.1028	-	1.97	3-Hydroxyoctanoic acid	C8H16O3	160.1099	M-H	1	1.25	1.21E-08	4.13
162.1126	+	8.52	L-Carnitine	C7H15NO3	161.1052	M+H	1	1.86	5.84E-05	1.44
175.0250	-	8.03	Ascorbic acid	C6H8O6	176.0321	M-H	1	1.10	1.27E-03	1.43
179.0564	-	8.62	Myoinositol	C6H12O6	180.0634	M-H	1	2.86	3.33E-16	1.34
191.0200	-	9.84	Citric acid/Isocitric acid	C6H8O7	192.0270	M-H	1	2.62	2.84E-04	1.41

Metaboloites in red were identified by using commercially available standards and the others were identified by comparison with the MS library.

Table 6.2 (Cont.) The details of significantly altered metabolites of MIN6 cells exposed with rotenone (10 μM in final concentration).

m/z	Polarity	RT (min)	Metabolites	Formula	M.W.	Adduct	Error (ppm)	VIP	FDR	Fold
198.0975	+	8.65	D-Glucose	C6H12O6	180.0634	M+NH4	1	1.09	0.00E+00	1.38
204.1232	+	7.58	L-Acetylcarnitine	C9H17NO4	203.1158	M+H	1	2.03	5.09E-07	2.12
223.1542	+	2.47	2-Hexenoylcholine	C11H22NO2	200.1651	M+H	0	1.14	2.33E-05	1.46
232.1546	+	6.65	Butyrylcarnitine	C11H21NO4	231.1471	M+H	1	1.64	3.65E-09	3.03
233.1861	+	2.60	N-Nonanoylglycine	C11H21NO3	215.1521	M+NH4	1	1.27	1.28E-06	2.47
240.1958	+	2.30	PC	C40H80NO7P	717.5672	M+3H	2	1.14	3.37E-04	1.42
243.1830	+	2.30	MG	C27H52O4	440.3866	M+2Na	2	1.10	2.10E-11	1.02
244.0933	+	7.61	Cytidine	C9H13N3O5	243.0855	M+H	2	1.48	1.36E-05	1.65
244.1909	+	2.16	N-Undecanoylglycine	C13H25NO3	243.1834	M+H	1	1.81	8.94E-05	2.40
245.1866	+	2.04	Dipeptide	C12H24N2O3	244.1787	M+H	2	1.22	6.46E-08	2.43
246.1702	+	6.48	Isovalerylcarnitine/Pivaloylcarnitine	C12H23NO4	245.1627	M+H	1	1.37	1.23E-06	4.12
248.1493	+	7.78	Hydroxybutyrylcarnitine	C11H21NO5	247.1420	M+H	0	1.74	4.55E-15	36.27
249.1699	+	2.21	Dodecanedioylcarnitine	C19H35NO6	373.2464	M+3ACN+2H	2	1.17	5.20E-04	1.47
258.2794	+	2.55	Palmitaldehyde	C16H32O	240.2453	M+NH4	1	1.31	1.25E-04	1.59
260.1858	+	2.60	Isohexanoylcarnitine	C13H25NO4	259.1784	M+H	1	1.88	1.28E-05	7.36
260.1859	+	6.16	Hexanoylcarnitine	C13H25NO4	259.1784	M+H	1	2.07	9.83E-07	4.26
280.2637	+	2.24	Hexadecenal	C16H30O	238.2297	M+ACN+H	1	2.17	3.53E-04	1.76
282.1199	+	8.87	N6-Methyladenosine	C11H15N5O4	281.1124	M+H	1	1.18	1.64E-04	1.88
284.0991	+	8.04	Guanosine	C10H13N5O5	283.0917	M+H	1	1.17	6.18E-06	2.36
284.2068	+	2.60	CerP(d18:1/26:1(17Z))	C46H90NO6P	783.6506	M+3Na	2	1.45	4.44E-05	1.86
288.2171	+	2.60	L-Octanoylcarnitine	C15H29NO4	287.2097	M+H	1	2.08	2.22E-07	9.85
289.2739	+	2.19	PG	C46H77O10P	820.5254	M+H+2Na	3	1.88	2.72E-07	1.93
290.2691	+	2.55	3-hydroxyhexadecanoic acid	C16H32O3	272.2351	M+NH4	1	1.32	7.40E-04	1.14

Metaboloites in red were identified by using commercially available standards and the others were identified by comparison with the MS library.

Table 6.2 (Cont.) The details of significantly altered metabolites of MIN6 cells exposed with rotenone (10 μM in final concentration).

m/z	Polarity	RT (min)	Metabolites	Formula	M.W.	Adduct	Error (ppm)	VIP	FDR	Fold
291.2168	+	2.21	LysoPE	C29H58NO7P	563.3951	M+H+NH4	4	1.12	6.03E-05	1.32
294.2429	+	2.24	PC	C52H98NO7P	879.7081	M+3H	1	1.50	5.28E-04	1.72
296.2584	+	2.24	Linolenic acid	C18H30O2	278.2246	M+NH4	0	2.22	1.96E-05	2.76
300.0495	-	8.70	N-Acetyl-D-Glucosamine 6-Phosphate	C8H16NO9P	301.0563	M-H	2	1.32	1.58E-03	18.08
302.1964	+	2.35	PC	C48H88NO8P	837.6248	M+3Na	3	1.10	6.94E-09	1.31
304.2121	+	6.50	3-hydroxyoctanoyl carnitine	C15H29NO5	303.2046	M+H	1	2.23	1.03E-07	121.40
304.2847	+	2.50	12-hydroxyheptadecanoic acid	C17H34O3	286.2508	M+NH4	0	1.08	5.51E-05	1.24
309.2273	+	2.30	N1,N12-Diacetylspermine	C14H30N4O2	286.2369	M+Na	4	1.28	7.46E-06	1.27
315.3008	+	2.30	Palmitoleoyl Ethanolamide	C18H35NO2	315.3006	M+NH4	0	1.10	2.72E-03	1.79
316.2122	+	2.27	PE	C51H94NO8P	879.6717	M+3Na	3	1.39	2.54E-11	2.05
324.2898	+	2.21	Oleic acid	C18H34O2	282.2559	M+ACN+H	0	1.35	1.63E-03	2.07
325.2487	+	2.44	3-Oxotetradecanoic acid	C14H26O3	242.1882	M+2ACN+H	1	1.15	2.31E-03	1.78
338.3419	+	2.16	Thromboxane	C20H40O	296.3079	M+ACN+H	0	1.48	4.31E-06	1.43
341.3165	+	2.21	Sphingosine	C18H37NO2	299.2824	M+ACN+H	1	1.95	3.44E-08	2.87
343.2958	+	2.60	TG	C68H114O6	1026.8615	M+3H	4	1.41	1.05E-03	2.12
343.3321	+	2.27	N-Oleoylethanolamine	C20H39NO2	325.2981	M+NH4	1	1.88	3.28E-06	1.85
345.2751	+	2.07	TG	C63H114O6	966.8615	M+3Na	4	1.16	1.35E-03	1.82
346.0564	-	8.22	Adenosine monophosphate	C10H14N5O7P	347.0631	M-H	2	1.81	3.44E-12	2.24
347.0405	-	8.87	Inosine 2'-phosphate	C10H13N4O8P	348.0471	M-H	2	1.19	5.09E-05	1.89
348.0706	+	8.04	Adenosine monophosphate	C10H14N5O7P	347.0631	M+H	1	1.87	4.35E-14	1.85
352.1652	+	6.26	Phenylalanyl-Tryptophan/Tryptophyl-Phenylalanine	C20H21N3O3	351.1583	M+H	1	1.65	3.80E-04	1.34
357.3114	+	2.27	Oleoyl glycine	C20H37NO3	339.2773	M+NH4	1	1.33	2.93E-03	1.71

Metaboloites in red were identified by using commercially available standards and the others were identified by comparison with the MS library.

Table 6.2 (Cont.) The details of significantly altered metabolites of MIN6 cells exposed with rotenone (10 μM in final concentration).

m/z	Polarity	RT (min)	Metabolites	Formula	M.W.	Adduct	Error (ppm)	VIP	FDR	Fold
359.1202	-	8.62	4-Deoxythreonic acid	C4H8O4	120.0423	3M-H	2	2.60	2.58E-13	1.47
359.3270	+	2.30	Phytosphingosine	C18H39NO3	317.2930	M+ACN+H	0	1.50	2.74E-05	2.65
364.0655	+	9.42	Guanosine monophosphate	C10H14N5O8P	363.0580	M+H	0	1.28	1.75E-13	6.72
373.3063	+	2.27	TG	C69H126O6	1050.9554	M+3Na	4	1.49	7.38E-05	2.38
375.3220	+	2.19	TG	C69H132O6	1057.0024	M+3Na	4	1.66	6.63E-09	2.00
382.1013	-	8.45	Succinyladenosine	C14H17N5O8	383.1077	M-H	2	1.25	2.69E-06	1.74
384.7724	+	2.21	TG	C73H134O6	1107.0180	M+H+2Na	1	1.20	4.37E-07	2.28
388.2543	+	2.50	PE	C41H68NO8P	733.4683	M+ACN+2H	1	1.36	1.82E-03	1.88
395.1492	+	2.21	Rotenone	C23H22O6	394.1416	M+H	1	7.98	2.85E-05	369.00
401.3704	-	14.67	TG	C52H100O5	804.7571	M-2H	2	1.16	1.38E-04	1.79
403.3534	+	2.19	TG	C75H144O6	1141.0963	M+3Na	3	1.16	3.88E-08	1.28
416.2855	+	2.55	PE	C45H76NO8P	789.5309	M+ACN+2H	1	1.08	9.34E-04	1.51
426.0229	-	8.90	ADP	C10H15N5O10P2	427.0294	M-H	2	1.31	5.65E-04	2.68
455.2902	+	2.30	9'-Carboxy-gamma-tocotrienol	C23H32O4	372.2301	M+2ACN+H	0	1.35	8.24E-06	2.16
460.2697	+	2.24	PIP	C43H84O16P2	918.5235	M+2H	1	1.87	1.87E-04	4.52
488.3586	+	2.13	Thyroxine glucuronide	C21H19I4NO10	952.7188	M+H+Na	2	1.19	8.20E-08	3.55
506.2034	+	6.21	PIP2	C41H77O19P3	966.4272	M+2Na	1	1.37	3.58E-03	1.18
538.5202	+	2.19	Ceramide (d18:1/16:0)	C34H67NO3	537.5121	M+H	1	1.48	6.89E-04	2.46
546.3650	+	2.13	Ganglioside GA2 (d18:1/9Z-18:1)	C56H102N2O18	1090.7128	M+2H	2	1.03	3.89E-11	11.98
565.0488	-	9.19	Uridine diphosphate glucose	C15H24N2O17P2	566.0550	M-H	2	1.33	4.35E-04	1.23
590.3925	+	2.10	LysoPE	C25H50NO7P	507.3325	M+2ACN+H	1	1.04	5.29E-10	2.91
598.0688	+	10.23	Uridine diphosphate glucuronic acid	C15H22N2O18P2	580.0343	M+NH4	1	1.11	1.72E-03	1.33
620.4376	+	2.19	LysoPE	C27H56NO7P	537.3794	M+2ACN+H	4	1.26	2.83E-14	2.96
707.0767	+	7.37	Nicotinamide ribotide	C11H15N2O8P	334.0566	2M+K	1	1.24	1.40E-03	1.25

Metaboloites in red were identified by using commercially available standards and the others were identified by comparison with the MS library.

Table 6.2 (Cont.) The details of significantly altered metabolites of MIN6 cells exposed with rotenone (10 μM in final concentration).

m/z	Polarity	RT (min)	Metabolites	Formula	M.W.	Adduct	Error (ppm)	VIP	FDR	Fold
752.5175	+	2.19	CL	C85H148O17P2	1503.0192	M+2H	1	1.16	2.18E-08	10.54
752.5584	+	2.01	PE	C43H78NO7P	751.5516	M+H	1	1.37	6.68E-06	9.40
904.5926	+	1.92	PI	C45H83O13P	862.5571	M+ACN+H	2	1.28	1.65E-04	2.71

Metaboloites in red were identified by using commercially available standards and the others were identified by comparison with the MS library.

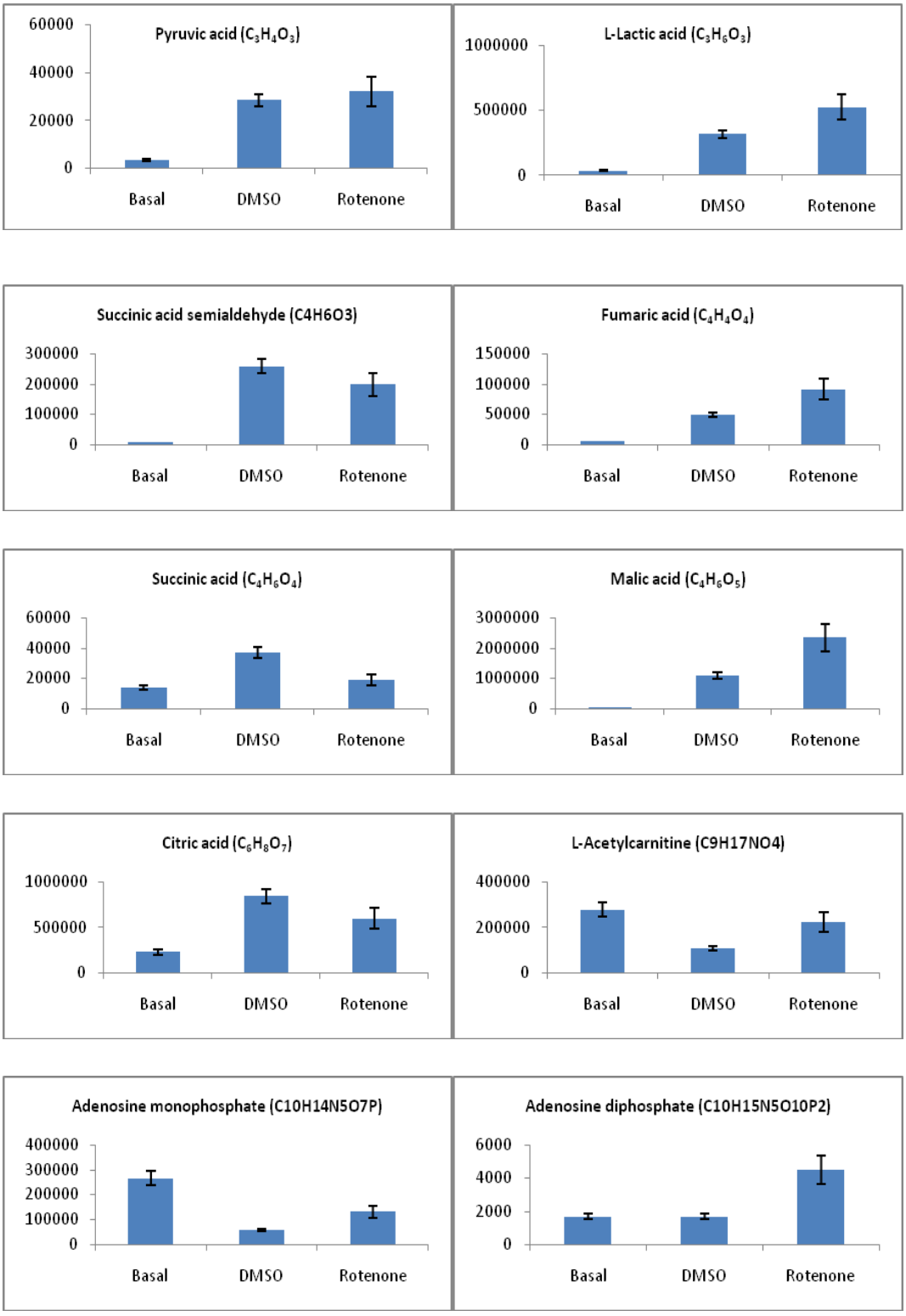


Figure 6.6 Level changes of ten altered metabolites (involved to bioenergetics) of 10 mM glucose treated MIN6 cells exposed to drugs compared to untreated cells: Basal = untreated, DMSO = glucose + DMSO and Rotenone = glucose + DMSO + Rotenone.

6.5.2.3 Metabolic signature of glucose-treated MIN6 cells exposure to antimycin A

Ethanol was used as a vehicle investigating how it compared with the glucose-treated samples. The OPLS-DA scores plot shown in Figure 6.7 illustrates that the ethanol-treated and the glucose-treated cells had metabolite profiles which were close together. We found that there were five significantly detected ions (VIP $\geq$1.0 and p-value < 0.05) as summarised in Supplementary Table 6.4. Based on exact mass (with mass error $\leq$ 5 ppm) and comparison to authentic standards (if they were available in our laboratory), none of them were identified. This could indicate that the amount of ethanol used as a vehicle has no effect on main metabolic profiles of glucose-treated MIN6 cells.

The effects of antimycin A on glucose-treated MIN6 cells were investigated. The OPLS-DA scores plot (Figure 6.8) shows that the metabolite profiles were separated among the antimycin A treatment from ethanol treatment and basal. This explained the significant separation of metabolites profiles among the treatments and indicated that metabolite profiles of glucose-treated MIN6 cells were altered by antimycin A. Then, applying the criteria for identifying the significant ions (VIP $\geq$ 1.00, FDR < 0.05) in order to study the effects of antimycin A on metabolite profile of glucose-treated MIN6 cells, 179 detected ions were significant observed (see

Supplementary Table 6.5). Based on exact mass (with mass error $\leq$ 5 ppm) and comparison to authentic standards, and data from free databases (HMDB and MetLin) and literatures, 92 of the significant ions were identified in our samples as summarised in Table 6.3. Figure 6.9 shows the level changes of the top ten significantly altered metabolites in MIN6 cells exposed to antimycin A compared with control.

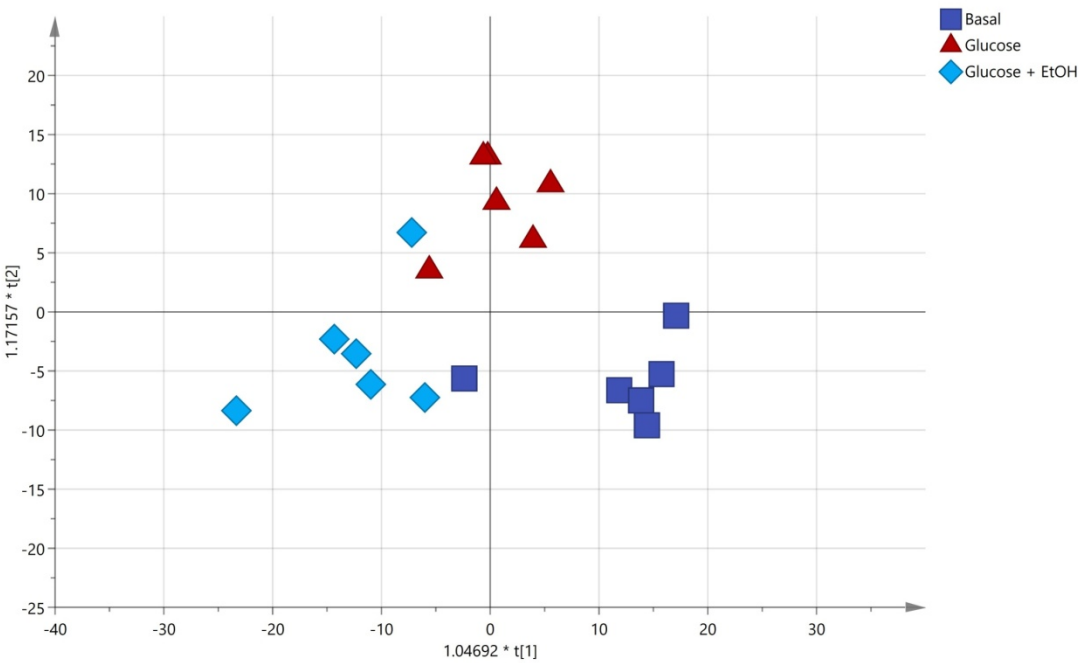


Figure 6.7 Scores plot from OPLS-DA analysis of basal, glucose and glucose+ ethanol treated MIN6 cells. Each point represents cell extracts from one sample of MIN6 cells under control or compound treatments. Extracts from the same condition are grouped: basal (pale blue diamonds), glucose (red triangles) and glucose + ethanol combined (dark blue squares).

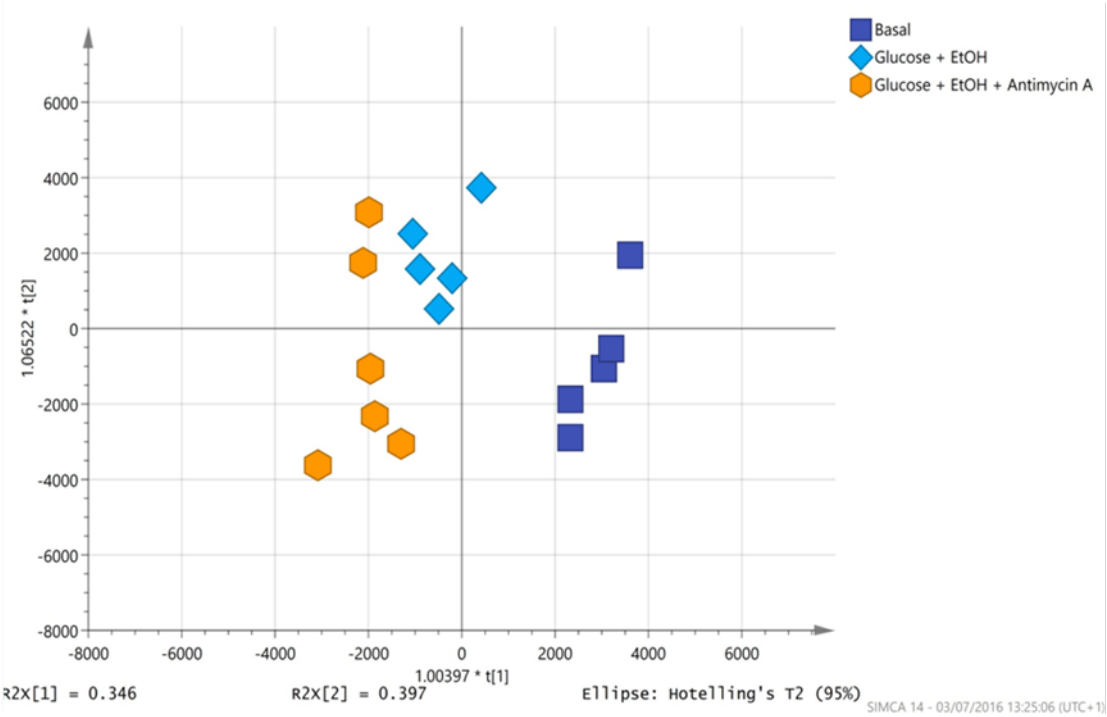


Figure 6.8 Scores plot from OPLS-DA analysis of basal, glucose + ethanol and glucose + ethanol + antimycin A treated MIN6 cells (with R^2X = 0.74, R^2Y = 0.99 and Q^2 =0.84). Each point represents cell extracts from one sample of MIN6 cells under control or compound treatments. Extracts from the same condition are grouped and enclosed with ellipses: basal (blue squares), glucose + ethanol (pale blue diamonds) and glucose + ethanol + antimycin A (brown hexagons).

Table 6.3 The details of significantly altered metabolites of MIN6 cells exposed to antimycin A (1 μM in final concentration).

RT (min)	Metabolites	Formula	M.W.	Adduct	Error (ppm)	VIP	FDR	Fold
2.54	Pyruvic acid	C3H4O3	88.0160	M-H	1	1.48	5.74E-05	0.31
8.62	Malonic semialdehyde	C3H4O3	88.0160	M-H	1	1.65	2.16E-03	1.14
2.63	Glyceraldehyde	C3H6O3	90.0317	M-H	2	3.16	8.76E-04	0.66
8.87	L-Alanine	C3H7NO2	89.0477	M+H	1	1.65	1.98E-07	1.30
8.60	2-Methyl-3-oxopropanoic acid	C4H6O3	102.0317	M-H	1	2.15	1.64E-06	1.30
10.47	L-Serine	C3H7NO3	105.0426	M+H	1	1.54	1.75E-14	2.00
8.11	Lactaldehyde	C3H6O2	74.0368	M+K-2H	0	1.76	1.19E-04	0.58
7.61	Cytosine	C4H5N3O	111.0433	M+H	1	1.15	6.30E-07	0.85
8.65	2-Hydroxy-2,4-pentadienoate	C5H6O3	114.0317	M-H	0	1.74	1.21E-04	1.34
8.87	Fumaric acid	C4H4O4	116.0110	M-H	1	1.77	4.05E-09	0.91
8.24	Succinic acid	C4H6O4	118.0266	M-H	1	2.19	6.45E-13	2.14
7.94	N4-Acetylaminobutanal	C6H11NO2	129.0790	M+H	1	1.22	6.19E-10	0.78
8.75	L-Aspartic acid	C4H7NO4	133.0375	M-H	1	2.54	2.54E-04	1.18
8.82	Malic acid	C4H6O5	134.0215	M-H	1	4.47	3.37E-07	0.96
9.10	L-Asparagine	C4H8N2O3	132.0535	M+H	2	1.20	9.54E-05	0.57
2.64	2-Keto-3-deoxy-D-gluconic acid	C6H10O6	178.0477	M+2Na+H	3	1.39	3.51E-05	2.61
2.60	(5R)-5-Hydroxyhexanoic acid	C6H12O3	132.0786	M+H	1	1.25	1.02E-09	1.15
7.29	Hypoxanthine	C5H4N4O	136.0385	M+H	1	1.46	1.05E-07	1.33
2.60	Nicotinamide N-oxide	C6H6N2O2	138.0429	M+H	1	1.18	6.98E-08	1.53
8.65	3-Methylglutaconic acid	C6H8O4	144.0423	M-H	1	1.91	6.52E-05	1.37
2.41	3-Dehydroxycarnitine	C7H15NO2	145.1103	M+H	1	1.24	1.47E-05	0.78
9.05	L-Glutamine	C5H10N2O3	146.0691	M+H	1	1.11	1.13E-05	0.30
5.46	L-Methionine	C5H11NO2S	149.0510	M+H	0	4.02	2.11E-08	9.62
7.75	Guanine	C5H5N5O	151.0494	M+H	0	1.25	1.22E-03	1.38

Metaboloites in red were identified by using commercially available standards and the others were identified by comparison with the MS library.

Table 6.3 (Cont) The details of significantly altered metabolites of MIN6 cells exposed to antimycin A (1 μM in final concentration).

RT (min)	Metabolites	Formula	M.W.	Adduct	Error (ppm)	VIP	FDR	Fold
9.45	L-Histidine	C6H9N3O2	155.0695	M+H	1	1.61	8.43E-08	0.48
8.52	L-Carnitine	C7H15NO3	161.1052	M+H	1	2.76	1.08E-10	0.75
8.67	Glycerol 3-phosphate	C3H9O6P	172.0137	M-H	1	2.43	7.08E-05	4.34
9.45	Citrulline	C6H13N3O3	175.0957	M+H	1	1.16	5.68E-04	1.00
8.62	D-Glucose	C6H12O6	180.0634	M-H	1	4.13	4.01E-05	1.16
7.58	L-Acetylcarnitine	C9H17NO4	203.1158	M+H	1	1.99	6.13E-06	0.97
2.47	2-Hexenoylcholine	C11H22NO2	200.1651	M+Na	0	1.22	4.89E-05	1.46
6.65	Isobutyryl-L-carnitine	C11H21NO4	231.1471	M+H	1	1.76	2.66E-05	0.86
2.60	N-Nonanoylglycine	C11H21NO3	215.1521	M+NH4	1	1.46	4.64E-05	2.62
2.30	MG	C27H52O4	440.3866	M+2Na	2	1.33	2.22E-16	0.95
7.61	Cytidine	C9H13N3O5	243.0855	M+H	2	1.23	4.80E-07	0.66
2.27	5Z-Tetradecenoic acid	C14H26O2	226.1933	M+NH4	1	1.18	6.92E-05	1.45
6.48	Pivaloylcarnitine	C12H23NO4	245.1627	M+H	1	1.23	0.00E+00	1.01
2.60	Myristic acid	C14H28O2	228.2089	M+NH4	0	1.89	3.22E-04	0.98
2.55	Palmitaldehyde	C16H32O	240.2453	M+NH4	1	1.72	1.74E-09	0.63
6.16	Hexanoylcarnitine	C13H25NO4	259.1784	M+H	1	2.98	1.83E-08	0.28
3.61	PA	C45H81O8P	780.5669	M+3H	0	1.53	1.96E-13	0.16
2.50	Hexadecenal	C16H30O	238.2297	M+Na	0	1.31	1.39E-08	0.79
1.74	4-(2-Amino-3-hydroxyphenyl)-2,4-dioxobutanoic acid	C10H9NO5	223.0481	M+ACN+H	1	1.48	4.00E-04	Infinity
2.21	2-Methyl-3-ketovaleric acid	C6H10O3	130.0630	2M+NH4	1	1.23	2.11E-03	0.60
2.60	CerP(d18:1/26:1(17Z))	C46H90NO6P	783.6506	M+3Na	2	1.45	1.38E-09	2.87
2.60	L-Octanoylcarnitine	C15H29NO4	287.2097	M+H	1	2.25	3.51E-06	0.92
2.27	All trans decaprenyl diphosphate	C50H90O7P2	864.6162	M+3H	1	1.33	8.30E-14	8.88

Metaboloites in red were identified by using commercially available standards and the others were identified by comparison with the MS library.

Table 6.3 (Cont) The details of significantly altered metabolites of MIN6 cells exposed to antimycin A (1 μM in final concentration).

RT (min)	Metabolites	Formula	M.W.	Adduct	Error (ppm)	VIP	FDR	Fold
2.19	PG	C46H77O10P	820.5254	M+H+2Na	3	2.05	1.33E-03	0.53
2.19	1-Methylnicotinamide	C7H9N2O	137.0715	2M+NH4	4	1.27	2.34E-04	0.62
1.94	Tyrosyl-Aspartate/Aspartyl-Tyrosine	C13H16N2O6	296.1008	M-H	2	2.53	4.66E-09	Infinity
2.04	Tyrosyl-Aspartate/Aspartyl-Tyrosine	C13H16N2O6	296.1008	M+H	1	1.88	2.30E-06	Infinity
8.70	N-Acetyl-D-Glucosamine 6-Phosphate	C8H16NO9P	301.0563	M-H	2	1.48	4.59E-05	0.72
2.35	PC	C48H88NO8P	837.6248	M+3Na	3	1.26	3.89E-14	0.90
2.30	N1,N12-Diacetylspermine	C14H30N4O2	286.2369	M+Na	4	1.49	1.37E-10	1.28
2.27	3-Hydroxytetradecanedioic acid	C14H26O5	274.1780	M+ACN+H	1	1.38	3.36E-05	1.46
8.67	Uridine 5'-monophosphate	C9H13N2O9P	324.0359	M-H	2	1.99	4.29E-06	2.92
2.16	Thromboxane	C20H40O	296.3079	M+ACN+H	0	1.86	1.19E-03	0.81
2.21	Sphingosine	C18H37NO2	299.2824	M+ACN+H	1	1.51	1.36E-06	1.17
2.60	TG	C68H114O6	1026.8615	M+3H	4	3.30	1.28E-04	4.41
2.27	N-Oleoylethanolamine	C20H39NO2	325.2981	M+NH4	1	1.76	9.90E-06	0.81
2.07	TG	C63H114O6	966.8615	M+3Na	4	1.77	1.61E-04	5.17
8.22	Adenosine monophosphate	C10H14N5O7P	347.0631	M-H	2	2.87	2.55E-05	6.24
8.87	Inosine 5'-monophosphate	C10H13N4O8P	348.0471	M-H	2	1.31	3.61E-05	1.91
8.04	Adenosine monophosphate	C10H14N5O7P	347.0631	M+H	1	3.08	7.86E-07	3.62
2.30	Phytosphingosine	C18H39NO3	317.2930	M+ACN+H	0	1.47	4.30E-06	0.58
9.42	Guanosine monophosphate	C10H14N5O8P	363.0580	M+H	0	1.44	8.88E-04	8.39
9.33	Galactinol	C12H22O11	342.1162	M+Na	1	1.54	0.00E+00	0.54
2.19	TG	C69H132O6	1057.0024	M+3Na	4	1.38	4.07E-04	2.67

Metaboloites in red were identified by using commercially available standards and the others were identified by comparison with the MS library.

Table 6.3 (Cont) The details of significantly altered metabolites of MIN6 cells exposed to antimycin A (1 μM in final concentration).

RT (min)	Metabolites	Formula	M.W.	Adduct	Error (ppm)	VIP	FDR	Fold
8.45	Succinyladenosine	C14H17N5O8	383.1077	M-H	2	2.06	8.08E-05	4.09
2.21	TG	C73H134O6	1107.0180	M+H+2Na	1	1.11	1.66E-05	2.49
14.67	TG	C52H100O5	804.7571	M-2H	2	1.26	1.08E-07	1.72
2.19	TG	C75H144O6	1141.0963	M+3Na	3	1.28	2.27E-06	2.01
8.90	ADP	C10H15N5O10P2	427.0294	M-H	2	1.80	1.29E-08	4.06
2.13	Glucosylsphingosine	C24H47NO7	461.3353	M+H-H2O	0	1.17	5.23E-09	0.36
2.10	Octacosanoic acid	C28H56O2	424.4280	M+Na	3	1.38	5.16E-07	7.58
2.30	9'-Carboxy-gamma-tocotrienol	C23H32O4	372.2301	M+2ACN+H	0	1.53	1.97E-04	0.35
2.13	Thyroxine glucuronide	C21H19I4NO10	952.7188	M+H+Na	2	1.17	2.11E-04	0.44
9.00	Citicoline	C14H26N4O11P2	488.1073	M+H	1	1.29	3.32E-04	0.83
2.21	Dodecanedioic acid	C12H22O4	230.1518	2M+ACN+H	2	1.13	0.00E+00	0.49
6.21	PIP2	C41H77O19P3	966.4272	M+2Na	1	2.63	4.83E-06	1.79
1.64	Pregnanediol-3-glucuronide	C27H44O8	496.3036	M+K-2H	2	2.41	0.00E+00	Infinity
2.19	Ceramide (d18:1/16:0)	C34H67NO3	537.5121	M+H	1	1.91	3.27E-06	0.35
2.13	Ganglioside GA2 (d18:1/9Z-18:1)	C56H102N2O18	1090.7128	M+2H	2	1.05	9.24E-04	0.37
9.15	Uridine diphosphate glucose	C15H24N2O17P2	566.0550	M+NH4	1	1.49	1.26E-07	0.86
2.10	LysoPE	C25H50NO7P	507.3325	M+2ACN+H	1	1.08	1.23E-12	0.82
2.19	LysoPE	C27H56NO7P	537.3794	M+2ACN+H	4	1.24	1.18E-04	0.77
2.13	CerP(d18:1/14:0)	C32H64NO6P	589.4471	M+2Na-H	0	1.09	1.39E-06	0.71
2.19	Ganglioside GD1b (d18:1/26:1(17Z))	C93H163N3O39	1946.0864	M+H+2Na	0	1.34	0.00E+00	0.99
2.13	lysoPC(26:1(5Z))	C34H68NO7P	633.4733	M+2Na-H	4	1.09	7.56E-10	0.44
7.37	Nicotinamide ribotide	C11H15N2O8P	334.0566	2M+K	1	1.44	1.67E-03	0.87
2.19	CL	C85H148O17P2	1503.0192	M+2H	1	1.17	7.74E-04	0.49
2.01	PE	C43H78NO7P	751.5516	M+H	1	1.56	1.39E-04	0.51

Metaboloites in red were identified by using commercially available standards and the others were identified by comparison with the MS library.

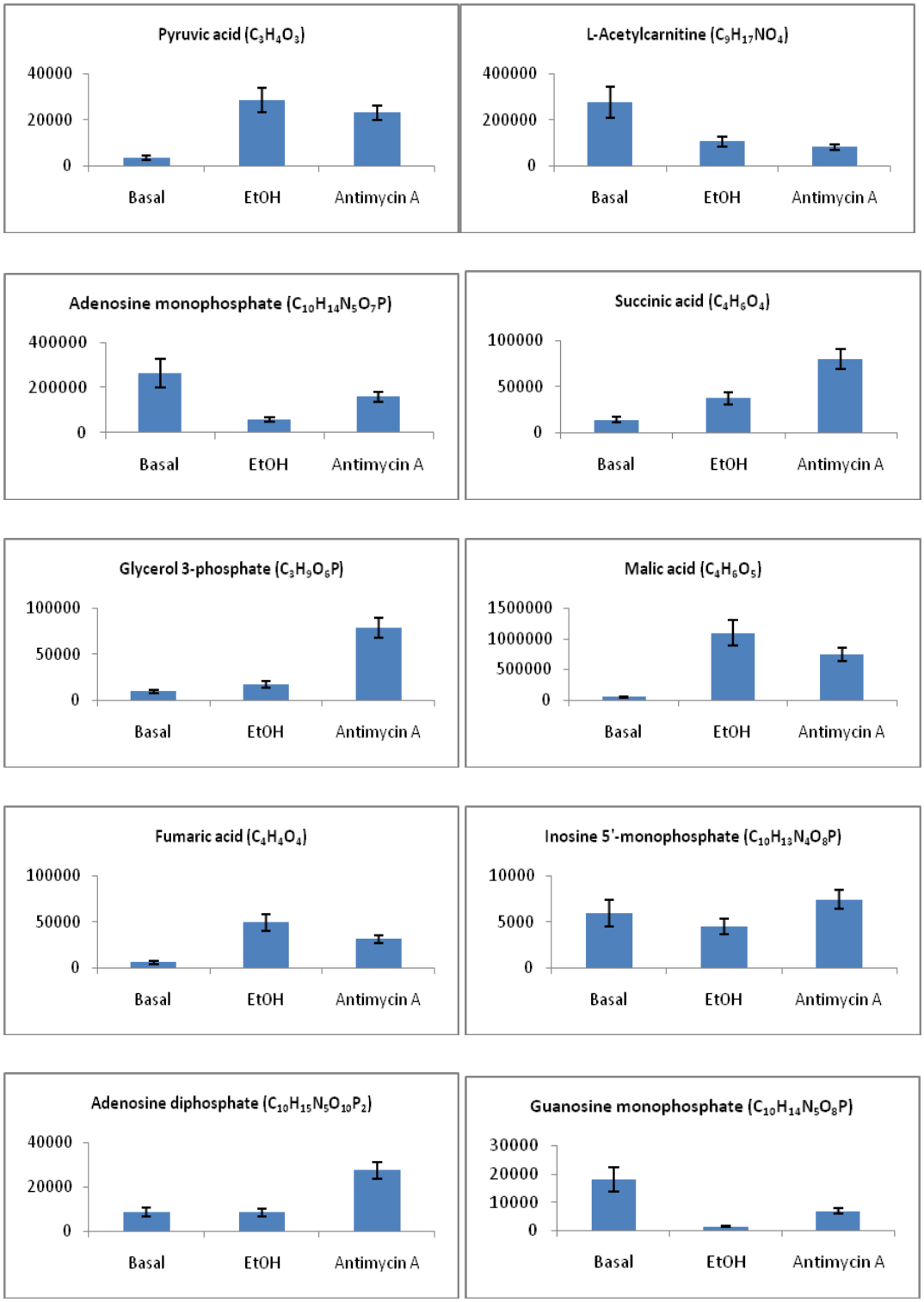


Figure 6.9 Level changes of ten altered metabolites (involved in bioenergetics) of 10 mM glucose-treated MIN6 cells exposed to 1 µM (in final concentration) of antimycin A and ethanol compared to untreated cells: Basal = untreated, EtOH = glucose + ethanol and Antimycin A = glucose + ethanol + antimycin A.

6.5.2.4 Metabolic signature of glucose-treated MIN6 cells exposure to azide

Glucose solution as a vehicle was used to dissolve azide. The OPLS-DA scores plot shown in Figure 6.10 indicates that the metabolite profiles of the azide-treated cells were separated from the glucose treated cells and basal cells. This explained the significant separation of metabolite profiles among the treatments and indicated that metabolite profiles of glucose-treated MIN6 cells were altered by azide. Then, applying the criteria for identifying the significant ions (VIP $\geq$ 1.00, FDR < 0.05) in order to study the effects of azide on metabolite profile of glucose-treated MIN6 cells, 208 significant ions were detected ions were significant observed (see Supplementary Table 6.6). Based on exact mass (with mass error $\leq$ 5 ppm) and comparison to authentic standards and data from free databases (HMDB and MetLin) and literature, 86 of the significant ions were identified in our samples as summarised in Table 6.4 Figure 6.11 shows the level changes of the top ten significantly altered metabolites in MIN6 cells exposed to azide compared with the control.

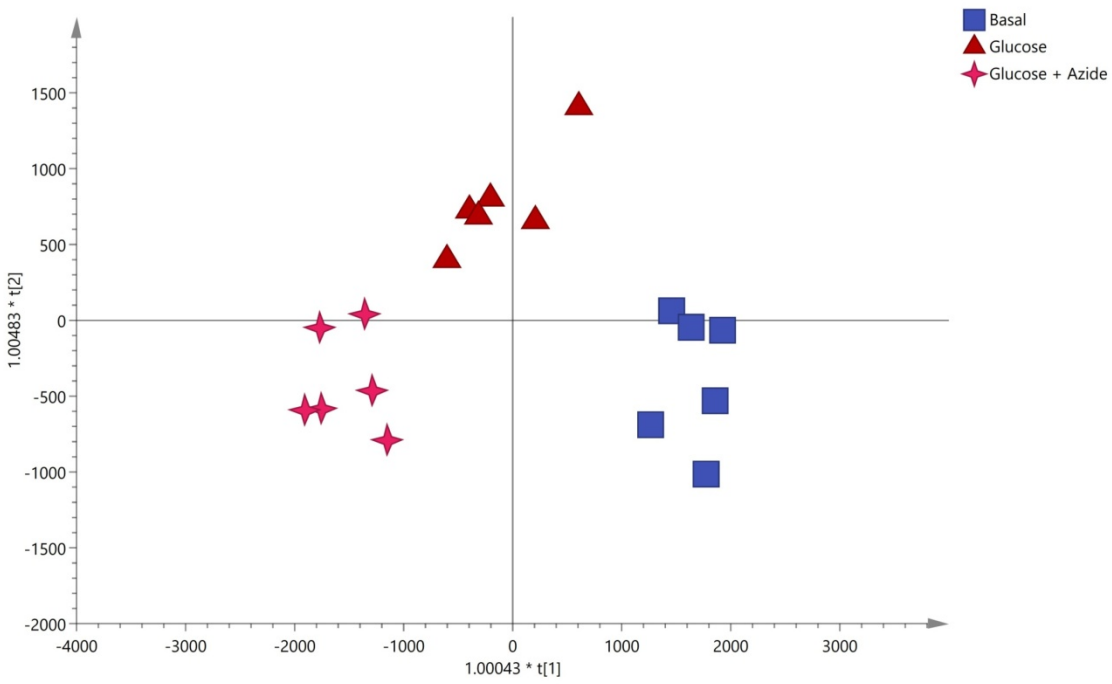


Figure 6.10 Scores plot from OPLS-DA analysis of basal, glucose and glucose + azide treated MIN6 cells (with R^2X =0.91, R^2Y = 0.96 and Q^2 = 0.94). Each point represents cell extracts from one sample of MIN6 cells under control or compound treatments. Extracts from the same condition are grouped: basal (blue squares), glucose (red triangles) and glucose + azide combined (pink four peak stars).

Table 6.4 The details of significantly altered metabolites of MIN6 cells exposed to azide (6 mM in final concentration).

m/z	Polarity	RT (min)	Metabolites	Formula	M.W.	Adduct	Error (ppm)	VIP	FDR	Fold
87.0089	-	2.54	Pyruvic acid	C3H4O3	88.0160	M-H	1	1.85	1.84E-04	4.28
89.0246	-	2.63	Glyceraldehyde	C3H6O3	90.0317	M-H	2	2.01	7.10E-04	13.73
90.0551	+	8.87	L-Alanine	C3H7NO2	89.0477	M+H	1	2.02	3.27E-07	1.68
101.0245	-	8.60	Succinic acid semialdehyde	C4H6O3	102.0317	M-H	1	2.03	1.10E-14	21.45
110.9854	-	8.11	Hydroxyacetone	C3H6O2	74.0368	M+K-2H	0	2.02	3.74E-08	1.07
112.0507	+	7.61	Cytosine	C4H5N3O	111.0433	M+H	1	1.94	1.43E-05	0.54
115.0038	-	8.87	Fumaric acid	C4H4O4	116.0110	M-H	1	2.02	4.11E-14	6.10
117.0195	-	8.24	Succinic acid	C4H6O4	118.0266	M-H	1	1.98	8.83E-06	1.81
128.0355	-	5.24	N-Acryloylglycine	C5H7NO3	129.0426	M-H	1	1.97	8.53E-04	0.40
130.0864	+	7.94	Acetylaminobutanal	C6H11NO2	129.0790	M+H	1	1.97	1.83E-05	1.34
132.0304	-	8.75	L-Aspartic acid	C4H7NO4	133.0375	M-H	1	1.99	1.19E-06	0.23
133.0144	-	8.82	Malic acid	C4H6O5	134.0215	M-H	1	2.03	3.66E-10	17.13
133.0610	+	9.10	L-Asparagine	C4H8N2O3	132.0535	M+H	2	2.04	3.25E-08	0.14
133.0860	+	2.60	6-Hydroxyhexanoic acid	C6H12O3	132.0786	M+H	1	1.94	2.14E-04	1.12
137.0459	+	7.29	Hypoxanthine	C5H4N4O	136.0385	M+H	1	1.96	9.81E-07	0.73
143.0351	-	8.65	3-Methylglutaconic acid	C6H8O4	144.0423	M-H	1	2.03	2.78E-08	49.73
146.1177	+	2.41	3-Dehydroxycarnitine	C7H15NO2	145.1103	M+H	1	1.97	5.06E-04	1.01
147.0765	+	9.05	L-Glutamine	C5H10N2O3	146.0691	M+H	1	1.91	2.10E-06	0.44
148.0605	+	8.47	L-Glutamate	C5H9NO4	147.0532	M+H	1	2.03	1.48E-03	2.40
150.1127	+	5.46	2-Hydroxy-3-methylpentanoic acid	C6H12O3	132.0786	M+NH4	1	1.83	4.59E-05	0.63
152.0566	+	7.75	Guanine	C5H5N5O	151.0494	M+H	0	2.04	8.38E-07	1.24
156.0769	+	9.45	L-Histidine	C6H9N3O2	155.0695	M+H	1	1.99	9.87E-04	1.11
162.1126	+	8.52	L-Carnitine	C7H15NO3	161.1052	M+H	1	1.95	8.75E-07	2.19
166.0725	+	7.91	Methylguanine	C6H7N5O	165.0651	M+H	1	1.94	2.94E-03	0.61

Metaboloites in red were identified by using commercially available standards and the others were identified by comparison with the MS library.

Table 6.4 (Cont) The details of significantly altered metabolites of MIN6 cells exposed to azide (6 mM in final concentration).

m/z	Polarity	RT (min)	Metabolites	Formula	M.W.	Adduct	Error (ppm)	VIP	FDR	Fold
171.0066	-	8.67	Glycerol 3-phosphate	C3H9O6P	172.0137	M-H	1	2.07	3.48E-04	4.15
173.0093	-	9.27	cis-Aconitic acid	C6H6O6	174.0164	M-H	1	1.91	2.70E-03	15.36
179.0564	-	8.62	D-Glucose	C6H12O6	180.0634	M-H	1	2.03	1.11E-16	31.98
188.1283	+	2.60	N-Heptanoylglycine	C9H17NO3	187.1208	M+H	1	1.85	4.02E-04	2.28
191.0200	-	9.84	Citric acid/Isocitric acid	C6H8O7	192.0270	M-H	1	1.95	3.31E-04	2.20
198.0975	+	8.65	myo-Inositol	C6H12O6	180.0634	M+NH4	1	1.99	0.00E+00	Infinity
204.1232	+	7.58	L-Acetylcarnitine	C9H17NO4	203.1158	M+H	1	1.94	3.90E-08	0.42
216.1596	+	2.50	N-Nonanoylglycine	C11H21NO3	215.1521	M+H	1	1.85	6.41E-04	1.49
216.1960	+	2.47	12-amino-dodecanoic acid	C12H25NO2	215.1885	M+H	0	1.94	1.26E-04	1.44
218.2118	+	3.32	Lauric acid	C12H24O2	200.1776	M+NH4	1	1.91	4.61E-04	1.96
223.1542	+	2.47	2-Hexenoylcholine	C11H22NO2	200.1651	M+Na	0	1.96	4.82E-06	1.58
229.0122	-	8.77	D-Ribose 5-phosphate	C5H11O8P	230.0192	M-H	1	2.20	8.53E-05	2.20
230.1753	+	2.24	N-Decanoylglycin	C12H23NO3	229.1678	M+H	1	1.98	8.61E-05	1.92
230.2481	+	7.17	Myristaldehyde	C14H28O	212.2140	M+NH4	1	2.03	4.50E-05	1.31
232.1546	+	6.65	Butyryl-L-carnitine/Isobutyryl carnitine	C11H21NO4	231.1471	M+H	1	2.04	3.49E-09	2.01
244.0933	+	7.61	Cytidine	C9H13N3O5	243.0855	M+H	2	1.93	7.53E-06	0.56
246.1702	+	6.48	2-Methylbutyroylcarnitine/Valerylcarnitine/Isovalerylcarnitine/Pivaloylcarnitine	C12H23NO4	245.1627	M+H	1	1.98	1.43E-05	1.84
246.2428	+	2.60	Myristic acid	C14H28O2	228.2089	M+NH4	0	2.00	2.68E-05	1.11
248.1493	+	7.78	Hydroxybutyrylcarnitine	C11H21NO5	247.1420	M+H	0	2.25	2.65E-09	4.66
258.2794	+	2.55	Palmitaldehyde	C16H32O	240.2453	M+NH4	1	1.94	7.66E-05	1.47
259.2381	+	2.35	(4E,6E,d14:2) sphingosine	C14H27NO2		M+NH4	0	2.21	2.93E-06	2.62

Metaboloites in red were identified by using commercially available standards and the others were identified by comparison with the MS library.

Table 6.4 (Cont) The details of significantly altered metabolites of MIN6 cells exposed to azide (6 mM in final concentration).

m/z	Polarity	RT (min)	Metabolites	Formula	M.W.	Adduct	Error (ppm)	VIP	FDR	Fold
260.1859	+	6.16	Hexanoylcarnitine	C13H25NO4	259.1784	M+H	1	2.05	6.40E-07	1.94
261.2190	+	2.50	Hexadecenal	C16H30O	238.2297	M+Na	0	1.94	1.31E-05	1.91
268.1043	+	6.24	Adenosine	C10H13N5O4	267.0968	M+H	1	1.91	1.56E-03	1.19
268.2272	+	2.30	5Z-Tetradecenoic acid	C14H26O2	226.1933	M+ACN+H	0	2.10	2.70E-04	1.91
269.0882	+	7.29	Inosine	C10H12N4O5	268.0808	M+H	1	1.83	2.28E-03	0.90
270.2068	+	2.47	11-Hydroxy-9-tridecenoic acid	C13H24O3	228.1725	M+ACN+H	2	2.09	6.34E-06	2.92
274.2742	+	2.57	C16 Sphinganine	C16H35NO2	273.2668	M+H	0	1.89	9.50E-05	1.14
284.0991	+	8.04	Guanosine	C10H13N5O5	283.0917	M+H	1	1.81	9.49E-04	1.13
288.2171	+	2.60	L-Octanoylcarnitine	C15H29NO4	287.2097	M+H	1	2.01	8.46E-07	1.87
290.2691	+	2.55	3-Hydroxy-hexadecanoic acid	C16H32O3	272.2351	M+NH4	1	1.90	1.08E-03	1.56
293.1962	+	2.24	3-hydroxyheptanoic acid	C7H14O3	146.0943	2M+H	1	1.92	8.56E-05	1.39
296.2584	+	2.24	Linolenic acid	C18H30O2	278.2246	M+NH4	0	1.78	1.82E-03	0.94
300.0495	-	8.70	N-Acetyl-D-Glucosamine 6-Phosphate	C8H16NO9P	301.0563	M-H	2	2.09	2.00E-06	1.20
304.2121	+	6.50	3-hydroxyoctanoyl carnitine	C15H29NO5	303.2046	M+H	1	2.13	1.48E-05	294.33
304.2847	+	2.50	12-hydroxyheptadecanoic acid	C17H34O3	286.2508	M+NH4	0	1.97	8.56E-07	0.37
309.2273	+	2.30	N1,N12-Diacetylspermine	C14H30N4O2	286.2369	M+Na	4	2.00	9.71E-06	1.39
316.2122	+	2.27	3-Hydroxytetradecanedioic acid	C14H26O5	274.1780	M+ACN+H	1	2.02	3.56E-10	3.17
338.3419	+	2.16	Thromboxane	C20H40O	296.3079	M+ACN+H	0	2.00	9.72E-06	0.37
340.2485	+	1.86	8E-Heptadecenedioic acid	C17H30O4	298.2144	M+ACN+H	0	1.89	1.46E-04	1.47
341.3165	+	2.21	Sphingosine	C18H37NO2	299.2824	M+ACN+H	1	1.85	7.09E-05	0.98
346.0564	-	8.22	Adenosine monophosphate	C10H14N5O7P	347.0631	M-H	2	2.17	5.17E-14	1.23
347.0405	-	8.87	Inosine 2'-phosphate	C10H13N4O8P	348.0471	M-H	2	2.27	1.81E-09	2.84
359.3270	+	2.30	Stearoylglycine	C20H39NO3	341.2930	M+NH4	0	1.96	1.66E-05	0.31

Metaboloites in red were identified by using commercially available standards and the others were identified by comparison with the MS library.

Table 6.4 (Cont) The details of significantly altered metabolites of MIN6 cells exposed to azide (6 mM in final concentration).

m/z	Polarity	RT (min)	Metabolites	Formula	M.W.	Adduct	Error (ppm)	VIP	FDR	Fold
360.1502	+	9.36	Galactinol	C12H22O11	342.1162	M+NH4	0	2.00	3.15E-07	2.52
363.2203	+	1.86	PG	C35H69O10P	680.4628	M+2Na	0	2.16	1.54E-06	7.83
364.0655	+	9.42	Guanosine monophosphate	C10H14N5O8P	363.0580	M+H	0	2.16	5.33E-15	1.32
365.1057	+	9.33	Galactinol	C12H22O11	342.1162	M+Na	1	2.01	5.30E-04	1.15
375.3220	+	2.19	N-palmitoyl threonine	C20H39NO4	357.2879	M+NH4	0	2.01	4.05E-09	0.93
382.1013	-	8.45	Succinyladenosine	C14H17N5O8	383.1077	M-H	2	2.23	3.08E-10	8.14
387.3584	+	2.27	N-palmitoyl isoleucine/N-palmitoyl leucine	C22H43NO3	369.3243	M+NH4	0	1.96	1.38E-03	0.34
390.2856	+	2.19	19(R)-hydroxy-PGF1α	C20H36O6	372.2512	M+NH4	0	1.85	1.17E-04	0.62
401.3704	-	14.67	TG	C52H100O5	804.7571	M-2H	2	1.93	4.76E-05	2.33
414.2851	+	2.13	Prostaglandin	C22H36O6	396.2512	M+NH4	0	1.91	3.08E-05	0.18
426.0229	-	8.90	Adenosine diphosphate	C10H15N5O10P2	427.0294	M-H	2	1.99	2.09E-04	2.99
444.3323	+	2.13	Glucosylsphingosine	C24H47NO7	461.3353	M+H-H2O	1	2.03	3.80E-11	0.02
460.2697	+	2.24	PIP	C43H84O16P2	918.5235	M+2H	1	2.02	1.15E-03	2.42
538.5202	+	2.19	Ceramide (d18:1/16:0)	C34H67NO3	537.5121	M+H	1	2.00	2.48E-04	0.72
565.0488	-	9.19	Uridine diphosphate glucose	C15H24N2O17P2	566.0550	M-H	2	2.02	3.47E-05	3.12
584.0896	+	9.15	Uridine diphosphate glucose	C15H24N2O17P2	566.0550	M+NH4	1	2.02	1.48E-10	2.61
752.5584	+	2.01	PE	C40H76NO8P	751.5516	M+H	1	2.05	6.58E-05	0.02
904.5926	+	1.92	PI	C47H83O13P	886.5571	M+NH4	2	2.03	1.89E-03	0.51

Metaboloites in red were identified by using commercially available standards and the others were identified by comparison with the MS library.

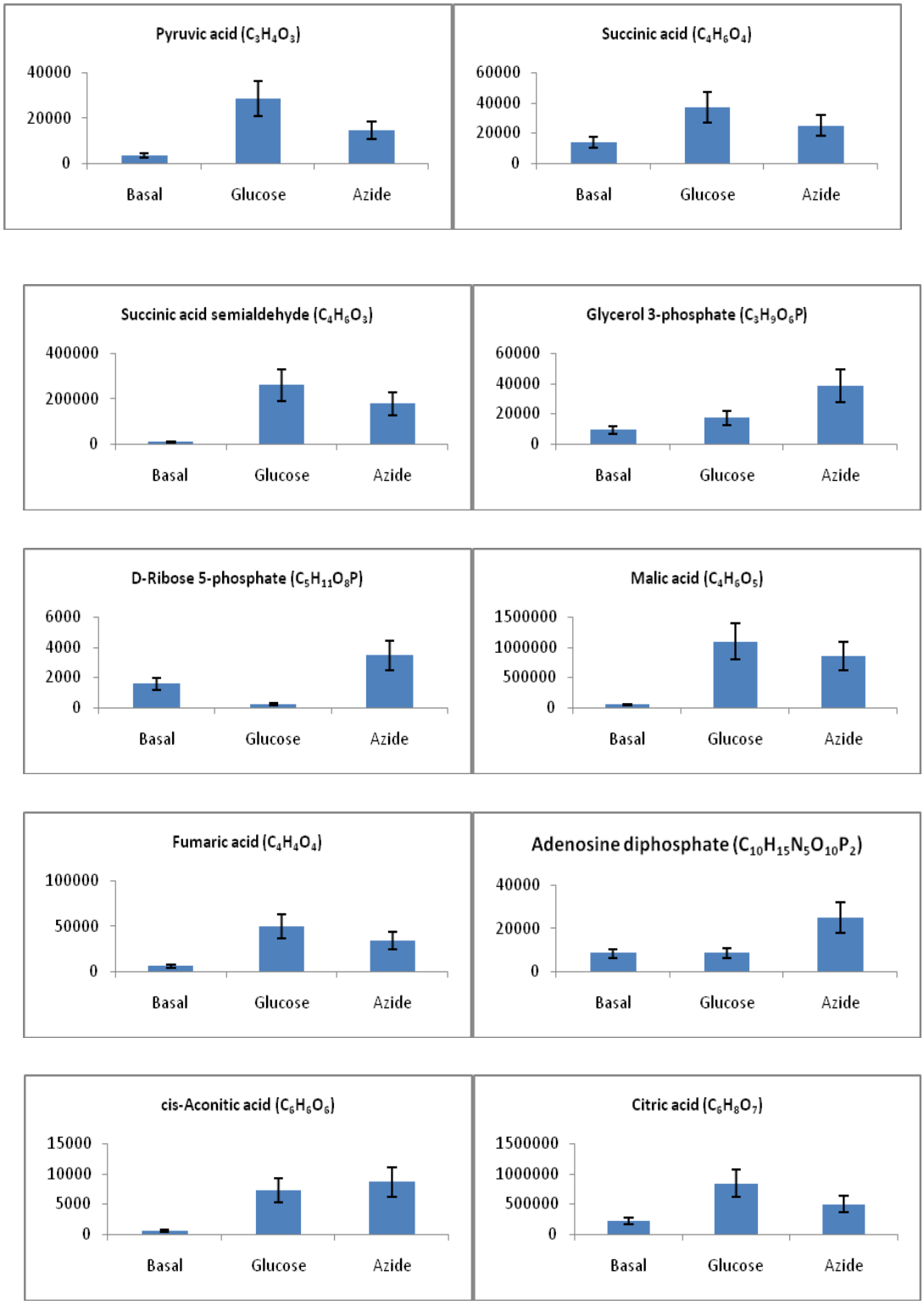


Figure 6.11 Level changes of ten altered metabolites (involved to bioenergetics) of 10 mM glucose treated MIN6 cells exposed with 6 mM (in final concentration) of azide compared to untreated cells: Basal = untreated, Glucose = glucose and Azide = glucose + azide. .

6.5.2.5 Metabolic signature of glucose-treated MIN6 cells exposure to fluoxetine

The effects of fluoxetine on glucose-treated MIN6 cells were studied. For dissolving fluoxetine, glucose solution was used as a vehicle. The OPLS-DA scores plot shown in Figure 6.12 indicates that the metabolite profiles of the fluoxetine treated cells were separated from glucose treated cells and basal cells. This explained the significant separation of metabolite profiles among the treatments and indicated that metabolite profiles of glucose-treated MIN6 cells were altered by fluoxetine. Then, applying the criteria for identifying the significant ions (VIP $\geq$ 1.00, FDR < 0.05) in order to study the effects of fluoxetine on the metabolite profile of glucose-treated MIN6 cells, 130 significant ions were detected (see Supplementary Table 6.7). Based on exact mass (with mass error $\leq$ 5 ppm) and comparison to authentic standards, and data from free databases (HMDB and MetLin) and literatures, 66 of the significant ions were identified in our samples as summarised in Table 6.5. Figure 6.13 shows the level changes of the top ten significantly altered metabolites in MIN6 cells exposed to fluoxetine compared with the control.

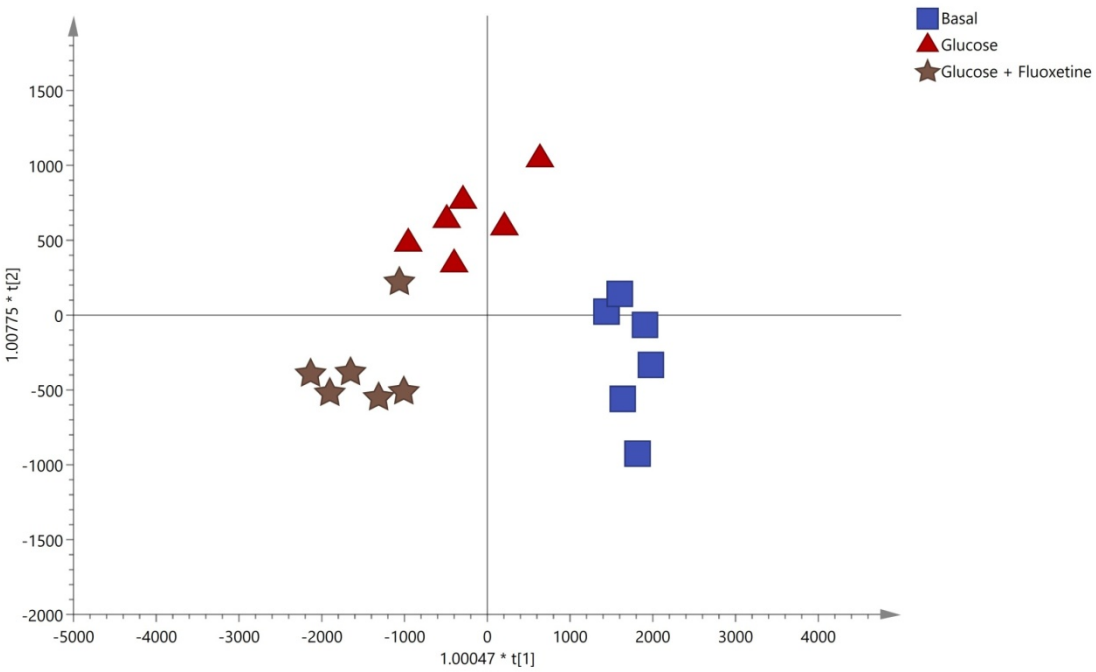


Figure 6.12 Scores plot from OPLS-DA analysis of basal, glucose and glucose + fluoxetine treated MIN6 cells (with R^2X = 0.96, R^2Y = 0.99 and Q^2 = 0.97). Each point represents cell extracts from one sample of MIN6 cells under control or compound treatments. Extracts from the same condition are grouped: basal (blue squares), glucose (red triangles) and glucose + fluoxetine (brown five peak star).

Table 6.5 The details of significantly altered metabolites of MIN6 cells exposed to fluoxetine (30 μM in final concentration).

m/z	Polarity	RT (min)	Metabolites	Formula	M.W.	Adduct	Error (ppm)	VIP	FDR	Fold
90.0551	+	8.87	L-Alanine	C3H7NO2	89.0477	M+H	1	1.04	1.10E-07	2.48
101.0245	-	8.60	Acetoacetic acid	C4H6O3	102.0317	M-H	1	1.09	1.73E-14	19.86
106.0500	+	9.33	L-Serine	C3H7NO3	105.0426	M+H	1	1.04	9.73E-04	2.78
112.0507	+	7.61	Cytosine	C4H5N3O	111.0433	M+H	1	1.05	6.30E-06	0.93
113.0246	-	8.65	2-Hydroxy-2,4-pentadienoate	C5H6O3	114.0317	M-H	0	1.09	6.62E-09	38.56
115.0038	-	8.87	Fumaric acid	C4H4O4	116.0110	M-H	1	1.06	1.20E-13	9.03
117.0195	-	8.24	Succinic acid	C4H6O4	118.0266	M-H	1	1.05	2.90E-08	3.51
120.0809	+	7.22	Tyramine	C8H11NO	137.0841	M+H-H2O	0	1.10	1.74E-03	1.77
130.0864	+	7.94	N4-Acetylaminobutanal	C6H11NO2	129.0790	M+H	1	1.04	4.43E-08	2.80
133.0144	-	8.82	Malic acid	C4H6O5	134.0215	M-H	1	1.06	3.02E-10	23.86
139.0503	+	2.60	Nicotinamide N-oxide	C6H6N2O2	138.0429	M+H	1	1.11	1.75E-09	6.62
143.0351	-	8.65	3-Methylglutaconic acid	C6H8O4	144.0423	M-H	1	1.09	3.49E-08	44.46
148.0605	+	8.47	L-Glutamic acid	C5H9NO4	147.0532	M+H	1	1.01	2.05E-03	2.40
150.0583	+	7.63	L-Methionine	C5H11NO2S	149.0510	M+H	0	1.09	1.45E-03	1.71
159.0300	-	2.12	3-Methyl-3-hydroxypentanedioate	C6H8O5	160.0372	M-H	1	1.10	3.66E-06	222.35
173.0093	-	9.27	cis-Aconitic acid	C6H6O6	174.0164	M-H	1	1.02	1.16E-03	33.27
176.1031	+	9.45	Citrulline	C6H13N3O3	175.0957	M+H	1	1.12	1.69E-13	5.59
179.0564	-	8.62	D-Glucose	C6H12O6	180.0634	M-H	1	1.10	1.11E-16	28.84
191.0200	-	9.84	Citric acid/Isocitric acid	C6H8O7	192.0270	M-H	1	1.02	6.77E-06	5.53
205.0973	+	7.75	L-Tryptophan	C11H12N2O2	204.0899	M+H	1	1.03	4.14E-03	1.30
223.1542	+	2.47	2-Hexenoylcholine	C11H22NO2	200.1651	M+Na	0	1.03	9.43E-06	1.18
232.1546	+	6.65	Isobutyryl-L-carnitine	C11H21NO4	231.1471	M+H	1	1.06	8.32E-11	6.08
243.1830	+	2.30	2-Hydroxyundecanoate	C11H21O3	201.1491	M+ACN+H	1	1.07	2.86E-11	4.71
244.0933	+	7.61	Cytidine	C9H13N3O5	243.0855	M+H	2	1.01	4.71E-06	0.94

Metaboloites in red were identified by using commercially available standards and the others were identified by comparison with the MS library.

Table 6.5 (Cont.) The details of significantly altered metabolites of MIN6 cells exposed to fluoxetine (30 µM in final concentration).

m/z	Polarity	RT (min)	Metabolites	Formula	M.W.	Adduct	Error (ppm)	VIP	FDR	Fold
246.1702	+	6.48	Pivaloylcarnitine	C12H23NO4	245.1627	M+H	1	1.02	2.54E-07	4.69
246.2428	+	2.60	Myristic acid	C14H28O2	228.2089	M+NH4	0	1.06	6.06E-07	0.76
260.1858	+	2.60	Hexanoylcarnitine	C13H25NO4	259.1784	M+H	1	1.02	3.82E-06	9.41
261.1962	+	3.61	PA	C45H81O8P	780.5669	M+3H	1	1.13	1.97E-07	8.84
284.0991	+	8.04	Guanosine	C10H13N5O5	283.0917	M+H	1	1.01	6.83E-06	1.64
284.2068	+	2.60	CerP(d18:1/26:1(17Z))	C46H90NO6P	783.6506	M+3Na	2	1.04	4.59E-05	1.13
300.0495	-	8.70	N-Acetyl-D-Glucosamine 6-Phosphate	C8H16NO9P	301.0563	M-H	2	1.11	1.30E-05	0.56
309.2273	+	2.30	N1,N12-Diacetylspermine	C14H30N4O2	286.2369	M+Na	4	1.05	5.04E-06	1.12
316.2122	+	2.27	3-Hydroxytetradecanedioic acid	C14H26O5	274.1780	M+ACN+H	1	1.02	1.69E-09	2.89
323.0292	-	8.67	Uridine 5'-monophosphate	C9H13N2O9P	324.0359	M-H	2	1.09	2.11E-05	2.76
325.2487	+	2.44	3-Oxotetradecanoic acid	C14H26O3	242.1882	M+2ACN+H	1	1.09	8.12E-05	5.69
340.2485	+	1.86	8E-Heptadecenedioic acid	C17H30O4	298.2144	M+ACN+H	0	1.03	1.46E-05	0.84
343.2958	+	2.60	TG	C68H114O6	1026.8615	M+3H	4	1.05	5.23E-06	2.60
344.2430	+	1.95	2,3-dinor-PGE1	C18H30O5	326.2093	M+NH4	1	1.05	7.87E-06	1.06
346.0564	-	8.22	Adenosine monophosphate	C10H14N5O7P	347.0631	M-H	2	1.06	6.36E-13	0.27
347.0405	-	8.87	Inosine 5'-monophosphate	C10H13N4O8P	348.0471	M-H	2	1.09	9.57E-07	1.95
348.0706	+	8.04	Inosine 2',3'-cyclic phosphate	C10H14N5O7P	347.0631	M+NH4	1	1.05	1.63E-14	0.29
364.0655	+	9.42	Guanosine monophosphate	C10H14N5O8P	363.0580	M+H	0	1.06	3.45E-14	0.50
365.1057	+	9.33	Galactinol	C12H22O11	342.1162	M+Na	1	1.03	4.08E-04	1.09
382.1013	-	8.45	Succinyladenosine	C14H17N5O8	383.1077	M-H	2	1.03	1.02E-06	3.06
384.7724	+	2.21	TG	C73H134O6	1107.0180	M+H+2Na	1	1.03	4.18E-06	5.55
401.3704	-	14.67	TG	C52H100O5	804.7571	M-2H	2	1.04	1.34E-04	1.21
444.3323	+	2.13	Glucosylsphingosine	C24H47NO7	461.3353	M+H-H2O	2	1.04	5.62E-11	0.02

Metaboloites in red were identified by using commercially available standards and the others were identified by comparison with the MS library.

Table 6.5 (Cont.) The details of significantly altered metabolites of MIN6 cells exposed to fluoxetine (30 µM in final concentration).

m/z	Polarity	RT (min)	Metabolites	Formula	M.W.	Adduct	Error (ppm)	VIP	p Value	Fold
455.2902	+	2.30	9'-Carboxy-gamma-tocotrienol	C23H32O4	372.2301	M+2ACN+H	0	1.10	7.05E-04	0.69
460.2947	+	1.74	N-stearoyl histidine	C24H43N3O3	421.3304	M+K	1	1.13	1.98E-05	5.23
466.4108	+	2.16	TG	C62H106O5	930.8040	M+2H	3	1.06	3.80E-05	2.64
488.3586	+	2.13	Thyroxine glucuronide	C21H19I4NO10	952.7188	M+H+Na	2	1.04	8.08E-10	0.02
502.3384	+	2.21	Dodecanedioic acid	C12H22O4	230.1518	2M+ACN+H	2	1.03	6.13E-09	0.01
533.2514	-	1.64	Pregnanediol-3-glucuronide	C27H44O8	496.3036	M+K-2H	2	1.13	6.20E-08	84.33
540.4464	+	1.74	PC	C56H110NO8P	955.7969	M+3ACN+2H	2	1.02	8.51E-06	2.23
546.3650	+	2.13	Ganglioside GA2 (d18:1/9Z-18:1)	C56H102N2O18	1090.7128	M+2H	2	1.05	1.75E-09	0.00
565.0488	-	9.19	Uridine diphosphate glucose	C15H24N2O17P2	566.0550	M-H	2	1.09	2.98E-07	6.21
590.3925	+	2.10	LysoPE	C25H50NO7P	507.3325	M+2ACN+H	1	1.05	1.38E-12	0.00
597.3055	-	2.26	1-Oleoylglycerophosphoinositol	C27H51O12P	598.3118	M-H	2	1.14	1.17E-10	8.63
598.0688	+	10.23	Uridine diphosphate glucuronic acid	C15H22N2O18P2	580.0343	M+NH4	1	1.06	1.81E-06	2.09
608.0898	+	8.67	Uridine diphosphate-N-acetylglucosamine	C17H27N3O17P2	607.0816	M+H	2	1.02	1.09E-04	1.77
620.4376	+	2.19	LysoPE	C27H56NO7P	537.3794	M+2ACN+H	4	1.04	1.55E-11	0.05
634.4197	+	2.13	CerP(d18:1/14:0)	C32H64NO6P	589.4471	M+2Na-H	2	1.04	8.46E-12	0.01
664.4618	+	2.19	Ganglioside GD1b (d18:1/26:1(17Z))	C93H163N3O39	1946.0864	M+H+2Na	0	1.03	3.71E-09	0.06
678.4469	+	2.13	lysoPC(26:1(5Z))	C34H68NO7P	633.4733	M+2Na-H	4	1.02	6.17E-08	0.00
707.0767	+	7.37	Nicotinamide ribotide	C11H15N2O8P	334.0566	2M+K	1	1.01	1.43E-03	1.04
752.5175	+	2.19	CL	C85H148O17P2	1503.0192	M+2H	1	1.02	3.76E-05	0.01

Metaboloites in red were identified by using commercially available standards and the others were identified by comparison with the MS library.

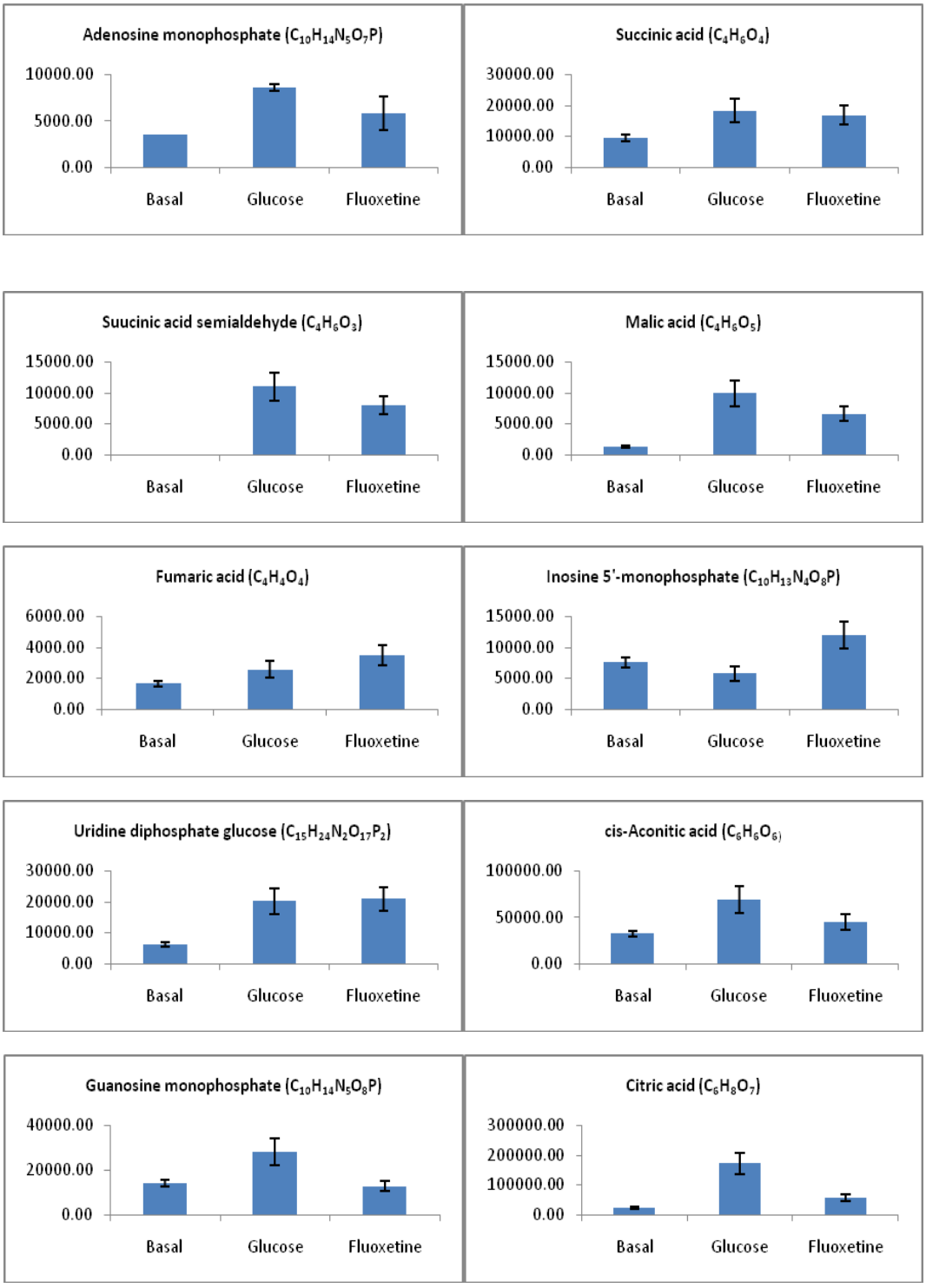


Figure 6.13 Level changes of ten altered metabolites (involved in bioenergetics) of 10 mM glucose treated MIN6 cells exposed to 30 µM (in final concentration) of fluoxetine compared to untreated cells: Basal = untreated, Glucose = glucose and Fluoxetine = glucose + fluoxetine. .

6.5.2.6 Overall effects

Based on the studies, it is found that rotenone, antimycin A, azide and fluoxetine mainly affected on bioenergetics (glycolysis, TCA cycle and ETC) as summarised in Tables 6.2 to 6.5. However, from the OPLS-DA scores plot shown in Figure 6.1, the indication is that the treatment compounds have an effect on glucose-treated MIN6 cells in distinguished metabolic pathways. Figure 6.14 shows the fold changes of some metabolites that were detected in all treatments. These metabolites are involved in mitochrondrial function.

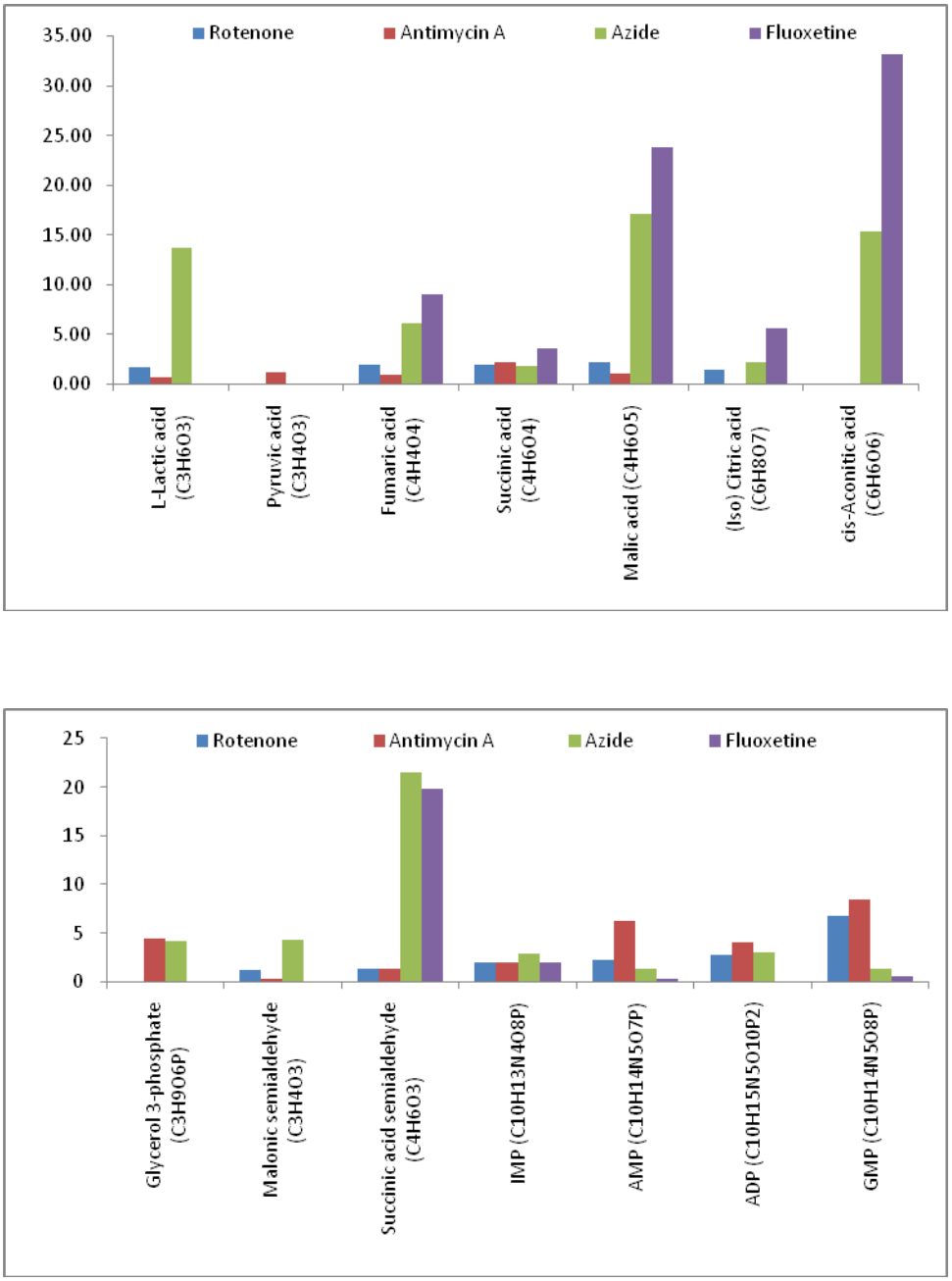


Figure 6.14 Fold changes of shared altered metabolites (involved in bioenergetics) of 10 mM glucose treated MIN6 cells exposed to glucose, rotenone, antimycin A and fluoxetine

6.5.3 Metabolic pathway analysis

The glycolysis and TCA cycle have a critical role in the insulin secretion response of β-cells to glucose (128). Key glycolytic metabolites identified in MIN6 cells exposed to glucose include glyceraldehydes (fold change = 14.14 times), lactate (fold change = 14.00 times) and pyruvate (fold change = 2.55 times). Other key metabolites were not detected in the experiments. Moreover, key TCA cycle metabolites identified include oxoglutarate (fold change = 16.66 times), fumarate (fold change = 8.86), citrate (fold change = 3.75 times) and malate (fold change = 22.10 times). Interestingly, other metabolites were also strongly associated with insulin secretion. For example, acyl carnitine compounds (carnitine (fold change = 2.65), hexanoylcarnitine (fold change = 7.61), octanolycarnitine (fold change = 7.85), etc.) are intermediate metabolites in fatty acid metabolism. These metabolites act as fatty acid carriers from the cytosol to the mitochondrion (269). Moreover, intermediates associated with fatty acid metabolism were also identified. In addition, amino acids alanine (fold change = 2.53), L-glutamate (fold change = 1.95), L-proline (fold change =1.69) and L-threonine (fold change = 2.45) were positively associated with MIN6 cell response to 10 mM glucose. The overall effects of glucose on MIN6 cells can be illustrated in Figure 6.15.

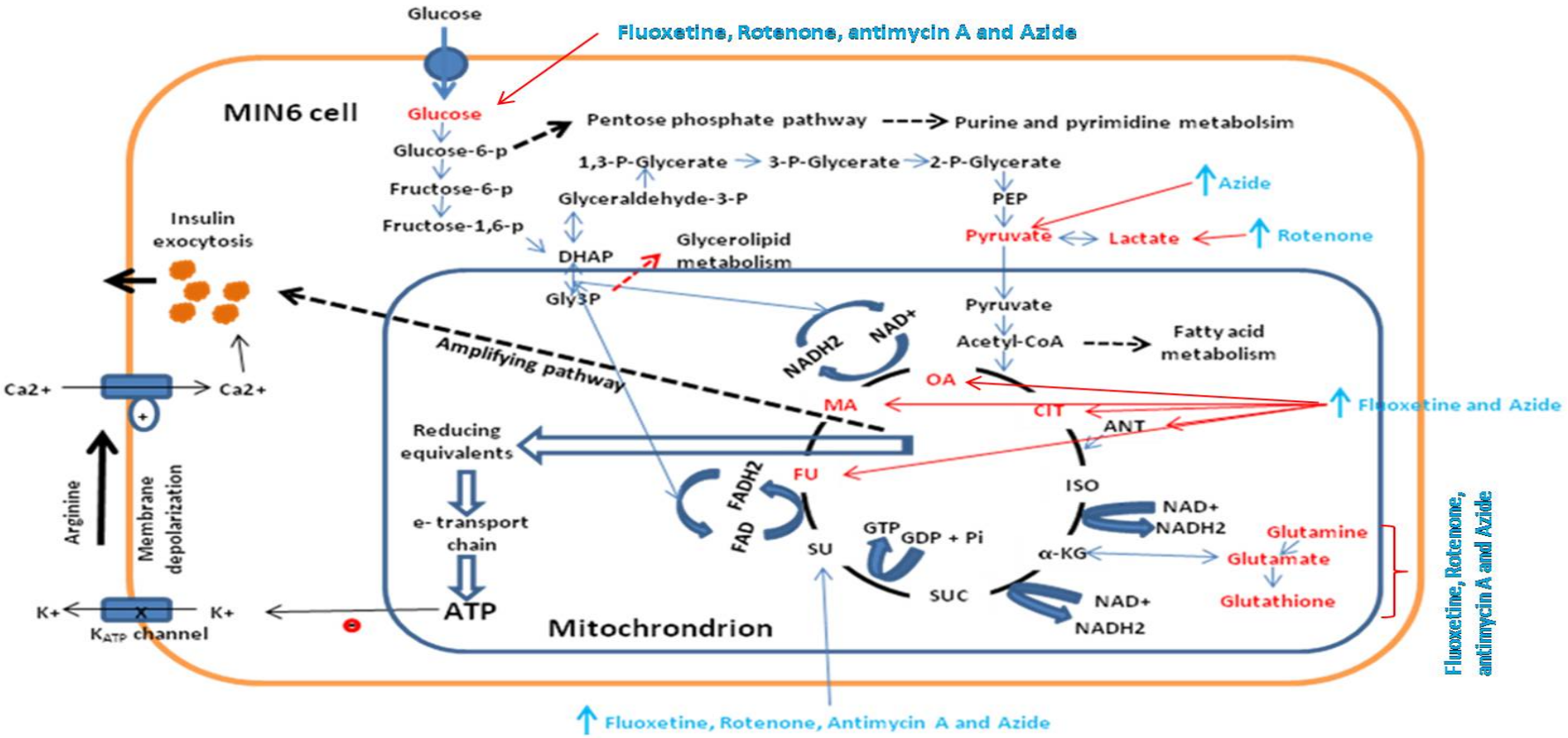


Figure 6.15 Model for the coupling of glucose metabolism to insulin secretion and the effects of fluoxetine, rotenone, antimycin A and azide in the MIN6 cell. Glycolysis converts glucose to pyruvate, which enters the mitochondrion and converts to acetyl-CoA. The acetyl-CoA feeds into the TCA cycle. The electrons occurring in the TCA cycle enter the electron transport chain (ETC) and generate ATP. High concentration of ATP inhibits the efflux of K+. This depolarises the plasma membrane which increases the influx of Ca2+ and triggers insulin exocytosis. Metabolites in red were detected in our investigation and their levels were raised in comparison to untreated cells. DHAP = dihydroxyacetone phosphate, Gly3P = glycerol-3-phosphate, OA = oxaloacetate, CIT = citrate, ISO = isocitrate, ANT = aconitate, α-KG = α-ketoglutarate, SUC = succinyl-CoA, SU = succinate, FU = fumarate, MA = malate.

Next, the effects of fluoxetine on glucose-treated MIN6 cells were examined and compared with three-known ETC inhibitors (rotenone (Complex I inhibitor), antimycin A (Complex III inhibitor) and azide (Complex IV inhibitor)). The concentration of fluoxetine, roteneone, antimycin A and azide used did not affect on MIN6 cell viability and caused no apoptosis (data not shown). When a comparison was made among glucose vs glucose + fluoxetine, glucose + DMSO vs glucose+ DMSO + rotenone, glucose + ethanol vs glucose + ethanol + antimycin A and glucose vs glucose + azide, it is found that TCA metabolites play a critical role in the insulin secretion response of glucose-treated MIN 6 cells to the compounds used as shown in Figure 6.15.

From the Figure 6.15, It was found that fluoxetine and azide affected on the levels of fumaric acid (fold change = 9.30 and 6.10), succinic acid (fold change = 3.51 and 1.81), malic acid (fold change = 23.86 and 17.13), cis-aconitic cid (fold change = 33.27 and 15.36) and (iso)citric acid (fold change = 5.53 and 2.20). Moreover, it was found that the level of succinic acid was increase (fold change = 2.14) in the antimycin A treatment group, and the levels of fumaric acid, succinic acid, and malic acid were increase (fold change = 1.85, 1.94 and 2.14, respectively) in rotenone treatment group. In addition, it is found that the level of pyruvic acid was increase only in the azide treatment group (fold change = 4.25). .

6.6 DISCUSSION

Fluoxetine is reported to be associated with both hyperglycaemia (121,123) and an increased risk of type 2 diabetes (260,270). The glucose stimulated-insulin secretion of beta cells is mainly controlled by glycolysis and the TCA cycle pathways (128). In the study, cell-based metabolomics using the HILIC-MS approach was applied to MIN6 cells in order to gain insight into the metabolic regulation of insulin secretion. The effects of rotenone (a complex I inhibitor of the ETC system), antimycin A (a complex III inhibitor of the ETC system) and azide (a complex IV inhibitor of the ETC system) were examined in order to compare their metabolite profiles with fluoxetine.

6.6.1 Glucose effects

First, the effect of glucose on metabolite profiles of MIN6 cells was investigated. The most significant difference in metabolites between untreated MIN6 cells and those treated with 10 mM glucose were identified by OPLS-DA combined with univariate analysis. OPLS-DA model forms a good summary and visualisation of the MS data set and has good predictability. Among all of the metabolites detected, 46 metabolites were found to be strongly associated with the metabolic response of MIN6 cells to glucose using our selected criteria (VIP $\geq$ 1.00 and FDR < 0.05). Huang et al. applied metabolomics in order to analyse pancreatic beta-cell insulin release

in response to glucose and suggested that glycolysis plays an important role in glucose-stimulated insulin secretion by beta cells (264). Glycolysis is the first important key step in glucose detection and it controls insulin secretion by beta cells (128). As expected, glycolytic intermediates and related metabolites, lactate, pyruvate, glucosamine, N-acetyneuraminic acid, CMP-N-acetylneuraminic acid, glyceraldehyde and UDP-glucose, were all increased in response to treating MIN6 cells with 10 mM glucose and these intermediates were strongly associated with glucose-stimulated insulin secretion by MIN6 cells in the OPLS-DA model. In addition to increasing glycolysis activity, several other cellular pathways were also shown to be associated with glucose-stimulated insulin secretion by MIN6 cells. One of these pathways could be lipid metabolism represented by many lipid compounds and acyl carnitine compounds in the study. The acyl carnitine compounds, such as L-carnitine, (iso)butyl carnitine, hexanoylcarnitine and octanoylcarnitine, are the lipid carriers between mitochondria matrix and the cytosol. When beta cells are exposed to an elevated glucose concentration, the intracellular levels of citrate, malonyl-CoA, palmitrate and acyl-CoA increases rapidly resulting in replenishment of oxaloacetate in the TCA cycle. This event leads to the accumulation and escape of citrate from the mitochondrial matrix into the cytosol for lipid synthesis. Moreover, glucose also inhibits fatty acid and lipid oxidation in beta cells. This inhibition results in an increase level of

malonyl-CoA and/or long chain acyl-CoA. These compounds promote nutrient storage in beta cells including fatty acid and lipid biosynthesis (271). In the studies, both of malonyl-CoA and or long chain acyl-CoA compounds were not detected because they could not be retained in our HILIC column used; however, the levels of intermediate metabolites in fatty acid and lipid metabolism, such as (iso)myristate, 3- or 2-hydroxyhexadecanoate and acyl carnitine compounds, were raised by treating MIN6 cells with 10 mM glucose and were also identified by our methods as significant metabolites contributing to clustering of high glucose treated MIN6 cells.

Amino acids and intermediates in metabolite metabolism; L-proline, L-glutamate, L- threonine, beta-alanine, and intermediates of amino acid metabolism were also shown to contribute significantly to clustering of high glucose treated MIN6 cells. Amino acid metabolism has shown that it may only be able to provide sufficient resources for insulin biosynthesis and may be indirectly/directly involved in regulating insulin release. Liu et al. showed that amino acids acutely stimulate insulin secretion from beta cells (272). McDaniel et al. showed that the increased level of glutamate in pancreatic beta cells treated with high glucose may act as a putative intracellular messenger in permeabilised beta cells resulting in direct stimulation of insulin exocytosis (273). Dixon et al. and McCleanaghan et al. found that the level of alanine was

increased in beta cells treated with high glucose and suggested that alanine has insulinotropic effects (274,275).

Glycolysis-derived pyruvate enters the TCA cycle resulting in net accumulation of TCA intermediates. Succinic acid semialdehyde, acetate, fumarate, malate, oxoglutarate, (iso) citrate were significantly elevated by glucose treatment of MIN6 cells in this study (see Table 6.1). The results obtained were similar to those produced by Huang's study; they showed that beta cells treated with high glucose increased the levels of all TCA intermediates (264). Moreover, it is found that the levels of dynophin (fold change = 2.06) and imidazoleacetic acid ribotide (fold change = 1.73) were significantly increased. The dynophin and imidazoleacetic acid ribotide are endogenous metabolites that regulate insulin secretion from pancreatic beta cells. The results were supported by the studies of Josefsen et al. and Prell et al. which showed the increased secretion of dynorphin and imidazoleacetic acid ribotide in glucose-treated beta cells (276,277). The increases of these metabolites could suggest that they could have a potentially significant role in regulating insulin secretion.

6.6.2 Fluoxetine effects on glucose-treated MIN6 cells

After it was confirmed the effects of glucose on metabolite profiles of MIN6 cells, the effects of fluoxetine on glucose-treated MIN6 cells was studied. Fluoxetine has been shown to inhibit mitochondrial function in pancreatic beta cells and other cells (122,124,125). Nevertheless, the molecular basis of fluoxetine on glucose-stimulated insulin secretion by beta cells remains largely unknown and requires further elucidation. The aim of this study was to identify different metabolites in glucose-treated MIN6 cells exposed to fluoxetine using cell-based metabolomics and the LC-MS approach. Moreover, these effects were compared with rotenone, antimycin A and azide. These compounds are well known ETC complex inhibitors in mitochondria (278).

Through cell-based metabolomics using a LC-MS approach coupled with OPLS-DA statistical analysis and Student's T-test, this study revealed a set of 66 differential metabolites. To develop further insight into the underlying molecular mechanism operating in glucose-treated MIN6 cells, the different metabolites were comprehensively analysed in terms of metabolic activity. They were found to be mainly involved in (i) lipids and lipid metabolism-related molecules and (ii) bioenergetics and other metabolites.

6.6.2.1 Lipids and lipid metabolism-related molecules

In the current study, the levels of 11 lipids and lipid-metabolism-related compounds (see Table 6.5) were decreased in glucose-treated MIN6 cells exposed to fluoxetine vs. glucose-treated MIN6 cells (as a control). This finding suggests that fluoxetine could affect lipid metabolism in glucose-treated MIN6 cells. As mentioned in above section, high glucose treatment in beta cells results in increased lipid metabolism. This event leads to the accumulation and escape of citrate from the mitochondrial matrix into the cytosol for lipid synthesis. Previous studies by Raeder and his colleagues have been reported that fluoxetine affects on lipid metabolism in cultured human glial cells (279). Therefore, as lipids and -metabolism-related compounds are an essential component in glucose-stimulated insulin secretion mechanism, alteration of lipid compounds would cause disturbances in fatty acid metabolism within MIN6 cells. Moreover, as vital components of the mitochondrial cell membrane, lipids provide important compounds for mitochondrial polarisation, which in turn supports the insulin exocytosis (280).

6.6.2.2 Bioenergetics

Glucose-induces insulin secretion is controlled by a signal generated in the mitochondria (281). The vital key signal is ATP which is produced from bioenergetics processes (glycolysis, TCA cycle and ETC) in mitochondria. The elevation of ATP concentration is important for the trigger of insulin exocytosis (282). Bioenergetics compounds (such as pyruvate, (iso) citrate, fumarate) seen Table 6.2 were identified in glucose-treated MIN6 cells exposed to fluoxetine, and were compared with glucose-treated MIN6 cells (as a control). Specifically increases in fumarate, succinate, malate, cis-aconitate and citric acid which are associated with the TCA cycle were observed as shown in Figure 6.16. The activation of the TCA cycle results in the production of vital electrons that are transferred to the ETC, resulting in the generation of ATP (281,282). Kao et al. have revealed that fluoxetine increases the TCA cycle activity in mice through mitochondrial function (283). De Long et al. have suggested that fluoxetine may contribute to decreased mitochondrial ETC enzyme activity and reduced glucose stimulated insulin secretion (124). In combination with the current results, it is found that fluoxetine may reduce glucose stimulated insulin secretion by affecting ATP generation through the inhibition of the ETC in mitochondria. This inhibition results in increased levels of TCA intermediate metabolites.

6.6.3 Comparison of the effects of fluoxetine and ETC inhibitors

In the previous section, it is found that fluoxetine may affect mitochondrial function in glucose-treated MIN6 cells. In order to understand how fluoxetine affect the mitochondrial function, the change of metabolite profile with well-known ETC inhibitors was compared: rotenone (a complex I inhibitor on the ETC system), antimycin A (a complex III inhibitor on the ETC system) and azide (a complex IV inhibitor on the ETC system).

The effects of fluoxetine and ETC inhibitor treatments on glucose-treated beta cells were observed in a diverse range of metabolic pathways and appear to be mediated by glycolysis and TCA cycle processes. These pathways are relevant to the beta cell secretory function and could represent target for fluoxetine and ETC inhibitor actions in beta cells.

6.6.3.1 Glycolysis

The first step in glucose metabolism which plays a crucial role in glucose-stimulated insulin metabolism is glycolysis. This step breaks glucose down to form pyruvate. In the study, it is found that the level of pyruvate did not significantly change in fluoxetine as similar to rotenone and azide treatment, but antimycin A treatment caused a slight increase. This could suggest that fluoxetine could not disturb glycolysis pathway. In addition, lactate is an end product

during adequate oxygenation. It is found that the rotenone treatment groups have an increased level of lactate in glucose-treated MIN6 cells (fold change = 1.66 and 13.73, respectively). In contrast, antimycin A decreased the level of lactate in glucose-treated MIN6 cells (fold change = -1.50) and fluoxetine did not cause a significant change. With antimycin A, the lactate could be changed to pyruvate because the level of pyruvate was significantly increased. The fluoxetine treatment has no significant effect on glycolysis; it may only disturb on other pathways.

6.6.3.2 TCA cycle

The next stage of glucose metabolism involves pyruvate produced during glycolysis entering the TCA cycle in order to produce NADH and $CoQH^2$. These then enter the ETC to generate ATP (284). In the TCA cycle, it is found that rotenone and fluoxetine increased the level of fumarate, succinate, malate and citrate (see Figure 6.16). The level of cis-aconitate was increased in the azide and fluoxetine samples. In addition, antimycin A mainly affected the level of succinate but did not affect other compounds. In the TCA cycle, as shown in Figure 6.16, citrate is dehydrated by enzyme aconitase into cis-aconitate. Cis-Aconitate is then changed by aconitase into isocitrate. In the study, it is found that the levels of (iso) citrate and cis-aconitate were significantly increased as shown in Figure 6.16, but not in the rotenone and antimycin A samples. This could

indicate that azide and fluoxetine may inhibit the enzyme aconitase. Furthermore, in this step NAD^+ receives an electron to become $NADH^+$-H^+. The $NADH^+$-H^+, then, moves to the ECT cycle for ATP generation (282). This could indicate that azide and fluoxetine may affect on the ETC by reducing the amount of $NADH^+$,H^+ present.

In addition, in the TCA cycle, succinate is dehydrated by the enzyme succinic dehydrogenase and using CoQ into form fumarate (128). It is found that the fold change ratio between succinate and fumarate was the highest in antimycin A treatment. This is not surprising because antimycin A blocks ETC complex III. In the ETC complex III, $CoQH_2$ transfers electrons to CytC and is reduced to CoQ (285). If the amount of CoQ is decreased, the succinate dehydrogenation is not complete. This may describe why the level of succinate is high in the antimycin A treated cells. In the next step, fumarate is dehydrated by the enzyme fumarase into malate. It is found that the level of malate was also decreased because the substrate (fumarate) was decreased. This finding confirmed that antimycin A can affect fumarate synthesis. Rotenone, azide and fluoxetine treatment may not affect this step.

In the final step of TCA cycle, malate is dehydrogenated by the enzyme malate dehydrogenase into oxaloacetate, and NAD is oxidised into NADH-H^+ (282). We found that azide and fluoxetine treatments increased the level of malate. This could indicate that

both azide and fluoxetine could inhibit malate dehydrogenase and/or NAD reduction. Rotenone and antimycin A may not affect this step.

Overall, it can be shown that fluoxetine and azide had similar effects on glucose-treated MIN6 cells in terms of metabolome changes, especially in metabolites related to bioenergetics. Recently De long et al have demonstrated that fluoxetine causes a significant reduction in ETC complex IV activity of pancreatic beta cells (124). Since azide is an ETC complex IV inhibitor, this could indicate that fluoxetine have a similar function.

While observation of MIN6 cells by using cell-based metabolomics and LC-MS may not be fully applicable to islets, the study performed affords several advantages over in vivo study, and more precise measurement, due to ease of manipulation and procurement. One limitation of these studies is the lack of accurate measurements to cover all of the glycolysis, TCA and ETC intermediate metabolites which are not detected by the method used, and incomplete authentic standards used for confirmation. In order to address this limitation, targeted metabolic profile could be used in order to cover only interested metabolites and MS fragmentation will be used to identify and confirm detected metabolites.

6.7 CONCLUSION

Data generated using cell-based metabolomics to study the effects of glucose-treated MIN6 cells with or without exposure to rotenone, antimycin A, azide and fluoxetine has provided a novel way to test and extend several hypotheses for studying the effects of drugs and other compounds on biochemical mechanisms of glucose stimulated insulin secretion. The simultaneous measurement of intermediate metabolites of glycolysis, the TCA cycle, ETC, amino acids, lipids and other compounds shows a novel interaction of metabolites that are vital in both the triggering and amplifying pathways of insulin secretion, thus helping to refine the global view. Support for the ETC hypothesis comes from our measurements which confirm previous findings, and reveal the exact biological pathways when compared that are well known biological inhibitors. Finally, we found that fluoxetine may have similar effects to azide on glucose-treated MIN6 cells. This suggests fluoxetine may affect ETC complex IV.

CHAPTER VII: SUMMARY AND FUTURE DIRECTIONS

7.1 SUMMARY

It is assumed that alterations in cellular metabolism, such as amino acid metabolism, energy metabolism, and fatty acid metabolism, either due to disease or drugs, results in cellular dysfunction. While several studies report alterations of metabolism by drugs and other compounds in many mammalian cells, holistic descriptions of HMVEC metabolism in response to antipsychotics, MCF-7 cell metabolism in response to cordycepin with and without pentostatin, and MIN6 cell metabolsim in response to fluoxetine are rare.

The works we have presented has developed, optimised, validated and applied cell-based metabolomics using LC-MS to assess the previously unknown effects of drugs on three mammalian cell lines, namely HMVECs exposed to antipsychotics, MCF-7 cells treated with cordycepin and MIN6 cells with fluoxetine, using untargeted metabolic profiling.

7.1.1 Optimisation and validation of a liquid chromatography-mass spectrometry method

Various analytical strategies have been designed in the past to study different aspects of metabolism in cells. Therefore

metabolomics is considered a tool for the different analytical approaches and data evaluation to acquire data about metabolites in cells (286). Mass spectrometry (MS), in combination with liquid chromatography (LC), is currently the key technology for cell-based metabolomics studies. The ongoing development of efficient and novel separations and the detection with excellent sensitivity and high mass resolution in LC-MS offer new opportunities in metabolomics studies (287). The determination and identification of a large number of metabolites in cells can be achieved in one single analysis by LC-MS (59).

MS is often used in cell based metabolomics due to its high sensitivity, selectivity and linear range. Moreover, MS allows a selective detection of many analytes at the same time because of its ability to separate ions according to mass to charge ratio (m/z) (288). In Orbitrap MS, it is even possible to distinguish between compounds with the same nominal mass. Nevertheless, the use of proper LC techniques is essential in metabolomics assays, especially when metabolites are to be quantified. LC is used widely for metabolomics studies, depending on the targeted or non-targeted analysis and on the metabolite class of interest. Some metabolite classes may be discriminated by the type of LC separation (33, 289).

Reversed phase-liquid chromatography (RP-LC) and hydrophilic interaction liquid chromatography (HILIC) are the most versatile techniques for targeted and non-targeted metabolomics because a wide spectrum of metabolites, from non-polar to polar, can be analysed without a derivatisation step as in gas chromatography (GC) (290). RP-LC is compatible with ESI-MS and is widely used for metabolomics studies. Because of high separation efficiency and robust retention times, RP-LC is often applied in quantification of non-polar metabolites and lipids. However, RP-LC separations are not effective in retention of polar metabolites (138). HILIC is the alternative LC separation technique for polar analytes and is fully compatible with ESI-MS and so it is used widely in metabolomics studies. Various types of HILIC exhibiting different selectivities are available today which makes the choice of the best separation system more complex (Neubauer, 2012). Recently, RP-LC and HILIC techniques have attracted much attention in optimising and validating methods for metabolomics analysis (138, 290, 291).

Currently, analytical technologies - especially LC-MS - are making great progress in optimising and validating methods for metabolomics analysis. Bajad et al. compared various different RP-LC and HILIC columns and found a column capable of separating some cellular metabolites. However, the methods are not suitable

for comprehensive coverage of cellular metabolites (292). Lorenz has developed a HILIC-MS method for metabolic profiling in beta-cells (291) and has shown that the developed technique is adequate for the detection of many metabolites. However, reproducibility and speed of this method can be improved further through an increase in column stability and lowered plate height. Later, Neubauer successfully applied RP-LC and HILIC methods for the measurement of a wide range of intracellular metabolites in yeast, but the method is not suitable for mammalian cell analysis (291). Fei et al. used HILIC-TOF-MS approach for the measurement of lipid and polar metabolites of gram-negative and gram-positive bacteria as well as mammalian macrophages; however, this method was not robust and had low reproducibility for highly polar metabolites (138). The optimal LC-MS method is still not a standard process for cell-based metabolomics in mammalian cells. Moreover, it is important to note that the effectiveness, reliability and reproducibility of LC-MS should be investigated before being applied to metabolomics studies.

In this study, efficiencies of both RP-LC and HILIC columns were evaluated. As shown in Chapter III, the polar fraction of QC samples was weakly retained under C18 RP-LC conditions and eluted near the column dead volume (1 min). On the C8 RP-LC column, the lipid fraction of QC sample was strongly retained and eluted in a high

aqueous mobile phase. This result indicates that the C8 RP-LC methods used are suitable for non-polar metabolites and lipids with excellent stability during the analysis procedure in terms of RSD less than 30%.

Consequently, experiments were designed to optimise and validate the parameters that affect the efficiency of a ZIC-HILIC column (betaine-sulfonate bonded phase). The intra-day precision of the proposed method was tested with six repeated injections of three standard solution mixtures. The inter-day precision was studied by analysing three standard solution mixtures, with six injections randomly executed between days. For retention time and peak area, the intra-day relative standard deviations were below 15%. Similar results were obtained for inter-day relative standard deviations.

From a global metabolomics perspective and using the ZIC-HILIC column approach, 164 metabolites including amino acids, nucleotides, organic acids, sugars and phosphate compounds were used as cellular metabolites. Detection of these metabolites was performed by their *m/z* within five ppm mass accuracy. As a result, 154 metabolites were identified in the standard mixtures.

RP-LC and HILIC separation methodologies for cell based metabolomics were optimised and validated. The C8 RP-LC column demonstrated adequate performance for the separation of non-polar

compounds and lipids. On the other hand, a simple, relatively rapid, and accurate HILIC methodology was successfully developed and validated for separating polar metabolites.

7.1.2 Effects of antipsychotic drugs applied to human microvascular endothelial cells on the intracellular metabolome

Over the past decades, several studies have stressed an important effect of a disrupted blood brain barrier (BBB) in antipsychotic treatment (86,87). The BBB is a complex structure located along the continuous cerebrovascular endothelium, which is selectively permeable to blood constituents and thereby protects the brain parenchyma from toxic compounds (89). Malfunction of the BBB can lead to enhanced permeability, which subsequently may cause damage to microvascular endothelium cells and surrounding brain tissue (88). Microvascular endothelium damage has been hypothesised to contribute to the associated neuropathologies observed with long term antipsychotic therapy (86). In addition, the damage of microvascular endothelium cells in the BBB may be the primary initiating factor of hypertension-related small vessel disease (292, 293). Interestingly, accumulating evidence also suggests that antipsychotics impaire HMVECs function of the BBB in patients with bipolar disorder (92). Moreover, Carrano et al. suggest a pivotal role of BBB disruption in cerebral amyloid angiopathy (294, 295).

Since this damage of the microvascular endothelial layer is associated with drugs and disorders, BBB disruption may consequently play a role in its development. Consistent with this hypothesis is evidence that suggests a role for BBB disruption in the pathogenesis of high dose antipsychotic treatment (86,87). To date, however, the exact link between BBB disruption and antipsychotics at high therapeutic dose remains poorly understood.

The aim of this work was to provide evidence to support currently available information on BBB disruption in in-vitro studies and its main underlying biological processes in terms of metabolome change in HMVECs. The application of cell-based metabolomics using LC-MS has enabled the measurement of drug effects for a wide range of metabolites in HMVECs. These measurements have allowed the testing of several prevailing hypotheses on the mechanism of antipsychotics at high dosage, and identification of cellular metabolites that may play a role in HMVEC metabolism. In this study, the cell-based metabolomics using LC-MS revealed that antipsychotics at high dosage may affect the bioenergetics pathway due to mitochondrial dysfunction resulting in ketoacidosis and inducing oxide stress by reactive oxygen species generation. These phenomena are involved with lipid metabolism.

In this study, RP-LC was applied to investigate lipids and related compounds. For identified metabolites, it was based on accurate

and exact mass measurement. Identification of known and unknown *m/z* was not successful as there were a number of metabolites in the available databases with the same *m/z*. However, as the intention of this was to find metabolites which are normally found in human cells, it was decided to present the results. The identification of lipids requires methods which cover the complexity of this structurally diverse group. Further studies are required using MS/MS data for unequivocal lipid identification.

Moreover, adequate retention and separation of polar metabolites is especially challenging. Many metabolites of interest in central metabolism are hydrophilic, polar molecules that are poorly retained by RP-LC approaches as shown in the data. HILIC has been increasingly used in the past decade for cell-based metabolomic analysis. The HILIC mode of separation is based on analyte interaction with an adsorbed water layer on the surface of a polar stationary phase and offers excellent retention of polar molecules. HILIC separation will be used for the analysis of those metabolites important in the study of central energy metabolism such as those from glycolysis, the TCA cycle, amino acids and other molecules. To get a broader view of the biochemical mechanisms of BBB dysfunction-related antipsychotics at high dosage, the combination data from RP-LC and HILIC approaches could provide a holistic evaluation of the metabolic profile that occurred in HMVECs.

7.1.3 LC-MS-based metabolomics revealed significant altered intracellular metabolites in human breast cancer (MCF-7) cells treated with cordycepin

Cordycepin (or 3'-deoxyadenosine) is a bioactive component extracted from the caterpillar fungi and its pharmacologic activities are reported to have nephroprotective, antiapoptotic, anti-metastatic, hepatoprotective, anti-inflammatory effects, antioxidant, anti-tumour, immunomodulatory and vasorelaxation activities (226, 297). Over the past decade, studies have focused on the effect of cordycepin on breast cancer with a view to its application in breast cancer treatment. Breast cancer develops in the cells of the breast and is hormone related. It is the most commonly diagnosed cancer and the second leading cause of cancer death in women worldwide. In 2015, there were approximately 231,840 new cases of breast cancer and 40,290 breast cancer deaths in the United States (99). Recent research, however, has studied the possible anti-breast cancer ability of cordycepin. Investigations have been done with breast cancer cell lines. Reports from these investigations have shown significant reductions in cancer cell proliferation (104, 110, 113, 116). Although cordycepin has shown that it effectively kills MCF7 human breast cancer cell lines in in-vitro studies, the clinical application of cordycepin in breast cancer treatment still remains elusive. Therefore, it is

essential to gain an understanding of the exact biological effects of cordycepin.

In recent years, further efforts have been made using genomic, proteomic and metabolomic approaches to investigate the cellular processes and their responses to anti-cancer drug as well as potential targets. Cell-based metabolomics in particular offers a unique strategy to detect metabolic changes that occur in a cell in response to drugs, and the outcome of such studies can provide insights into their corresponding mode of action (298, 299). In addition, chemical analysis methods such as LC-MS have already been developed for cell-based metabolomic studies of cancer cells to new candidate drugs. In cell-based metabolomics the investigations carried out so far have focused on studying changes in the intracellular metabolism in response to anti-cancer drugs. An untargeted metabolic profiling approach could give rise to a more complete mechanistic insight of cordycepin on MCF-7 cells. Therefore, cell-based metabolomics using LC-MS has been used to analyse metabolic changes in MCF-7 cell extracts.

Within the frame work of this study, the effect of cordycepin on MCF-7 metabolome was investigated by untargeted metabolic profiling analysis. The metabolic profiling of MCF-7 cells was affected in a distinct manner and provided complementary information regarding intracellular targets such as purine and

pyrimidine metabolism and bioenergetics. In addition, the level of topaquinone is increased in MCF-7 cells treated with cordycepin. Topaquinone is a natural compound involved in the degradation of DNA. This may indicate that cordycepin is involved in the inhibition of cell proliferation and differentiation, and the activation of cell apoptosis. A recent study analysed cordycepin-treated MCF-7 cells and found that mRNAs, down-regulated through the inhibition of polyadenylation, were predominantly involved in transcriptional regulation, cell proliferation, cell cycle and cell migration (300). Since polyadenylation is a process that is required for cell survival and occurs independently of DNA synthesis, targeting polyadenylation (301) may be an effective RNA-directed strategy for cordycepin application in breast cancer therapy.

Polyadenylation is a template-independent step catalysed by poly (A) polymerase (PAP), which uses ATP as its substrate (301). The data shows that the levels of cordycepin phosphate increased, but the level of ATP decreased. We can hypothesise that cordycepin phosphate compounds may be a substrate for PAP and affect polyadenylation efficiency. Cordycepin is metabolised intracellularly into its corresponding triphosphate derivatives; it may be incorporated efficiently into poly (A)-tails by PAP (302). Alternately, cordycepin phosphates may inhibit polyadenylation via two different mechanisms. First, cordycepin phosphate compounds may be directly incorporated into nascent RNAs during either transcription

or polyadenylation. This prevents further primer elongation causing subsequent chain termination (303). Second, cordycepin phosphate may act as an inhibitor for PAP and reduce the Poly (A)-tailed length of newly synthesised RNAs. This would reduce the stability of the transcript as well as negatively affecting the nuclear transport and translation efficiency (302). The investigations may indicate that cordycepin phosphate compounds - especially cordycepin triphosphates - may be key to the inhibition of polyadenylation in MCF-7 cells.

7.1.4 Cell-based metabolomics using LC-MS to study the metabolic effects of fluoxetine on glucose-treated murine pancreatic beta (MIN6) cells

Fluoxetine is used for the treatment of major depressive disorders including bulimia nervosa, obsessive-compulsive disorder, panic disorder, and premenstrual dysphoria (120). In the last decade, reports have indicated that the use of fluoxetine is associated with an increased risk of pancreatic beta cell dysfunction to reduced insulin secretion and hyperglycaemia (124). Despite extensive research, the biochemical mechanisms for deterioration of β-cell function are not fully understood.

In these studies, cell-based metabolomics using LC-MS, was employed to identify and quantify the level s of cellular metabolites present in glucose-exposed MIN6 cells following fluoxetine

exposure, and their relationship to biological pathways. Electron transport chain inhibitors were used in the studies to fully understand the dynamics of metabolite changes.

It was found that fluoxetine could impair glycolysis, TCA and fatty acid metabolism. The decline in MIN6 cell function plays a central role in insulin secretion and several intermediates are associated with MIN6 cell insulin secretion. It has been suggested that intermediate metabolites in bioenergetics could be significant signals for inducing MIN6 cell toxicity by fluoxetine (304).

Nevertheless, use of fluoxetine for depression treatment is important because it could improve the quality of life and increase treatment compliance, which may reduce long term complications and emergencies. Fluoxetine might also be used as a prophylactic treatment in patients. However, the effect on blood glucose control of fluoxetine and its interaction with other drugs or insulin needs to be investigated. As was observed in previous studies, fluoxetine can induce hyperglycaemia in patients and other animal species.

In this study, the results demonstrate that fluoxetine causes diverse changes in MIN6 cells, after glucose overload. The biggest changes in cellular metabolites in glucose-treated MIN6 cells occurred after the administration of fluoxetine, which caused an increase in glucose level in MIN6 cells. This in turn caused an inhibition of insulin secretion in beta cells. The changes in cellular metabolite

levels during the glucose test induced by ETC inhibitors was pronounced in both glucose-treated and untreated MIN6 cells and showed that ETC inhibitors have a different action profile in each treatment. Interestingly, a complex VI inhibitor in ETC was suggested as a toxicity effect of fluoxetine on MIN6 cells.

Although fluoxetine is very effective and frequently used, the drug is considered to have few adverse reactions such as the impairment of beta cell function. In this study, fluoxetine induced changes of metabolite levels that are involved with glycolysis, TCA and fatty acid metabolism. Further studies are needed to determine whether this effect will be still demonstrable after long-term treatment.

The use of stable-labelled internal standards can provide improved precision and accuracy in metabolite quantification. MIN6 cells could be grown in media containing [U-^{13}C]-glucose as the primary glucose source. Theoretically, extracts from these cells should contain similar metabolite concentrations to those grown in non-labelled media, except with the incorporation of a large percentage of ^{13}C in all endogenously synthesised metabolites, involved in the glycolysis pathway. These labelled metabolites can then be quantified using non-labelled standards to determine their absolute level. The extracts can then be added to experimental extracts and endogenous non-labelled metabolites quantified by isotope dilution. Alternatively, these ^{13}C labelled extracts could simply be used as

internal references to improve precision by correcting ionisation suppression and instrument drift. Metabolomic investigations into glucose-treated MIN6 cells with or without fluoxetine or other drugs could benefit from this approach by improving precision to discern smaller but significant changes in metabolite levels in experiments. This approach will be applied for an assessment of how fluoxetine affects on the glycolysis pathway in beta cells.

7.1.5 Overall summary

Analysis of viability and reliability of drug mode of action studies are essential for assessing drug effects and toxicity prospects in a clinical setting. In-vivo analysis is used to provide quantitative information on each step of the pharmacological effect, including critical in-vivo parameters for drug pre-clinical and clinical decision-making on therapeutic efficacy and index, and safety profiles. However, increasing numbers of reports reveal that in-vivo studies based on plasma, urine and other media do not correlate with drug pharmacological effects in target organs or cells, since some drugs do not reach concentrations sufficient to exert therapy in their intracellular targets (305).

Moreover, traditionally, in vitro study have relied on the use of single-endpoint measurements aimed to estimate cell viability and/or the functional metabolic state of cells previously exposed to drug candidates. These assays normally monitor events that occur

late in the cell injury process, and have unfortunately shown poor prediction of cytotoxicity (306). Therefore, the development of reliable screening methods to detect cytotoxicity early in the drug development process remains a challenge. With the advance of the 'omics' technologies, new methods have been developed to propose predictive signatures and to determine drug toxicity mechanisms. The simultaneous measurement of multiple parameters could contribute to the development of more accurate and predictive strategies (232). Multiparametric methods integrate information obtained simultaneously from different cell function indicators, which may indicate the mechanism of drug and/or toxic action of a candidate drug and help in prioritising compounds in drug discovery based on their potential cytotoxicity to humans (307). In this sense, genomic- and transcriptomic-based analyses and cell imaging approaches have been proposed for cytotoxicity screening in cultured cells. Although these methods provide the possibility of detecting subtle toxicity-related changes, they fail to provide translational biomarkers and report limited mechanism information from a global view. Cell-based metabolomics, which is aided by the unbiased measurement of all the downstream products of genes and proteins, could complete the informatics mechanism provided by other 'omics' and other technologies. The capability of cell-based metabolomics to assess the cell response to drugs and other compounds has been widely used; several reports have

demonstrated the use of cell-based metabolomics in biomarker discovery and in providing new insight into drug mode of action and/or toxicity. Cell-based metabolomics offers the closest data to the phenotype of the system under investigation, which, in the case of patients, could be used to obtain new toxicity- or efficiency-related biomarkers and would therefore be clinically beneficial (232).

In this work, the capabilities of cell-based metabolomics using LC-MS based untargeted metabolite profiling as a tool to detect the potential mechanism of drugs were assessed. This application is beneficial for at least a subset of toxicity and mechanisms of action, but there continues to be a debate about whether drugs and other compounds can directly affect cell metabolism or if they can actually reduce the risk of toxicity at all. The majority of existing data regarding the effects of drugs on mammalian cells has focused on HMVECs, MCF-7 and MIN6 cells. The literature is currently lacking data specific to the metabolomic effects of antipsychotics, cordycepin and fluoxetine on combined in-vitro, in-vivo, and ex-vivo data for BBB, breast cancer and pancreatic beta cells, respectively, and this was the inspiration to systematically determine these agents' specific effects on HMVEC, MCF-7 and MIN6 cells in these settings. First, experiments to evaluate in-vitro cellular and molecular mechanisms were designed to determine how HMVEC,

MCF-7 and MIN6 cells respond to antipsychotics, cordycepin and fluoxetine, respectively.

Metabolomics can be broadly divided into untargeted and targeted metabolomics. Untargeted metabolomics involves analysing various chemical classes with wide ranges of polarity, solubility, and volatility. It includes - and is not limited to -the analyses of amino acids, organic acids, sugars, sugar alcohols, lipids, fatty acids and those metabolites which undergo post-modifications such as phosphorylation or methylation (308). Moreover, it is often used to provide a real-time, global investigation of the biological state of a cell as a result of biotic and abiotic perturbations. More importantly, the major advantage of untargeted metabolomics is the ability to identify a drug-mediated response at the biochemical level with no prior knowledge of the mode of action of a particular drug candidate (309). This method can be used to classify compounds according to their mode of action based on a metabolic signature and, in many cases, can highlight the specific metabolic enzyme or pathway that the drug targets. The primary limitation of this approach is that some drugs do not act by disruption of metabolic pathways. In addition, drugs may induce non-specific metabolic changes in response oxidative stress, or as secondary responses to the initial drug action (309). Targeted metabolomics approaches are often required in these circumstances to provide a detailed characterisation of the temporal and dose-dependent biochemical

effects of drugs (309). Additional studies, such as transcriptomics, may also be required to delineate primary and secondary metabolic responses to drug treatment (310). Generally, measurements of RNA or protein levels are unlikely to reveal the primary targets of drugs that inhibit metabolic enzymes. Nevertheless, transcriptomic and proteomic approaches are likely to detect the secondary cellular responses to drug treatment, which may be relevant in determining potential toxicity mechanisms. A systems biology approach, that combines metabolomics with other functional genomics tools, is a promising tool to obtain comprehensive descriptions of the modes of action and toxicity for candidate drugs (309). Cell-based metabolomics may also be combined with chemical biology (e.g. protein or ligand microarrays (311)) and chemoinformatic methods (e.g. similarity ensemble approach (312)) to improve identification of unknown drug targets in an untargeted manner.

Furthermore, cell-based metabolomics methods offer effective tools for the identification and characterisation of mechanisms of drug action, which should optimise drug discovery by allowing detailed pre-clinical pharmacokinetic/pharmacodynamic descriptions of candidate drugs, and have the potential to translate into clinical studies to monitor patient responses to drug treatment (313).

7.2 FUTURE WORK

7.2.1 Expanding metabolite identification

More than 1,000 mass signals in mammalian cells were analysed in this study, but only about 200 named metabolites were identified. In order to truly understand the metabolome of mammalian cells, all metabolites need to be identified. One of the ways to increase the number of metabolites identified is through the use of tandem mass spectrometry, the identification of metabolites through fragmentation of parent ions. The number of chemical fragmentation patterns for mammalian metabolites is constantly increasing (314, 315). Now that a reliable extraction and analysis process is in place, it is possible to employ fragmentation patterns, and accurate mass and retention times in order to confidently identify metabolites. Using fragmentation patterns is a cost effective way of identifying metabolites, however, it does have the drawback of being incredibly time-consuming, and it will only work with one method. A single method will consist of using a specific column, with two specific mobile phases that will run through the column in various amounts as dictated by a pre-determined gradient. If the fragments of a metabolite are identified with a specific mass eluting at a specific time using any one method, changing the method will require the MS/MS fragmentation to be repeated to ensure the same metabolites are being identified. This study used authentic standards for metabolic identification. Future studies will use MS/MS

fragmentation of metabolites for metabolomics analysis to create an in-house database of fragmentation patterns for comparison with fragmentation data which is already available. This will maximise the number of metabolites that can be identified during analysis.

7.2.2 Expanding coverage of the metabolites

In the future, expanded coverage of the metabolome will be possible using columns that can resolve very small polar metabolites, or differentiate between molecule isomers. Non-polar compounds and lipids can be resolved on a C8 and C18 based column and polar metabolites can be resolved on a HILIC based column. Furthermore, isomers can be separated in porous graphitised carbon columns (314). There is currently an abundance of literature on the detection and resolution of non-polar and polar metabolites. In addition, it is known that D-form, L-form, R-form and S-form of some metabolites make up the majority of what is present in the metabolome so it is unclear how much information can actually be gained from resolving isomers (315). For these reasons mentioned, it would be easier and more informative to develop a ZIC-HILIC based column method first. In order to develop a method with the use of a HILIC based column, the variety of authentic standards that are found ubiquitously in mammalian cells will need to be purchased. The ability to run and confidently identify cellular metabolites will allow the development of a method that effectively separates most cellular metabolites.

7.2.3 Improving metabolomics methods to obtain more quantitative data using multiple internal standards

The success of cell based metabolomics as a method for studying the effect of drugs on mammalian cells largely depends on its ability to detect various sources of biological variability. Removal of platform-specific sources of variability such as systemic error is therefore one of the foremost priorities in data processing. However, the chemical diversity of metabolite results in different responses to variations in experimental conditions and so this makes normalisation a very demanding task.

Targeted analysis uses an isotope labelled internal standard for each metabolite measured for absolute quantification. However, in untargeted metabolic profiling methods this is not practical. The number of metabolites is large, they are chemically too diverse to afford a common labelling molecule, and many of them may not even be known. In addition, the availability of stable isotope labelled references is generally very limited. In this study, statistical models were used to derive optimal scaling factors for each sample, based on complete sets of data using intensity. However, this method lacks multiple normalisation factors for a variety of chemical species. In addition, constraining the data to a specific normalisation factor based on total signal affects its covariance structure, therefore requiring special caution when performing multivariate analysis of data (50).

In future studies, the choice of multiple internal standard molecules will be a more reasonable approach. This normalisation approach will reduce variability across the full spectrum of metabolites. Furthermore, it can be used directly as either a one-step or two-step normalisation method where the normalisation parameters containing data about the variability of internal standard compounds and their association to variability of metabolites are first calculated from a study performed under reproducible conditions. Finally, the method can be used to select standard compounds for normalisation and to evaluate their influence on variability of all detected metabolites.

7.2.4 Integration of metabolomics data with metabolic pathway maps

Future work will integrate metabolomics data into metabolic maps. Metabolite levels together with their corresponding metabolic fluxes are integrative outcomes of biochemical transformations and regulatory processes and they can be used to characterise the response of drugs on mammalian cells. Change in fluxes and particularly changes in metabolite levels do not follow such rationale and are often the outcome of complex interactions of several components. The increasing quality and coverage of metabolomics into metabolic pathway maps has fostered the understanding of drug effects on cellular processes.

7.2.5 Metabolomics for off-target effects of drugs in cells potential adverse effects in toxicology studies

Cell-based metabolomics has been used to evaluate the effects of drugs on mammalian cells in order to help develop new agents and to maximise the benefits of drugs currently on the market. LC-MS is a key method in cell-based metabolomics and the technology continues to improve, allowing LC-MS to remain involved in future drug research and development. The new drugs represent new types of therapeutic agents that are designed to provide increased specificity, higher efficiency, and fewer side effects. Cell-based metabolomics can identify new biological targets, find new use for drugs already on the market, and can be applied further in drug development studies to provide insight into the biological mechanisms of the drug action and its off-target effects which are related to cell toxicity.

APPENDIX

Supplementary Table 2.1 List of the first group of metabolite mixture.

Metabolites	Formula	M.W.
Imidazole	$C_3H_4N_2$	68.0374
methylglyoxal	$C_3H_4O_2$	72.0211
Glyoxylate	$C_2H_2O_3$	74.0004
1-Butanol	$C_4H_{10}O$	74.0732
Glycine	$C_2H_5NO_2$	75.0320
glycolate	$C_2H_4O_3$	76.0160
Pyruvate	$C_3H_4O_3$	88.0160
Putrescine	$C_4H_{12}N_2$	88.1000
L-Alanine	$C_3H_7NO_2$	89.0477
glyceraldehyde	$C_3H_6O_3$	90.0317
Glycerol	$C_3H_8O_3$	92.0473
2-oxobutanoate	$C_4H_6O_3$	102.0317
Malonate	$C_3H_4O_4$	104.0110
(R)-3-Hydroxybutanoate	$C_4H_8O_3$	104.0473
L-Serine	$C_3H_7NO_3$	105.0426
Phenylhydrazine	$C_6H_8N_2$	108.0687
Creatinine	$C_4H_7N_3O$	113.0589
L-Proline	$C_5H_9NO_2$	115.0633
Fumarate	$C_4H_4O_4$	116.0110
L-Valine	$C_5H_{11}NO_2$	117.0790
Methylmalonate	$C_4H_6O_4$	118.0266
L-2,4-Diaminobutanoate	$C_4H_{10}N_2O_2$	118.0742
L-Threonine	$C_4H_9NO_3$	119.0582
D-Erythrose	$C_4H_8O_4$	120.0423
Nicotinate	$C_6H_5NO_2$	123.0320
pyrazinoate	$C_5H_4N_2O_2$	124.0273
Taurine	$C_2H_7NO_3S$	125.0147
Imidazole-4-acetate	$C_5H_6N_2O_2$	126.0429
trans-4-Hydroxy-L-proline	$C_5H_9NO_3$	131.0582
L-Leucine	$C_6H_{13}NO_2$	131.0946
Oxaloacetate	$C_4H_4O_5$	132.0059
L-Asparagine	$C_4H_8N_2O_3$	132.0535
L-Aspartate	$C_4H_7NO_4$	133.0375

Supplementary Table 2.1 (Cont.) List of the first group of metabolite mixture.

Metabolites	Formula	M.W.
Adenine	$C_5H_5N_5$	135.0545
4-Aminobenzoate	$C_7H_7NO_2$	137.0477
Ethanolamine phosphate	$C_2H_8NO_4P$	141.0191
Spermidine	$C_7H_{19}N_3$	145.1579
L-Glutamine	$C_5H_{10}N_2O_3$	146.0691
L-Lysine	$C_6H_{14}N_2O_2$	146.1055
L-Glutamate	$C_5H_9NO_4$	147.0532
(R)-2-Hydroxyglutarate	$C_5H_8O_5$	148.0372
L-Methionine	$C_5H_{11}NO_2S$	149.0510
Guanine	$C_5H_5N_5O$	151.0494
2-Phenylglycine	$C_8H_9NO_2$	151.0633
Xanthine	$C_5H_4N_4O_2$	152.0334
3-Hydroxyphenylacetate	$C_8H_8O_3$	152.0473
L-Histidine	$C_6H_9N_3O_2$	155.0695
Orotate	$C_5H_4N_2O_4$	156.0171
4-Coumarate	$C_9H_8O_3$	164.0473
L-Rhamnose	$C_6H_{12}O_5$	164.0685
L-Phenylalanine	$C_9H_{11}NO_2$	165.0790
Phthalate	$C_8H_6O_4$	166.0266
Phosphoenolpyruvate	$C_3H_5O_6P$	167.9824
3_4-Dihydroxyphenylacetate	$C_8H_8O_4$	168.0423
L-Cysteate	$C_3H_7NO_5S$	169.0045
Pyridoxine	$C_8H_{11}NO_3$	169.0739
Gallate	$C_7H_6O_5$	170.0215
cis-Aconitate	$C_6H_6O_6$	174.0164
L-Arginine	$C_6H_{14}N_4O_2$	174.1117
L-Citrulline	$C_6H_{13}N_3O_3$	175.0957
Serotonin	$C_{10}H_{12}N_2O$	176.0950
D-Glucosamine	$C_6H_{13}NO_5$	179.0794
D-glucose	$C_6H_{12}O_6$	180.1559
1-Naphthylacetic acid	$C_{12}H_{10}O_2$	186.0681
N2-Acetyl-L-lysine	$C_8H_{16}N_2O_3$	188.1161
meso-2_6-Diaminoheptanedioate	$C_7H_{14}N_2O_4$	190.0954

Supplementary Table 2.1 (Cont.) List of the first group of metabolite mixture.

Metabolites	Formula	M.W.
D-Galacturonate	$C_6H_{10}O_7$	194.0427
D-Gluconic acid	$C_6H_{12}O_7$	196.0583
Selenomethionine	$C_5H_{11}NO_2Se$	196.9955
L-Tryptophan	$C_{11}H_{12}N_2O_2$	204.0899
2-Methylcitrate	$C_7H_{10}O_7$	206.0427
MOPS	$C_7H_{15}NO_4S$	209.0722
D-Galactarate	$C_6H_{10}O_8$	210.0376
N-Acetyl-D-glucosamine	$C_8H_{15}NO_6$	221.0899
Deoxyuridine	$C_9H_{12}N_2O_5$	228.0746
D-ribose 5-phosphate	$C_5H_{11}O_8P$	230.0192
Melatonin	$C_{13}H_{16}N_2O_2$	232.1212
L-Cystine	$C_6H_{12}N_2O_4S_2$	240.0238
Thymidine	$C_{10}H_{14}N_2O_5$	242.0903
Cytidine	$C_9H_{13}N_3O_5$	243.0855
Thymidine	$C_{10}H_{14}N_2O_5$	242.0903
Cytidine	$C_9H_{13}N_3O_5$	243.0855
Uridine	$C_9H_{12}N_2O_6$	244.0695
Pyridoxal phosphate	$C_8H_{10}NO_6P$	247.0246
sn-glycero-3-Phosphocholine	$C_8H_{20}NO_6P$	257.1028
D-glucose 6-phosphate	$C_6H_{13}O_9P$	260.0297
Thiamin	$C_{12}H_{16}N_4OS$	265.1123
2_3-Bisphospho-D-glycerate	$C_3H_8O_{10}P_2$	265.9593
Inosine	$C_{10}H_{12}N_4O_5$	268.0808
6-Phospho-D-gluconate	$C_6H_{13}O_{10}P$	276.0246
CMP	$C_9H_{14}N_3O_8P$	323.0519
UMP	$C_9H_{13}N_2O_9P$	324.0359
3'_5'-Cyclic AMP	$C_{10}H_{12}N_5O_6P$	329.0525
D-Fructose 1_6-bisphosphate	$C_6H_{14}O_{12}P_2$	339.9960
Maltose	$C_{12}H_{22}O_{11}$	342.1162
dGMP	$C_{10}H_{14}N_5O_7P$	347.0631
IMP	$C_{10}H_{13}N_4O_8P$	348.0471
Phenolsulfonphthalein	$C_{19}H_{14}O_5S$	354.0562
riboflavin	$C_{17}H_{20}N_4O_6$	376.1383
Cholesterol	$C_{27}H_{46}O$	386.3549

Supplementary Table 2.1 (Cont.) List of the first group of metabolite mixture.

Metabolites	Formula	M.W.
S-Adenosyl-L-methionine	$C_{15}H_{22}N_6O_5S$	399.1451
Thiamin diphosphate	$C_{12}H_{18}N_4O_7P_2S$	425.0450
ADP	$C_{10}H_{15}N_5O_{10}P_2$	427.0294
IDP	$C_{10}H_{14}N_4O_{11}P_2$	428.0134
Deoxyribose	C5H10O4	134.0579

Supplementary Table 2.2 List of the second group of metabolite mixture.

Metabolites	Formula	M.W.
Methylguanidine	$C_2H_7N_3$	73.0640
L-Alanine	$C_3H_7NO_2$	89.0477
(R)-Lactate	$C_3H_6O_3$	90.0317
4-Aminobutanoate	$C_4H_9NO_2$	103.0633
cytosine	$C_4H_5N_3O$	111.0433
Uracil	$C_4H_4N_2O_2$	112.0273
Betaine	$C_5H_{11}NO_2$	117.0790
Succinate	$C_4H_6O_4$	118.0266
Nicotinamide found in Std	$C_6H_6N_2O$	122.0480
L-isoleucine found in Std	$C_6H_{13}NO_2$	131.0946
Glycylglycine	$C_4H_8N_2O_3$	132.0535
L-Ornithine	$C_5H_{12}N_2O_2$	132.0899
(S)-Malate	$C_4H_6O_5$	134.0215
Hypoxanthine	$C_5H_4N_4O$	136.0385
2-Oxoglutarate	$C_5H_6O_5$	146.0215
D-Ribose	$C_5H_{10}O_5$	150.0528
L-Carnitine found in Std	$C_7H_{15}NO_3$	161.1052
DL-Glyceraldehyde 3-phosphate	$C_3H_7O_6P$	169.9980
L-Tyrosine	$C_9H_{11}NO_3$	181.0739
3-Phospho-D-glycerate	$C_3H_7O_7P$	185.9929
Citrate	$C_6H_8O_7$	192.0270
Deoxyadenosine	$C_{10}H_{13}N_5O_3$	251.1018
sucrose	$C_{12}H_{22}O_{11}$	342.1162
AMP	$C_{10}H_{14}N_5O_7P$	347.0631
HEPES	$C_8H_{18}N_2O_4S$	348.1573
GMP	$C_{10}H_{14}N_5O_8P$	363.0580
S-Adenosyl-L-homocysteine	$C_{14}H_{20}N_6O_5S$	384.1216
Folate	$C_{19}H_{19}N_7O_6$	441.1397
GDP	$C_{10}H_{15}N_5O_{11}P_2$	443.0243
ATP	$C_{10}H_{16}N_5O_{13}P_3$	506.9957
GTP	$C_{10}H_{16}N_5O_{14}P_3$	522.9907
NAD+	$C_{21}H_{27}N_7O_{14}P_2$	664.1169

Supplementary Table 2.3 List of the third group of metabolite mixture.

Metabolites	Formula	M.W.
Urea	CH_4N_2O	60.0324
2-Hydroxy isobutyric acid	$C_4H_8O_3$	104.0473
L-cysteine	$C_3H_7NO_2S$	121.0197
Benzoate	$C_7H_6O_2$	122.0368
Creatine found in Std	$C_4H_9N_3O_2$	131.0695
L-Homocysteine	$C_4H_9NO_2S$	135.0354
Acetylcholine	$C7H_{16}NO_2$	146.1181
D-Arabinose	$C_5H_{10}O_5$	150.0528
4-Hydroxyphenyl acetate	$C_8H_8O_3$	152.0473
Uric acid	$C_5H_4N_4O_3$	168.0283
3-Methylhistidine	$C_7H_{11}N_3O_2$	169.0851
ascorbate	$C_6H_8O_6$	176.0321
Hippuric acid	$C_9H_9NO_3$	179.0582
D-Fructose	$C_6H_{12}O_6$	180.0634
Myoinositol	$C_6H_{12}O_6$	180.0634
D-Mannitol	$C_6H_{14}O_6$	182.0790
Isocitric acid	$C_6H_8O_7$	192.0270
2-Hydroxyhippuric acid	$C_9H_9NO_4$	195.0532
L-Cystine	$C_6H_{12}N_2O_4S_2$	240.0238
D-Fructose 6-phosphate	$C_6H_{13}O_9P$	260.0297
Homocystine	$C_8H_{16}N_2O_4S_2$	268.0551
Stearic acid	$C_{18}H_{36}O_2$	284.2715
glutathione	$C_{10}H_{17}N_3O_6S$	307.0838
D-Fructose-1,6-diphosphate	$C_6H_{14}O_{12}P_2$	339.9960
Trehalose	$C_{12}H_{22}O_{11}$	342.1162
CDP	$C_9H_{15}N_3O_{11}P_2$	403.0182
UDP	$C_9H_{14}N_2O_{12}P_2$	404.0022

Supplementary Table 3.1 Formula, monoisotopic molecular weight, type of adduct, detected mass, retention time and relative standard error of metabolites.

Metabolites	[M+H]-	[M+H]+	m/z	RT	%RSD (n=6)
1-Naphthylacetic acid	/		185.0608	2.51	0.38
Benzoate	/		121.0295	2.59	0.32
Gallate	/		169.0143	2.61	0.57
Melatonin	/		231.1139	2.71	0.52
2-Hydroxyhippuric acid	/		194.0459	2.88	0.33
Hippuric acid	/		178.0510	2.92	0.43
2-Hydroxy isobutyric acid	/		103.0401	2.95	0.17
D-Arabinose	/		149.0455	2.96	0.85
4-Hydroxyphenyl acetate	/		151.0401	2.97	1.01
3-Hydroxyphenylacetate	/		151.0401	2.98	0.17
Phosphoenolpyruvate		/	168.9897	3.06	0.82
(R)-3-Hydroxybutanoate	/		103.0401	3.12	0.16
(R)-Lactate	/		89.0244	3.15	0.18
glyceraldehyde	/		89.0244	3.20	0.16
Succinate	/		117.0193	3.20	0.74
Methylmalonate	/		117.0193	3.25	0.31
Nicotinamide		/	123.0553	3.25	0.53
Phthalate	/		165.0193	3.25	0.15
3_4-Dihydroxyphenylacetate	/		167.0350	3.27	0.40
2-oxobutanoate	/		101.0244	3.67	0.41
Fumarate	/		115.0037	3.90	0.57

RT = Retention time in minute.

Supplementary Table 3.1 (Cont.) Formula, monoisotopic molecular weight, type of adduct, detected mass, and retention time and its relative standard error of metabolites.

Metabolites	[M+H]-	[M+H]+	m/z	RT	%RSD (n =6)
glycolate	/		75.0088	4.33	0.61
6-Phospho-D-gluconate	/		275.0174	4.51	0.84
Pyruvate	/		87.0088	4.56	0.45
Deoxyuridine	/		227.0673	5.12	0.19
(R)-2-Hydroxyglutarate	/		147.0299	5.39	0.28
Malonate	/		103.0037	5.53	0.18
Deoxyadenosine		/	252.1091	6.19	0.28
Xanthine	/		151.0261	6.22	0.24
(S)-Malate	/		133.0142	6.23	0.23
Hypoxanthine	/		135.0312	6.28	0.23
Uridine	/		243.0623	6.31	0.20
L-Rhamnose	/		163.0612	6.59	0.20
Phenolsulfonphthalein	/		353.0489	6.72	0.53
D-Ribose	/		149.0455	6.94	0.22
Inosine	/		267.0735	7.03	0.21
Isocitric acid	/		191.0197	7.10	0.16
Glyoxylate	/		72.9931	7.13	0.40
Adenine	/		134.0472	7.15	0.29
2-Phenylglycine	/	/	150.0561	7.15	0.31
Pyridoxine	/		168.0666	7.15	0.34
2-Oxoglutarate	/		145.0142	7.20	0.29

RT = Retention time in minute.

Supplementary Table 3.1 (Cont.) Formula, monoisotopic molecular weight, type of adduct, detected mass, and retention time and its relative standard error of metabolites.

Metabolites	[M+H]-	[M+H]+	m/z	RT	%RSD (n =6)
L-Leucine	/	/	130.0874	7.27	0.24
Folate	/		440.1324	7.28	0.21
L-isoleucine	/	/	130.0874	7.33	0.24
ascorbate	/		175.0248	7.33	0.14
L-Tryptophan	/	/	203.0826	7.51	0.37
D-Erythrose	/		119.0350	7.56	0.19
N-Acetyl-D-glucosamine	/		220.0827	7.56	0.19
Methylguanidine		/	74.0713	7.64	0.22
Selenomethionine	/		195.9882	7.74	0.27
Uric acid	/		167.0211	7.78	0.13
Guanine	/		150.0421	7.79	0.34
L-Carnitine		/	162.1125	7.86	0.42
L-Methionine	/	/	148.0438	7.89	0.16
Myoinositol	/		179.0561	7.98	0.10
Creatinine	/		112.0516	8.00	0.60
cis-Aconitate	/		173.0092	8.02	0.65
D-Fructose	/		179.0561	8.11	0.06
L-Valine	/	/	116.0717	8.12	0.30
Imidazole-4-acetate	/		125.0357	8.20	0.50
L-Tyrosine	/	/	180.0666	8.25	0.51
L-Homocysteine	/	/	134.0281	8.32	0.06

RT = Retention time in minute.

Supplementary Table 3.1 (Cont.) Formula, monoisotopic molecular weight, type of adduct, detected mass, and retention time and its relative standard error of metabolites.

Metabolites	[M+H]-	[M+H]+	m/z	RT	%RSD (n = 6)
cytosine		/	112.0505	8.66	0.15
Orotate	/		155.0098	8.74	0.28
Betaine		/	118.0863	8.91	0.06
L-cysteine	/	/	120.0125	8.98	0.00
N2-Acetyl-L-lysine	/		187.1088	8.99	0.31
D-Gluconic acid	/		195.0510	9.02	0.21
glutathione	/		306.0765	9.11	0.09
sucrose	/		341.1089	9.12	0.18
Cytidine	/		242.0782	9.14	0.06
3'_5'-Cyclic AMP	/		328.0452	9.20	0.27
4-Aminobutanoate	/		102.0561	9.21	2.25
trans-4-Hydroxy-L-proline	/		130.0510	9.35	0.15
L-Glutamate	/		146.0459	9.43	0.22
L-Threonine	/	/	118.0510	9.44	0.16
Taurine	/	/	124.0074	9.45	0.00
Maltose	/		341.1089	9.48	0.06
Trehalose	/		341.1089	9.53	0.10
S-Adenosyl-L-homocysteine	/		383.1143	9.56	0.39
D-Galacturonate	/		193.0354	9.66	0.29
L-Aspartate	/	/	132.0302	9.85	0.21
L-Alanine	/	/	88.0404	9.86	0.18

RT = Retention time in minute.

Supplementary Table 3.1 (Cont.) Formula, monoisotopic molecular weight, type of adduct, detected mass, and retention time and its relative standard error of metabolites.

Metabolites	[M+H]-	[M+H]+	m/z	RT	%RSD (n =6)
L-Asparagine	/	/	131.0462	9.88	0.15
Deoxyribose	/		133.0506	9.89	0.00
L-Serine	/	/	104.0353	9.90	0.10
Glycine	/		74.0248	9.91	0.35
L-Citrulline	/		174.0884	9.97	0.13
Serotonin		/	177.1022	9.97	0.29
D-Galactarate	/		209.0303	10.07	0.82
Glycylglycine		/	133.0608	10.08	0.30
UDP	/		402.9949	10.39	0.21
Homocystine	/		267.0479	10.41	0.09
Ethanolamine phosphate	/		140.0118	10.58	0.14
sn-glycero-3-Phosphocholine		/	258.1101	10.61	0.12
D-Glucosamine	/		178.0721	10.62	0.54
AMP	/		346.0558	10.73	0.08
GDP		/	444.0316	10.75	0.42
L-Cystine	/	/	239.0166	10.89	0.26
CMP	/		322.0446	10.91	0.12
3-Methylhistidine	/		168.0779	11.23	0.09
L-Histidine	/	/	154.0622	11.23	0.44
L-Ornithine	/	/	131.0826	11.24	1.91
meso-2_6-Diaminoheptanedioate	/		189.0881	11.32	0.20

RT = Retention time in minute.

Supplementary Table 3.1 (Cont.) Formula, monoisotopic molecular weight, type of adduct, detected mass, and retention time and its relative standard error of metabolites.

Metabolites	[M+H]-	[M+H]+	m/z	RT	%RSD (n = 6)
UMP	/		323.0286	11.50	0.50
L-Lysine	/	/	145.0983	11.51	0.34
L-2_4-Diaminobutanoate	/		117.0670	11.56	0.34
L-Cysteate	/		167.9972	11.72	0.29
dGMP	/		346.0558	11.74	0.36
IMP	/		347.0398	11.84	0.53
D-ribose 5-phosphate	/		229.0119	12.14	0.44
GMP	/		362.0507	12.43	0.11
D-Fructose 6-phosphate	/		259.0224	12.47	0.15
DL-Glyceraldehyde 3-phosphate	/		168.9907	12.51	0.40
D-glucose 6-phosphate	/		259.0224	12.80	0.37
CDP	/		402.0109	16.06	0.82

RT = Retention time in minute.

Supplementary Table 5.1 List of identified metabolites in MCF-7 cell extracts

m/z	RT (min)	Mean abundance												Metabolites	Formula	Error (ppm)
		DMSO			Pentostatin			Cordycepin			Cordycepin + Pentostatin					
		2 h	8 h	24 h	2 h	8 h	24 h	2 h	8 h	24 h	2 h	8 h	24 h			
166.0975	2.12	3940	4226	4119	4165	4083	4151	4081	4279	4252	4056	3710	3900	Methylimidazole acetaldehyde	C6H8N2O	0
629.5518	2.37	901	731	496	1265	209	306	993	277	1811	162	64	362	DG	C41H74O5	1
369.3518	2.40	11469	10616	10326	14913	7668	8527	15444	8123	26623	6827	8481	21287	3-Deoxyvitamin D3	C27H44	0
538.5204	2.43	24865	20977	13392	33026	8729	14158	31641	14449	62537	6600	8329	51492	N-Palmitoylsphingosine	C34H67NO3	2
385.2226	2.43	1433	7	10	1783	65	16	1638	0	0	1885	16	50	20-Trihydroxy-leukotriene-B4	C20H32O7	1
338.3422	2.43	56646	32803	24366	119614	22782	24811	103930	35439	63502	37400	26471	68832	Eicosanoyl-EA	C22H45NO2	0
353.2693	2.43	1052	463	514	1374	395	360	1613	362	462	1162	457	379	MG	C21H36O4	2
267.1724	2.43	1089	4657	1122	1721	3988	1660	1395	3464	2090	1205	1720	1336	Myristic acid	C14H28O2	1
427.2700	2.45	930	0	0	1100	23	1	815	0	0	928	1	28	Prostaglandin PGE2 glyceryl ester/Prostaglandin PGE2 1-glyceryl ester	C23H38O7	2
329.1965	2.48	1524	438	260	1725	536	293	1888	265	337	1896	466	224	Kynuramine	C9H12N2O	2
342.3011	2.50	1326	794	738	1563	777	655	1794	647	1855	1042	677	1885	Stearoylglycine	C20H39NO3	2
265.2168	2.50	1753	274	467	2322	198	261	2338	356	516	2210	461	740	TG	C51H84O6	2
298.2383	2.52	6008	7039	6681	4810	5937	7093	5299	6659	7417	4993	6987	6202	Decanoyl-L-carnitine	C17H33NO4	0
342.2647	2.52	4254	6126	5314	4221	5398	6564	4654	5657	7158	3706	5754	6670	trans-2-Dodecenoylcarnitine	C19H35NO4	2
312.2173	2.55	4240	5481	5715	3441	4749	6405	4144	5193	5719	4047	5231	4765	2-trans,4-cis-Decadienoylcarnitine	C17H29NO4	1
272.2226	2.55	1192	1197	1152	948	1034	1346	1133	981	1159	1056	1022	1053	Tridecanoylglycine	C15H29NO3	2
244.2275	2.57	3530	2851	3065	3306	2487	3015	3306	2375	3037	2765	2971	2789	(4E,d14:1) sphingosine	C14H29NO2	2
207.1745	2.57	2407	1535	1929	2299	1659	1889	2191	1778	1579	2229	1728	1556	4a-Formyl-5a-cholesta-8,24-dien-3b-ol	C28H44O2	1
203.1393	2.57	1735	1439	1737	1457	1229	1626	1239	1478	1060	1627	1181	1359	Alanyl-Isoleucine/Alanyl-Leucine/Isoleucyl-Alanine/Leucyl-Alanine	C9H18N2O3	1
300.2541	2.57	4763	4477	4331	4811	4088	4635	4654	3988	4434	4397	4487	4253	Pentadecanoylglycine	C17H33NO3	2
227.1279	2.60	5008	1106	1126	5569	1029	1251	5329	1262	894	6208	979	980	3,4-Methylenesebacic acid	C12H18O4	1
286.2382	2.60	18197	17491	20335	16001	15889	20175	16505	16824	17219	16241	18218	17145	Myristoylglycine	C16H31NO3	2
244.1912	2.60	15748	16476	16506	12710	11984	19053	18753	13159	19372	13671	11082	19464	N-Undecanoylglycine	C13H25NO3	2
216.1960	2.62	3726	2769	3111	3022	2523	2989	3764	2487	3424	3000	2408	3142	12-amino-dodecanoic acid	C12H25NO2	1
226.1439	2.62	4975	5475	5841	3599	4836	6688	3953	6040	5694	4814	5612	5658	2-Ethylacrylylcarnitine	C12H21NO4	2
230.1754	2.62	20014	18804	20024	17458	16173	23153	21292	17711	18473	18547	15766	18574	N-Decanoylglycine	C12H23NO3	1
268.1913	2.62	1288	1490	1407	948	1272	1759	1181	1391	1289	1137	1151	1075	PS	C43H80NO10P	0
216.1596	2.65	29321	31260	28908	23050	25504	32399	23942	27843	31138	24546	26290	28643	N-Nonanoylglycine	C11H21NO3	1

Supplementary Table 5.1 (Cont.) List of identified metabolites in MCF-7 cell extracts

m/z	RT (min)	Mean abundance												Metabolites	Formula	Error (ppm)
		DMSO			Pentostatin			Cordycepin			Cordycepin + Pentostatin					
		2 h	8 h	24 h	2 h	8 h	24 h	2 h	8 h	24 h	2 h	8 h	24 h			
302.2332	2.70	7911	5699	6760	6645	5248	6975	6621	6076	6000	6787	5897	5474	2,6 Dimethylheptanoyl carnitine/Nonanoylcarnitine	C16H31NO4	2
202.1437	2.72	27860	27124	25507	22697	24362	32338	23000	27544	25813	25368	24246	25671	Capryloylglycine	C10H19NO3	0
339.2653	2.72	4152	978	4296	2504	862	754	3193	1324	4706	1080	3122	2418	PE-Cer	C36H73N2O7P	1
201.1599	2.72	8926	1901	490	6653	6000	448	12816	7440	4097	6319	2159	566	Spermine dialdehyde	C10H20N2O2	1
258.1705	2.75	2517	2786	2729	2241	2420	3641	2418	2871	2705	2461	2233	2562	2-Hexenoylcarnitine	C13H23NO4	2
174.1489	2.75	3862	5721	6206	3580	4545	5825	3373	4747	5099	2959	5016	5573	9-Aminononanoic acid/3R-aminononanoic acid	C9H19NO2	0
355.2598	2.75	3251	2447	2562	2876	1823	3012	3259	2539	3373	3377	2581	2515	9-Decenoylcarnitine	C17H31NO4	2
230.1390	2.75	14173	12879	12895	11543	12108	15639	12007	13587	12493	12205	12151	11573	Butyrylcarnitine/Isobutyryl-L-carnitine	C11H19NO4	1
215.1394	2.75	908	863	869	644	726	1012	665	933	783	863	751	739	N-Acetyl(iso)leucine/Isovalerylsarcosine/Hexanoylglycine	C8H15NO3	2
188.1281	2.75	175533	152542	156442	134863	132840	181531	142271	153586	165876	141872	146231	147453	N-Heptanoylglycine	C9H17NO3	0
244.1547	2.75	8938	8068	7896	6667	6983	10023	6581	8816	7547	7603	6841	7028	Tiglylcarnitine	C12H21NO4	2
346.2594	2.80	24866	13774	17900	20037	13275	17436	20766	16478	16040	21505	16763	15747	3-hydroxyundecanoyl carnitine	C18H35NO5	2
810.6836	2.80	8240	5979	3411	8980	3250	3500	7897	4955	7918	3687	3419	4823	Glucosylceramide (d18:1/24:1(15Z))/Galactosylceramide (d18:1/24:1(15Z))	C48H91NO8	2
216.1233	2.80	4269	4218	4142	3147	3937	5049	3664	4532	4290	3573	4093	3827	Propenoylcarnitine	C10H17NO4	1
302.1609	2.81	474	609	1131	329	554	605	457	616	739	447	501	1023	Pimelylcarnitine	C14H25NO6	0
160.1332	2.82	14420	10236	12286	11134	8883	12170	11879	10012	11094	11098	9994	11341	DL-2-Aminooctanoic acid	C8H17NO2	0
174.1125	2.82	54601	48090	49349	41656	44921	59044	44529	51454	48042	42898	46540	46399	Isovalerylalanine/Hexanoylglycine	C8H15NO3	0
131.0348	2.84	735	820	1239	709	257	330	657	559	505	792	708	1283	2-Acetolactate	C5H8O4	2
418.2810	2.89	1626	667	1170	979	605	438	1609	655	795	1280	907	1006	3-hydroxytridecanoyl carnitine	C20H39NO5	0
748.5309	2.90	26386	17147	18803	32665	10870	14930	32371	13575	44023	15156	12334	30731	CL	C84H152O17P2	2
429.2426	2.90	9458	5846	5866	7331	4966	1726	12656	6309	3361	28837	10168	5335	Glycyl-Lysine/Lysyl-Glycine	C8H17N3O3	1
248.1496	2.90	1137	774	654	946	775	952	1005	754	636	862	535	613	Hydroxybutyrylcarnitine	C11H21NO5	1
220.1181	2.90	51159	73283	103652	55767	69232	88690	62043	67829	70248	51818	40961	56789	Pantothenic acid	C9H17NO5	1
161.0453	2.91	2426	1650	2605	2955	3482	9888	2774	2685	2103	2502	1362	1645	2-Hydroxyadipic acid	C6H10O5	1
89.0243	2.91	111921	113270	172915	66403	55326	91965	131113	106745	148336	108672	121677	164841	Lactic acid	C3H6O3	0
147.0661	2.91	312	328	516	343	474	1132	356	460	646	350	307	413	Mevalonic acid/(R) 2,3-Dihydroxy-3-methylvalerate	C6H12O4	1
117.0192	2.91	6026	9689	19541	6616	32353	89971	6467	25015	39469	6062	8762	13921	Succinic acid	C4H6O4	0
690.5076	2.92	5080	3500	3001	5635	1854	2522	6284	2541	6154	3612	2240	3229	PE/PC	C37H72NO8P	1
461.3377	2.92	1108	4	291	867	0	10	894	4	377	52	89	179	Stearidonyl carnitine	C25H41NO4	1
764.5241	2.93	10024	9304	9766	9056	8149	5791	11968	8021	11030	11108	9073	7475	PE/PC	C43H76NO8P	1

Supplementary Table 5.1 (Cont.) List of identified metabolites in MCF-7 cell extracts

m/z	RT (min)	Mean abundance												Metabolites	Formula	Error (ppm)
		DMSO			Pentostatin			Cordycepin			Cordycepin + Pentostatin					
		2 h	8 h	24 h	2 h	8 h	24 h	2 h	8 h	24 h	2 h	8 h	24 h			
129.0556	2.96	10749	16701	41284	4656	7467	16908	16784	14984	27155	14644	14980	30817	4-Acetylbutyrate/2-Methyl-3-ketovaleric acid	C6H10O3	1
714.5082	2.96	2973	2840	2796	2614	2046	1183	3360	2057	2463	3599	2511	2486	PE	C39H74NO8P	0
766.5399	2.96	13943	15381	12305	11425	10084	6904	15033	11970	13910	14369	12796	11895	PE/PC	C43H78NO8P	1
738.5429	2.99	2697	1734	1942	3414	1160	1356	3487	1284	4818	1494	1562	4111	PC	C42H76NO7P	0
190.0896	2.99	550	516	232	902	597	221	1571	293	179	888	611	21	S-Prenyl-L-cysteine	C8H15NO2S	0
115.0036	3.06	2016	5345	6666	807	824	1146	1697	3742	3087	946	5823	10397	Fumaric acid	C4H4O4	1
298.0975	3.07	6251	6090	9908	6189	5727	8188	4998	2072	2832	1858	395	2288	5'-Methylthioadenosine	C11H15N5O3S	2
344.2803	3.14	482	506	941	676	508	680	302	628	1044	170	337	447	Dodecanoylcarnitine	C19H37NO4	2
350.3060	3.17	1026	228	282	897	114	67	1540	110	310	298	54	247	Dihomo-gamma-Linolenoyl ethanolamide	C22H39NO2	2
386.2907	3.22	965	1279	1668	1202	1314	1761	533	1405	1362	272	352	302	3-Hydroxy-cis-5-tetradecenoylcarnitine	C21H39NO5	2
288.2174	3.25	748	727	1152	913	570	981	383	684	707	118	202	238	L-Octanoylcarnitine	C15H29NO4	2
115.0399	3.29	2328	3323	9708	1242	1477	3633	3777	2916	5998	3278	2847	6736	2-Methylacetoacetic acid/2-Oxovaleric acid/Glutarate semialdehyde/Alpha-ketoisovaleric acid	C5H8O3	1
332.2437	3.33	509	880	1246	606	923	1568	255	873	1099	148	177	76	3-hydroxydecanoyl carnitine	C17H33NO5	2
260.1861	3.33	1776	1898	3739	2311	1497	2780	1100	2226	1976	777	1805	1308	Hexanoylcarnitine	C13H25NO4	2
188.0562	3.34	1236	1671	3278	931	962	1461	1172	1139	1554	1273	1146	1754	Glutarylglycine	C7H11NO5	1
190.0719	3.42	121	243	1586	84	116	410	97	148	526	107	163	846	2-Amino-3,7-dideoxy-D-threo-hept-6-ulosonic acid	C7H13NO5	1
246.1704	3.44	37441	25468	42492	43744	23172	32524	31587	19440	47648	20478	11873	6674	2-Methylbutyroylcarnitine/Pivaloylcarnitine/Isovalerylcarnitine/Valerylcarnitine		2
79.0212	3.55	13731	37882	19513	5849	10195	8127	19438	23388	29667	48227	21638	32444	Dimethyl sulfoxide	C2H6OS	0
748.5708	3.57	26	2	9	156	416	1321	465	2	371	39	1	1	Glucosylceramide/Galactosylceramide	C42H81NO8	0
232.1546	3.58	76817	94595	170662	88550	83036	137422	62732	85946	95641	45263	51638	28051	Butyrylcarnitine/Isobutyryl-L-carnitine	C11H21NO4	1
140.0818	4.15	1323	1714	1589	1275	1705	1438	1967	1209	1436	1740	1781	1644	Histidinal	C6H9N3O	0
131.0759	4.44	1743	1965	4258	1433	1688	2458	2290	1417	2653	1745	1479	2697	L-gamma-glutamyl-L-(iso)leucine	C11H20N2O5	0
153.0659	4.61	188	773	1224	210	426	789	141	565	835	253	421	1059	N1-Methyl-2-pyridone-5-carboxamide/N1-Methyl-4-pyridone-3-carboxamide	C7H8N2O2	0
188.0562	4.72	1142	1579	3176	1068	943	1338	1202	1176	1626	1159	1396	2341	N-Acetylglutamic acid	C7H11NO5	1
218.1389	4.89	111719	96532	151220	129932	88101	123204	109593	70287	108371	96912	29596	7444	Propionylcarnitine	C10H19NO4	1
148.0604	5.25	3664	4354	6716	4035	3851	5380	3693	3278	3420	3231	1956	1551	L-Glutamic acid	C5H9NO4	0
176.0554	5.27	15265	19661	34550	16403	16492	25391	15188	15375	15875	13975	13306	17469	N-Formyl-L-glutamic acid	C6H9NO5	0

m/z	RT (min)	Mean abundance												Metabolites	Formula	Error (ppm)
		DMSO			Pentostatin			Cordycepin			Cordycepin + Pentostatin					
		2 h	8 h	24 h	2 h	8 h	24 h	2 h	8 h	24 h	2 h	8 h	24 h			
204.1231	5.61	175575	248133	400776	162858	230703	314557	127245	212858	185188	267647	189051	95618	L-Acetylcarnitine	C9H17NO4	0
252.1091	5.63	0	0	0	0	0	0	15192	3467	1589	48958	53001	26202	Cordycepin	C10H13N5O3	0
674.5126	5.67	2087	2025	671	877	1505	3641	2216	1419	3673	2258	1021	932	PE	C37H74NO7P	1
702.5433	5.67	1132	954	150	491	851	1426	1307	610	1573	1366	247	229	PE/PC	C39H78NO7P	1
115.0035	5.72	3210	4269	7863	2538	1957	2658	3511	3378	4221	3192	4018	5949	Maleic acid	C4H4O4	1
133.0141	5.72	97179	138450	276778	72054	47512	69766	115313	102580	136536	106175	131564	212406	Malic acid	C4H6O5	1
189.0870	5.74	1502	1482	3723	1279	1308	1661	1267	1005	1215	840	871	1547	N-Acetylglutamine	C7H12N2O4	0
219.0977	5.76	625	1809	11247	619	1373	5681	497	958	2488	448	682	2177	Serinyl-Hydroxyproline/Hydroxyprolyl-Serine/5-L-Glutamyl-L-alanine	C8H14N2O5	1
771.5193	5.78	285	112	126	268	1136	2887	394	281	1200	495	89	78	PG	C42H77O10P	1
253.0934	5.79	21	56	101	12	48	63	14706	5274	7686	17	1864	4429	Deoxyinosine	C10H12N4O4	1
217.0827	5.80	617	1369	5045	574	834	2201	499	1011	2048	639	1212	4046	5-L-Glutamyl-L-alanine	C8H14N2O5	1
137.0458	5.81	2453	2271	922	894	532	2095	13816	13992	7950	1467	3098	7542	Hypoxanthine	C5H4N4O	0
262.1653	5.87	2225	2354	4228	2403	2012	3231	2154	1631	2810	1758	1383	1485	3-Hydroxyisovalerylcarnitine	C12H23O5N1	2
315.2285	5.87	1425	261	2587	820	57	87	1611	355	1777	123	1200	525	Heptanoylcarnitine	C14H27NO4	2
289.0676	5.93	288	2768	5983	595	207	993	114	1001	1228	156	1856	4526	Uridine	C9H12N2O6	1
245.0772	5.95	67	868	2441	8	521	1722	10	251	373	126	16	202	Pseudouridine	C9H12N2O6	1
810.5296	6.00	2240	1006	1143	2607	0	158	2510	597	2689	1104	1599	4460	PS/PE	C44H76NO10P	2
305.0985	6.08	6688	8968	16613	6774	7545	11786	5434	8095	10428	4955	5621	16946	N-Acetylaspartylglutamic acid	C11H16N2O8	2
788.5456	6.10	11953	7128	8881	8287	2302	1609	11264	3550	10331	10170	9659	11907	PS	C42H78NO10P	2
848.5456	6.17	914	536	536	1077	1003	1194	1323	400	1215	1227	359	215	PC	C46H78NO8P	1
231.0620	6.22	1843	2151	2693	1963	2172	1151	1698	1478	1525	1641	1904	2016	Pyroglutamylglycine	C7H10N2O4	1
268.1046	6.28	565	8193	13448	423	6293	9276	371	2494	4469	4132	598	5787	Adenosine/deoxyguanosine	C10H13N5O4	2
229.1549	6.33	15800	16762	25733	16327	15386	21959	14866	12799	6941	12717	4369	3106	Pro (iso)Leu/(iso)Leu Pro	C11H20N2O3	1
146.1175	6.43	11487	12335	23087	12368	12422	18776	10438	13110	11660	10068	7490	6394	3-Dehydroxycarnitine	C7H15NO2	0
261.1272	6.46	21918	7668	4540	18902	8184	2340	23457	6470	4071	32534	14470	3197	Pantetheine	C11H22N2O4S	0
168.0655	6.48	731	750	2190	484	404	1348	458	596	923	501	283	796	Isopyridoxal/Pyridoxal	C8H9NO3	0
170.0811	6.55	15696	18711	30769	12704	20167	23772	18109	16457	16308	20433	17155	16092	Pyridoxine	C8H11NO3	0
294.2434	6.58	73273	62537	62516	56497	57683	75508	55933	65262	51846	47937	44816	47942	4,8 dimethylnonanoyl carnitine	C18H35NO4	2
352.2918	6.60	3808	2677	1255	4785	1440	1449	4579	2089	6923	1510	1385	4554	sphingomyelin	C39H79N2O6P	2
269.0885	6.63	677	2409	1396	0	541	3357	0	3114	982	132	0	2543	Inosine	C10H12N4O5	1

Supplementary Table 5.1 (Cont.) List of identified metabolites in MCF-7 cell extracts

m/z	RT (min)	Mean abundance												Metabolites	Formula	Error (ppm)
		DMSO			Pentostatin			Cordycepin			Cordycepin + Pentostatin					
		2 h	8 h	24 h	2 h	8 h	24 h	2 h	8 h	24 h	2 h	8 h	24 h			
148.0427	6.65	699	742	3	1385	1123	0	3025	432	26	1793	426	0	Thiomorpholine 3-carboxylate	C5H9NO2S	0
136.0617	6.67	1297	1356	3546	2086	1718	2495	5021	630	416	3421	1656	3186	Adenine	C5H5N5	0
101.0243	6.69	715	975	2394	606	718	1063	827	757	1102	836	829	1500	(S)-Methylmalonic acid semialdehyde/Succinic acid semialdehyde/2-Methyl-3-oxopropanoic acid/2-Ketobutyric acid/Acetic anhydride	C4H6O3	1
145.0140	6.69	9562	14515	41387	6919	8183	15329	11738	10482	17279	11866	11897	27571	α-Oxoglutaric acid	C5H6O5	1
166.0863	6.70	474275	504693	725861	466392	457547	546392	525326	425947	485150	496677	542369	579492	L-Phenylalanine	C9H11NO2	0
283.0682	6.74	554	652	1287	447	2367	2741	312	605	887	502	628	1133	Xanthosine	C10H12N4O6	0
831.6591	6.79	2582	1965	570	1023	1820	4624	3346	1310	3790	3239	934	1308	SM	C45H91N2O6P	1
247.1114	6.82	3791	1499	1100	3826	1755	443	4358	1265	708	6966	3200	449	Methionyl-Proline/Prolyl-Methionine	C10H18N2O3S	1
215.1392	6.82	3368	3571	5724	3462	3459	4982	3026	2983	1516	2831	953	607	Prolyl-Valine/Valyl-Proline	C10H18N2O3	1
191.0195	6.88	76750	89786	196302	51877	34750	33520	110343	20778	128637	52011	52613	59508	D-Glucaro-1,4-lactone	C6H8O7	1
221.0922	6.89	1439	1796	4506	2910	1425	2107	2324	1793	3019	2677	2147	2702	5-Hydroxy-L-tryptophan	C11H12N2O3	1
111.0087	6.91	965	1148	2494	628	496	450	1406	264	1578	637	662	696	Nicotinate beta-D-ribonucleotide	C11H15NO9P	2
205.0972	6.92	90014	102627	145459	85943	92325	109206	102648	83416	94239	93259	109517	119179	L-Tryptophan	C11H12N2O2	0
240.0511	6.93	2356	3189	6180	2076	2215	3157	1940	2959	4724	2787	2759	5114	3-Hydroxyhippuric acid	C9H9NO4	1
132.0300	6.93	135	1174	4449	143	43	954	56	166	4531	151	433	3076	L-Aspartic acid	C4H7NO4	1
173.0089	6.96	636	684	1517	394	245	282	769	224	941	483	414	554	Dehydroascobic acid	C6H6O6	1
213.1234	6.99	32844	33337	42251	33461	32264	41482	28511	32065	11770	26999	16914	9371	L-prolyl-L-proline	C10H16N2O3	0
627.5364	7.02	4607	1640	677	6621	172	358	4731	1403	7216	2094	1074	6111	DG	C41H72O5	2
156.0768	7.02	244	585	1049	297	527	892	286	502	563	366	561	759	Dihydrouracil	C4H6N2O2	0
306.0937	7.25	1494	2534	6440	1324	1851	4104	1311	1264	4901	1217	848	1776	7-Methylinosine	C11H15N4O5	1
162.1124	7.27	83876	70164	95972	90362	67476	87676	87268	51488	79871	57709	38678	33635	L-Carnitine	C7H15NO3	0
150.0583	7.27	90261	99442	123198	86343	87599	96502	105939	76935	88291	96588	106486	114094	L-Methionine	C5H11NO2S	0
162.0761	7.32	549	1708	7601	189	1967	3642	176	1385	1939	1109	885	2768	Aminoadipic acid	C6H11NO4	1
247.1292	7.37	1052	1255	1826	1004	1252	1476	1001	903	1283	957	791	731	Leucyl-Aspartate/Isoleucyl-Aspartate/Aspartyl-Isoleucine/Aspartyl-Leucine	C10H18N2O5	1
284.0994	7.40	329	4163	7990	16	2251	5803	85	1482	2475	1355	1321	3387	Guanosine	C10H13N5O5	1
230.1866	7.42	419	429	1245	385	303	538	532	161	443	213	98	96	N6,N6,N6-Trimethyl-L-lysine	C9H20N2O2	1
671.4079	7.55	319	278	468	276	87	20	708	211	272	1182	589	349	PA(18:4(6Z,9Z,12Z,15Z)/18:4(6Z,9Z,12Z,15Z))	C39H61O8P	0
551.2377	7.60	3710	812	2344	2653	537	1111	2246	705	1261	2456	1383	1777	Retinylphosphate mannose	C26H41O9P	0

Supplementary Table 5.1 (Cont.) List of identified metabolites in MCF-7 cell extracts

m/z	RT (min)	Mean abundance												Metabolites	Formula	Error (ppm)
		DMSO			Pentostatin			Cordycepin			Cordycepin + Pentostatin					
		2 h	8 h	24 h	2 h	8 h	24 h	2 h	8 h	24 h	2 h	8 h	24 h			
182.0813	7.68	259626	277295	406567	248414	242891	295395	295325	218258	260825	281553	306308	323915	L-Tyrosine	C9H11NO3	0
187.1077	7.68	2008	1989	2783	1997	1733	2271	1983	1439	641	1685	517	156	Prolyl-Alanine/Alanyl-Proline	C8H14N2O3	0
243.0983	7.69	1926	1960	2947	1393	750	364	1925	1593	1041	2120	1872	2463	Hydroxyprolyl-Hydroxyproline	C10H16N2O5	1
350.1024	7.75	4161	1186	4123	4627	918	1867	3593	712	1943	2247	486	913	5-(Formylmethyl)glutathione	C12H19N3O7S	2
173.0089	7.76	501	497	3550	366	26	51	600	403	784	608	480	2048	cis-Aconitic cid	C6H6O6	1
205.0683	7.83	946	708	251	637	1144	194	2430	944	728	2840	2142	786	Galactitol	C6H14O6	0
772.4859	7.85	314	286	1536	459	154	333	773	380	368	784	351	477	CL	C89H140O17P2	0
217.1185	7.90	3265	3149	4562	3153	2736	3771	3173	2455	1133	2656	1164	241	γ-Glutamyl-γ-aminobutyraldehyd	C9H16N2O4	1
277.0899	7.90	1551	978	382	1156	1521	506	2219	1343	1155	2139	1658	1089	Galactosylglycerol	C9H18O8	2
269.1248	7.90	9	3	1	5106	3	0	6	8	6	11560	9	0	Pentostatin	C11H16N4O4	1
410.1586	7.90	0	1511	0	0	1517	63	72	775	76	60	668	41	Tetrahydrofolic acid	C19H23N7O6	1
167.0815	7.93	3430	3743	6494	5301	2584	2736	3109	2108	7184	5119	3783	4276	Tryptophyl-Glutamine/Glutaminyl-Tryptophan	C16H20N4O4	0
119.0348	7.94	15667	11903	9807	28209	22285	16858	22574	11109	13837	13593	14021	9129	(S)-3,4-Dihydroxybutyric acid/A,b-Dihydroxyisobutyric acid	C4H8O4	1
267.0718	7.94	1696	1091	966	2116	1662	1826	1993	1607	1630	1884	1382	1110	3-Deoxy-D-glycero-D-galacto-2-nonulosonic acid	C9H16O9	1
143.0347	7.94	10859	8174	6483	19662	16001	11651	15896	7593	9133	9323	9737	5780	3-Methylglutaconic acid/(E)-2-Methylglutaconic acid/3-Hexenedioic acid	C6H8O4	2
131.0348	7.94	5418	4167	3519	9634	8082	6203	7878	3987	4899	4677	4942	3232	Ethylmalonic acid/Glutaric acid	C5H8O4	2
225.0613	7.94	524679	413791	315246	1013138	760822	585751	814946	365385	480513	449172	492726	272996	Glucoheptonic acid	C7H14O8	1
136.0481	7.95	5131	3149	1592	4386	4125	1659	5776	3960	3912	7942	7066	5416	Creatinine	C4H7N3O	0
130.0620	7.96	8661	17266	53968	7136	12042	25493	5221	12185	18909	9775	11224	36540	Creatine	C4H9N3O2	1
277.0326	7.96	3448	2813	1770	5185	3626	4023	4624	1527	3043	3213	5637	1971	D-Ribitol 5-phosphate	C5H13O8P	1
217.0821	8.07	2532	5162	3248	2247	3683	3224	2073	3951	3370	2187	3666	4803	Aspartyl-Threonine/Threoninyl-Aspartate/Glu Ser/Ser Glu	C8H14N2O6	1
70.0652	8.14	2011	2294	4125	2173	2120	3763	2457	2695	2695	1459	1441	1351	1-Pyrroline	C4H7N	1
672.1752	8.17	1137	584	2886	1255	953	1372	2129	1334	1529	2552	1413	1472	CMP-N-glycoloylneuraminate	C20H31N4O17P	1
203.0525	8.17	2153	430	0	1292	918	23	3969	709	584	5897	3748	761	Myoinositol	C6H12O6	1
166.0177	8.20	9036	2313	9731	1208	817	1777	8829	1855	4802	6040	2311	6020	Homocysteinesulfinic acid	C4H9NO4S	2
140.0682	8.22	25281	7585	3149	22354	9038	3696	30993	11551	11777	34686	28315	16321	L-Valine	C5H11NO2	0
695.4283	8.26	566	370	893	366	129	66	1015	138	374	1161	490	667	PG	C38H65O10P	1
155.0096	8.28	276	5639	14904	1391	264	1624	40	2457	16179	425	3107	12269	Orotic acid	C5H4N2O4	1
111.0199	8.28	35	441	1149	107	27	141	13	198	1227	43	245	1007	Uracil	C4H4N2O2	0
173.0921	8.31	4324	4962	6047	4614	4877	5884	4189	4845	2548	3455	2838	2423	Glycylproline/L-prolyl-L-glycine	C7H12N2O3	0

Supplementary Table 5.1 (Cont.) List of identified metabolites in MCF-7 cell extracts

m/z	RT (min)	Mean abundance												Metabolites	Formula	Error (ppm)
		DMSO			Pentostatin			Cordycepin			Cordycepin + Pentostatin					
		2 h	8 h	24 h	2 h	8 h	24 h	2 h	8 h	24 h	2 h	8 h	24 h			
601.3357	8.34	800	783	1286	746	856	1390	604	424	579	432	209	177	2-Stearoylglycerophosphoinositol/1-Stearoylglycerophosphoinositol	C27H53O12P	2
310.1138	8.36	1463	5807	3902	1647	6183	3341	2184	3153	3352	1741	4249	3033	N-Acetylneuraminic acid	C11H19NO9	2
229.1187	8.36	845	3006	3140	1095	4396	4377	804	3014	2060	654	832	1389	Prolyl-Hydroxyproline/Hydroxyprolyl-Proline	C10H16N2O4	2
620.3941	8.41	143	80	1427	450	440	742	343	643	249	486	382	206	PS	C31H60NO10P	2
231.0978	8.43	3085	3286	4347	2946	2971	3770	2652	3073	1942	2118	1508	1106	Aspartyl-L-proline/Prolyl-Aspartate	C9H14N2O5	1
156.0421	8.48	5683	3067	1374	4087	2845	1607	5758	2819	3567	5101	5468	4287	N-Methylethanolaminium phosphate	C3H10NO4P	0
320.0918	8.53	1074	3867	1452	759	3099	5746	571	2770	1991	382	1254	1183	S-(Hydroxymethyl)glutathione	C11H19N3O7S	0
189.0523	8.53	1043	916	494	849	894	701	785	783	883	639	729	798	Phenyllactic acid/ Dihydro-3-coumaric acid	C9H10O3	1
371.9899	8.55	5249	3591	1127	7778	8155	5919	6557	3408	4014	3571	2992	690	Nicotinic acid mononucleotide	C11H14NO9P	2
719.0968	8.59	1531	1734	1019	1665	2675	2350	1900	1840	1654	982	2050	284	cyclic GMP-AMP	C20H24N10O13P2	2
203.1025	8.61	890	810	1324	929	825	1252	793	652	250	630	223	24	Alanyl-Hydroxyproline/Hydroxyprolyl-Alanine/Prolyl-Serine/Serinyl-Proline	C8H14N2O4	0
148.0604	8.61	289649	379542	488606	299812	383743	475946	280443	325852	361556	213364	264709	354247	N-Acetylserine	C5H9NO4	0
74.0601	8.65	2887	2770	3261	2797	2704	3030	2849	2300	2566	2320	2784	3081	3-Aminopropionaldehyde/Aminoacetone	C3H7NO	0
164.0294	8.65	2987	2486	1392	2637	2154	1279	3507	2174	2188	3748	4055	3405	L-Threonine	C4H9NO3	0
393.0293	8.67	1426	836	487	1087	1166	1232	1267	855	915	1298	814	605	Diguanosine triphosphate	C20H27N10O18P3	2
148.0039	8.70	21379	23094	19156	20671	20661	24433	16501	20266	23070	13636	15593	15866	Taurine	C2H7NO3S	0
213.0491	8.74	15394	9229	1201	4895	10374	8993	6597	5876	5290	10462	8551	4187	Serinyl-Serine	C6H12N2O5	1
170.0617	8.75	1883	1259	916	1607	1213	907	1176	1028	933	938	1498	1466	Indolelactic acid/ 5-Methoxyindoleacetate	C11H11NO3	4
152.0318	8.75	1659	1154	814	1444	1021	787	1015	831	752	724	1330	1213	N-Acryloylglycine	C5H7NO3	0
147.0764	8.75	109346	68370	46690	92848	63312	61755	56028	46532	46400	37336	62934	66277	Ureidoisobutyric acid	C5H10N2O3	0
694.4820	8.80	317	434	1139	385	389	505	759	677	858	664	592	671	PE/PC	C39H70NO8P	1
712.4525	8.80	181	390	1195	109	232	282	624	521	606	638	509	489	PS(P-16:0/14:1(9Z))	C36H68NO9P	0
264.9734	8.80	5182	4448	1267	5377	4269	4278	3584	3250	2956	2121	3751	3641	Uridine triphosphate	C9H15N2O15P3	0
714.4489	8.83	484	585	1504	714	710	754	918	805	851	979	413	676	PE(18:4(6Z,9Z,12Z,15Z)/18:4(6Z,9Z,12Z,15Z))	C41H66NO8P	1
214.8362	8.85	6500	7343	11611	7273	7280	7813	8967	8441	8731	9614	7080	7713	GlcCer(d14:2(4E,6E)/16:0)	C36H67NO8	0
248.9993	8.85	1990	3556	6726	2418	3170	2808	4393	3607	2931	4680	4855	4906	Oxaloglutarate	C7H8O7	5
698.4755	8.85	988	1020	2045	1236	1182	1160	1281	1260	1409	1284	1032	1094	PE/PC	C38H68NO8P	0
678.5076	8.90	917	1141	1956	1058	1009	1020	1400	1556	1430	1691	1295	1251	PE/PC	C36H72NO8P	1
488.6558	8.92	6648	8503	17334	7820	8906	8098	14422	12151	12072	19290	13213	12608	(2E)-Tetradecenoyl-CoA	C35H60N7O17P3S	1

Supplementary Table 5.1 (Cont.) List of identified metabolites in MCF-7 cell extracts

m/z	RT (min)	Mean abundance												Metabolites	Formula	Error (ppm)
		DMSO			Pentostatin			Cordycepin			Cordycepin + Pentostatin					
		2 h	8 h	24 h	2 h	8 h	24 h	2 h	8 h	24 h	2 h	8 h	24 h			
76.0393	8.97	525	741	1396	530	646	1231	477	619	756	381	299	452	Glycine	C2H5NO2	0
150.0139	8.99	591	727	1044	613	613	651	662	691	571	612	752	1025	L-Serine	C3H7NO3	1
692.6200	9.02	2137	2156	1549	1956	2135	1635	2623	2180	2210	2741	2572	2517	DG	C41H78O5	2
392.7963	9.02	6949	7859	8143	6787	7500	6429	9126	8054	8271	10086	9558	9357	PC	C44H82NO8P	0
790.6938	9.04	1078	1262	937	1105	1189	930	1023	1155	1090	1233	1149	1257	TG	C47H88O6	2
947.7855	9.12	1203	1465	3111	2183	2476	1921	2513	1328	1965	1176	1671	1351	TG	C65H106O5	0
260.0275	9.18	1911	1878	3352	1839	1562	2507	1595	2433	3342	1320	1627	2906	Glycerylphosphorylethanolamine	C5H14NO6P	2
623.3492	9.33	502	392	1538	538	600	511	864	473	645	1037	960	989	Arginyl-Histidine/Histidinyl-Arginine	C12H21N7O3	1
237.9966	9.35	5565	2846	905	5384	3634	3652	4620	3547	4028	3281	952	407	Phosphocreatinine	C4H8N3O4P	1
210.0283	9.39	12783	5001	1609	6048	1728	830	9309	5792	7082	12339	6791	7419	Phosphocreatine	C4H10N3O5P	1
332.0760	9.43	0	0	0	0	0	0	820	760	20	2513	8356	3962	Cordycepin monophosphate	C10H14N5O6P	2
178.0240	9.43	1412	1776	2100	1433	1539	1797	1199	1681	1713	1060	1171	1554	dIMP	C10H13N4O7P	2
147.0764	9.43	3908	3142	3328	3747	2856	3027	3285	2435	2296	2986	3081	3142	L-Glutamine	C5H10N2O3	0
203.1504	9.51	610	553	1285	579	430	878	535	392	594	351	543	594	Asymmetric dimethylarginine	C8H18N4O2	1
170.0577	9.54	908	978	1121	917	877	1207	643	835	764	492	532	668	Phosphorylcholine	C4H12NO4P	0
258.1107	9.62	71982	61317	82945	74572	57551	78809	43982	75024	95711	32180	44765	113044	Glycerophosphocholine	C8H20NO6P	2
142.0264	9.62	3019	3894	2957	3098	3485	2694	2668	3126	1239	2133	3511	10762	O-Phosphoethanolamine	C2H8NO4P	0
132.0300	9.65	1233	1832	2141	805	1345	1303	993	1514	1463	1313	1597	1537	8-Hydroxyadenosine	C5H5N5O	2
307.1074	9.67	1007	337	571	992	325	433	625	322	391	438	330	224	Glutathione amide	C10H18N4O5S	1
275.1246	9.68	42	45	73	12	993	4277	15	93	99	40	12	62	Valyl-Hydroxyproline/Hydroxyprolyl-Valin	C10H18N2O4	1
348.0711	9.72	4174	42072	130161	2415	16456	69313	1548	7561	20546	4807	3602	69372	Adenosine monophosphate/dGMP/Inosine-2',3'-cyclic phosphate	C10H14N5O7P	2
307.1006	9.72	1020	487	571	1048	273	472	525	309	437	527	448	212	His Glu/Glu His	C11H16N4O5	2
307.0838	9.72	974959	463541	597182	917870	345995	481276	617354	344064	470923	501579	428004	323168	Oxidized glutathione	C20H32N6O12S2	2
928.2119	9.73	5167	911	1165	979	852	117	2101	295	1003	5224	460	760	Nonanoyl-CoA	C30H52N7O17P3S	2
161.1285	9.74	13	2671	1650	23	1827	2281	11	1604	1533	5	1114	1800	Isoputreanine/N(6)-Methyllysine	C7H16N2O2	0
324.0598	9.87	1831	4839	13332	1682	3160	7359	1275	1990	2606	1525	2110	7082	Cytidine monophosphate	C9H14N3O8P	2
170.0925	9.98	1245	940	1147	1146	999	1326	971	778	846	827	1014	1051	Methylhistidine	C7H11N3O2	1
223.0748	10.01	3514	5744	14355	3844	5200	11370	3240	3921	5580	2314	1755	2166	L-Cystathionine	C7H14N2O4S	1
156.0768	10.01	21434	20160	28394	21701	18678	22765	23933	17734	19308	23502	22314	24922	L-Histidine	C6H9N3O2	0
629.4937	10.10	908	1005	1545	591	644	957	1200	725	1164	1141	1028	1204	DG	C43H68O5	0

Supplementary Table 5.1 (Cont.) List of identified metabolites in MCF-7 cell extracts

m/z	RT (min)	Mean abundance												Metabolites	Formula	Error (ppm)
		DMSO			Pentostatin			Cordycepin			Cordycepin + Pentostatin					
		2 h	8 h	24 h	2 h	8 h	24 h	2 h	8 h	24 h	2 h	8 h	24 h			
467.0346	10.14	4409	3735	3621	5087	9208	6120	5208	3254	3753	3330	3817	2906	CDP-ethanolamine	C11H20N4O11P2	1
175.1190	10.15	13903	14931	15271	12841	14274	12151	17962	12327	13735	16448	28158	24274	L-Arginine	C6H14N4O2	0
673.5208	10.22	705	1325	704	964	788	782	659	727	657	669	437	771	DG	C45H70O5	2
664.1168	10.22	43100	45641	63413	41308	40520	69987	29275	33312	50641	22544	16748	30538	NAD	C21H27N7O14P2	0
184.0734	10.24	212936	269299	263246	220084	238918	248266	163197	202563	222561	137503	141912	236898	Phosphocholine	C5H14NO4P	0
147.1128	10.24	14723	15842	14383	13173	15108	13151	18261	13205	13687	16387	25215	22915	L-Lysine	C6H14N2O2	0
678.4117	10.24	675	931	589	687	779	610	956	1069	759	343	328	928	PE	C35H62NO8P	2
579.1675	10.32	514	731	676	649	1086	1171	742	752	1048	957	652	922	N-Succinyl-2-amino-6-ketopimelate	C11H15NO8	1
230.9908	10.38	561	1005	1715	461	139	372	755	694	828	695	1009	1709	(2R)-2-Hydroxy-3-(phosphonatooxy)propanoate	C3H7O7P	1
247.0581	10.39	874	927	1190	823	839	1476	625	723	1092	507	638	1049	Phosphatidyl glycerol	C6H15O8P	1
191.0195	10.40	36789	72172	115891	42558	16760	27540	43261	77993	68262	42615	65694	100749	Isocitric acid	C6H8O7	1
517.0847	10.45	0	0	0	173	737	1211	62	45	18	0	0	0	Glucosamine 6-phosphate	C6H14NO8P	1
331.0545	10.53	249	669	1184	51	389	666	151	631	774	308	632	810	Glycineamideribotide	C7H15N2O8P	1
323.0283	10.64	2656	19795	62524	2751	3263	15686	1800	4552	8784	1926	12357	38464	Uridine monophosphate	C9H13N2O9P	1
399.1453	10.69	1846	2112	2987	1830	1853	2456	1192	1547	1611	556	181	1129	S-Adenosylmethionine	C15H22N6O5S	2
171.0062	10.78	333	233	263	115	719	2492	279	977	1465	336	188	288	Glycerol 3-phosphate	C3H9O6P	1
347.0395	10.84	1223	2381	1224	64	17	14063	20	4744	1157	188	1114	5679	Inosine-5'-monophosphate (IMP)	C10H13N4O8P	0
245.0613	10.86	103	466	871	71	286	560	68	239	190	88	900	1577	Cytidine diphosphate choline (CDPcholine)	C14H26N4O11P2	1
168.9905	10.96	1703	10684	30009	3228	7689	17852	1040	6455	8001	800	9082	20536	Glyceraldehyde-3-phosphate	C3H7O6P	1
300.0487	10.96	1592	1699	1965	2278	3951	8982	2181	2580	3136	1742	1631	2442	N-Acetyl-D-Glucosamine 6-Phosphate/N-Acetyl-glucosamine 1-phosphate	C8H16NO9P	1
204.0868	10.97	286	182	225	306	153	309	322	364	400	240	459	1246	N-Acetylglucosamine	C8H15NO6	2
229.0116	11.02	1063	3401	10160	1839	2926	5154	1066	2421	2809	772	3292	7245	Ribose-5-phosphate/Ribulose-6-phosphate/Xylusoe-5-phosphate	C5H11O8P	1
364.0659	11.17	130	3365	18730	144	1567	10266	72	851	2145	538	1089	8663	Guanosine monophosphate	C10H14N5O8P	1
381.1987	11.19	0	8873	3707	0	5458	230	23	1743	994	4	945	696	Threoninyl-Alanine/Alanyl-Threonine	C7H14N2O4	2
333.0590	11.20	6879	5857	9190	4664	2781	2666	5305	5385	9391	6552	5881	8543	1-(sn-Glycero-3-phospho)-1D-myo-inositol	C9H19O11P	1
184.0014	11.25	6398	2089	670	2835	3620	6525	5572	2222	2158	7164	3071	2066	Phosphoserine	C3H8NO6P	1
291.1079	11.27	0	1245	1077	1	1062	1946	4	1590	396	0	485	117	Methylglutaric acid/(S)-2-Aceto-2-hydroxybutanoic acid	C6H10O4	2
243.0268	11.28	830	441	716	624	602	1468	1235	627	1281	1048	669	852	Inositol cyclic phosphate	C6H11O8P	2
261.0373	11.40	1334	334	419	888	864	1786	2362	839	1986	2116	962	1010	Glucose-6-phosphate/Fructose-6-Phosphate	C6H13O9P	0

Supplementary Table 5.1 (Cont.) List of identified metabolites in MCF-7 cell extracts

m/z	RT (min)	Mean abundance												Metabolites	Formula	Error (ppm)
		DMSO			Pentostatin			Cordycepin			Cordycepin + Pentostatin					
		2 h	8 h	24 h	2 h	8 h	24 h	2 h	8 h	24 h	2 h	8 h	24 h			
196.0068	11.67	1489	0	0	1347	0	0	1191	0	0	1289	0	0	Indoxylsulfuric acid	C8H7NO4S	0
411.0300	11.69	408	4631	11731	450	5726	6580	820	5133	7217	844	5511	7240	1-Phosphatidyl-D-myo-inositol	C11H19O13P	2
472.0981	11.72	14	86857	138416	83	72441	82726	21	62944	86965	108	76349	91717	CMP-2-aminoethylphosphonate	C11H20N4O10P2	2
153.0395	11.72	404	729	1310	480	654	1022	462	625	837	443	647	800	Glycolic acid	C2H4O3	1
413.0446	11.88	27	2045	4265	73	2632	2476	103	2320	2424	54	2111	2713	1-Phosphatidyl-D-myo-inositol	C11H19O13P	2
191.0195	12.03	5378	51538	76585	4740	13968	21519	6728	54793	51176	8125	48081	79214	Citric acid	C6H8O7	1
123.1126	12.18	7513	7460	7486	7155	7405	6633	8060	6293	8751	8573	6641	7707	Ethanolamine	C2H7NO	2
477.0760	12.50	5	12776	16698	18	15564	48436	132	10018	13310	36	11563	9474	2-Methyl-1-hydroxypropyl-ThPP	C16H26N4O8P2S	1
184.9854	12.55	1432	2619	4170	1686	3325	9814	2095	2553	3360	1423	2766	3472	2-Phosphoglycerate/3-Phosphoglycerate	C3H7O7P	1
333.0544	13.31	32	42	915	14	0	257	27	0	3681	12	0	88	Deamino nicotinamide adenine dinucleotide	C21H26N6O15P2	2
146.1652	13.85	685	3742	6310	858	3112	2480	3170	3951	2842	4009	4419	2721	Spermidine	C7H19N3	0
372.5457	14.33	2540	2931	4180	2583	2556	3659	2387	2146	3239	1774	1851	2769	Nicotinamide Adenine Dinucleotide Phosphate (NADP+)	C21H28N7O17P3	2
274.5110	14.87	0	0	11	0	97	0	0	0	0	41	1099	75	PI	C42H77O13P	1
428.0375	14.92	8416	26382	50957	9852	15927	27916	8190	13027	19829	5706	8258	33383	Adenosine diphosphate/dGDP	C10H15N5O10P2	1
412.0424	14.92	356	967	3145	34	3653	519	816	733	137	4543	46859	9201	dADP	C10H15N5O9P2	1
784.1502	16.00	1150	1373	4007	1671	1418	2577	1812	1854	2195	1205	1101	2617	Flavin adenine dinucleotide	C27H33N9O15P2	0
341.0041	16.33	13568	6987	11755	24979	8418	25362	20406	4450	22146	4521	12783	6304	Fructose-1,6-bisphosphate	C6H14O12P2	2
201.1121	16.43	2940	3055	3237	2823	3067	3006	2884	3123	3097	2797	3353	3321	cis-4-Decenedioic acid	C10H16O4	0
173.0302	16.73	7084	6075	6681	8192	7270	8517	6915	7785	6088	7506	5545	5896	Dihydrothymine	C5H8N2O2	3
201.1848	16.73	2703	2659	2849	2671	2774	2892	2534	2823	2651	2519	2893	2782	Isobutyl octanoate/Lauric acid	C12H24O2	0
734.5710	17.99	2941	2001	1157	3338	896	1315	3259	1066	4771	1063	1024	2462	PE/PC	C40H80NO8P	2

Supplementary Table 6.1 Details of detected ions (*m/z*) from cell extracts of untreated MIN6 cells (basal) and 10 mM glucose treated MIN6 cells.

m/z	Charge	RT (min)	Mean Abundance		VIP	p-Value	Fold (Glucose/Basal)
			Control	Glucose			
251.1855	+	2.32	9199.49	18099.85	1.86	4.04E-04	1.97
760.5858	+	2.35	29545.75	49629.08	2.64	4.06E-02	1.68
193.1437	+	2.47	5381.14	8298.49	1.05	7.41E-03	1.54
290.2691	+	2.55	6491.52	12435.36	1.56	6.32E-04	1.92
344.2281	+	2.55	5500.54	8661.44	1.09	1.07E-02	1.57
300.2018	+	2.57	7401.29	12859.82	1.44	1.75E-03	1.74
703.5758	+	2.57	7096.85	15781.13	1.74	3.14E-02	2.22
195.1230	+	2.60	32720.79	56620.02	3.03	1.12E-03	1.73
239.1490	+	2.60	8840.61	21234.66	2.18	1.24E-03	2.40
240.1806	+	2.60	4837.25	9343.21	1.36	1.30E-03	1.93
246.2428	+	2.60	3202.80	6860.57	1.20	2.11E-03	2.14
260.1858	+	2.60	815.46	9936.59	1.88	4.42E-03	12.19
284.2068	+	2.60	2505.43	5294.35	1.08	1.22E-04	2.11
288.2171	+	2.60	1832.96	14392.91	2.19	4.83E-03	7.85
151.0967	+	2.62	11457.16	18581.43	1.63	1.09E-02	1.62
89.0246	-	2.63	3193.73	31628.64	3.26	1.09E-02	9.90
834.3546	+	2.66	51582.88	115731.14	4.86	3.51E-02	2.24
953.4039	+	2.71	167085.69	371230.92	8.63	3.75E-02	2.22
953.9057	+	2.71	10854.66	28556.26	2.53	2.92E-02	2.63
87.0089	-	3.36	451.67	4530.05	1.14	1.55E-02	10.03
89.0246	-	3.67	2710.92	38322.73	3.89	1.08E-05	14.14
122.9759	-	4.77	4080.68	6178.21	1.05	4.78E-02	1.51
713.2904	-	5.05	164089.46	283864.26	6.59	1.66E-02	1.73
951.3896	-	5.05	49433.68	97441.12	4.18	1.32E-02	1.97
834.3547	+	5.09	44042.98	71514.13	3.20	1.03E-03	1.62
953.4040	+	5.09	127693.19	206098.46	5.43	1.64E-03	1.61
953.9056	+	5.09	7575.61	13445.20	1.45	1.13E-02	1.77
89.0246	-	5.48	9885.41	138368.20	7.12	1.83E-03	14.00
260.1859	+	6.16	2252.10	17134.79	2.50	9.60E-05	7.61
232.1546	+	6.65	1338.94	6714.53	1.51	2.92E-04	5.01
304.3001	+	6.67	815.73	7154.34	1.53	6.70E-03	8.77
237.0918	-	6.97	2237867.32	4671713.08	31.29	2.74E-04	2.09
299.0923	-	6.97	54792.04	121568.55	5.08	3.96E-04	2.22
953.9057	+	6.98	13519.33	24540.48	2.00	3.91E-02	1.82
951.3897	-	6.99	59962.58	127068.77	5.15	2.02E-04	2.12
1189.4883	-	6.99	2693.97	8308.69	1.44	3.89E-03	3.08

Supplementary Table 6.1 (Cont.) Details of detected ions (*m/z*) from cell extracts of untreated MIN6 cells (basal) and 10 mM glucose treated MIN6 cells.

m/z	Charge	RT (min)	Mean Abundance		VIP	p-Value	Fold (Glucose/Basal)
			Control	Glucose			
239.1063	+	7.00	7920464.95	12812961.28	45.08	1.55E-05	1.62
715.3046	+	7.00	960658.96	1705866.54	17.23	1.71E-04	1.78
715.8067	+	7.00	5625.06	12354.94	1.63	1.67E-04	2.20
834.3546	+	7.00	76033.69	135465.53	4.80	9.97E-03	1.78
953.4041	+	7.00	189487.15	336962.33	7.66	3.77E-03	1.78
477.2510	+	7.03	3561.01	6228.28	1.01	2.15E-05	1.75
134.8948	-	7.13	4449.64	13179.14	1.79	4.77E-02	2.96
450.1944	+	7.14	7644.09	16429.82	1.81	6.96E-03	2.15
132.8680	-	7.15	7825.07	11836.87	1.24	9.20E-03	1.51
389.1257	-	7.15	200.19	2969.20	1.02	3.62E-03	14.83
342.1696	+	7.17	7023.82	12452.46	1.39	3.52E-02	1.77
404.1855	+	7.19	2602.93	6901.79	1.34	5.00E-05	2.65
370.2010	+	7.34	1512.85	7462.96	1.58	1.94E-03	4.93
336.0534	+	7.37	4452.37	7248.17	1.07	7.39E-03	1.63
338.0504	+	7.37	9060.01	14791.07	1.53	6.82E-03	1.63
340.0475	+	7.37	7202.30	11807.90	1.37	6.09E-03	1.64
707.0767	+	7.37	2497.80	5003.05	1.03	2.36E-03	2.00
711.0709	+	7.37	43259.15	75128.77	3.66	3.14E-03	1.74
713.0679	+	7.37	39728.46	69689.03	3.56	2.34E-03	1.75
715.0650	+	7.37	40721.58	70638.84	3.55	2.80E-03	1.73
96.9699	-	7.55	189655.77	323642.84	7.08	2.17E-03	1.71
98.9670	-	7.55	63389.15	107721.63	4.08	2.37E-03	1.70
349.1178	+	7.83	5654.25	17572.84	2.12	1.73E-02	3.11
308.0992	-	7.84	2037.77	6287.48	1.20	3.85E-02	3.09
354.1695	+	7.96	834.80	5270.08	1.27	2.42E-02	6.31
110.9854	-	8.11	522.33	3889.28	1.12	6.51E-03	7.45
116.0707	+	8.12	87452.02	148004.93	4.85	7.08E-04	1.69
117.0740	+	8.12	4758.48	8071.26	1.14	6.55E-04	1.70
180.0868	+	8.20	53.42	9194.82	1.91	8.23E-03	172.13
291.0492	-	8.22	33.73	13184.86	2.09	3.34E-02	390.93
146.0460	-	8.40	52022.29	101501.91	4.45	2.64E-03	1.95
147.0494	-	8.40	2928.26	7497.75	1.39	5.41E-04	2.56
326.1098	-	8.47	0.00	34147.86	3.83	4.41E-05	> 1,000,000.00
102.0551	+	8.47	3743.67	7720.51	1.28	5.26E-03	2.06
148.0605	+	8.47	91051.03	197760.27	6.69	2.35E-03	2.17
149.0639	+	8.47	5270.59	11619.89	1.63	2.32E-03	2.20
664.1176	+	8.50	14512.97	22081.02	1.72	3.32E-03	1.52
304.0712	-	8.52	83.71	47837.18	4.54	3.32E-05	571.44

Supplementary Table 6.1 (Cont.) Details of detected ions (*m/z*) from cell extracts of untreated MIN6 cells (Basal) and 10 mM glucose treated MIN6 cells.

m/z	Charge	RT (min)	Mean Abundance		VIP	p-Value	Fold (Glucose/Basal)
			Control	Glucose			
162.1126	+	8.52	8550.80	22620.98	2.35	7.38E-04	2.65
145.0144	-	8.55	532.65	8873.24	1.91	1.23E-04	16.66
215.0331	-	8.55	209.09	92104.46	6.26	3.93E-04	440.50
217.0301	-	8.55	45.54	30557.00	3.61	4.37E-04	671.00
242.0521	-	8.55	18.98	3651.38	1.24	8.25E-05	192.41
382.0489	-	8.57	0.00	3375.25	1.16	1.44E-02	> 1,000,000.00
101.0245	-	8.60	821.05	25792.17	3.31	3.00E-06	31.41
87.0089	-	8.62	2033.04	5183.29	1.11	2.27E-04	2.55
131.0351	-	8.62	885.67	5026.35	1.33	2.60E-05	5.68
179.0564	-	8.62	2963.34	152379.89	8.07	8.70E-06	51.42
359.1202	-	8.62	996.48	100048.03	6.60	9.29E-06	100.40
113.0246	-	8.65	176.55	11252.31	2.21	1.88E-06	63.73
143.0351	-	8.65	176.65	13995.63	2.45	4.40E-06	79.23
239.0233	-	8.67	9.14	4803.04	1.35	2.95E-02	525.33
312.0942	-	8.67	0.00	5267.32	1.46	9.05E-04	> 1,000,000.00
392.5660	-	8.67	0.00	34067.94	3.83	8.47E-04	> 1,000,000.00
436.1597	-	8.67	0.73	8104.68	1.62	5.41E-02	11094.23
482.5976	-	8.67	0.00	17994.52	2.77	1.01E-03	> 1,000,000.00
298.9901	-	8.70	0.00	3005.69	1.07	3.11E-02	> 1,000,000.00
317.0008	-	8.70	0.00	3591.15	1.17	3.12E-02	> 1,000,000.00
479.5486	-	8.70	0.00	5984.87	1.51	3.18E-02	> 1,000,000.00
120.0657	+	8.72	1861.44	4551.75	1.05	3.40E-03	2.45
613.1412	-	8.77	5045.06	10064.40	1.40	1.12E-02	1.99
133.0144	-	8.82	4939.68	109183.10	6.64	7.82E-05	22.10
90.0551	+	8.87	5433.32	13723.37	1.89	3.79E-05	2.53
132.0769	+	8.87	7939.22	13901.63	1.50	1.42E-03	1.75
115.0038	-	8.87	552.73	4899.10	1.35	1.23E-04	8.86
417.1556	-	8.87	0.00	3456.03	1.09	2.03E-02	> 1,000,000.00
258.1103	+	8.92	476698.63	983603.64	13.86	4.72E-02	2.06
565.0488	-	9.19	3958.87	11489.28	1.79	1.92E-03	2.90
444.9244	-	9.39	66.52	6700.32	1.58	3.53E-02	100.72
191.0200	-	9.84	22424.47	84033.33	4.92	2.37E-03	3.75
272.9222	-	14.65	57883.48	102442.59	4.32	2.67E-04	1.77
824.7269	-	14.65	3160.39	7891.25	1.41	1.91E-03	2.50
367.8832	-	14.67	4049.37	11193.90	1.74	2.20E-04	2.76
389.8777	-	14.67	1673.04	5098.76	1.19	4.27E-04	3.05
144.9756	-	14.70	70625.61	107664.49	3.68	4.74E-03	1.52
166.9576	-	14.70	119811.98	182710.87	5.11	2.00E-04	1.52

Supplementary Table 6.1 (Cont.) Details of detected ions (*m/z*) from cell extracts of untreated MIN6 cells (Basal) and 10 mM glucose treated MIN6 cells.

m/z	Charge	RT (min)	Mean Abundance		VIP	p-Value	Fold (Glucose/Basal)
			Control	Glucose			
188.9396	-	14.70	82497.14	124800.55	4.28	8.31E-04	1.51
250.9401	-	14.70	28394.92	51501.50	2.90	5.96E-03	1.81
294.9039	-	14.70	58197.44	100412.77	4.26	1.15E-03	1.73
325.9044	-	14.70	1205.33	3847.51	1.01	2.22E-03	3.19
336.8954	-	14.70	1879.66	5695.83	1.23	1.07E-03	3.03
347.8864	-	14.70	6321.61	18618.84	2.26	1.74E-04	2.95
356.9047	-	14.70	29975.85	59412.95	3.44	8.51E-04	1.98
378.8867	-	14.70	8022.22	17695.13	2.02	4.47E-04	2.21
400.8685	-	14.70	42278.43	90197.35	4.53	4.11E-04	2.13
440.8868	-	14.70	11179.61	23315.06	2.22	1.32E-03	2.09
484.8511	-	14.70	16465.85	39536.74	3.08	5.28E-04	2.40
546.8259	-	14.70	1906.56	5317.30	1.19	4.40E-04	2.79
612.7976	-	14.70	5202.78	14495.94	1.98	1.09E-04	2.79
128.9536	+	14.71	108732.02	169328.80	5.09	1.90E-04	1.56
274.9105	+	14.71	14438.26	24916.49	2.08	4.57E-03	1.73
296.9183	+	14.71	97262.32	176328.09	5.79	1.22E-04	1.81
340.8823	+	14.71	9518.93	16764.89	1.73	4.66E-03	1.76
380.9007	+	14.71	59391.64	112938.54	4.76	2.28E-04	1.90
424.8647	+	14.71	8401.88	15943.84	1.78	2.22E-03	1.90
486.8653	+	14.71	27474.97	56273.91	3.48	2.06E-04	2.05
508.8477	+	14.71	4154.14	8398.29	1.33	2.15E-03	2.02
526.8840	+	14.71	20106.32	40123.50	2.90	2.06E-04	2.00
654.8304	+	14.71	6068.47	13154.29	1.73	7.11E-04	2.17
694.8488	+	14.71	5919.85	13273.74	1.76	2.94E-04	2.24
592.8298	+	14.73	2993.74	6162.16	1.16	1.18E-03	2.06
632.8484	+	14.73	15163.69	32810.48	2.72	2.80E-04	2.16
800.8134	+	14.73	5894.13	13975.66	1.84	6.70E-04	2.37
416.8427	-	14.83	2858.92	8156.24	1.41	5.02E-02	2.85
288.8960	-	14.85	6853.99	14494.39	1.69	3.61E-02	2.11
204.9135	-	14.88	5768.99	10626.87	1.35	1.21E-02	1.84
266.9140	-	14.88	2540.44	5533.46	1.04	5.19E-02	2.18
250.8918	+	14.88	3301.50	7424.24	1.24	1.38E-02	2.25
312.8922	+	14.88	5357.56	13928.83	1.77	2.77E-02	2.60
396.8746	+	14.88	3011.75	8777.59	1.45	3.41E-02	2.91
502.8392	+	14.88	1967.62	6129.07	1.23	4.18E-02	3.11
542.8578	+	14.88	2812.12	9091.76	1.50	4.47E-02	3.23
648.8222	+	14.88	1215.44	4141.98	1.02	4.57E-02	3.41
184.9201	+	14.91	4315.30	8442.32	1.25	7.66E-03	1.96

Supplementary Table 6.1 (Cont.) Details of detected ions (*m/z*) from cell extracts of untreated MIN6 cells (Basal) and 10 mM glucose treated MIN6 cells.

m/z	Charge	RT (min)	Mean Abundance		VIP	p-Value	Fold (Glucose/Basal)
			Control	Glucose			
144.9275	+	14.94	6601.00	11749.82	1.39	6.62E-03	1.78

Supplementary Table 6.2 Details of detected ions (*m/z*) from cell extracts of MIN6 cells treated with DMSO.

m/z	Charge	RT (min)	VIP	p-Value	Mean Abundance	
					Glucose	DMSO
499.1863	+	5.89	5.03	4.00E-02	583356.00	1145111.00
261.0876	+	5.96	4.53	2.00E-02	466899.00	984661.00
519.1536	-	6.01	1.05	3.84E-02	7692.63	18247.15
79.0211	+	7.26	1.84	2.00E-02	864.00	109257.00
757.2524	-	7.84	1.39	3.27E-02	10848.26	28676.22
759.2672	+	7.85	2.63	3.00E-02	104989.00	258668.00
519.1537	-	7.89	1.71	2.22E-02	17574.61	45977.66
343.0556	-	7.91	2.03	2.08E-02	32726.84	74605.30
603.1362	-	7.91	1.30	1.73E-02	12195.68	31942.42
521.1683	+	7.95	2.02	2.00E-02	62944.00	161929.00
299.0658	-	7.98	1.28	1.79E-02	12023.36	30445.72
365.0375	-	7.98	1.46	2.10E-02	17962.55	45697.06
144.9753	-	8.75	1.42	3.68E-02	18988.54	38949.89
128.9534	+	9.28	1.14	5.00E-02	27492.00	60324.00
166.9572	-	9.38	2.37	3.51E-02	47564.64	104582.92
188.9392	-	9.38	2.67	4.39E-02	59628.91	135121.01
400.8676	-	9.38	1.36	5.18E-02	15807.41	35892.31
100.9855	-	9.41	2.21	3.74E-02	44651.32	92588.24
272.9216	-	9.41	1.17	4.79E-02	10977.31	25525.61

Supplementary Table 6.3 Details of detected ions (*m/z*) from cell extracts of MIN6 cells treated rotenone: glucose, DMSO (glucose + DMSO) and rotenone (glucose + DMSO + rotenone).

m/z	Charge	RT (min)	VIP	FDR	Mean Abundance		
					Glucose	DMSO	Rotenone
425.1251	-	1.76	1.58	1.04E-07	31.65	41.50	38696.08
472.1970	+	1.83	1.51	7.66E-05	0.00	0.00	30666.95
427.1396	+	1.83	2.02	4.37E-07	1833.65	2041.56	122450.06
340.2485	+	1.86	1.13	1.61E-03	2074.58	3961.21	2158.39
377.2427	+	1.89	1.21	2.31E-03	9634.79	7934.25	13156.45
904.5926	+	1.92	1.26	1.65E-04	12884.24	14525.66	5356.60
344.2430	+	1.95	1.25	2.22E-07	5844.32	12987.77	12384.59
159.1028	-	1.97	1.24	3.44E-12	1146.17	2111.93	8732.34
752.5584	+	2.01	1.59	6.68E-06	49181.82	18014.19	1915.72
317.1896	+	2.04	1.13	9.83E-07	4534.82	4929.58	6841.08
245.1866	+	2.04	1.22	0.00E+00	3799.29	3756.86	9117.49
314.2092	-	2.06	1.22	3.05E-04	3538.79	514.95	5974.05
345.2751	+	2.07	1.16	2.72E-07	5115.29	3378.35	6139.95
590.3925	+	2.10	1.43	9.22E-06	21045.71	348.79	119.87
393.1351	-	2.12	1.62	2.93E-03	0.00	0.00	44957.57
409.1299	-	2.12	1.84	6.63E-09	49.89	30.45	81862.50
303.1740	+	2.13	1.14	6.46E-08	3631.10	4728.45	6543.43
357.2168	+	2.13	1.17	1.85E-04	733.63	1102.79	4452.35
448.2910	+	2.13	1.24	9.34E-04	5865.71	8169.70	15009.82
316.2228	+	2.13	1.34	1.28E-05	16107.05	22170.93	32575.85
678.4469	+	2.13	1.38	5.61E-07	16431.40	440.01	156.86
546.3650	+	2.13	1.41	8.20E-08	18461.68	129.92	10.84
634.4197	+	2.13	1.43	3.69E-03	20843.77	522.93	257.00
444.3323	+	2.13	2.18	3.51E-05	160380.79	6953.69	4312.11
488.3586	+	2.13	2.30	3.24E-04	191533.41	7634.81	2150.47
583.3805	+	2.16	1.25	2.36E-05	2862.16	3403.58	10589.32
380.3376	+	2.16	1.33	5.48E-04	19194.72	8105.63	5883.14
441.7884	+	2.16	1.34	3.88E-08	4277.00	6953.07	20055.95
244.1909	+	2.16	1.79	2.57E-07	90967.85	135905.40	56525.66
338.3419	+	2.16	2.01	3.33E-03	237146.32	144568.51	100907.54
576.4112	+	2.16	2.31	3.89E-11	196143.13	9995.67	1547.85
532.3850	+	2.16	2.35	0.00E+00	212063.58	13625.91	5745.94
390.2856	+	2.19	1.12	3.80E-04	4333.87	2502.42	4247.42
357.3479	+	2.19	1.12	1.60E-03	2067.82	1755.18	4070.80
198.1855	+	2.19	1.22	3.65E-06	6265.93	9906.49	3997.70
430.2440	+	2.19	1.28	1.28E-03	4753.79	4286.00	14232.75
322.2953	+	2.19	1.29	3.47E-06	11691.75	22152.79	18370.18

Supplementary Table 6.3 (Cont.) Details of detected ions (*m/z*) from cell extracts of MIN6 cells treated rotenone: glucose, DMSO (glucose + DMSO) and rotenone (glucose + DMSO + rotenone).

m/z	Charge	RT (min)	VIP	FDR	Mean Abundance		
					Glucose	DMSO	Rotenone
403.3534	+	2.19	1.62	2.37E-05	66898.87	23799.64	18643.10
752.5175	+	2.19	1.63	2.18E-08	47499.85	3907.32	370.62
375.3220	+	2.19	1.88	1.63E-03	132258.91	47608.70	95290.55
289.2739	+	2.19	1.90	2.33E-05	146450.74	91091.34	175478.57
664.4618	+	2.19	2.07	1.97E-08	137816.53	15747.20	5383.96
620.4376	+	2.19	2.21	1.72E-03	171600.81	13282.77	4486.38
291.2168	+	2.21	1.18	3.65E-09	3550.39	7480.13	5673.87
278.1600	+	2.21	1.18	6.95E-05	7694.39	4983.91	7356.33
384.7724	+	2.21	1.22	3.28E-06	1084.79	3546.94	8074.46
249.1699	+	2.21	1.22	8.48E-04	4452.10	10172.66	6915.15
398.1576	+	2.21	1.33	2.74E-05	0.00	0.00	12432.50
502.3384	+	2.21	1.34	1.82E-03	13798.44	971.16	219.27
291.2530	+	2.21	1.34	1.28E-06	10043.69	23381.18	15286.80
324.2898	+	2.21	1.35	2.21E-04	16943.62	14329.43	29635.26
341.3165	+	2.21	1.91	1.64E-04	80347.15	53228.00	152777.93
440.2071	+	2.21	4.93	0.00E+00	6083.60	5657.40	1814653.20
395.1492	+	2.21	7.72	3.04E-03	19830.15	13920.01	5136451.96
293.1962	+	2.24	1.23	1.75E-04	6762.48	12974.19	12230.24
371.3635	+	2.24	1.23	1.60E-03	12821.95	11984.17	18090.10
294.2429	+	2.24	1.51	1.18E-06	39415.98	38902.87	66849.54
482.2177	+	2.24	1.54	4.67E-05	388.60	1944.39	34252.77
432.2385	+	2.24	1.63	2.85E-05	11449.45	12475.66	59851.30
383.1493	+	2.24	1.67	1.05E-03	0.00	0.00	50672.87
460.2697	+	2.24	1.82	6.19E-04	29999.63	24854.84	112377.34
280.2637	+	2.24	2.16	1.26E-10	235470.88	204132.25	359687.79
296.2584	+	2.24	2.18	3.37E-04	137258.66	94560.22	260814.68
393.1336	+	2.24	3.08	7.30E-08	949.89	1208.63	489818.62
367.2692	+	2.27	1.16	2.72E-03	2346.65	5517.11	5503.09
357.3114	+	2.27	1.34	6.94E-09	16085.98	16241.96	27849.03
316.2122	+	2.27	1.44	4.13E-04	5164.57	15773.02	32320.07
373.3063	+	2.27	1.47	2.44E-03	25754.47	19147.08	45601.48
278.2480	+	2.27	1.56	1.01E-04	47839.91	54148.16	84500.43
343.3321	+	2.27	1.87	4.44E-05	127725.70	105456.03	195566.01
315.3008	+	2.30	1.10	1.25E-04	1905.92	1832.37	3270.78
236.2010	+	2.30	1.13	1.11E-16	2033.63	2181.96	4224.70
240.1958	+	2.30	1.15	3.16E-04	3522.13	4750.22	6763.29

Supplementary Table 6.3 (Cont.) Details of detected ions (*m/z*) from cell extracts of MIN6 cells treated rotenone: glucose, DMSO (glucose + DMSO) and rotenone (glucose + DMSO + rotenone).

m/z	Charge	RT (min)	VIP	FDR	Mean Abundance		
					Glucose	DMSO	Rotenone
254.2116	+	2.30	1.18	5.07E-07	4265.27	4846.28	8258.32
268.2121	+	2.30	1.24	5.84E-05	6307.09	12615.61	11588.31
243.1830	+	2.30	1.28	9.51E-06	1328.99	9857.31	10095.72
310.2367	+	2.30	1.35	5.20E-04	13969.68	19998.54	30589.94
455.2902	+	2.30	1.41	1.11E-15	439.85	11443.36	24770.25
309.2273	+	2.30	1.45	4.55E-15	15623.56	39143.43	30833.59
359.3270	+	2.30	1.50	5.51E-05	30501.09	16714.25	44268.35
131.0715	-	2.31	1.17	1.32E-11	327.06	986.92	4090.73
295.2114	+	2.32	1.17	5.16E-05	1654.07	4868.63	2790.07
251.1855	+	2.32	1.89	4.44E-07	91994.91	180998.45	146039.48
302.1964	+	2.35	1.18	8.94E-05	1307.60	4879.37	3727.66
259.2381	+	2.35	1.21	2.34E-06	5711.35	5630.87	11298.76
214.1803	+	2.35	1.37	1.62E-12	20410.09	21088.88	36323.89
237.1698	+	2.41	1.29	4.35E-04	7650.27	16530.80	11206.82
205.0796	+	2.41	1.46	1.38E-04	1401.39	5949.56	28144.27
325.2487	+	2.44	1.17	2.87E-03	1823.11	3690.14	6550.28
231.2069	+	2.44	1.20	5.14E-04	4647.57	5501.95	9893.68
209.1386	+	2.44	1.22	2.13E-03	3819.34	9123.05	8099.94
245.2229	+	2.44	1.30	0.00E+00	13926.96	19492.37	27132.24
223.1542	+	2.47	1.19	5.65E-04	3128.72	7204.81	4942.08
270.2068	+	2.47	1.20	0.00E+00	3381.42	5756.62	8946.30
216.1960	+	2.47	1.22	1.54E-08	3447.04	8585.83	4219.75
304.2847	+	2.50	1.14	6.04E-06	4978.54	2754.96	3421.43
402.2336	+	2.50	1.14	1.16E-04	3684.30	2329.62	676.20
198.1491	+	2.50	1.17	8.68E-04	4329.04	7932.30	7882.61
237.1059	+	2.50	1.18	1.16E-05	59.07	514.17	4085.28
261.2190	+	2.50	1.19	9.90E-05	4216.54	8425.28	7228.59
388.2543	+	2.50	1.37	2.71E-06	28287.77	33038.60	17547.28
87.0089	-	2.54	1.46	1.68E-07	3393.78	28421.44	32047.08
416.2855	+	2.55	1.11	8.35E-07	4448.74	3751.54	2487.88
258.2794	+	2.55	1.37	3.24E-05	14077.73	27955.95	17558.54
290.2691	+	2.55	1.69	3.12E-04	64915.23	124353.57	108743.65
300.2018	+	2.57	1.81	1.36E-05	74012.90	128598.21	63732.74
133.0860	+	2.60	1.20	0.00E+00	4758.21	9313.50	6116.20
196.1546	+	2.60	1.41	1.42E-04	19704.38	38138.56	26303.47
233.1861	+	2.60	1.42	1.11E-16	25661.57	5911.23	14606.41

Supplementary Table 6.3 (Cont.) Details of detected ions (*m/z*) from cell extracts of MIN6 cells treated rotenone: glucose, DMSO (glucose + DMSO) and rotenone (glucose + DMSO + rotenone).

m/z	Charge	RT (min)	VIP	FDR	Mean Abundance		
					Glucose	DMSO	Rotenone
284.2068	+	2.60	1.52	4.46E-06	25054.34	52943.52	28414.46
246.2428	+	2.60	1.65	3.28E-07	32027.96	68605.73	28725.47
260.1858	+	2.60	1.98	4.03E-08	8154.62	99365.94	13502.94
288.2171	+	2.60	2.18	4.03E-04	18329.57	143929.06	14612.68
89.0246	-	2.63	2.77	5.66E-04	31937.26	316286.44	525091.87
133.0762	+	2.64	1.23	1.45E-12	580.19	3193.79	8248.95
80.0247	+	2.76	1.40	6.07E-04	0.00	0.00	18175.51
81.0171	+	2.78	1.61	4.12E-14	0.00	0.00	43701.41
79.0213	+	2.78	4.01	6.63E-05	759.44	502.61	1047449.00
261.1962	+	3.61	1.30	2.09E-06	20.93	8180.55	309.03
202.1804	+	3.87	1.42	0.00E+00	3603.83	15828.83	28930.94
150.1127	+	5.46	1.46	1.71E-05	57292.21	33934.77	52607.80
260.1859	+	6.16	2.24	2.58E-03	22521.03	171347.89	40249.99
506.2034	+	6.21	1.54	1.87E-04	144880.91	102211.96	120230.43
114.0664	+	6.26	1.42	2.83E-08	37257.50	42662.64	59426.30
352.1652	+	6.26	1.74	5.22E-05	107904.21	139291.68	186966.01
246.1702	+	6.48	1.40	3.12E-08	6091.96	20165.09	4892.34
304.2121	+	6.50	2.20	1.23E-06	20.28	1378.49	167349.35
232.1546	+	6.65	1.75	4.44E-06	13389.44	67145.28	22127.06
389.1257	-	7.15	1.48	1.35E-03	2001.87	29692.04	16362.36
404.1855	+	7.19	1.62	1.38E-04	26029.31	69017.94	72528.21
137.0459	+	7.29	1.53	6.51E-04	46091.44	13770.60	27916.22
370.2010	+	7.34	1.69	3.16E-06	15128.53	74629.55	60232.51
707.0768	+	7.37	1.44	1.40E-03	24977.99	50030.52	39952.98
262.1651	+	7.44	1.11	2.58E-07	2616.72	3226.79	4296.31
125.0012	-	7.47	1.23	3.33E-16	421.55	6511.89	5561.03
204.1232	+	7.58	2.29	4.23E-04	276364.60	104631.54	222025.84
112.0507	+	7.61	1.38	1.12E-08	25940.32	9546.64	19486.16
244.0933	+	7.61	1.60	8.16E-08	84166.17	41743.30	68901.80
152.0566	+	7.75	1.29	3.83E-05	13137.18	8589.01	18708.94
574.2838	+	7.75	1.51	6.89E-04	37729.51	10832.88	38366.56
248.1493	+	7.78	1.72	2.68E-05	1031.26	1690.66	61327.21
130.0864	+	7.94	1.14	8.48E-14	1930.73	4170.16	3008.12
175.0250	-	8.03	1.11	8.05E-05	2062.93	2650.19	3781.92
284.0991	+	8.04	1.17	9.67E-14	2977.24	2594.54	6115.40
348.0706	+	8.04	2.42	6.02E-05	328111.68	98261.28	182224.04

Supplementary Table 6.3 (Cont) Details of detected ions (*m/z*) from cell extracts of MIN6 cells treated rotenone: glucose, DMSO (glucose + DMSO) and rotenone (glucose + DMSO + rotenone).

m/z	Charge	RT (min)	VIP	FDR	Mean Abundance		
					Glucose	DMSO	Rotenone
110.9854	-	8.11	1.58	4.26E-07	5223.29	38892.76	10346.30
70.0653	+	8.12	1.37	2.32E-05	23842.17	36284.29	41529.65
117.0740	+	8.12	1.58	1.27E-03	47584.84	80712.58	88987.81
116.0707	+	8.12	3.49	7.04E-05	874520.21	1480049.30	1636361.59
114.0562	-	8.16	1.22	5.58E-11	5646.84	9698.35	12060.13
286.0607	-	8.22	1.44	5.35E-04	82.04	22921.88	19548.50
346.0564	-	8.22	2.34	7.40E-04	265428.94	58338.33	130404.11
117.0195	-	8.24	1.47	6.65E-04	13772.29	36983.33	19040.91
382.1013	-	8.45	1.35	3.44E-08	4103.26	12916.47	22489.79
662.1031	-	8.47	1.43	7.29E-09	75913.64	63850.81	85093.23
326.1098	-	8.47	2.74	6.82E-04	0.00	341478.64	268584.43
664.1176	+	8.50	1.87	4.00E-04	145129.71	220810.24	241881.98
304.0712	-	8.52	3.06	8.53E-05	837.14	478371.84	392117.64
162.1126	+	8.52	2.14	5.09E-05	85507.98	226209.76	156854.63
242.0521	-	8.55	1.49	7.72E-06	189.77	36513.81	34878.89
101.0245	-	8.60	2.49	2.06E-04	8210.50	257921.67	197563.34
125.0245	-	8.62	1.22	2.84E-04	111.90	5689.18	4738.53
359.1202	-	8.62	3.97	1.03E-07	9964.82	1000480.29	680944.99
179.0564	-	8.62	4.66	2.58E-13	29633.36	1523798.87	1138040.08
198.0975	+	8.65	1.21	2.69E-06	0.00	5151.34	3723.81
225.0619	-	8.65	1.31	2.75E-06	4.39	10957.81	7262.79
113.0246	-	8.65	1.99	1.64E-04	1765.54	112523.10	84235.78
143.0351	-	8.65	2.11	9.18E-05	1766.45	139956.32	102672.24
351.0705	-	8.67	1.31	5.28E-04	199.89	11695.56	7864.90
491.2330	-	8.67	1.42	7.21E-11	0.00	20328.79	16183.27
312.0942	-	8.67	1.67	1.01E-04	0.00	52673.20	48552.46
503.0930	-	8.70	1.27	8.24E-06	0.00	6270.39	10342.64
300.0495	-	8.70	1.35	2.10E-11	1197.22	11698.49	646.98
132.0304	-	8.75	2.62	7.19E-04	718063.57	331216.27	372444.48
428.0372	+	8.82	1.20	1.82E-03	1832.85	2801.07	8714.15
133.0144	-	8.82	5.02	2.62E-07	49396.84	1091831.00	2341130.14
91.0584	+	8.87	1.16	1.06E-04	1449.98	4031.27	5127.16
282.1199	+	8.87	1.18	5.09E-07	3578.96	4010.73	7542.42
90.0551	+	8.87	1.92	4.33E-15	54333.16	137233.72	169407.76
347.0405	-	8.87	1.18	6.03E-05	5940.44	4496.13	8495.65
115.0038	-	8.87	1.77	1.21E-08	5527.34	48990.97	90730.22

Supplementary Table 6.3 (Cont.) Details of detected ions (*m/z*) from cell extracts of MIN6 cells treated rotenone: glucose, DMSO (glucose + DMSO) and rotenone (glucose + DMSO + rotenone).

m/z	Charge	RT (min)	VIP	FDR	Mean Abundance		
					Basal	DMSO	Rotenone
426.0229	-	8.90	1.30	0.00E+00	8368.02	8360.99	22424.19
147.0765	+	9.05	1.26	0.00E+00	10540.80	1901.03	3128.15
133.0610	+	9.10	1.24	1.58E-03	9332.10	2449.98	5950.42
584.0896	+	9.15	1.37	5.81E-12	4068.40	18710.80	19265.11
565.0488	-	9.19	1.84	3.58E-03	39588.72	114892.85	141058.10
341.1095	-	9.30	1.24	3.53E-04	1119.86	8313.11	6067.72
360.1502	+	9.36	1.26	7.46E-06	3177.20	11189.09	7314.50
364.0655	+	9.42	1.38	6.86E-04	17889.35	1515.85	10181.48
191.0200	-	9.84	3.35	2.73E-06	224244.70	840333.33	596285.07
598.0688	+	10.23	1.16	4.35E-11	4787.45	6785.12	9015.58
401.3704	-	14.67	1.22	1.75E-13	2053.91	7567.84	4239.54
389.8777	-	14.67	1.57	4.35E-14	16730.37	50987.64	30233.51
367.8832	-	14.67	1.81	2.54E-11	40493.69	111939.00	73284.31
165.9735	-	14.70	1.24	7.11E-06	4344.10	10436.59	7566.82
568.8336	-	14.70	1.39	7.75E-12	5346.76	20992.51	10183.85
431.8687	-	14.70	1.40	6.76E-06	7177.97	24268.65	14557.53
325.9044	-	14.70	1.50	1.33E-03	12053.25	38475.09	21086.73
546.8259	-	14.70	1.57	9.11E-06	19065.60	53173.01	33576.67
336.8954	-	14.70	1.61	2.33E-04	18796.61	56958.25	31346.59
612.7976	-	14.70	1.92	5.29E-10	52027.80	144959.38	92986.48
378.8867	-	14.70	1.94	4.31E-06	80222.17	176951.32	124414.07
440.8868	-	14.70	2.05	5.18E-09	111796.09	233150.58	172072.58
347.8864	-	14.70	2.08	8.64E-04	63216.07	186188.41	112490.53
484.8511	-	14.70	2.47	3.71E-05	164658.47	395367.37	265699.49
356.9047	-	14.70	2.65	1.96E-05	299758.53	594129.53	434321.45
400.8685	-	14.70	3.06	2.84E-05	422784.29	901973.48	662555.51
694.8488	+	14.71	1.78	2.09E-03	59198.45	132737.38	106125.65
632.8484	+	14.73	2.20	2.83E-14	151636.86	328104.77	266207.44
260.8800	-	14.91	1.17	1.76E-06	3963.70	6807.73	7633.84
404.8265	-	14.96	1.19	7.38E-05	3354.51	6833.69	8188.13

Supplementary Table 6.4 Details of detected ions (*m/z*) from cell extracts of MIN6 cells treated ethanol (EtOH).

m/z	Charge	RT (min)	VIP	p-Value	Mean Abundance	
					Glucose	EtOH
499.1863	+	5.89	6.27	3.39E-02	583355.87	1393456.77
759.2672	+	5.89	2.28	2.43E-02	62154.96	204827.02
497.1719	-	5.92	1.86	4.23E-02	60096.14	139306.51
759.2672	+	7.85	3.47	4.03E-02	104988.76	327341.54
310.1408	+	9.12	4.45	5.84E-03	34866.23	682713.85

Supplementary Table 6.5 Details of detected ions (*m/z*) from cell extracts of MIN6 cells treated antimycin A: glucose, EtOH (glucose + ethanol) and antimycin A (glucose + ethanol + antimycin A).

m/z	Charge	RT (min)	VIP	FDR	Mean Abundance		
					Glucose	EtOH	Antimycin A
519.2356	-	1.64	2.29	0.00E+00	0.00	0.00	105294.97
533.2514	-	1.64	2.29	2.89E-09	104.70	0.00	58935.17
547.2670	-	1.64	2.29	2.41E-07	413.88	66.56	194933.42
265.0822	+	1.74	2.19	0.00E+00	0.00	0.00	6736.95
521.2500	+	1.74	2.24	0.00E+00	0.00	0.00	17766.47
535.2668	+	1.74	2.22	5.29E-04	1151.80	159.86	12824.29
549.2814	+	1.74	2.21	1.45E-07	93.52	362.86	55779.47
340.2485	+	1.86	2.15	2.23E-04	2074.58	3961.21	1927.99
295.0940	-	1.94	2.29	0.00E+00	0.00	0.00	66989.82
344.2430	+	1.95	1.99	6.18E-05	5844.32	12987.77	8734.29
752.5584	+	2.01	1.95	1.07E-06	49181.82	18014.19	7165.78
297.1084	+	2.04	2.29	0.00E+00	0.00	0.00	21626.69
345.2751	+	2.07	2.21	1.16E-08	5115.29	3378.35	20511.19
447.4159	+	2.10	2.16	5.45E-05	136.99	292.68	4771.20
590.3925	+	2.10	1.98	1.05E-08	21045.71	348.79	123.49
414.2851	+	2.13	1.86	1.04E-05	5038.25	2319.16	1156.42
444.3323	+	2.13	1.97	8.35E-12	160380.79	6953.69	5020.66
448.2910	+	2.13	2.17	5.73E-07	5865.71	8169.70	19605.01
488.3586	+	2.13	1.98	8.85E-12	191533.41	7634.81	5437.94
546.3650	+	2.13	1.98	1.59E-10	18461.68	129.92	34.29
634.4197	+	2.13	1.98	6.48E-08	20843.77	522.93	207.85
678.4469	+	2.13	1.96	8.89E-07	16431.40	440.01	133.92
338.3419	+	2.16	1.90	6.14E-06	237146.32	144568.51	104424.73
350.3267	+	2.16	1.92	4.72E-05	116148.31	115352.82	78302.03
380.3376	+	2.16	1.94	1.59E-09	19194.72	8105.63	5875.48
532.3850	+	2.16	1.98	1.78E-12	212063.58	13625.91	10411.25
576.4112	+	2.16	1.97	1.99E-12	196143.13	9995.67	7713.75
289.2739	+	2.19	1.96	5.23E-09	146450.74	91091.34	52582.39
292.1757	+	2.19	1.84	2.11E-04	10585.09	7338.52	5030.52
322.2953	+	2.19	1.91	1.67E-03	11691.75	22152.79	17083.90
375.3220	+	2.19	1.89	2.46E-05	132258.91	47608.70	57345.78
390.2856	+	2.19	1.94	4.80E-06	4333.87	2502.42	1538.04
399.3948	+	2.19	2.04	9.23E-05	56551.40	64445.07	36590.96
403.3534	+	2.19	1.92	7.23E-07	66898.87	23799.64	26196.57
538.5202	+	2.19	2.06	7.05E-04	22317.57	48025.78	19797.32
620.4376	+	2.19	1.97	3.51E-13	171600.81	13282.77	10464.44
664.4618	+	2.19	1.97	1.73E-09	137816.53	15747.20	10955.92

Supplementary Table 6.5 (Cont.) Details of detected ions (*m/z*) from cell extracts of MIN6 cells treated antimycin A: glucose, EtOH (glucose + ethanol) and antimycin A (glucose + ethanol + antimycin A).

m/z	Charge	RT (min)	VIP	FDR	Mean Abundance		
					Basal	EtOH	Antimycin A
249.1699	+	2.21	1.90	9.90E-06	4452.10	10172.66	10029.98
278.1600	+	2.21	1.85	8.08E-05	7694.39	4983.91	2983.92
291.2168	+	2.21	1.93	5.16E-07	3550.39	7480.13	9316.66
291.2530	+	2.21	1.87	1.97E-04	10043.69	23381.18	20254.57
341.3165	+	2.21	1.82	6.77E-05	80347.15	53228.00	49943.05
384.7724	+	2.21	1.82	5.51E-04	1084.79	3546.94	3577.63
502.3384	+	2.21	1.97	6.72E-07	13798.44	971.16	326.30
293.1962	+	2.24	1.93	3.32E-04	6762.48	12974.19	9423.05
244.2272	+	2.27	1.95	4.29E-06	1660.60	2563.94	3490.60
289.2124	+	2.27	2.27	1.29E-08	493.34	192.73	3370.30
316.2122	+	2.27	1.96	7.56E-10	5164.57	15773.02	19210.29
343.3321	+	2.27	1.79	9.60E-04	127725.70	105456.03	86473.17
367.2692	+	2.27	1.85	2.24E-04	2346.65	5517.11	4605.36
243.1830	+	2.30	2.01	1.37E-10	1328.99	9857.31	6585.71
309.2273	+	2.30	1.91	1.39E-06	15623.56	39143.43	38933.44
359.3270	+	2.30	1.91	1.31E-05	30501.09	16714.25	9648.27
455.2902	+	2.30	2.14	1.97E-04	439.85	11443.36	2732.83
219.1879	+	2.32	2.12	1.38E-09	877.98	2335.80	5214.74
251.1855	+	2.32	1.88	1.61E-04	91994.91	180998.45	150086.98
295.2114	+	2.32	1.92	4.83E-06	1654.07	4868.63	4789.46
302.1964	+	2.35	2.05	1.26E-07	1307.60	4879.37	2735.99
146.1177	+	2.41	1.90	1.22E-03	3281.82	6194.61	4452.04
205.0796	+	2.41	2.20	1.96E-13	1401.39	5949.56	22765.24
237.1698	+	2.41	1.91	4.59E-05	7650.27	16530.80	12853.93
209.1386	+	2.44	2.02	1.39E-08	3819.34	9123.05	14970.49
216.1960	+	2.47	1.90	4.00E-04	3447.04	8585.83	5829.01
223.1542	+	2.47	1.89	3.51E-06	3128.72	7204.81	6750.73
198.1491	+	2.50	1.98	3.22E-04	4329.04	7932.30	5520.48
261.2190	+	2.50	1.96	8.88E-04	4216.54	8425.28	5506.57
304.2847	+	2.50	1.86	1.18E-04	4978.54	2754.96	3911.97
402.2336	+	2.50	1.89	1.50E-06	3684.30	2329.62	1623.86
548.3558	+	2.50	2.25	5.29E-04	841.62	723.38	3113.24
87.0089	-	2.54	1.86	5.74E-05	3393.78	28421.44	23004.43
258.2794	+	2.55	2.16	2.55E-05	14077.73	27955.95	12651.62
344.2281	+	2.55	2.01	1.32E-03	55005.41	86614.40	46161.90
274.2742	+	2.57	1.81	4.07E-04	920600.21	795914.03	649722.56

Supplementary Table6.5 (Cont.) Details of detected ions (*m/z*) from cell extracts of MIN6 cells treated antimycin A: glucose, EtOH (glucose + ethanol) and antimycin A (glucose + ethanol + antimycin A).

m/z	Charge	RT (min)	VIP	FDR	Mean Abundance		
					Glucose	EtOH	Antimycin A
133.0860	+	2.60	1.80	6.52E-05	4758.21	9313.50	9206.58
139.0503	+	2.60	1.96	1.13E-05	1541.03	3143.61	4105.84
195.1230	+	2.60	1.89	4.80E-07	327207.87	566200.18	651079.25
196.1546	+	2.60	1.98	6.92E-05	19704.38	38138.56	28070.56
230.2481	+	2.60	2.04	1.33E-03	41408.58	62421.08	34655.48
233.1861	+	2.60	1.91	2.30E-06	25661.57	5911.23	12476.17
246.2428	+	2.60	1.95	1.28E-04	32027.96	68605.73	44594.37
260.1858	+	2.60	2.07	3.61E-05	8154.62	99365.94	31642.18
284.2068	+	2.60	1.91	1.66E-05	25054.34	52943.52	52919.98
288.2171	+	2.60	1.88	2.27E-06	18329.57	143929.06	106901.57
343.2958	+	2.60	2.17	1.75E-08	33629.89	35491.53	190099.94
89.0246	-	2.63	1.95	8.76E-04	31937.26	316286.44	448333.12
133.0762	+	2.64	2.11	6.98E-08	580.19	3193.79	7845.91
218.2118	+	3.32	1.84	2.11E-03	9378.31	18154.10	16719.09
261.1962	+	3.61	2.23	4.30E-06	20.93	8180.55	306.14
202.1804	+	3.87	2.03	1.74E-09	3603.83	15828.83	23832.77
244.2637	+	4.02	2.08	1.19E-03	7577.35	5753.62	11936.82
150.1127	+	5.46	2.28	1.08E-10	57292.21	33934.77	303516.88
260.1859	+	6.16	2.14	7.86E-07	22521.03	171347.89	56178.68
506.2034	+	6.21	2.04	2.48E-04	144880.91	102211.96	187488.10
246.1702	+	6.48	1.96	1.36E-06	6091.96	20165.09	20846.00
232.1546	+	6.65	1.98	4.66E-09	13389.44	67145.28	49769.89
389.1257	-	7.15	2.02	1.30E-03	2001.87	29692.04	10176.69
230.2481	+	7.17	1.93	2.34E-04	123996.01	101673.27	143595.80
404.1855	+	7.19	1.97	3.62E-04	26029.31	69017.94	46614.94
137.0459	+	7.29	1.93	1.47E-05	46091.44	13770.60	20872.32
370.2010	+	7.34	1.94	2.93E-05	15128.53	74629.55	45550.27
707.0767	+	7.37	1.90	1.45E-03	24977.99	50030.52	43188.62
125.0012	-	7.47	1.98	2.54E-04	421.55	6511.89	4450.36
204.1232	+	7.58	1.93	1.83E-08	276364.60	104631.54	80327.21
112.0507	+	7.61	1.95	1.21E-04	25940.32	9546.64	10945.16
244.0933	+	7.61	1.94	3.36E-05	84166.17	41743.30	38487.51
152.0566	+	7.75	1.83	7.08E-05	13137.18	8589.01	10664.75
574.2838	+	7.75	1.87	2.09E-04	37729.51	10832.88	14483.00
130.0864	+	7.94	2.03	9.54E-05	1930.73	4170.16	2718.66
348.0706	+	8.04	2.03	3.54E-13	328111.68	98261.28	225681.15

Supplementary Table 6.5 (Cont.) Details of detected ions (*m/z*) from cell extracts of MIN6 cells treated antimycin A: glucose, EtOH (glucose + ethanol) and antimycin A (glucose + ethanol + antimycin A).

m/z	Charge	RT (min)	VIP	FDR	Mean Abundance		
					Glucose	EtOH	Antimycin A
110.9854	-	8.11	1.95	6.30E-07	5223.29	38892.76	20096.55
286.0607	-	8.22	2.01	1.08E-07	82.04	22921.88	29243.24
346.0564	-	8.22	2.06	5.24E-13	265428.94	58338.33	159556.36
117.0195	-	8.24	2.15	6.19E-10	13772.29	36983.33	79591.98
382.1013	-	8.45	2.21	1.06E-09	4103.26	12916.47	48158.27
326.1098	-	8.47	2.02	0.00E+00	0.00	341478.64	237664.59
662.1031	-	8.47	1.86	6.63E-07	75913.64	63850.81	54006.89
304.0712	-	8.52	2.00	1.23E-12	837.14	478371.84	399514.58
162.1126	+	8.52	2.00	4.01E-05	85507.98	226209.76	133326.20
242.0521	-	8.55	2.00	3.89E-14	189.77	36513.81	28949.66
101.0245	-	8.60	2.01	1.75E-14	8210.50	257921.67	217632.09
87.0089	-	8.62	1.86	2.16E-03	20330.44	51832.92	40591.31
125.0245	-	8.62	1.98	3.37E-07	111.90	5689.18	5259.14
179.0564	-	8.62	2.01	2.22E-16	29633.36	1523798.87	1233489.21
359.1202	-	8.62	2.00	1.37E-13	9964.82	1000480.29	808739.34
198.0975	+	8.65	1.99	0.00E+00	0.00	5151.34	4318.91
113.0246	-	8.65	2.01	4.05E-09	1765.54	112523.10	95148.83
143.0351	-	8.65	2.01	2.11E-08	1766.45	139956.32	116053.40
225.0619	-	8.65	1.98	8.30E-14	4.39	10957.81	7919.38
171.0066	-	8.67	2.08	2.66E-05	9200.10	17009.87	78027.24
312.0942	-	8.67	1.99	0.00E+00	0.00	52673.20	31440.95
323.0292	-	8.67	1.98	7.74E-04	45363.15	71548.47	99980.13
351.0705	-	8.67	2.13	7.19E-07	199.89	11695.56	123047.49
491.2329	-	8.67	1.99	0.00E+00	0.00	20328.79	19638.86
300.0495	-	8.70	2.08	3.27E-06	1197.22	11698.49	4593.09
503.0930	-	8.70	1.98	0.00E+00	0.00	6270.39	9854.41
132.0304	-	8.75	1.96	3.51E-05	718063.57	331216.27	255072.90
428.0372	+	8.82	2.20	1.35E-05	1832.85	2801.07	12749.87
133.0144	-	8.82	2.01	1.02E-09	49396.84	1091831.00	740668.46
90.0551	+	8.87	1.98	1.98E-07	54333.16	137233.72	132117.85
91.0584	+	8.87	1.99	1.64E-06	1449.98	4031.27	3968.38
115.0038	-	8.87	2.02	6.45E-13	5527.34	48990.97	31313.00
347.0405	-	8.87	2.11	6.84E-05	5940.44	4496.13	7397.97
426.0229	-	8.90	2.20	1.24E-05	8368.02	8360.99	27315.62
489.1152	+	9.00	1.91	1.35E-04	10300.81	8992.43	6114.77
147.0765	+	9.05	1.93	8.43E-08	10540.80	1901.03	1106.28

Supplementary Table 6.5 (Cont.) Details of detected ions (*m/z*) from cell extracts of MIN6 cells treated antimycin A: glucose, EtOH (glucose + ethanol) and antimycin A (glucose + ethanol + antimycin A).

m/z	Charge	RT (min)	VIP	FDR	Mean Abundance		
					Glucose	EtOH	Antimycin A
584.0896	+	9.15	2.04	2.20E-11	4068.40	18710.80	11532.21
565.0488	-	9.19	1.88	1.60E-03	39588.72	114892.85	91818.82
341.1095	-	9.30	1.96	6.54E-06	1119.86	8313.11	10600.74
365.1057	+	9.33	1.97	3.78E-04	17956.98	36927.64	27633.78
360.1502	+	9.36	2.00	1.32E-06	3177.20	11189.09	10259.93
364.0655	+	9.42	2.00	4.84E-14	17889.35	1515.85	7112.84
156.0769	+	9.45	2.01	5.68E-04	17678.75	33861.52	22426.60
176.1031	+	9.45	1.82	4.64E-05	2518.71	4023.06	4240.48
779.5209	+	10.38	2.21	1.17E-03	582.72	1210.54	10346.05
106.0864	+	10.47	1.95	1.19E-04	9551.97	11209.61	19927.56
367.8832	-	14.67	1.96	7.46E-08	40493.69	111939.00	88906.29
389.8777	-	14.67	1.95	4.39E-07	16730.37	50987.64	39900.21
401.3704	-	14.67	1.87	8.88E-04	2053.91	7567.84	5556.46
409.8868	-	14.67	1.87	1.59E-03	1101.40	9113.85	5774.40
165.9735	-	14.70	1.93	6.13E-06	4344.10	10436.59	8650.99
325.9044	-	14.70	1.93	1.39E-04	12053.25	38475.09	26097.78
336.8954	-	14.70	1.93	3.44E-05	18796.61	56958.25	41109.57
347.8864	-	14.70	1.95	4.68E-06	63216.07	186188.41	140144.62
356.9047	-	14.70	1.97	8.74E-08	299758.53	594129.53	490383.83
378.8867	-	14.70	1.97	1.69E-07	80222.17	176951.32	147397.13
400.8685	-	14.70	1.96	3.02E-06	422784.29	901973.48	764255.56
431.8687	-	14.70	1.94	6.78E-06	7177.97	24268.65	18163.15
440.8868	-	14.70	1.96	7.99E-07	111796.09	233150.58	194394.43
484.8511	-	14.70	1.95	3.01E-07	164658.47	395367.37	311927.89
546.8259	-	14.70	1.93	1.26E-05	19065.60	53173.01	40889.83
568.8336	-	14.70	1.95	9.30E-05	5346.76	20992.51	14546.98
612.7976	-	14.70	1.95	2.32E-06	52027.80	144959.38	112672.65
486.8653	+	14.71	1.95	1.66E-03	274749.68	562739.07	510319.56
694.8488	+	14.71	1.95	5.99E-04	59198.45	132737.38	117433.81
632.8484	+	14.73	1.94	1.28E-03	151636.86	328104.77	293245.93

Supplementary Table 6.6 Details of detected ions (*m/z*) from cell extracts of MIN6 cells treated azide.

m/z	Charge	RT (min)	VIP	FDR	Mean Abundance		
					Basal	Glucose	Azide
340.2485	+	1.86	1.89	1.46E-04	2074.58	3961.21	3058.69
363.2203	+	1.86	2.16	1.54E-06	534.92	1578.26	4187.21
377.2427	+	1.89	1.91	1.70E-06	9634.79	7934.25	10650.34
904.5926	+	1.92	2.03	1.89E-03	12884.24	14525.66	6591.67
344.2430	+	1.95	1.94	1.84E-05	5844.32	12987.77	9543.98
752.5584	+	2.01	2.05	6.58E-05	49181.82	18014.19	1063.98
317.1896	+	2.04	2.17	1.63E-07	4534.82	4929.58	9274.63
314.2092	-	2.06	2.03	8.85E-04	3538.79	514.95	3899.41
345.2751	+	2.07	1.78	9.07E-04	5115.29	3378.35	4977.09
590.3925	+	2.10	2.03	9.91E-11	21045.71	348.79	56.10
303.1740	+	2.13	2.09	5.12E-05	3631.10	4728.45	6828.23
357.2168	+	2.13	2.20	6.63E-07	733.63	1102.79	3408.71
414.2851	+	2.13	1.91	3.08E-05	5038.25	2319.16	901.81
444.3323	+	2.13	2.03	3.80E-11	160380.79	6953.69	2807.42
488.3586	+	2.13	2.03	3.81E-09	191533.41	7634.81	2266.07
546.3650	+	2.13	2.03	5.83E-12	18461.68	129.92	6.79
634.4197	+	2.13	2.03	3.45E-10	20843.77	522.93	147.54
678.4469	+	2.13	2.01	1.17E-07	16431.40	440.01	68.53
338.3419	+	2.16	2.00	9.72E-06	237146.32	144568.51	87546.70
380.3376	+	2.16	2.00	2.49E-09	19194.72	8105.63	5598.78
532.3850	+	2.16	2.03	2.34E-11	212063.58	13625.91	6849.22
576.4112	+	2.16	2.03	3.01E-09	196143.13	9995.67	2620.59
583.3805	+	2.16	2.14	1.14E-03	2862.16	3403.58	6281.45
289.2739	+	2.19	1.89	1.88E-06	146450.74	91091.34	88112.33
292.1757	+	2.19	1.91	1.22E-04	10585.09	7338.52	4519.90
322.2953	+	2.19	1.94	2.16E-03	11691.75	22152.79	13690.91
357.3479	+	2.19	2.19	1.74E-05	2067.82	1755.18	4491.34
375.3220	+	2.19	2.01	4.05E-09	132258.91	47608.70	122775.66
390.2856	+	2.19	1.85	1.17E-04	4333.87	2502.42	2692.07
399.3948	+	2.19	2.03	1.58E-04	56551.40	64445.07	32873.56
403.3534	+	2.19	1.96	3.15E-07	66898.87	23799.64	21584.78
430.2440	+	2.19	2.18	2.50E-04	4753.79	4286.00	8438.25
538.5202	+	2.19	2.00	2.48E-04	22317.57	48025.78	16152.91
614.4841	+	2.19	1.79	3.77E-03	15027.39	11621.52	9796.61
620.4376	+	2.19	2.03	1.16E-11	171600.81	13282.77	6416.85
664.4618	+	2.19	2.03	1.55E-08	137816.53	15747.20	5490.20
752.5175	+	2.19	2.02	1.06E-05	47499.85	3907.32	355.00
249.1699	+	2.21	1.96	5.86E-05	4452.10	10172.66	6542.87

Supplementary Table 6.6 (Cont.) Details of detected ions (*m/z*) from cell extracts of MIN6 cells treated azide.

m/z	Charge	RT (min)	VIP	FDR	Mean Abundance		
					Basal	Glucose	Azide
278.1600	+	2.21	1.86	5.12E-04	7694.39	4983.91	3575.00
291.2168	+	2.21	1.91	2.00E-05	3550.39	7480.13	5983.15
291.2530	+	2.21	1.96	7.93E-04	10043.69	23381.18	12598.09
341.3165	+	2.21	1.85	7.09E-05	80347.15	53228.00	78503.65
384.7724	+	2.21	2.11	5.90E-06	1084.79	3546.94	4745.11
502.3384	+	2.21	2.02	1.13E-08	13798.44	971.16	196.92
230.1753	+	2.24	1.98	8.61E-05	7696.82	10860.97	14747.31
293.1962	+	2.24	1.92	8.56E-05	6762.48	12974.19	9394.11
296.2584	+	2.24	1.78	1.82E-03	137258.66	94560.22	129152.87
432.2385	+	2.24	1.99	2.13E-03	11449.45	12475.66	28155.85
460.2697	+	2.24	2.02	1.15E-03	29999.63	24854.84	72544.22
173.1174	+	2.27	1.82	1.69E-03	8361.02	12744.52	12691.27
192.1385	+	2.27	1.94	1.23E-04	4854.26	5118.13	3066.42
316.2122	+	2.27	2.02	3.56E-10	5164.57	15773.02	16377.52
367.2692	+	2.27	1.87	1.35E-04	2346.65	5517.11	4235.88
373.3063	+	2.27	1.80	3.88E-03	25754.47	19147.08	27936.41
387.3584	+	2.27	1.96	1.38E-03	3082.91	3077.32	1052.31
236.2010	+	2.30	2.15	3.70E-06	2033.63	2181.96	4810.54
240.1958	+	2.30	2.07	2.77E-05	3522.13	4750.22	7114.57
243.1830	+	2.30	2.01	6.02E-11	1328.99	9857.31	6038.18
254.2116	+	2.30	2.05	3.13E-05	4265.27	4846.28	8176.31
268.2121	+	2.30	1.94	2.91E-03	6307.09	12615.61	7560.75
268.2272	+	2.30	2.10	2.70E-04	3532.67	3103.84	6753.39
288.2535	+	2.30	1.88	3.93E-03	12977.30	23980.79	17691.41
309.2273	+	2.30	2.00	9.71E-06	15623.56	39143.43	21722.04
359.3270	+	2.30	1.96	1.66E-05	30501.09	16714.25	9358.21
455.2902	+	2.30	2.10	6.24E-05	439.85	11443.36	69.40
251.1855	+	2.32	1.93	8.81E-05	91994.91	180998.45	125560.69
295.2114	+	2.32	1.99	2.03E-05	1654.07	4868.63	2765.29
212.1647	+	2.35	1.91	3.33E-04	5628.84	8412.30	10500.27
214.1803	+	2.35	2.15	4.82E-07	20410.09	21088.88	46335.25
259.2381	+	2.35	2.21	2.93E-06	5711.35	5630.87	14935.95
302.1964	+	2.35	2.00	2.11E-10	1307.60	4879.37	3188.55
200.1647	+	2.38	1.93	1.68E-04	22049.72	30454.92	39485.41
236.1859	+	2.38	2.00	1.53E-04	2648.04	3817.74	4447.64
146.1177	+	2.41	1.97	5.06E-04	3281.82	6194.61	3327.53
205.0796	+	2.41	2.18	5.93E-12	1401.39	5949.56	10635.14
237.1698	+	2.41	1.95	9.41E-06	7650.27	16530.80	11279.63

Supplementary Table 6.6 (Cont.) Details of detected ions (*m/z*) from cell extracts of MIN6 cells treated azide.

m/z	Charge	RT (min)	VIP	FDR	Mean Abundance		
					Basal	Glucose	Azide
275.1425	+	2.41	2.16	1.71E-03	4270.94	4730.13	8207.28
209.1386	+	2.44	1.96	6.77E-06	3819.34	9123.05	6029.39
231.2069	+	2.44	2.12	3.67E-04	4647.57	5501.95	8960.70
245.2229	+	2.44	1.98	1.48E-04	13926.96	19492.37	24632.59
216.1960	+	2.47	1.94	1.26E-04	3447.04	8585.83	4954.67
223.1542	+	2.47	1.96	4.82E-06	3128.72	7204.81	4936.68
270.2068	+	2.47	2.09	6.34E-06	3381.42	5756.62	9888.13
172.1334	+	2.50	1.86	5.98E-04	38106.04	53169.95	63344.94
198.1491	+	2.50	2.01	7.49E-07	4329.04	7932.30	8648.64
216.1596	+	2.50	1.85	6.41E-04	10526.57	15584.49	15645.55
261.2190	+	2.50	1.94	1.31E-05	4216.54	8425.28	8059.25
304.2847	+	2.50	1.97	8.56E-07	4978.54	2754.96	1841.75
388.2543	+	2.50	1.96	2.87E-04	28287.77	33038.60	17500.09
402.2336	+	2.50	2.06	2.37E-08	3684.30	2329.62	854.10
87.0089	-	2.54	1.85	1.84E-04	3393.78	28421.44	14534.60
258.2794	+	2.55	1.94	7.66E-05	14077.73	27955.95	20635.09
290.2691	+	2.55	1.90	1.08E-03	64915.23	124353.57	101016.81
344.2281	+	2.55	1.97	7.69E-04	55005.41	86614.40	44637.97
274.2742	+	2.57	1.89	9.50E-05	920600.21	795914.03	1049066.41
133.0860	+	2.60	1.94	2.14E-04	4758.21	9313.50	5340.79
188.1283	+	2.60	1.85	4.02E-04	3167.83	6226.34	7221.93
196.1546	+	2.60	2.06	1.02E-05	19704.38	38138.56	19936.33
233.1861	+	2.60	1.91	4.36E-07	25661.57	5911.23	13269.21
246.2428	+	2.60	2.00	2.68E-05	32027.96	68605.73	35401.19
260.1858	+	2.60	2.00	1.06E-05	8154.62	99365.94	22350.93
284.2068	+	2.60	1.95	5.21E-04	25054.34	52943.52	32885.42
288.2171	+	2.60	2.01	8.46E-07	18329.57	143929.06	34253.96
89.0246	-	2.63	2.01	7.10E-04	31937.26	316286.44	438355.52
218.2118	+	3.32	1.91	4.61E-04	9378.31	18154.10	18424.31
261.1962	+	3.61	2.12	4.89E-07	20.93	8180.55	40.67
202.1804	+	3.87	2.03	4.55E-09	3603.83	15828.83	15137.41
244.2637	+	4.02	2.15	1.59E-04	7577.35	5753.62	12304.70
128.0355	-	5.24	1.97	8.53E-04	12136.28	15432.98	4873.36
150.1127	+	5.46	1.83	4.59E-05	57292.21	33934.77	36252.66
260.1859	+	6.16	2.05	6.40E-07	22521.03	171347.89	43754.49
506.2034	+	6.21	1.96	1.78E-04	144880.91	102211.96	172671.00
268.1043	+	6.24	1.91	1.56E-03	109588.69	62700.34	130019.41
246.1702	+	6.48	1.98	1.43E-05	6091.96	20165.09	11178.82

Supplementary Table 6.6 (Cont.) Details of detected ions (*m/z*) from cell extracts of MIN6 cells treated azide.

m/z	Charge	RT (min)	VIP	FDR	Mean Abundance		
					Basal	Glucose	Azide
304.2121	+	6.50	2.13	1.48E-05	20.28	1378.49	5968.59
232.1546	+	6.65	2.04	3.49E-09	13389.44	67145.28	26904.99
715.3046	+	7.00	1.98	3.20E-03	9606589.58	17058665.39	9415072.81
389.1257	-	7.15	1.97	1.40E-03	2001.87	29692.04	7798.94
230.2481	+	7.17	2.03	4.50E-05	123996.01	101673.27	161816.85
404.1855	+	7.19	2.03	2.89E-04	26029.31	69017.94	27805.54
137.0459	+	7.29	1.96	9.81E-07	46091.44	13770.60	33459.72
269.0882	+	7.29	1.83	2.28E-03	62168.94	26337.72	56076.72
370.2010	+	7.34	1.99	4.10E-05	15128.53	74629.55	21489.89
707.0767	+	7.37	1.91	1.51E-03	24977.99	50030.52	34722.74
125.0012	-	7.47	2.01	3.44E-04	421.55	6511.89	3165.28
204.1232	+	7.58	1.94	3.90E-08	276364.60	104631.54	114784.57
112.0507	+	7.61	1.94	1.43E-05	25940.32	9546.64	14025.37
244.0933	+	7.61	1.93	7.53E-06	84166.17	41743.30	46949.71
152.0566	+	7.75	2.04	8.38E-07	13137.18	8589.01	16246.95
574.2838	+	7.75	1.84	2.83E-05	37729.51	10832.88	26324.15
248.1493	+	7.78	2.25	2.65E-09	1031.26	1690.66	4806.99
326.0654	-	7.84	1.96	3.85E-04	547.06	5594.13	68.38
166.0725	+	7.91	1.94	2.94E-03	23505.91	28477.48	14452.55
130.0864	+	7.94	1.97	1.83E-05	1930.73	4170.16	2594.03
284.0991	+	8.04	1.81	9.49E-04	2977.24	2594.54	3355.25
348.0706	+	8.04	2.16	3.11E-15	328111.68	98261.28	405024.19
166.0545	-	8.09	1.76	7.42E-05	51637.19	38795.69	45790.35
110.9854	-	8.11	2.02	3.74E-08	5223.29	38892.76	5596.35
286.0607	-	8.22	2.04	1.26E-07	82.04	22921.88	23190.03
346.0564	-	8.22	2.17	5.17E-14	265428.94	58338.33	327419.86
117.0195	-	8.24	1.98	8.83E-06	13772.29	36983.33	24901.25
147.0494	-	8.40	2.08	1.27E-03	29282.57	74977.54	85490.62
382.1013	-	8.45	2.23	3.08E-10	4103.26	12916.47	33399.53
326.1098	-	8.47	2.04	0.00E+00	0.00	341478.64	295222.99
662.1031	-	8.47	1.80	4.59E-06	75913.64	63850.81	76554.89
148.0605	+	8.47	2.03	1.48E-03	910510.31	1977602.66	2182781.44
149.0639	+	8.47	2.02	1.33E-03	52705.91	116198.90	128110.56
273.0753	+	8.47	1.90	6.35E-04	12767.53	24901.43	18788.97
304.0712	-	8.52	2.02	1.35E-12	837.14	478371.84	333213.06
162.1126	+	8.52	1.95	8.75E-07	85507.98	226209.76	187277.43
242.0521	-	8.55	2.02	6.06E-14	189.77	36513.81	18720.15
101.0245	-	8.60	2.03	1.10E-14	8210.50	257921.67	176080.89

Supplementary Table 6.6 (Cont.) Details of detected ions (*m/z*) from cell extracts of MIN6 cells treated azide.

m/z	Charge	RT (min)	VIP	FDR	Mean Abundance		
					Basal	Glucose	Azide
125.0245	-	8.62	2.01	4.43E-07	111.90	5689.18	3981.59
179.0564	-	8.62	2.03	1.11E-16	29633.36	1523798.87	947547.34
359.1202	-	8.62	2.02	9.75E-14	9964.82	1000480.29	592241.99
198.0975	+	8.65	1.99	0.00E+00	0.00	5151.34	3574.95
113.0246	-	8.65	2.02	5.02E-09	1765.54	112523.10	76596.49
143.0351	-	8.65	2.03	2.78E-08	1766.45	139956.32	87847.25
225.0619	-	8.65	2.01	1.12E-13	4.39	10957.81	5384.27
171.0066	-	8.67	2.07	3.48E-04	9200.10	17009.87	38167.28
312.0942	-	8.67	2.03	0.00E+00	0.00	52673.20	15014.74
351.0705	-	8.67	2.23	2.01E-06	199.89	11695.56	49838.22
491.2329	-	8.67	2.03	0.00E+00	0.00	20328.79	17957.00
300.0495	-	8.70	2.09	2.00E-06	1197.22	11698.49	1431.55
503.0930	-	8.70	2.00	2.22E-16	0.00	6270.39	6510.43
132.0304	-	8.75	1.99	1.19E-06	718063.57	331216.27	162223.11
229.0122	-	8.77	2.20	8.53E-05	1569.18	249.73	3444.51
428.0372	+	8.82	1.98	2.76E-04	1832.85	2801.07	10069.40
133.0144	-	8.82	2.03	3.66E-10	49396.84	1091831.00	845937.13
90.0551	+	8.87	2.02	3.27E-07	54333.16	137233.72	91277.74
91.0584	+	8.87	2.02	4.32E-06	1449.98	4031.27	2604.29
115.0038	-	8.87	2.02	4.11E-14	5527.34	48990.97	33711.09
347.0405	-	8.87	2.27	1.81E-09	5940.44	4496.13	16883.14
88.0405	-	8.90	2.08	6.24E-06	10057.28	15533.02	7984.71
426.0229	-	8.90	1.99	2.09E-04	8368.02	8360.99	25023.15
147.0765	+	9.05	1.91	2.10E-06	10540.80	1901.03	4682.92
133.0610	+	9.10	2.04	3.25E-08	9332.10	2449.98	1268.25
584.0896	+	9.15	2.02	1.48E-10	4068.40	18710.80	10607.17
565.0488	-	9.19	2.02	3.47E-05	39588.72	114892.85	123361.59
173.0093	-	9.27	1.91	2.70E-03	563.29	7248.25	8654.68
341.1095	-	9.30	1.95	1.75E-05	1119.86	8313.11	6858.99
365.1057	+	9.33	2.01	5.30E-04	17956.98	36927.64	20696.74
360.1502	+	9.36	2.00	3.15E-07	3177.20	11189.09	8018.63
364.0655	+	9.42	2.16	5.33E-15	17889.35	1515.85	23615.41
156.0769	+	9.45	1.99	9.87E-04	17678.75	33861.52	19677.81
191.0200	-	9.84	1.95	3.31E-04	224244.70	840333.33	493581.34
306.0756	+	10.05	2.05	2.88E-03	7652.68	8159.67	13266.98
367.8832	-	14.67	2.00	7.52E-08	40493.69	111939.00	69522.01
389.8777	-	14.67	2.00	5.82E-07	16730.37	50987.64	29971.25
401.3704	-	14.67	1.93	4.76E-05	2053.91	7567.84	4788.65

Supplementary Table 6.6 (Cont.) Details of detected ions (*m/z*) from cell extracts of MIN6 cells treated azide.

m/z	Charge	RT (min)	VIP	FDR	Mean Abundance		
					Basal	Glucose	Azide
409.8868	-	14.67	1.95	2.04E-03	1101.40	9113.85	3011.27
165.9735	-	14.70	1.96	1.03E-03	4344.10	10436.59	6611.41
325.9044	-	14.70	1.98	1.04E-04	12053.25	38475.09	18664.00
336.8954	-	14.70	1.99	1.96E-05	18796.61	56958.25	29420.84
347.8864	-	14.70	1.99	6.77E-06	63216.07	186188.41	109235.02
356.9047	-	14.70	1.99	5.77E-08	299758.53	594129.53	418533.37
378.8867	-	14.70	2.00	2.87E-07	80222.17	176951.32	124666.57
400.8685	-	14.70	1.98	6.64E-07	422784.29	901973.48	670606.01
431.8687	-	14.70	2.00	8.53E-07	7177.97	24268.65	13789.06
440.8868	-	14.70	1.98	1.40E-06	111796.09	233150.58	162838.26
484.8511	-	14.70	1.99	8.62E-07	164658.47	395367.37	254694.98
546.8259	-	14.70	1.99	1.53E-05	19065.60	53173.01	30966.21
568.8336	-	14.70	1.96	7.96E-05	5346.76	20992.51	12582.81
612.7976	-	14.70	1.99	3.58E-06	52027.80	144959.38	88901.23
380.9007	+	14.71	1.96	2.23E-03	593916.41	1129385.44	910030.22
486.8653	+	14.71	1.96	9.23E-04	274749.68	562739.07	447266.06
694.8488	+	14.71	1.97	3.65E-04	59198.45	132737.38	101976.00
632.8484	+	14.73	1.96	5.99E-04	151636.86	328104.77	257167.71

Supplementary Table 6.7 Details of detected ions (*m/z*) from cell extracts of MIN6 cells treated fluoxetine.

m/z	Charge	RT (min)	VIP	FDR	Mean		
					Basal	Glucose	Fluoxetine
533.2514	-	1.64	1.13	6.20E-08	104.70	0.00	8829.78
473.2836	-	1.67	1.09	3.07E-03	1979.99	734.75	6119.32
556.4429	+	1.71	1.09	6.44E-07	1500.53	1478.94	4264.27
460.2947	+	1.74	1.13	1.98E-05	1606.37	1444.88	8407.56
540.4464	+	1.74	1.02	8.51E-06	1682.48	1811.63	3746.87
193.0906	-	1.76	1.14	2.58E-10	0.00	31.17	4850.41
340.2485	+	1.86	1.03	1.46E-05	2074.58	3961.21	1748.48
344.2430	+	1.95	1.05	7.87E-06	5844.32	12987.77	6211.72
245.1866	+	2.04	1.10	1.09E-09	3799.29	3756.86	10081.76
314.2092	-	2.06	1.08	6.68E-04	3538.79	514.95	5137.74
590.3925	+	2.10	1.05	1.38E-12	21045.71	348.79	52.64
159.0300	-	2.12	1.10	3.66E-06	17.64	1255.51	3923.00
444.3323	+	2.13	1.04	5.62E-11	160380.79	6953.69	3874.24
634.4197	+	2.13	1.04	8.46E-12	20843.77	522.93	119.69
546.3650	+	2.13	1.05	1.75E-09	18461.68	129.92	20.49
678.4469	+	2.13	1.02	6.17E-08	16431.40	440.01	54.12
488.3586	+	2.13	1.04	8.08E-10	191533.41	7634.81	3415.45
466.4108	+	2.16	1.06	3.80E-05	3725.22	2553.06	9831.45
510.4366	+	2.16	1.07	8.28E-05	3207.22	2637.16	9719.91
532.3850	+	2.16	1.04	1.55E-11	212063.58	13625.91	10305.14
554.4634	+	2.16	1.07	1.16E-03	2181.34	1791.10	8541.46
576.4112	+	2.16	1.04	2.82E-09	196143.13	9995.67	3495.62
583.3805	+	2.16	1.01	4.13E-05	2862.16	3403.58	10287.65
752.5175	+	2.19	1.02	3.76E-05	47499.85	3907.32	512.49
664.4618	+	2.19	1.03	3.71E-09	137816.53	15747.20	8262.88
620.4376	+	2.19	1.04	1.55E-11	171600.81	13282.77	8246.38
438.3792	+	2.19	1.02	2.87E-06	8401.89	8212.68	16587.48
526.4321	+	2.19	1.03	1.54E-05	8879.03	9768.32	20081.03
570.4581	+	2.19	1.09	3.53E-07	6642.46	7867.26	24503.42
614.4841	+	2.19	1.02	3.78E-04	15027.39	11621.52	21753.22
658.5106	+	2.19	1.10	1.77E-06	2397.53	3598.72	17608.51
502.3384	+	2.21	1.03	6.13E-09	13798.44	971.16	160.61
384.7724	+	2.21	1.03	4.18E-06	1084.79	3546.94	6023.90
249.1699	+	2.21	1.06	9.03E-06	4452.10	10172.66	4314.90
291.2530	+	2.21	1.01	1.79E-04	10043.69	23381.18	9300.24
293.1962	+	2.24	1.01	2.18E-05	6762.48	12974.19	6877.83
597.3055	-	2.26	1.14	1.17E-10	1966.34	0.00	16973.06
316.2122	+	2.27	1.02	1.69E-09	5164.57	15773.02	14944.38

Supplementary Table 6.7 (Cont.) Details of detected ions (*m/z*) from cell extracts of MIN6 cells treated fluoxetine.

m/z	Charge	RT (min)	VIP	FDR	Mean		
					Basal	Glucose	Fluoxetine
243.1830	+	2.30	1.07	2.86E-11	1328.99	9857.31	6257.98
455.2902	+	2.30	1.10	7.05E-04	439.85	11443.36	305.24
309.2273	+	2.30	1.05	5.04E-06	15623.56	39143.43	17448.87
251.1855	+	2.32	1.01	4.01E-05	91994.91	180998.45	96397.99
295.2114	+	2.32	1.06	2.05E-05	1654.07	4868.63	2051.23
302.1964	+	2.35	1.09	4.75E-10	1307.60	4879.37	2298.38
205.0796	+	2.41	1.05	3.88E-10	1401.39	5949.56	6492.54
237.1698	+	2.41	1.02	1.01E-05	7650.27	16530.80	8635.34
325.2487	+	2.44	1.09	8.12E-05	1823.11	3690.14	10368.36
209.1386	+	2.44	1.04	3.67E-06	3819.34	9123.05	4064.20
223.1542	+	2.47	1.03	9.43E-06	3128.72	7204.81	3698.77
216.1960	+	2.47	1.01	3.45E-05	3447.04	8585.83	3266.40
344.2281	+	2.55	1.01	6.85E-07	55005.41	86614.40	30720.29
300.2018	+	2.57	1.02	2.38E-06	74012.90	128598.21	53845.38
284.2068	+	2.60	1.04	4.59E-05	25054.34	52943.52	28390.31
260.1858	+	2.60	1.02	3.82E-06	8154.62	99365.94	76743.43
246.2428	+	2.60	1.06	6.06E-07	32027.96	68605.73	24418.01
139.0503	+	2.60	1.11	1.75E-09	1541.03	3143.61	10199.77
343.2958	+	2.60	1.05	5.23E-06	33629.89	35491.53	87492.75
196.1546	+	2.60	1.08	3.82E-05	19704.38	38138.56	16531.39
261.1962	+	3.61	1.13	1.97E-07	20.93	8180.55	184.97
202.1804	+	3.87	1.05	5.84E-09	3603.83	15828.83	13537.56
246.1702	+	6.48	1.02	2.54E-07	6091.96	20165.09	28555.70
232.1546	+	6.65	1.06	8.32E-11	13389.44	67145.28	81379.10
166.0864	+	7.19	1.03	4.03E-03	42593.42	44477.80	71229.50
120.0809	+	7.22	1.10	1.74E-03	3236.89	2829.26	5725.67
707.0767	+	7.37	1.01	1.43E-03	24977.99	50030.52	26085.36
125.0012	-	7.47	1.06	2.26E-04	421.55	6511.89	4457.79
244.0933	+	7.61	1.01	4.71E-06	84166.17	41743.30	79385.72
112.0507	+	7.61	1.05	6.30E-06	25940.32	9546.64	24110.00
150.0583	+	7.63	1.09	1.45E-03	34866.34	22566.86	59760.37
205.0973	+	7.75	1.03	4.14E-03	43893.80	22336.81	57094.95
130.0864	+	7.94	1.04	4.43E-08	1930.73	4170.16	5400.91
348.0706	+	8.04	1.05	1.63E-14	328111.68	98261.28	96341.14
284.0991	+	8.04	1.01	6.83E-06	2977.24	2594.54	4884.17
346.0564	-	8.22	1.06	6.36E-13	265428.94	58338.33	70840.79
286.0607	-	8.22	1.06	1.21E-07	82.04	22921.88	25276.26
117.0195	-	8.24	1.05	2.90E-08	13772.29	36983.33	48405.70

Supplementary Table 6.7 (Cont.) Details of detected ions (*m/z*) from cell extracts of MIN6 cells treated fluoxetine.

m/z	Charge	RT (min)	VIP	FDR	Mean		
					Basal	Glucose	Fluoxetine
147.0494	-	8.40	1.05	2.50E-03	29282.57	74977.54	81215.57
382.1013	-	8.45	1.03	1.02E-06	4103.26	12916.47	12552.49
326.1098	-	8.47	1.08	0.00E+00	0.00	341478.64	266095.08
148.0605	+	8.47	1.01	2.05E-03	910510.31	1977602.66	2182738.20
304.0712	-	8.52	1.08	1.63E-12	837.14	478371.84	301930.11
242.0521	-	8.55	1.10	8.57E-14	189.77	36513.81	14471.46
101.0245	-	8.60	1.09	1.73E-14	8210.50	257921.67	163094.41
179.0564	-	8.62	1.10	1.11E-16	29633.36	1523798.87	854758.35
125.0245	-	8.62	1.07	5.46E-07	111.90	5689.18	3520.48
113.0246	-	8.65	1.09	6.62E-09	1765.54	112523.10	68086.92
143.0351	-	8.65	1.09	3.49E-08	1766.45	139956.32	78533.36
225.0619	-	8.65	1.08	1.35E-13	4.39	10957.81	4648.66
608.0898	+	8.67	1.02	1.09E-04	168981.10	232660.93	299484.07
312.0942	-	8.67	1.04	0.00E+00	0.00	52673.20	35991.82
351.0705	-	8.67	1.10	3.20E-06	199.89	11695.56	37680.33
491.2329	-	8.67	1.07	0.00E+00	0.00	20328.79	16743.39
323.0292	-	8.67	1.09	2.11E-05	45363.15	71548.47	125178.75
300.0495	-	8.70	1.11	1.30E-05	1197.22	11698.49	675.57
503.0930	-	8.70	1.11	0.00E+00	0.00	6270.39	16320.58
133.0144	-	8.82	1.06	3.02E-10	49396.84	1091831.00	1178395.54
90.0551	+	8.87	1.04	1.10E-07	54333.16	137233.72	134512.48
91.0584	+	8.87	1.04	5.25E-07	1449.98	4031.27	4060.59
115.0038	-	8.87	1.06	1.20E-13	5527.34	48990.97	49932.10
347.0405	-	8.87	1.09	9.57E-07	5940.44	4496.13	11595.35
584.0896	+	9.15	1.06	5.91E-13	4068.40	18710.80	22763.22
565.0488	-	9.19	1.09	2.98E-07	39588.72	114892.85	246037.41
173.0093	-	9.27	1.02	1.16E-03	563.29	7248.25	18739.05
365.1057	+	9.33	1.03	4.08E-04	17956.98	36927.64	19485.06
106.0500	+	9.33	1.04	9.73E-04	6644.12	14664.76	18496.33
364.0655	+	9.42	1.06	3.45E-14	17889.35	1515.85	8961.25
176.1031	+	9.45	1.12	1.69E-13	2518.71	4023.06	14071.24
191.0200	-	9.84	1.02	6.77E-06	224244.70	840333.33	1239770.11
306.0756	+	10.05	1.01	1.04E-03	7652.68	8159.67	14656.58
598.0688	+	10.23	1.06	1.81E-06	4787.45	6785.12	10010.42
401.3704	-	14.67	1.04	1.34E-04	2053.91	7567.84	2479.25
367.8832	-	14.67	1.09	2.13E-07	40493.69	111939.00	47866.11
389.8777	-	14.67	1.09	1.20E-06	16730.37	50987.64	19699.53
165.9735	-	14.70	1.06	2.18E-05	4344.10	10436.59	5228.97

Supplementary Table 6.7 (Cont.) Details of detected ions (*m/z*) from cell extracts of MIN6 cells treated fluoxetine.

m/z	Charge	RT (min)	VIP	FDR	Mean		
					Basal	Glucose	Fluoxetine
325.9044	-	14.70	1.05	3.53E-05	12053.25	38475.09	12154.11
336.8954	-	14.70	1.06	9.12E-06	18796.61	56958.25	20393.63
347.8864	-	14.70	1.08	4.28E-06	63216.07	186188.41	69824.08
356.9047	-	14.70	1.08	3.32E-08	299758.53	594129.53	333827.94
378.8867	-	14.70	1.09	3.16E-07	80222.17	176951.32	96040.92
400.8685	-	14.70	1.07	2.84E-06	422784.29	901973.48	504481.10
431.8687	-	14.70	1.08	1.62E-06	7177.97	24268.65	9441.59
440.8868	-	14.70	1.07	3.43E-07	111796.09	233150.58	128912.06
484.8511	-	14.70	1.07	8.91E-07	164658.47	395367.37	186209.72
546.8259	-	14.70	1.07	6.00E-06	19065.60	53173.01	21381.93
568.8336	-	14.70	1.05	1.71E-04	5346.76	20992.51	6255.48
612.7976	-	14.70	1.08	4.86E-06	52027.80	144959.38	60964.95
380.9007	+	14.71	1.05	3.79E-03	593916.41	1129385.44	719963.83
486.8653	+	14.71	1.05	1.80E-03	274749.68	562739.07	346650.36
694.8488	+	14.71	1.06	5.48E-04	59198.45	132737.38	77542.77
632.8484	+	14.73	1.04	1.07E-03	151636.86	328104.77	194429.21

REFERENCES

1. Zhang A, Sun H, Yan G, Wang P, Wang X. Metabolomics for Biomarker Discovery: Moving to the Clinic. Biomed Res Int. 2015;1–6.

2. Rahman M, Hasan MR. Cancer Metabolism and Drug Resistance. Metabolites. 2015;5(4):571–600.

3. Spratlin JL, Serkova NJ, Gail Eckhardt S. Clinical Applications of Metabolomics in Oncology: A Review. Clin Cancer Res. 2009 2009;15(2):431–440.

4. Medina-Cleghorn D, Nomura DK. Exploring Metabolic Pathways and Regulation through Functional Chemoproteomic and Metabolomic Platforms. Chem Biol. 2014;21(9):1171–1184.

5. Birkemeyer C, Luedemann A, Wagner C, Erban A, Kopka J. Metabolome analysis: The potential of in vivo labeling with stable isotopes for metabolite profiling. Trends Biotechnol. 2005;23(1):28–33.

6. Gowda GAN, Djukovic D. Overview of Mass Spectrometry-Based Metabolomics: Opportunities and Challenges. Methods Mol Biol. 2014;1198:3–12.

7. Dettmer K, Aronov PA, Hammock BD. MASS SPECTROMETRY-BASED METABOLOMICS. Mass Spectrom Rev. 2007;26(1):51–

78.

8. Griffiths WJ, Koal T, Wang Y, Kohl M, Enot DP, Deigner H-P. Targeted Metabolomics for Biomarker Discovery. Angew Chemie Int Ed .2010;49(32):5426–5445.

9. Roberts LD, Souza AL, Gerszten RE, Clish CB. Targeted Metabolomics. Curr Protoc Mol Biol. 2012;CHAPTER:Unit30.2-Unit30.2.

10. Lu W, Bennett BD, Rabinowitz JD. Analytical strategies for LC–MS-based targeted metabolomics. J Chromatogr B. 2008;871(2):236–242.

11. Dudley E, Yousef M, Wang Y, Griffiths WJ. Targeted metabolomics and mass spectrometry. Adv Protein Chem Struct Biol. Netherlands; 2010;80:45–83.

12. Sheridan H, Krenn L, Jiang R, Sutherland I, Ignatova S, Marmann A, et al. The potential of metabolic fingerprinting as a tool for the modernisation of TCM preparations. J Ethnopharmacol. 2012;140(3):482–491.

13. Kosmides AK, Kamisoglu K, Calvano SE, Corbett SA, Androulakis IP. Metabolomic Fingerprinting: Challenges and Opportunities. Crit Rev Biomed Eng. 2013;41(3):205–221.

14. Ellis DI, Dunn WB, Griffin JL, Allwood JW, Goodacre R. Metabolic fingerprinting as a diagnostic tool.

Pharmacogenomics. England; 2007;8(9):1243–1266.

15. Ellis DI, Goodacre R. Metabolic fingerprinting in disease diagnosis: biomedical applications of infrared and Raman spectroscopy. Analyst. England; 2006;131(8):875–885.

16. Christians U, Klawitter J, Hornberger A, Klawitter J. How unbiased is non-targeted metabolomics and is targeted pathway screening the solution. Curr Pharm Biotechnol. Netherlands; 2011;12(7):1053–1066.

17. Jun H, Raju D, Sammy C and CHB. Mass spectrometry-based technologies for high-throughput metabolomic. Bioanalysis. 2009;1(9):1665–1684.

18. Cajka T, Fiehn O. Toward Merging Untargeted and Targeted Methods in Mass Spectrometry-Based Metabolomics and Lipidomics. Anal Chem. 2016;88(1):524–545.

19. Pan Z, Raftery D. Comparing and combining NMR spectroscopy and mass spectrometry in metabolomics. Anal Bioanal Chem. 2007;387(2):525–527.

20. Dieterle F, Riefke B, Schlotterbeck G, Ross A, Senn H, Amberg A. NMR and MS Methods for Metabonomics BT - Drug Safety Evaluation: Methods and Protocols. In: Gautier J-C, editor. Totowa, NJ: Humana Press; 2011:385–415.

21. Lei Z, Huhman D V, Sumner LW. Mass spectrometry strategies

in metabolomics. J Biol Chem. 2011;286(29):25435–25442.

22. Imperlini E, Santorelli L, Orrù S, Scolamiero E, Ruoppolo M, Caterino M. Mass Spectrometry-Based Metabolomic and Proteomic Strategies in Organic Acidemias. 2016.

23. Huang M-Z, Yuan C-H, Cheng S-C, Cho Y-T, Shiea J. Ambient Ionization Mass Spectrometry. Annu Rev Anal Chem [Internet]. Annual Reviews; 2010;3(1):43–65.

24. Tsugawa H, Tsujimoto Y, Sugitate K, Sakui N, Nishiumi S, Bamba T, et al. Highly sensitive and selective analysis of widely targeted metabolomics using gas chromatography/triple-quadrupole mass spectrometry. J Biosci Bioeng. 2014;117(1):122–128.

25. Hu Q, Noll RJ, Li H, Makarov A, Hardman M, Graham Cooks R. The Orbitrap: a new mass spectrometer. J Mass Spectrom. 2005;40(4):430–443.

26. Crutchfield CA, Thomas SN, Sokoll LJ, Chan DW. Advances in mass spectrometry-based clinical biomarker discovery. Clin Proteomics. 2016;13(1):1.

27. Kingdon KH. A Method for the Neutralization of Electron Space Charge by Positive Ionization at Very Low Gas Pressures. Phys Rev. 1923;21(4):408–418.

28. Knight RD. Storage of ions from laser produced plasmas. Appl

Phys Lett. American Institute of Physics; 1981 Feb 15;38(4):221–223.

29. Makarov A. Electrostatic Axially Harmonic Orbital Trapping:□ A High-Performance Technique of Mass Analysis. Anal Chem. 2000;72(6):1156–1162.

30. Makarov A, Scigelova M. Coupling liquid chromatography to Orbitrap mass spectrometry. J Chromatogr A. 2010;1217(25):3938–3945.

31. Patti GJ. Separation strategies for untargeted metabolomics. J Sep Sci. 2011;34(24):3460–3469.

32. Kuehnbaum NL, Britz-McKibbin P. New Advances in Separation Science for Metabolomics: Resolving Chemical Diversity in a Post-Genomic Era. Chem Rev. 2013;113(4):2437–2468.

33. Iwasaki Y, Sawada T, Hatayama K, Ohyagi A, Tsukuda Y, Namekawa K, et al. Separation Technique for the Determination of Highly Polar Metabolites in Biological Samples. Metabolites. 2012;2(4):496–515.

34. Zhou B, Xiao JF, Tuli L, Ressom HW. LC-MS-based metabolomics. Mol BioSyst. 2012;8(2):470–81.

35. Becker S, Kortz L, Helmschrodt C, Thiery J, Ceglarek U. LC–MS-based metabolomics in the clinical laboratory. J Chromatogr B. 2012;883–884:

36. Fujimori T, Sasaki K. LC-MS-based Metabolomics BT - Encyclopedia of Systems Biology. In: Dubitzky W, Wolkenhauer O, Cho K-H, Yokota H, editors. New York, NY: Springer New York; 2013:1109–1111.

37. Mirnaghi FS, Caudy AA. Challenges of analyzing different classes of metabolites by a single analytical method. Bioanalysis. 2014;6(24):3393–3416.

38. Aretz I, Meierhofer D. Advantages and Pitfalls of Mass Spectrometry Based Metabolome Profiling in Systems Biology. Han T-L (Morgan), editor. Int J Mol Sci. 2016;17(5):632.

39. Ackermann BL, Berna MJ, Eckstein JA, Ott LW, Chaudhary AK. Current Applications of Liquid Chromatography/Mass Spectrometry in Pharmaceutical Discovery After a Decade of Innovation. Annu Rev Anal Chem. 2008;1(1):357–96.

40. Piteni AI, Kouskoura MG. HILIC Chromatography – An Insight on the Retention Mechanism. J Chromatogr & Sep Tech. 2016;7(3).

41. Isabelle K, Rico J.E. Derks MG. The Rise of Hydrophilic Interaction Chromatography in Untargeted Clinical Metabolomics. LCGC Eur. 2016;30(1):60–75.

42. Wernisch S, Pennathur S. Evaluation of coverage, retention patterns, and selectivity of seven liquid chromatographic

methods for metabolomics. Anal Bioanal Chem. Germany; 2016;408(22):6079–6091.

43. Shubhakar A, Kozak RP, Reiding KR, Royle L, Spencer DIR, Fernandes DL, et al. Automated High-Throughput Permethylation for Glycosylation Analysis of Biologics Using MALDI-TOF-MS. Anal Chem. 2016 .

44. Gunda V, Yu F, Singh PK. Validation of Metabolic Alterations in Microscale Cell Culture Lysates Using Hydrophilic Interaction Liquid Chromatography (HILIC)-Tandem Mass Spectrometry-Based Metabolomics. PLoS One. 2016;11(4):e0154416.

45. Gao S, Yang R, Peng Z, Lu H, Li N, Ding J, et al. Metabolomics analysis for hydroxy-L-proline-induced calcium oxalate nephrolithiasis in rats based on ultra-high performance liquid chromatography quadrupole time-of-flight mass spectrometry. Sci Rep. England; 2016;6:30142.

46. Deda O, Chatziioannou AC, Fasoula S, Palachanis D, Raikos N, Theodoridis GA, et al. Sample preparation optimization in fecal metabolic profiling. J Chromatogr B, Anal Technol Biomed life Sci. 2016 .

47. Zhang T, Watson DG. Evaluation of the technical variations and the suitability of a hydrophilic interaction liquid chromatography-high resolution mass spectrometry (ZIC-

pHILIC-Exactive orbitrap) for clinical urinary metabolomics study. J Chromatogr B, Anal Technol Biomed life Sci. 2016;1022:199–205.

48. Tang D-Q, Zou L, Yin X-X, Ong CN. HILIC-MS for metabolomics: An attractive and complementary approach to RPLC-MS. Mass Spectrom Rev. 2016;35(5):574–600.

49. Xiao JF, Zhou B, Ressom HW. Metabolite identification and quantitation in LC-MS/MS-based metabolomics. Trends Analyt Chem. 2012;32:1–14.

50. Draper J, Enot DP, Parker D, Beckmann M, Snowdon S, Lin W, et al. Metabolite signal identification in accurate mass metabolomics data with MZedDB, an interactive m/z annotation tool utilising predicted ionisation behaviour "rules." BMC Bioinformatics. 2009;10(1):1–16.

51. May JC, McLean JA. Advanced Multidimensional Separations in Mass Spectrometry: Navigating the Big Data Deluge. Annu Rev Anal Chem. 2016;9(1):387–409.

52. van den Berg R a, Hoefsloot HCJ, Westerhuis J a, Smilde AK, van der Werf MJ. Centering, scaling, and transformations: improving the biological information content of metabolomics data. BMC Genomics. 2006;7:142.

53. Stein SE. An integrated method for spectrum extraction and

compound identification from gas chromatography/mass spectrometry data. J Am Soc Mass Spectrom. 1999;10(8):770–781.

54. Shurubor YI, Paolucci U, Krasnikov BF, Matson WR, Kristal BS. Analytical precision, biological variation, and mathematical normalization in high data density metabolomics. Metabolomics. 2005;1(1):75–85.

55. Worley B, Powers R. Multivariate Analysis in Metabolomics. Curr Metabolomics. 2013;1(1):92–107.

56. Johnstone IM, Titterington DM. Statistical challenges of high-dimensional data. Philosophical transactions. Series A, Mathematical, physical, and engineering sciences. England; 2009. p. 4237–53.

57. Zhang A, Sun H, Yan G, Wang P, Wang X. Mass spectrometry-based metabolomics: Applications to biomarker and metabolic pathway research. Biomed Chromatogr. 2016;30(1):7–12.

58. Tebani A, Abily-Donval L, Afonso C, Marret S, Bekri S. Clinical Metabolomics: The New Metabolic Window for Inborn Errors of Metabolism Investigations in the Post-Genomic Era. Int J Mol Sci. 2016;17(7):1167.

59. Zhang A, Sun H, Xu H, Qiu S, Wang X. Cell metabolomics. OMICS. 2013;17(10):495–501.

60. Halama A. Metabolomics in cell culture—A strategy to study crucial metabolic pathways in cancer development and the response to treatment. Arch Biochem Biophys. 2014;564:100–109.

61. Cuperlovic-Culf M, Barnett DA, Culf AS, Chute I. Cell culture metabolomics: applications and future directions. Drug Discov Today. 2010;15(15–16):610–621.

62. Sweet B V, Schwemm AK, Parsons DM. Review of the processes for FDA oversight of drugs, medical devices, and combination products. J Manag Care Pharm. 2011;17(1):40–50.

63. Singh SS. Preclinical pharmacokinetics: an approach towards safer and efficacious drugs. Curr Drug Metab. 2006;7(2):165–182.

64. Attia SM. Deleterious effects of reactive metabolites. Oxid Med Cell Longev. 2010;3(4):238–53.

65. Pugsley MK, Authier S, Curtis MJ. Principles of Safety Pharmacology. Br J Pharmacol. 2008;154(7):1382–1399.

66. Paul SM, Mytelka DS, Dunwiddie CT, Persinger CC, Munos BH, Lindborg SR, et al. How to improve R&D productivity: the pharmaceutical industry's grand challenge. Nat Rev Drug Discov. 2010;9(3):203–214.

67. Tolstikov V. Metabolomics: Bridging the Gap between Pharmaceutical Development and Population Health. Metabolites. 2016;6(3):20.

68. Wishart DS. Emerging applications of metabolomics in drug discovery and precision medicine. Nat Rev Drug Discov. 2016;15(7):473–484.

69. Miyamoto S, Duncan GE, Marx CE, Lieberman JA. Treatments for schizophrenia: a critical review of pharmacology and mechanisms of action of antipsychotic drugs. Mol Psychiatry. 2004;10(1):79–104.

70. Meltzer HY. Update on typical and atypical antipsychotic drugs. Annu Rev Med. 2013;64:393–406.

71. Leucht S, Cipriani A, Spineli L, Mavridis D, Örey D, Richter F, et al. Comparative efficacy and tolerability of 15 antipsychotic drugs in schizophrenia: a multiple-treatments meta-analysis. Lancet. 2016;382(9896):951–962.

72. Liperoti R, Pedone C, Corsonello A. Antipsychotics for the Treatment of Behavioral and Psychological Symptoms of Dementia (BPSD). Curr Neuropharmacol. 2008;6(2):117–124.

73. Ban TA. Fifty years chlorpromazine: a historical perspective. Neuropsychiatr Dis Treat. 2007;3(4):495–500.

74. Donlon PT, Hopkin J, Tupin JP. Overview: Efficacy and safety

of the rapid neuroleptization method with injectable haloperidol. The American Journal of Psychiatry. U1979.:273–278.

75. Ayd FJ. Haloperidol: Twenty years' clinical experience. Journal of Clinical Psychiatry. 1978:807–814.

76. Tardy M, Huhn M, Kissling W, Engel RR, Leucht S. Haloperidol versus low-potency first-generation antipsychotic drugs for schizophrenia. Adv Psychiatr Treat. 2014;20(5):296.

77. Scarff JR, Casey DA. Newer Oral Atypical Antipsychotic Agents: A Review. Pharm Ther. 2011;36(12):832–838.

78. Meltzer HY. An overview of the mechanism of action of clozapine. Journal of Clinical Psychiatry. 1994:47–52.

79. Byerly MJ, DeVane CL. Pharmacokinetics of Clozapine and Risperidone: A Review of Recent Literature. J Clin Psychopharmacol. 1996;16(2).

80. Janssen PA, Niemegeers CJ, Awouters F, Schellekens KH, Megens AA, Meert TF. Pharmacology of risperidone (R 64 766), a new antipsychotic with serotonin-S2 and dopamine-D2 antagonistic properties. J Pharmacol Exp Ther. 1988;244(2):685–693.

81. Ereshefsky L, Lacombe S. Pharmacological profile of risperidone. The Canadian Journal of Psychiatry / La Revue

canadienne de psychiatrie. 1993:S80–88.

82. Levine M, Ruha AM. Overdose of atypical antipsychotics: Clinical presentation, mechanisms of toxicity and management. CNS Drugs. 2012;26(7):601–611.

83. Minns AB, Clark RF. Toxicology and overdose of atypical antipsychotics. J Emerg Med. 2012;43(5):906–913.

84. Murphy SL, Xu J, Kochanek KD, Statistics V. National Vital Statistics Reports Deaths : Final Data for 2010. 2013;61(4).

85. Fearn V. Deaths Related to Drug Poisoning in England and Wales : 2014 registrations. 2015;1–30.

86. Elmorsy E, Elzalabany LM, Elsheikha HM, Smith PA. Adverse effects of antipsychotics on micro-vascular endothelial cells of the human blood-brain barrier. Brain Res. 2014;1583:255–68.

87. Elmorsy E, Smith PA. Bioenergetic disruption of human micro-vascular endothelial cells by antipsychotics. Biochem Biophys Res Commun. 2015;460(3):857–862.

88. Abbott NJ, Patabendige AAK, Dolman DEM, Yusof SR, Begley DJ. Structure and function of the blood-brain barrier. Neurobiol Dis. 2010;37(1):13–25.

89. Abbott NJ. Physiology of the blood-brain barrier and its consequences for drug transport to the brain. Int Congr Ser.

2005;1277:3–18.

90. Marchi N, Angelov L, Masaryk T, Fazio V, Granata T, Hernandez N, et al. Seizure-promoting effect of blood-brain barrier disruption. Epilepsia. 2007;48(4):732–742.

91. Abdul Muneer PM, Alikunju S, Szlachetka AM, Murrin LC, Haorah J. Impairment of brain endothelial glucose transporter by methamphetamine causes blood-brain barrier dysfunction. Mol Neurodegener. 2011;6:23.

92. Ben-Shachar D, Livne E, Spanier I, Leenders KL, Youdim MB. Typical and atypical neuroleptics induce alteration in blood-brain barrier and brain 59FeCl3 uptake. J Neurochem. 1994;62:1112–1118.

93. Pardridge WM, Crawford IL, Connor JD. Permeability Changes Induced by Nortriptyline in the Blood-Brain Barrier or parenteral loading with its percursor , L-dopa , especially when peripherally acting dopa decarboxylase inhibitors are administered concurrently (Lotti and Porter , 1970). Somew. 1973;49–57.

94. Anderson N, Borlak J. Drug-induced phospholipidosis. FEBS Lett. 2006;580(23):5533–5540.

95. Halliwell WH. Cationic amphiphilic drug-induced phospholipidosis. Toxicol Pathol. 1997;25(1):53–60.

96. Muehlbacher M, Tripal P, Roas F, Kornhuber J. Identification of Drugs Inducing Phospholipidosis by Novel in vitro Data. ChemMedChem. 2012;7(11):1925–1934.

97. Reasor MJ, Hastings KL, Ulrich RG. Drug-induced phospholipidosis: issues and future directions. Expert Opin Drug Saf. England; 2006;5(4):567–583.

98. Sellers WR, Fisher DE. Apoptosis and cancer drug targeting. J Clin Invest. 1999;104(12):1655–1661.

99. Rick A, Tracie B, Louise AB, Stacey F, Rachel AF, Ted G, Mia MG, Joan K, Chun CL, Marji M, Kimberly M, Lisa AN, Dearell N, Anthony, Piercy C, Richards AX. Breast Cancer Facts & Figures 2015-2016. Atlanta, Geogria; 2016.

100. McPherson, K; Stell, CM DJ. Breast Cancer-Epidermiology, Risk Factors and Genetics Risk Factors for Breast Cancer. Br Med J. 2000;321(9):624–628.

101. Sledge GW, Mamounas EP, Health F, Hortobagyi GN, Burstein HJ. Past , Present , and Future Challenges in Breast Cancer Treatment. J Clin Oncol. 2014;32(19):1979–1986.

102. Yeo B, Turner NC, Jones A. An update on the medical management of breast cancer. BMJ Br Med J. 2014;348.

103. Sugar AM, Caffrey RPMC. Antifungal Activity of 3 J - Deoxyadenosine (Cordycepin)†. 1998;42(6):1424–1427.

104. Choi S, Lim M-H, Kim KM, Jeon BH, Song WO, Kim TW. Cordycepin-induced apoptosis and autophagy in breast cancer cells are independent of the estrogen receptor. Toxicol Appl Pharmacol. 2011;257(2):165–173.

105. Choi YH, Kim G-Y, Lee HH. Anti-inflammatory effects of cordycepin in lipopolysaccharide-stimulated RAW 264.7 macrophages through Toll-like receptor 4-mediated suppression of mitogen-activated protein kinases and NF-kappaB signaling pathways. Drug Des Devel Ther. 2014;8:1941–1953.

106. Jeong JW, Jin CY, Kim GY, Lee JD, Park C, Kim G Do, et al. Anti-inflammatory effects of cordycepin via suppression of inflammatory mediators in BV2 microglial cells. Int Immunopharmacol. 2010;10(12):1580–1586.

107. Jeong MH, Lee CM, Lee SW, Seo SY, Seo MJ, Kang BW, et al. Cordycepin-enriched Cordyceps militaris induces immunomodulation and tumor growth delay in mouse-derived breast cancer. Oncol Rep. 2013;30(4):1996–2002.

108. Ko BS, Lu YJ, Yao WL, Liu TA, Tzean SS, Shen TL, et al. Cordycepin Regulates GSK-3-beta,beta-Catenin Signaling in Human Leukemia Cells. PLoS One. 2013;8(9):1–7.

109. Kredich NM. Inhibition of nucleic acid methylation by

cordycepin. J Biol Chem. 1980;255(15):7380–7385.

110. Lee JH, Hong SM, Yun JY, Myoung H, Kim M-J. Anti-Cancer Effects of Cordycepin on Oral Squamous Cell Carcinoma Proliferation and Apoptosis in Vitro. J Cancer Ther 2011;2(2):224–234.

111. Lee SY, Debnath T, Kim SK, Lim B. Anti-cancer effect and apoptosis induction of cordycepin through DR3 pathway in the human colonic cancer cell HT-29. Food Chem Toxicol. 2013;60:439–447.

112. Wang D, Zhang Y, Lu J, Wang Y, Wang J, Meng Q, et al. Cordycepin, a Natural Antineoplastic Agent, Induces Apoptosis of Breast Cancer Cells via Caspase-dependent Pathways. Nat Prod Commun. 2016;11(1):63–68.

113. Lee HJ, Burger P, Vogel M, Friese K, Brüning A. The nucleoside antagonist cordycepin causes DNA double strand breaks in breast cancer cells. Invest New Drugs. 2012;30(5):1917–1925.

114. Lu H, Li X, Zhang J, Shi H, Zhu X, He X. Effects of cordycepin on HepG2 and EA.hy926 cells: Potential antiproliferative, antimetastatic and anti-angiogenic effects on hepatocellular carcinoma. Oncol Lett. 2014;7:1556–1562.

115. Thomadaki H, Tsiapalis CM, Scorilas A. Polyadenylate

polymerase modulations in human epithelioid cervix and breast cancer cell lines, treated with etoposide or cordycepin, follow cell cycle rather than apoptosis induction. Biol Chem. 2005;386(5):471–480.

116. Noh, E., Youn, H. j., Jung, S. H., Han, J., jeong, y., Chung, E., Jung, J., Kim, B., Lee, S., Lee, Y., Kim J. Cordycepin inhibits TPA-induced matrix metalloproteinase-9 expression by suppressing the MAPK/AP-1 pathway in MCF-7 human breast cancer cells. Int J Mol Med. 2010;25(2):255–260.

117. Cristalli G, Costanzi S, Lambertucci C, Lupidi G, Vittori S, Volpini R, et al. Adenosine deaminase: functional implications and different classes of inhibitors. Med Res Rev. 2001;21(2):105–128.

118. Frederiksen S, MALLING H, KLENOW H. ISOLATION OF 3'-DEOXYADENOSINE (CORDYCEPIN) FROM THE LIQUID MEDIUM OF CORDYCEPS MILITARIS (L. EX FR.) LINK. Biochim Biophys Acta. 1965 Feb;95:189–193.

119. Rodman LE, Farnell DR, Coyne JM, Allan PW, Hill DL, Duncan KL, et al. Toxicity of cordycepin in combination with the adenosine deaminase inhibitor 2'-deoxycoformycin in beagle dogs. Toxicol Appl Pharmacol. 1997;147(1):39–45.

120. Sm C, Kl G. Fluoxetine: a review of its therapeutic potential in

the treatment of depression associated with physical illness. Drugs. 2001;61(1):81–110.

121. Yamada J, Sugimoto Y, Inoue K. Selective serotonin reuptake inhibitors fluoxetine and fluvoxamine induce hyperglycemia by different mechanisms. Eur J Pharmacol. 1999;382(3):211–215.

122. Isaac R, Boura-Halfon S, Gurevitch D, Shainskaya A, Levkovitz Y, Zick Y. Selective serotonin reuptake inhibitors (SSRIs) inhibit insulin secretion and action in pancreatic beta cells. J Biol Chem. 2013;288(8):5682–5693.

123. Biagetti B, Corcoy R. Hypoglycemia associated with fluoxetine treatment in a patient with type 1 diabetes. World J Clin cases. 2013;1(5):169–171.

124. De Long NE, Hyslop JR, Raha S, Hardy DB, Holloway AC. Fluoxetine-induced pancreatic beta cell dysfunction: New insight into the benefits of folic acid in the treatment of depression. J Affect Disord. 2014;166:6–13.

125. Cataldo LR, Cortes VA, Mizgier ML, Aranda E, Mezzano D, Olmos P, et al. Fluoxetine impairs insulin secretion without modifying extracellular serotonin levels in MIN6 beta-cells. Exp Clin Endocrinol Diabetes. 2015;123(8):473–478.

126. Paul S. University of Nottingham, Nottingham UK. Fluoxetine

and clomipramine inhibit mitochondrial respiration in a murine pancreatic beta-cell line. Fluoxetine and clomipramine inhibit mitochondrial respiration in a murine pancreatic beta-cell line. 2008:2008.

127. Goren HJ. Role of insulin in glucose-stimulated insulin secretion in beta cells. Curr Diabetes Rev. 2005;1(3):309–330.

128. German MS. Glucose sensing in pancreatic islet beta cells: the key role of glucokinase and the glycolytic intermediates. Proc Natl Acad Sci U S A. 1993;90(5):1781–1785.

129. Korfmacher WA. Foundation review: Principles and applications of LC-MS in new drug discovery. Drug Discov Today. 2005;10(20):1357–1367.

130. Kumar PR, Dinesh SR, Rini R. Lcms- a Review and a Recent Update. 2016;5(5):377–391.

131. Pitt JJ. Principles and Applications of Liquid Chromatography-Mass Spectrometry in Clinical Biochemistry. Clin Biochem Rev. 2009;30(1):19–34.

132. Ponnayyan SS, Sharma K, Mullangi R, Sukumaran SK. Review of the validated HPLC and LC-MS/MS methods for determination of drugs used in clinical practice for Alzheimer's disease. Biomed Chromatogr. 2014;28(11):1431–1490.

133. Zhou S, Song Q, Tang Y, Naidong W. Critical Review of Development, Validation, and Transfer for High Throughput Bioanalytical LC-MS/MS Methods. Curr Pharm Anal. 2005;1(1):3–14.

134. Cubbon S, Antonio C, Wilson J, Thomas-Oates J. Metabolomic applications of HILIC-LC-MS. Mass Spectrom Rev. 2010;29(5):671–684.

135. Creek DJ, Jankevics A, Breitling R, Watson DG, Barrett MP, Burgess KE V. Toward Global Metabolomics Analysis with Hydrophilic Interaction Liquid Chromatography–Mass Spectrometry: Improved Metabolite Identification by Retention Time Prediction. Anal Chem. 2011;83(22):8703–8710.

136. Contrepois K, Jiang L, Snyder M. Optimized Analytical Procedures for the Untargeted Metabolomic Profiling of Human Urine and Plasma by Combining Hydrophilic Interaction and Reverse-Phase Liquid Chromatography - Mass Spectrometry. Mol Cell Proteomics. 2015.

137. Dejaegher B, Vander Heyden Y. HILIC methods in pharmaceutical analysis. J Sep Sci. 2010;33(6–7):698–715.

138. Fei F, Bowdish DME, McCarry BE. Comprehensive and simultaneous coverage of lipid and polar metabolites for endogenous cellular metabolomics using HILIC-TOF-MS. Anal

Bioanal Chem. 2014;406(15):3723–3733.

139. Bajad S, Shulaev V. LC-MS-based metabolomics. Methods Mol Biol. 2011;708:213–228.

140. Nakanishi H, Ogiso H, Taguchi R. Qualitative and quantitative analyses of phospholipids by LC-MS for lipidomics. Methods Mol Biol. 2009;579:287–313.

141. Milne S, Ivanova P, Forrester J, Alex Brown H. Lipidomics: an analysis of cellular lipids by ESI-MS. Methods. 2006;39(2):92–103.

142. Haoula Z, Ravipati S, Stekel DJ, Ortori CA, Hodgman C, Daykin C, et al. Lipidomic analysis of plasma samples from women with polycystic ovary syndrome. Metabolomics. 2015;11(3):657–666.

143. Bligh EG, Dyer WJ. A rapid method of total lipid extraction and purification. Can J Biochem Physiol. 1959;37:911–917.

144. Muller DC, Degen C, Scherer G, Jahreis G, Niessner R, Scherer M. Metabolomics using GC-TOF-MS followed by subsequent GC-FID and HILIC-MS/MS analysis revealed significantly altered fatty acid and phospholipid species profiles in plasma of smokers. J Chromatogr B, Anal Technol Biomed life Sci. 2014;966:117–126.

145. Calderon-Santiago M, Priego-Capote F, Jurado-Gamez B,

Luque de Castro MD. Optimization study for metabolomics analysis of human sweat by liquid chromatography-tandem mass spectrometry in high resolution mode. J Chromatogr A. 2014;1333:70–78.

146. Paglia G, Magnusdottir M, Thorlacius S, Sigurjonsson OE, Guethmundsson S, Palsson BO, et al. Intracellular metabolite profiling of platelets: evaluation of extraction processes and chromatographic strategies. J Chromatogr B, Anal Technol Biomed life Sci. 2012;898:111–120.

147. Holčapek M, Kolářová L, Nobilis M. High-performance liquid chromatography–tandem mass spectrometry in the identification and determination of phase I and phase II drug metabolites. Anal Bioanal Chem. 2008;391(1):59–78.

148. Cheng M-L, Shiao M-S, Chiu DT-Y, Weng S-F, Tang H-Y, Ho H-Y. Biochemical disorders associated with antiproliferative effect of dehydroepiandrosterone in hepatoma cells as revealed by LC-based metabolomics. Biochem Pharmacol. 2011;82(11):1549–1561.

149. Hao Z, Xiao B, Weng N. Impact of column temperature and mobile phase components on selectivity of hydrophilic interaction chromatography (HILIC). J Sep Sci. 2008;31(9):1449–1464.

150. Spagou K, Tsoukali H, Raikos N, Gika H, Wilson ID, Theodoridis G. Hydrophilic interaction chromatography coupled to MS for metabonomic/metabolomic studies. J Sep Sci. 2010;33(6–7):716–727.

151. Yang S, Sadilek M, Lidstrom ME. Streamlined pentafluorophenylpropyl column liquid chromatography–tandem quadrupole mass spectrometry and global 13C-labeled internal standards improve performance for quantitative metabolomics in bacteria. J Chromatogr A. 2010;1217(47):7401–7410.

152. Sato S, Soga T, Nishioka T, Tomita M. Simultaneous determination of the main metabolites in rice leaves using capillary electrophoresis mass spectrometry and capillary electrophoresis diode array detection. Plant J. 2004;40(1):151–163.

153. Tolstikov V V, Fiehn O. Analysis of Highly Polar Compounds of Plant Origin: Combination of Hydrophilic Interaction Chromatography and Electrospray Ion Trap Mass Spectrometry. Anal Biochem. 2002;301(2):298–307.

154. Allwood JW, Goodacre R. An introduction to liquid chromatography-mass spectrometry instrumentation applied in plant metabolomic analyses. Phytochem Anal. 2010;21(1):33–47.

155. Thomas A, Déglon J, Steimer T, Mangin P, Daali Y, Staub C. On-line desorption of dried blood spots coupled to hydrophilic interaction/reversed-phase LC/MS/MS system for the simultaneous analysis of drugs and their polar metabolites. J Sep Sci. 2010;33(6–7):873–879.

156. Hsieh Y. Potential of HILIC-MS in quantitative bioanalysis of drugs and drug metabolites. J Sep Sci. 2008;31(9):1481–1491.

157. Lindenmayer J-P, Kaur A. Antipsychotic Management of Schizoaffective Disorder: A Review. Drugs. 2016;76(5):589–604.

158. Rajagopalan K, Hassan M, Boswell K, Sarnes E, Meyer K, Grossman F. Review of outcomes associated with restricted access to atypical antipsychotics. Am J Manag Care. 2016;22(6):e208-214.

159. Correll CU, Detraux J, De Lepeleire J, De Hert M. Effects of antipsychotics, antidepressants and mood stabilizers on risk for physical diseases in people with schizophrenia, depression and bipolar disorder. World Psychiatry. 2015;14(2):119–136.

160. Benich III JJ, Bragg SW, Freedy JR. Psychopharmacology in Primary Care Settings. Prim Care Clin Off Pract. 2016;43(2):327–340.

161. Gopalakrishna G, Ithman MH, Lauriello J. Update on New and Emerging Treatments for Schizophrenia. Psychiatr Clin North Am. 2016;39(2):217–238.

162. Siskind D, McCartney L, Goldschlager R, Kisely S. Clozapine v. first- and second-generation antipsychotics in treatment-refractory schizophrenia: systematic review and meta-analysis. Br J Psychiatry. 2016.

163. Gaillard PJ, De Boer AG. Relationship between permeability status of the blood-brain barrier and in vitro permeability coefficient of a drug. Eur J Pharm Sci. 2000;12(2):95–102.

164. Jeffrey P, Summerfield S. Assessment of the blood-brain barrier in CNS drug discovery. Neurobiol Dis. 2010;37(1):33–37.

165. Xu G, Mahajan S, Roy I, Yong KT. Theranostic quantum dots for crossing blood-brain barrier in vitro and providing therapy of HIV-associated encephalopathy. Front Pharmacol. 2013;4:1–8.

166. Williams C a, Lavik EB, Manuscript A, Amini AR, Laurencin CT, Nukavarapu SP, et al. Engineering the human pluripotent stem cell microenvironment to direct cell fate. Nat Biotechnol. 2012;30(6):2014.

167. Weiss N, Miller F, Cazaubon S, Couraud PO. The blood-brain

barrier in brain homeostasis and neurological diseases. Biochim Biophys Acta - Biomembr. 2009;1788(4):842–857.

168. Obermeier B, Daneman R, Ransohoff RM. Development, maintenance and disruption of the blood-brain barrier. Nat Med. 2013;19(12):1584–1596.

169. Sharma HS, Muresanu D, Sharma A, Patnaik R. Chapter 11 - Cocaine-Induced Breakdown of the Blood–Brain Barrier and Neurotoxicity. In: Neurobiology BT-IR of, editor. New Concepts of Psychostimulant Induced Neurotoxicity. 2009:297–334.

170. Gandhi N, Saiyed ZM, Napuri J, Samikkannu T, Reddy PVB, Agudelo M, et al. Interactive role of human immunodeficiency virus type 1 (HIV-1) clade-specific Tat protein and cocaine in blood-brain barrier dysfunction: implications for HIV-1-associated neurocognitive disorder. J Neurovirol. 2010;16(4):294–305.

171. Torres E, Gutierrez-Lopez MD, Mayado A, Rubio A, O'Shea E, Colado MI. Changes in interleukin-1 signal modulators induced by 3,4-methylenedioxymethamphetamine (MDMA): regulation by CB2 receptors and implications for neurotoxicity. J Neuroinflammation. 2011;8:53.

172. Zetterberg H, Jakobsson J, Redsäter M, Andreasson U, Pålsson E, Ekman CJ, et al. Blood-cerebrospinal fluid barrier

dysfunction in patients with bipolar disorder in relation to antipsychotic treatment. Psychiatry Res. 2014;217(3):143–146.

173. Wang M, Bai J, Chen WN, Ching CB. Metabolomic profiling of cellular responses to carvedilol enantiomers in vascular smooth muscle cells. PLoS One. 2010;5(11).

174. Gika HG, Theodoridis G a, Wingate JE, Wilson ID. Within-Day Reproducibility of an HPLC MS Based Method for Metabonomic Analysis: Application to Human Urine. JProteome Res. 2007;6:3291–303.

175. Gika HG, Macpherson E, Theodoridis GA, Wilson ID. Evaluation of the repeatability of ultra-performance liquid chromatography-TOF-MS for global metabolic profiling of human urine samples. J Chromatogr B Anal Technol Biomed Life Sci. 2008;871(2):299–305.

176. Food and Drug Administration. Guidance for industry. Bioanalytical method validation. 2013.

177. Chan TL, Gershon S. Chlorpromazine metabolism in humans. Part I. Microchim Acta. 1973;61(3):435–452.

178. Yeung PK, Hubbard JW, Korchinski ED, Midha KK. Pharmacokinetics of chlorpromazine and key metabolites. Eur J Clin Pharmacol. Germany; 1993;45(6):563–569.

179. Rousu T, Hokkanen J, Pelkonen OR, Tolonen A. Applicability of Generic Assays Based on Liquid Chromatography–Electrospray Mass Spectrometry to Study in vitro Metabolism of 55 Structurally Diverse Compounds . Front Pharmacol. 2010;1:10.

180. Schaber G, Wiatr G, Wachsmuth H, Dachtler M, Albert K, Gaertner I, et al. Isolation and identification of clozapine metabolites in patient urine. Drug Metab Dispos. 2001;29(6):923–931.

181. Schaber G, Stevens I, Gaertner HJ, Dietz K, Breyer-Pfaff U. Pharmacokinetics of clozapine and its metabolites in psychiatric patients: plasma protein binding and renal clearance. Br J Clin Pharmacol. 1998;46(5):453–459.

182. Pereira de Sousa I, Bernkop-Schnurch A. Pre-systemic metabolism of orally administered drugs and strategies to overcome it. J Control Release. 2014;192:301–309.

183. Dauchy S, Dutheil F, Weaver RJ, Chassoux F, Daumas-Duport C, Couraud P-O, et al. ABC transporters, cytochromes P450 and their main transcription factors: expression at the human blood-brain barrier. J Neurochem. 2008;107(6):1518–1528.

184. Shawahna R, Uchida Y, Decleves X, Ohtsuki S, Yousif S, Dauchy S, et al. Transcriptomic and quantitative proteomic

analysis of transporters and drug metabolizing enzymes in freshly isolated human brain microvessels. Mol Pharm. 2011;8(4):1332–1341.

185. Anthrieu S, Azzi PB El, Dumont J, Abdel-Razzak Z, Guguen-Guillouzo C, Fromenty B, et al. Oxidative stress plays a major role in chlorpromazine-induced cholestasis in human HepaRG cells. Hepatology. 2013;57(4):1518–1529.

186. Sajja RK, Rahman S, Cucullo L. Drugs of abuse and blood-brain barrier endothelial dysfunction: A focus on the role of oxidative stress. J Cereb Blood Flow Metab. 2015;0271678X15616978.

187. REDDY MKC. Haart Drugs Induce Oxidative Stress and Mitochondrial Dysfunction in Blood-Brain Barrier. In Vivo. 2010.

188. Martindale JL, Holbrook NJ. Cellular response to oxidative stress: Signaling for suicide and survival. J Cell Physiol. 2002;192(1):1–15.

189. Nadanaciva S, Rana P, Beeson GC, Chen D, Ferrick DA, Beeson CC, et al. Assessment of drug-induced mitochondrial dysfunction via altered cellular respiration and acidification measured in a 96-well platform. J Bioenerg Biomembr. 2012;44(4):421–437.

190. Napolitano JSM, Lagace CJ, Brennan WA, June R. Differential Effects of Typical and Atypical Neuroleptics on Mitochondrial Function In Vitro. 2003;26(11):951–959.

191. Takami G, Ota M, Nakashima A, Kaneko YS, Mori K, Nagatsu T, et al. Effects of atypical antipsychotics and haloperidol on PC12 cells: Only aripiprazole phosphorylates AMP-activated protein kinase. J Neural Transm. 2010;117(10):1139–1153.

192. Canfrán-Duque A, Pastor O, Reina M, Lerma M, Cruz-Jentoft AJ, Lasunción MA, et al. Curcumin mitigates the intracellular lipid deposit induced by antipsychotics in vitro. PLoS One. 2015;10(10):1–18.

193. Halliwell WH. Amphiphilic Drug-Induced Phospholipidosis. Toxicol Pathol. 1997;25(39):53–60.

194. Cohen BH. Pharmacologic effects on mitochondrial function. Dev Disabil Res Rev. 2010;16(2):189–199.

195. Hroudov J, Fiar Z. In vitro inhibition of mitochondrial respiratory rate by antidepressants. Toxicol Lett. 2012;213(3):345–352.

196. Hoppel C. The role of carnitine in normal and altered fatty acid metabolism. Am J Kidney Dis. 2003;41(4 Suppl 4):S4--S12.

197. Guzmn M, Blzquez C. Ketone body synthesis in the brain: Possible neuroprotective effects. Prostaglandins Leukot Essent

Fat Acids. 2004;70(3):287–292.

198. Sterx R. of Ketone. 1961;236(11):2892–2897.

199. Wu Y-T, Wei S-BW and Y-H. Metabolic Reprogramming of Human Cells in Response to Oxidative Stress: Implications in the Pathophysiology and Therapy of Mitochondrial Diseases. Current Pharmaceutical Design. 2014:5510–5526.

200. Escribá P V., Busquets X, Inokuchi J, Balogh G, Török Z, Horváth I, et al. Membrane lipid therapy: Modulation of the cell membrane composition and structure as a molecular base for drug discovery and new disease treatment. Prog Lipid Res. 2015;59:38–53.

201. Cichoz-Lach H, Michalak A. Oxidative stress as a crucial factor in liver diseases. World J Gastroenterol. 2014;20(25):8082–8091.

202. Stress O, Controlled ARE, The T, Phosphate P, Transaldolase PBY. Are Controlled Through the Pentose Phosphate. 2012;17(7):395–403.

203. Walss-Bass C, Weintraub ST, Hatch J, Mintz J, Chaudhuri AR. Clozapine causes oxidation of proteins involved in energy metabolism: a possible mechanism for antipsychotic-induced metabolic alterations. Int J Neuropsychopharmacol. 2008;11:1097–1104.

204. Quincozes-Santos A, Bobermin LD, Tonial RPL, Bambini-Junior V, Riesgo R, Gottfried C. Effects of atypical (risperidone) and typical (haloperidol) antipsychotic agents on astroglial functions. Eur Arch Psychiatry Clin Neurosci. 2010;260(6):475–481.

205. Collaborators MWS. Breast cancer and hormone-replacement therapy in the Million Women Study. Lancet. 2003;362(9382):419–427.

206. Ferlay J, Soerjomataram I, Dikshit R, Eser S, Mathers C, Rebelo M, et al. Cancer incidence and mortality worldwide: Sources, methods and major patterns in GLOBOCAN 2012. Int J Cancer. 2015;136(5):E359–386.

207. Siegel RL, Miller KD, Jemal A. Cancer statistics, 2015. CA Cancer J Clin. 2015;65(1):5–29.

208. U.S. Cancer Statistics Working Group. United States Cancer Statistics: 1999–2013 Incidence and Mortality Web-based Report. Atlanta: U.S. Department of Health and Human Services, Centers for Disease Control and Prevention and National Cancer Institute. 2016.

209. National Cancer Intelligence Network. Recurrent and metastatic breast cancer data collection project. 2012.

210. Ferlay J, Steliarova-Foucher E, Lortet-Tieulent J, Rosso S,

Coebergh JWW, Comber H, et al. Cancer incidence and mortality patterns in Europe: Estimates for 40 countries in 2012. Eur J Cancer. 2013;49(6):1374–1403.

211. Coughlin SS, Ekwueme DU. Breast cancer as a global health concern. Cancer Epidemiol. 2009;33(5):315–318.

212. Nemoto T, Vana J, Bedwani RN, Baker HW, McGregor FH, Murphy GP. Management and survival of female breast cancer: Results of a national survey by the American college of surgeons. Cancer. 1980;45(12):2917–2924.

213. Fowble BL, Solin LJ, Schultz DJ, Goodman RL. Ten year results of conservative surgery and irradiation for stage I and II breast cancer. Int J Radiat Oncol. 1991;21(2):269–277.

214. Bodai BI, Tuso P. Breast Cancer Survivorship: A Comprehensive Review of Long-Term Medical Issues and Lifestyle Recommendations. Perm J. 2015;19(2):48–79.

215. Hassett MJ, O'Malley AJ, Pakes JR, Newhouse JP, Earle CC. Frequency and Cost of Chemotherapy-Related Serious Adverse Effects in a Population Sample of Women With Breast Cancer. J Natl Cancer Inst. 2006;98(16):1108–1117.

216. Shapiro CL, Recht A. Side Effects of Adjuvant Treatment of Breast Cancer. N Engl J Med. 2001;344(26):1997–2008.

217. Carlson RW, Anderson BO, Chopra R, Eniu AE, Jakesz R, Love

RR, et al. Treatment of breast cancer in countries with limited resources. Breast J. 2003;9 Suppl 2:S67-74.

218. Eniu A, Carlson RW, Aziz Z, Bines J, Hortobágyi GN, Bese NS, et al. Breast cancer in limited-resource countries: Treatment and allocation of resources. Breast J. 2006;12(SUPPL. 1).

219. André F, Zielinski CC. Optimal strategies for the treatment of metastatic triple-negative breast cancer with currently approved agents. Ann Oncol. 2012;23(suppl 6):vi46-vi51.

220. Kayl AE, Meyers CA. Side-effects of chemotherapy and quality of life in ovarian and breast cancer patients. Curr Opin Obstet Gynecol. 2006;18(1):24–28.

221. Azim HA, de Azambuja E, Colozza M, Bines J, Piccart MJ. Long-term toxic effects of adjuvant chemotherapy in breast cancer. Ann Oncol. 2011

222. Aslam MS, Naveed S, Ahmed A, Abbas Z, Gull I, Athar MA. Side Effects of Chemotherapy in Cancer Patients and Evaluation of Patients Opinion about Starvation Based Differential Chemotherapy. 2014:817–822.

223. da Rocha AB, Lopes RM, Schwartsmann G. Natural products in anticancer therapy. Curr Opin Pharmacol. 2001;1(4):364–369.

224. Mann J. Natural products in cancer chemotherapy: past, present and future. Nat Rev Cancer. 2002;2(2):143–148.

225. Bonofiglio D, Giordano C, Amicis F De, Andò ML and S. Natural Products as Promising Antitumoral Agents in Breast Cancer: Mechanisms of Action and Molecular Targets.. Mini-Reviews in Medicinal Chemistry. 2016: 596–604.

226. Tuli HS, Sandhu SS, Sharma AK. Pharmacological and therapeutic potential of Cordyceps with special reference to Cordycepin. 3 Biotech. 2014;4(1):1–12.

227. Yoon J, Kim J, Baek K-S, Kim G, Lee S, Lee D, et al. A direct protein kinase B-targeted anti inflammatory activity of cordycepin from artificially cultured fruit body of *Cordyceps militaris* YR - 2015//1. Pharmacogn Mag. 2015;11(43):485-477.

228. Nakamura K, Shinozuka K, Yoshikawa N. Anticancer and antimetastatic effects of cordycepin, an active component of Cordyceps sinensis. J Pharmacol Sci. 2015;127(1):53–56.

229. Wong YY, Moon A, Duffin R, Barthet-Barateig A, Meijer HA, Clemens MJ, et al. Cordycepin Inhibits Protein Synthesis and Cell Adhesion through Effects on Signal Transduction. J Biol Chem. 2010;285(4):2610–2621.

230. Frederiksen S. Inhibition of ribonucleic acid and deoxyribonucleic acid synthesis in Ehrlich ascites cells by cordycepin-N1-oxide. Biochim Biophys Acta - Spec Sect

Nucleic Acids Relat Subj. 1963;76:366–371.

231. Siev M, Weinberg R, Penman S. The selective interruption of nucleolar RNA synthesis in HeLa cells by cordycepin. J Cell Biol. 1969;41:510–520.

232. García- Cañaveras JC, Castell J V., Donato MT, Lahoz A. A metabolomics cell-based approach for anticipating and investigating drug-induced liver injury. Sci Rep. 2016;6:27239.

233. Sun J. Metabolomics in Drug-induced Toxicity and Drug Metabolism. J Drug Metab Toxicol. 2012;3(5).

234. Li F, Gonzalez FJ, Ma X. LC–MS-based metabolomics in profiling of drug metabolism and bioactivation. Acta Pharm Sin B. 2012;2(2):118–125.

235. Utami W. Ion pairing LC-MS/MS method for analysis of intracellular phosphorylated metabolites. The University of Nottingham; 2015.

236. Utami W. Ion pairing LC-MS/MS method for analysis of intracellular phosphorylated metabolites. 2015.

237. Sumner LW, Amberg A, Barrett D, Beale MH, Beger R, Daykin CA, et al. Proposed minimum reporting standards for chemical analysis Chemical Analysis Working Group (CAWG) Metabolomics Standards Initiative (MSI). Metabolomics. 2007

Sep;3(3):211–221.

238. Pohjanen E, Thysell E, Lindberg J, Schuppe-Koistinen I, Moritz T, Jonsson P, et al. Statistical multivariate metabolite profiling for aiding biomarker pattern detection and mechanistic interpretations in GC/MS based metabolomics. Metabolomics. 2006;2(4):257–268.

239. Dalla Rosa L, da Silva AS, Gressler LT, Oliveira CB, Dambrós MGC, Miletti LC, et al. Cordycepin (3'-deoxyadenosine) pentostatin (deoxycoformycin) combination treatment of mice experimentally infected with Trypanosoma evansi. Parasitology. 2013;140(5):663–671.

240. Li G, Nakagome I, Hirono S, Itoh T, Fujiwara R. Inhibition of adenosine deaminase (ADA)-mediated metabolism of cordycepin by natural substances. Pharmacol Res Perspect. 2015;3(2):e00121.

241. Rottenberg ME, Masocha W, Ferella M, Petitto-Assis F, Goto H, Kristensson K, et al. Treatment of African trypanosomiasis with cordycepin and adenosine deaminase inhibitors in a mouse model. J Infect Dis. 2005;192(9):1658–1665.

242. Hu Z, Lee C Il, Shah VK, Oh EH, Han JY, Bae JR, et al. Cordycepin increases nonrapid eye movement sleep via adenosine receptors in rats. Evidence-based Complement

Altern Med. 2013;2013.

243. Tsai YJ, Lin LC, Tsai TH. Pharmacokinetics of adenosine and cordycepin, a bioactive constituent of cordyceps sinensis in rat. J Agric Food Chem. 2010;58:4638–4643.

244. al-Razzak LA, Benedetti AE, Waugh WN, Stella VJ. Chemical stability of pentostatin (NSC-218321), a cytotoxic and immunosuppressant agent. Pharm Res. 1990;7(5):452–460.

245. Kraut EH, Neff JC, Bouroncle BA, Gochnour D, Grever MR. Immunosuppressive effects of pentostatin. J Clin Oncol . 1990;8(5):848–855.

246. O'DWYER PJ, WAGNER B, LEYLAND-JONES B, WITTES RE, CHESON BD, HOTH DF. 2'-Deoxycoformycin (Pentostatin) for Lymphoid MalignanciesRational Development of an Active New Drug. Ann Intern Med. 1988;108(5):733–743.

247. Soares AS, Costa VM, Diniz C, Fresco P. Inosine strongly enhances proliferation of human C32 melanoma cells through PLC-PKC-MEK1/2-ERK1/2 and PI3K pathways. Basic Clin Pharmacol Toxicol. 2015;116(1):25–36.

248. Lane AN, Fan TWM. Regulation of mammalian nucleotide metabolism and biosynthesis. Nucleic Acids Res. 2015;43(4):2466–2485.

249. Weber G, Nakamura H, Natsumeda Y, Szekeres T, Nagai M.

Regulation of GTP biosynthesis. Adv Enzyme Regul. 1992;32:57–69.

250. Chiarugi A, Dolle C, Felici R, Ziegler M. The NAD metabolome [mdash] a key determinant of cancer cell biology. Nat Rev Cancer. 2012;12(11):741–752.

251. Genschel U. Coenzyme A biosynthesis: Reconstruction of the pathway in archaea and an evolutionary scenario based on comparative genomics. Mol Biol Evol. 2004;21(7):1242–1251.

252. Carter NS, Yates P, Arendt CS, Boitz JM, Ullman B. Purine and pyrimidine metabolism in Leishmania. Adv Exp Med Biol. 2008;625:141–154.

253. Trigg PI, Gutteridge WE, Williamson J. The effects of cordycepin on malaria parasites. Trans R Soc Trop Med Hyg]. 1971;65(4):514–520.

254. Ahmad Z, Okafor F, Azim S, Laughlin TF. ATP synthase: a molecular therapeutic drug target for antimicrobial and antitumor peptides. Curr Med Chem. 2013;20(15):1956–1973.

255. Pelicano H, Martin DS, Xu R-H, Huang P. Glycolysis inhibition for anticancer treatment. Oncogene. 2006;25(34):4633–4646.

256. Bessman SP, Carpenter CL. The creatine-creatine phosphate energy shuttle. Annu Rev Biochem. 1985;54:831–862.

257. Greenhaff PL. The creatine-phosphocreatine system: there's more than one song in its repertoire. J Physiol. 2001;537(Pt 3):657.

258. Rinaldi AC, Porcu CM, Oliva S, Curreli N, Rescigno A, Sollai F, et al. Biosynthesis of the topaquinone cofactor in copper amine oxidases--evidence from model studies. Eur J Biochem. 1998 Jan;251(1–2):91–97.

259. Houen G. Mammalian Cu-containing amine oxidases (CAOs): new methods of analysis, structural relationships, and possible functions. APMIS Suppl. DENMARK; 1999;96:1–46.

260. Ye Z, Chen L, Yang Z, Li Q, Huang Y, He M, et al. Metabolic Effects of Fluoxetine in Adults with Type 2 Diabetes Mellitus: A Meta-Analysis of Randomized Placebo-Controlled Trials. PLoS One. 2011;6(7):e21551.

261. Marken PA, Munro JS. Selecting a Selective Serotonin Reuptake Inhibitor: Clinically Important Distinguishing Features. Prim Care Companion J Clin Psychiatry. 2000;2(6):205–210.

262. Preskorn S. Clinically relevant pharmacology of selective serotonin reuptake inhibitors. Clin Pharmacokinet. 1997;1–21.

263. Bergstrom RF, Lemberger L, Farid NA, Wolen RL. Clinical pharmacology and pharmacokinetics of fluoxetine: A review.

Br J Psychiatry. 1988;153(SUPPL. 3):47–50.

264. Huang M, Joseph JW. Metabolomic analysis of pancreatic ??-cell insulin release in response to glucose. Islets. 2012;4(3):210–222.

265. Lorenz MA, El Azzouny MA, Kennedy RT, Burant CF. Metabolome response to glucose in the beta-cell line INS-1 832/13. J Biol Chem. 2013 Apr;288(15):10923–10935.

266. ElAzzouny MA, Evans CR, Burant CF, Kennedy RT. Metabolomics Analysis Reveals that AICAR Affects Glycerolipid, Ceramide and Nucleotide Synthesis Pathways in INS-1 Cells. PLoS One. 2015;10(6):e0129029.

267. Ahn JK, Kim S, Kim J, Hwang J, Kim KH, Cha H-S. A Comparative Metabolomic Evaluation of Behcet's Disease with Arthritis and Seronegative Arthritis Using Synovial Fluid. PLoS One. 2015;10(8):e0135856.

268. Stewart DA, Winnike JH, McRitchie SL, Clark RF, Pathmasiri WW, Sumner SJ. Metabolomics Analysis of Hormone-Responsive and Triple-Negative Breast Cancer Cell Responses to Paclitaxel Identify Key Metabolic Differences. J Proteome Res. 2016 Sep;15(9):3225–3240.

269. Clay HB, Parl AK, Mitchell SL, Singh L, Bell LN, Murdock DG. Altering the Mitochondrial Fatty Acid Synthesis (mtFASII)

Pathway Modulates Cellular Metabolic States and Bioactive Lipid Profiles as Revealed by Metabolomic Profiling. PLoS One. 2016;11(3):e0151171.

270. Fluoxetine for Depression in Diabetes. 2000.

271. Gehrmann W, Elsner M, Lenzen S. for Lipotoxicity in Pancreatic B-Cells. Diabetes, Obes & Metab. 2010;12:149–158.

272. Liu Z, Jeppesen PB, Gregersen S, Chen X, Hermansen K. Dose- and Glucose-Dependent Effects of Amino Acids on Insulin Secretion from Isolated Mouse Islets and Clonal INS-1E Beta-Cells. Rev Diabet Stud. 2008;5(4):232–244.

273. McDaniel ML, Marshall CA, Pappan KL, Kwon G. Metabolic and Autocrine Regulation of the Mammalian Target of Rapamycin by Pancreatic β-Cells. Diabetes. 2002;51(10):2877-2885.

274. Dixon G, Nolan J, McClenaghan N, Flatt PR, Newsholme P. A comparative study of amino acid consumption by rat islet cells and the clonal beta-cell line BRIN-BD11 - the functional significance of L-alanine. J Endocrinol. 2003;179(3):447–454.

275. McClenaghan NH, Barnett CR, Ah-Sing E, Abdel-Wahab YHA, O'Harte FPM, Yoon T-W, et al. Characterization of a Novel Glucose-Responsive Insulin-Secreting Cell Line, BRIN-BD11, Produced by Electrofusion. Diabetes. 1996;45(8):1132-1140.

276. Josefsen K, Buschard K, Sorensen LR, Wollike M, Ekman R, Birkenbach M. Glucose stimulation of pancreatic beta-cell lines induces expression and secretion of dynorphin. Endocrinology. 1998;139(10):4329–4336.

277. Prell GD, Martinelli GP, Holstein GR, Matulić-Adamić J, Watanabe KA, Chan SLF, et al. Imidazoleacetic acid-ribotide: An endogenous ligand that stimulates imidazol(in)e receptors. Proc Natl Acad Sci U S A. 2004;101(37):13677–13682.

278. Rodrigues T, Lopes F, Moreira R. Inhibitors of the mitochondrial electron transport chain and de novo pyrimidine biosynthesis as antimalarials: The present status. Curr Med Chem. 2010;17(10):929–956.

279. Raeder MB, Ferno J, Glambek M, Stansberg C, Steen VM. Antidepressant drugs activate SREBP and up-regulate cholesterol and fatty acid biosynthesis in human glial cells. Neurosci Lett. 2006;395(3):185–190.

280. Bardini G, Rotella CM, Giannini S. Dyslipidemia and diabetes: reciprocal impact of impaired lipid metabolism and Beta-cell dysfunction on micro- and macrovascular complications. Rev Diabet Stud. 2012;9(2–3):82–93.

281. Maechler P, Wollheim CB. Mitochondrial signals in glucose-stimulated insulin secretion in the beta cell. J Physiol.

2000;529(Pt 1):49–56.

282. Wiederkehr A, Wollheim CB. Minireview: Implication of Mitochondria in Insulin Secretion and Action. Endocrinology. 2006;147(6):2643–2649.

283. Kao C-Y, He Z, Henes K, Asara JM, Webhofer C, Filiou MD, et al. Fluoxetine Treatment Rescues Energy Metabolism Pathway Alterations in a Posttraumatic Stress Disorder Mouse Model. Mol neuropsychiatry. 2016;2(1):46–59.

284. Wallace M, Whelan H, Brennan L. Metabolomic analysis of pancreatic beta cells following exposure to high glucose. Biochim Biophys Acta. 2013;1830(3):2583–2590.

285. Ma X, Jin M, Cai Y, Xia H, Long K, Liu J, et al. Mitochondrial electron transport chain complex III is required for antimycin A to inhibit autophagy. Chem Biol. 2011 Nov;18(11):1474–1481.

286. Alonso A, Marsal S, Julia A. Analytical methods in untargeted metabolomics: State of the art in 2015. Front Bioeng Biotechnol. 2015;3:23

287. Arnold JM, Choi WT, Sreekumar A, Maletic-Savatic M. Analytical strategies for studying stem cell metabolism. Front Biol, 2015;10(2):141-153.

288. Scalbert A, Brennan L, Fiehn O, Hankemeier T, Kristal BS, van Ommen B, Pujos-Guillot E, Verheij, Wishart D, Wopereis S.

Mass-spectrometry-based metabolomics: Limitation and recommendations for future progress with particular focus on nutrition research. Metabolomics. 2009;5(4):435-458.

289. Neubauer S. Metabolomics in yeast by LC-MS. University of Natural Resources and Life Scieces-BOKU, Austria, 2012.

290. Lorenz MA. Development and application of metabolomic techniques for identification and quantification of intracellular etabolites relevant to glucose stimulated insulin secreation in β-cells. University of Michigan, USA. 2011.

291. Bajad SU, Lu W, Kimball EH, Yuan J, Peterson C, Rabinowitz JD. Separation and quantification of water soluble cellular metabolites by hydrophilic interaction chromatography-tandem mass spectrometry. J Chromato A. 2006;1125(1):76-88.

292. Wardlaw JM, Doubal F, Armitage P, Chappell F, Carpenter T, Maniega SM. Lacunar stroke is associated with diffuse blood-brain barrier dysfunction. Annals of Neurology. 2009;65:194-202.

293. Wardlaw JM. Blood-brain barrier and cerebral small vessel disease. J of the Neuro Sciences.2010;299:66-71.

294. Carrano A, Hoozemans JJM, van der Vies SM, Rozemuller AJM, can Horssen J, de Vries HE. Amyloid beta induce oxidative stress-mediated blood-brain barrier changes in capillary

amyloid angiopathy. Antioxidants & Redox Signaling. 2011;15(5):1167-1178.

295. Carrano A, Hoozemans JJM, van der Vies SM, van Horssen J, de Vries HE, Rozemuller AJM. Neuroinflammation and blood-brain barrier changes in capillary amyloid angiopathy. Antioxidants & Redox Signaling. 2012;10:329-331.

296. Noh EM, Youn HJ, Jung SH, Han JH, Jeong YJ, Chung EY, Jung JY, Kim BS, Lee SH, Lee YR, Kim JS. Cordycepin inhibit TPA-induced matrix metalloproteinase-9 expression by suppressing the MAPK/AP-1 pathway in MCF-7 human breast cancer cells. Inter J of Molecular Medicine. 2010;25:255-260.

297. Tuli HS, Sharma AK, Sandhu SS, Kashyap D. Cordycepin: A bioactive metabolite with therapeutic potential. Life Sciences. 2013;93:863-869.

298. Dorries K, Schluter R, Lalk M. Impact of antibiotics with various target sites on the metabolome of staphylococcus aureus. Antimicro Agents & Chemother. 2014;58(12)

299. Hoerr V, Duggan GE, Zbytnuik L, Poon KKH, Grobe C, Neugebauer U, Methling K, Loffler B, Vogel HJ. Characterization and prediction of the mechanism of action of antibiotics through NMR metabolomics. BMC Microbiol. 2016;16:82.

300. Khurshid A. The effect of the polyadenylation inhibitor

Cordycepin on MCF-7 cells. Universitu of Nottingham, UK. 2015.

301. Chen LS, Plunkett W, Gandhi V. Polyadenylation inhibition by the triphosphates of deoxyadenosine analogues. Leuk Res. 2008;32(10):1573-1581.

302. Kondrashov A, Meijier HA, Barthet-Barateig A, Parker HN, Khurshid A, Tessier S, Sicard M, Knox AJ, Pang L, de Moor CH. Inhibition of polyadenylation reduces inflammatory gene induction. RNA, 2012;18(2)2236-2250.

303. Curanovic D, Cohen M, Singh I, Slagle CE, Leslie CS, Jaffrey SR. Global profiling of stimulus-induced polyadenylation in cells using a poly(A) trap. Nat Chem Biol. 2013;9(11):671-673.

304. Ahmed SH. Mitochondrial function of pancreatic beta cells as a target of antidepressants. University of Nottingham, UK. 2015.

305. Worth A, Barroso J, Bremer S, Burton J, Casati S, Coecke S, Corvi R, Desprez B, Dumont C, Gouliarmou V, Grapel R, Griesinger C, Halder M, Roi AJ, Kienzler A, Madia F, Munn S, Nepelska M, Paini A, Price A, Prieto P, Rolaki A, Schaffer M, Triebe J, Whelan M, Wittehr C, Zuang V. Alternative methods for regulatory toxicology-a state-of-art-review. JRC Science and policy reports. 2014.

306. Atienzar FA, Blomme EA, Chen M, Hewitt P, Kenna JG, Labbe

G, Moulin F, Pognan F, Roth AB, Suter-Dick L, Ukairo O, Weaver RJ, Will Y, Dambach DM. Key challenge and opportunities associated with the use of in vitro models to detect human DILI: Integrated risk assessment and mitigation plans. Biomed Res Inter. 2016;2016.

307. Gomez-Lechon MJ, Lahoz A, Gombau L, Castell JV, Donato MT. In vitro evaluation of potential hepatotoxicity induced by drugs. Current Pharm Design. 2010;16.

308. Fei F. The development of cellular metabolomic platforms and their application. Dissertation submitted in partial fulfilment of the requirements for the degree of Doctor of Philosophy, McMaster University, 2015.

309. Creek DJ, Barrett MP. Determination of antiprotozoal drug mechanisms by metabolomics approaches.Parasitology. 2014;141:83-92.

310. Van Brummelen AC, Olszewski KL, Wilinski D, Llinas M, Louw AI. Birkholtz LM. Co-inhibition of Plasmodium falciparum S-adenosylmethionine decarboxylase/ornitine decarboxylase reveals perturbation-specific compensatory mechanisms by transcriptome, proteome, and metabolome analyses. J of Biological Chem. 2009;284:4635-4646.

311. MacBeath G, Koehler AN, Schreiber SL. Printing small

molecules as microarrays and detecting protein-ligand interactions en masse. J of the American Chem Society. 1999;121:7967-7968.

312. Keiser MJ, Irwin JJ, Shoichet BK. The chemical basis of pharmacology. Biochemistry. 2010;49:10267.

313. Beyoglu D, Idle JR. Metabolomics and its potential in drug development. Biochemical Pharmacology. 2013;85.

314. Esch C, Hui DS, Lee R, Edwards JL. Quantitation of thiol metabolites from mammalian cells using fluorous tagging and HILIC MS. Analytical Method. 2015;7:7164-7169.

315. Dias DA, Jones OAH, Beale DJ, Boughton BA, Benheim D, Kouremenos KA, Wolfender JL, Wishart DS. Current and future perspectives on the structural identification of small molecules in biological systems. Metabolites. 2016;6(4):46.